International Journal of

Biology

andChemistry

Al-Farabi Kazakh National University

EDITORIAL

The most significant achievements in the field of natural sciences are reached in joint collaboration, where important roles are taken by biology and chemistry. Therefore publication of a Journal, displaying results of current studies in the field of biology and chemistry, facilitates highlighting of theoretical and practical issues and distribution of scientific discoveries.

One of the basic goals of the Journal is to promote the extensive exchange of information between the scientists from all over the world. We welcome publishing original papers and materials of biological and chemical conferences, held in different countries (by prior agreement, after the process of their subsequent selection).

Creation of special International Journal of Biology and Chemistry is of great importance, since scientists worldwide, including other continents, might publish their articles, which will help to widen the geography of future collaboration.

The Journal aims to publish the results of the experimental and theoretical studies in the field of biology, biotechnology, chemistry and chemical technology. Among the emphasized subjects are: modern issues of technologies for organic synthesis; scientific basis of the production of physiologically active preparations; modern issues of technologies for processing of raw materials; production of new materials and technologies; study on chemical and physical properties and structure of oil and coal; theoretical and practical issues in processing of hydrocarbons; modern achievements in the field of nanotechnology; results of studies in various branches of biology, biotechnology, genetics, nanotechnology, etc.

We hope to receive papers from the leading scientific centers, which are involved in the application of the scientific principles of biological and chemical sciences on practice and carrying out research on the subject, related to production of new materials, technologies and ecological issues.

G.A. Mun[1*] , I. Moldakhan[2] , A.M. Serikbay[1] ,
D. Kaldybekov[1] , I.E. Suleimenov[3] , Kinam Park[4]

[1]Al-Farabi Kazakh National University, Almaty, Kazakhstan
[2]Almaty University of Power Engineering and Telecommunications, Almaty, Kazakhstan
[3]Institute of Information and Computational Technologies, Almaty, Kazakhstan
[4]Purdue University, West Lafayette, USA
*e-mail: mungrig@yandex.ru

Hydrophilic interpolymer associates – the key to solving the problem of pre-biological evolution

Abstract. A new approach to the analysis of the processes that led to the appearance of Life on Earth was proposed. The approach is based on the idea of the evolution of the Earth's shells as a system whole, which corresponds to the interpretation of the concept of "complex system" based on the analogy with neural networks. This analogy allows us to show that there are evolutionary mechanisms for which the primary one is the evolution of an analog of a neural network that is complementary to a specific complex system. The transformation of the system in this case takes place at the level of restructuring its structure, which at the next stage of evolution creates prerequisites for the "selection" of elements that correspond to the new state of the system as a whole. Experimental evidence of the validity of this approach for the interpretation of the origin of Life has been obtained based on the analysis of the formation of a comparative new class of macromolecular systems – hydrophilic interpolymer associates. It was shown that a solution of two interacting polymers, in which hydrophilic interpolymer associates are formed, is a direct analog of a neural network in a defined range of conditions. This object is capable of evolving as a whole, which proves the possibility of implementing an alternative mechanism of evolution considered in the framework of Darwinian theories.

Key words: complex system, polymers, interpolymer complexes, hydrophilic interpolymer associates, origin of life, neural network analog, evolution.

Introduction

Currently, active research is continuing to uncover the mystery of the origin of Life on our planet [1-3]. The authors of the vast majority of works carried out in this direction, either way, are guided by an approach that dating back to the theory of the origin of Darwinian's species [1-3].

However, there is every reason to believe that attempts to interpret the mechanisms of evolution that precede biological evolution, based on theories that go back to Darwin's point of view, cannot lead to success. This follows, among other things, from philosophical (methodological) judgments [4, 5]. Darwinian theories have faced and will continue to face insurmountable difficulties in trying to establish the

mechanisms of evolution that led to the emergence of Life on Earth for fundamental reasons.

Darwin's theory the origin of species successfully describes the evolution of existing biological species, but is unable to adequately answer the question of where Life came from as a system whole. The last clarification (the systemic integrity of the phenomenon of Life) is extremely important. It is on this basis that even purely philosophical methods can show that mutational mechanisms are not able to give an adequate picture of the evolution that preceded the biological one.

Namely, Life exists in the form of ecosystems, therefore mutation mechanisms cannot be consistent even from the point of view of General philosophical concepts: they can explain the transformation of

ecosystems, but they cannot explain the instantaneous emergence of an ecosystem with a rather complex and well-developed structure. Thus, the appearance of Life can only be the result of a certain qualitative leap (the emergence of a new quality), otherwise called aromorphosis, the prerequisites for this point of view are set out in well-known review papers [6, 7].

In [4, 5] it was shown that it is possible to propose a mechanism of evolution alternative to those that follow Darwinian theories. The corresponding theory is based on fundamentally new ideas about complex systems.

In the cited works, a hypothesis was put forward that a system of arbitrary nature should be interpreted as complex, when there is a complementary analog of a neural network. This means that for any complex system (a system that meets the category of complex in the philosophical sense), first of all, certain processes of information processing must be characterized that qualitatively different from the processes of information processing, characteristic to its individual components. The system (in the philosophical sense of this term) is something that qualitatively different from a simple set of its constituent elements – this idea is characteristic of the entire system approach, which goes back to the works of L. von Bertalanffy.

The proposed interpretation of the concept of "complex system" based on the analogy with neural networks, as well as the resulting philosophical understanding of the category of complex, indeed allow to propose a mechanism of evolution that is fundamentally different from Darwin's.

Indeed, a complex system can evolve even when the characteristics of its individual elements remain unchanged. In fact, this means that in this system, it is not the elements themselves that change, but the architecture of the relationships between them. The analogy with a neural network is important in that way because the rearrangement of links between system elements can be interpreted in the language of information theory as the evolution of an analog of a neural network that is complementary to the complex system under consideration.

We emphasize that this paper uses these representations. The evolution of an analog of the neural network that is complementary to a complex system of arbitrary nature suggests that a complex system could become a system for processing information even if it is composed of extremely simple elements. It is appropriate to emphasize that the existing artificial neural networks are also built from very simple elements that perform extremely simple functions,

but when combined into a single system, they allow to implement a new quality, new information processing systems.

If a complex system experiences a quantitative and qualitative transition associated with the emergence of a qualitatively new information processing system, then it could be converted into a filter that creates preferential conditions for the existence or appearance (reproduction) of those elements that correspond to its qualitatively new state.

In other words, from the proposed point of view, the primary one is not the evolution of elements that are driven by mutations, but the evolution of the system as a whole; it can cause the very qualitative leap that, in particular, could lead to the emergence of Life as a system whole, i.e. already in the form of an ecosystem.

In other words, according to this point of view, Life on our planet arose due to a very specific complex system was able to process information in a very specific way.

The relationship between the philosophical interpretation of the category of information reflected in [8] and the proposed interpretation of prebiological evolution in this paper is as follows.

The simplest form of life, namely a virus, can be considered as a macromolecular object that performs a single function – the preservation of its genetic code, "its information". The virus contains a single informational macromolecule, and all the rest perform auxiliary functions. This example clearly shows that the origin of life can and should be interpreted purely from the position of information theory.

Further, as was shown in [9] based on the concept of dialectical positivism [8], information systems have a well-defined hierarchy.

What is called a message is an information object of the simplest type. At the next level are information systems, which are some rules for processing information. The simplest example of a more complex information system is a set of operating rules with binary numbers (addition, multiplication, etc.) or any other algorithm. At the highest level of the hierarchy of information objects is human intelligence, understood as a purely informational object (this object cannot be identified with the brain or processes occurring in it, just as you cannot identify a punched card and information written on it).

We emphasize that this work is not about identifying certain protocells, but about identifying the conditions when these protocells could have occurred. Returning to the idea of the existence of Life in the form of ecosystems, this means that the entire system

as a whole is rebuilt and all the attributes of Life are created simultaneously in it. This, in particular, excludes the criticism that was addressed to Darwinian theories, and which was based on the extremely low probability of spontaneous occurrence of such molecules as DNA. From this point of view, this question is not worth it at all. It is not about the probabilities of random processes; it is about the evolution of the system as a whole.

Thus, to solve the problem of the origin of Life on our planet, it is necessary to show how such physical and chemical systems as solutions of hydrophilic macromolecules can be transformed into information processing systems. The choice of these systems as the base object is obvious: the main information macromolecules (DNA and RNA) are hydrophilic polymers.

In the present paper, we assume that the first step in this direction already has all the prerequisites. Namely, it is shown that there are quite certain conditions under which a solution containing two types of hydrophilic macromolecules interacting with each other is transformed into a non-trivial information processing system.

This transformation becomes possible due to the fact that hydrophilic interpolymer associates (HIA) could be formed in systems of this type [10, 11], and their formation can be accompanied by phase transitions of a stadial character. Experimental proof of the existence of staged phase transitions for the same system was given in [12] by the example of reactions between polyvinylcaprolactam (PVCL) and polyacrylic acid (PAA).

In this paper, the same system is experimentally studied and the conditions when phase transitions become stadial are analyzed. We emphasize that the multiplicity of phase transitions in such systems is quite easy to interpret from the point of view of the physical chemistry of polymers. Namely, in [10-12], it was shown that hydrophilic interpolymer associates are product that is intermediate by its properties with respect to both classical interpolymer complexes, true solutions, and cross-linked hydrophilic networks (Figure 1).
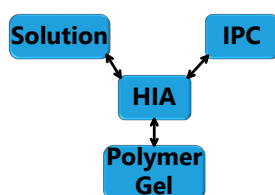
Figure 1 – An intermediate position
of the HIA among the known macromolecular objects

The hydrophilic interpolymer associate (HIA), as shown in [11, 12], is an analog of a cross-linked polymer network and HIA is a dynamic system. In other words, the hydrogen bonds that stabilize it are disrupted constantly and appeared again.

Experimental

Materials
Polyacrylic acid (PAA) with molecular weights of 2×10^3; 2.5×10^5; 4.5×10^5; 7.5×10^5 and 1.079×10^6 Da was purchased from Sigma-Aldrich (St. Louis, MO, USA). Polyvinylcaprolactam (PVCL) was synthesized according to a report using free-radical polymerization technique [19].

Molecular weight characteristics and polydispersity of the PVCL were determined using a gel permeation chromatography (GPC Aligent 1100 series RI detector).

Methods
The pH of polymer solution mixtures was gradually decreased by adding 0.1M HCl dropwise and the optical density (D) of mixtures was determined using a Shimadzu UV-2401PC UV-Vis spectrophotometer (Shimadzu Corp., Kyoto, Japan) with a Shimadzu CPS-240A thermoelectrically temperature controlled cell positioner at 400 nm wavelength and at 25 °C.

Results

The dependence of the optical density (turbidity) of polymer mixtures on pH, containing equimolar amounts of PVCL and PAA of different molecular weights, are presented in Figures 2-4. The turbidimetric titration curves are shown in Figure 7 for the case of PAA with Mw 4.5×10^5 Da.
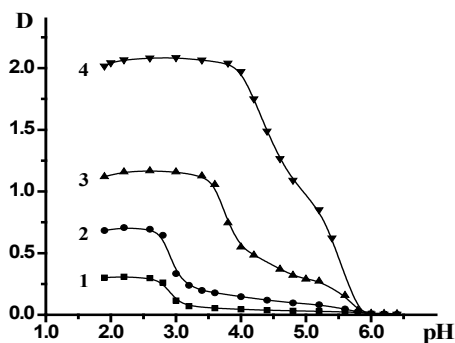
Figure 2 – The dependence of the optical density
of polymer solution mixtures of PVCL and PAA on pH;
Mw (PAA) = 2.5×10^5 Da, $C_{polymers}$ = 0.005 (1); 0.01 (2);
0.02 (3) and 0.05 mol/L (4)
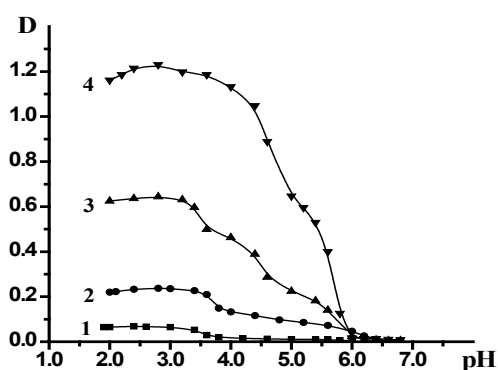
Figure 3 – The dependence of the optical density of polymer solution mixtures of PVCL and PAA on pH; Mw (PAA) = 4.5×10^5 Da, $C_{polymers}$ = 0.0025 (1); 0.005 (2); 0.01 (3) and 0.02 mol/L (4)
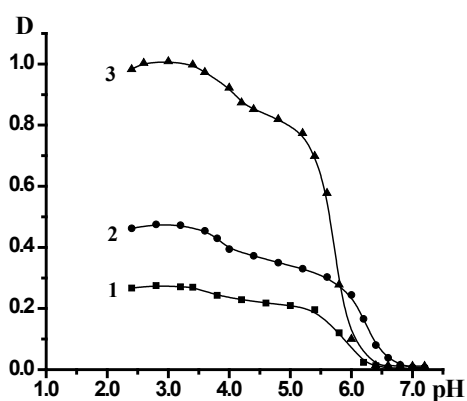
Figure 4 – The dependence of the optical density of polymer solution mixtures of PVCL and PAA on pH; Mw (PAA) = 7.5×10^5 Da, $C_{polymers}$ = 0.0025 (1); 0.005 (2) and 0.01 mol/L (3)

Discussion

PVCL belongs to a class of thermo-responsive polymers which possess a lower critical solution temperature (LCST) due to hydrophobic interactions in solutions [13, 14]. Complexes formed by such polymers are usually also sensitive to variations in other parameters that could shift the hydrophobic-hydrophilic balance, in particular, to variations in pH. This is confirmed by the data displayed in Figures 2-4.

In particular, it is clear that there is a critical pH value that limits the pH range, in which there is a sharp increase in the optical density of the solution and this is usually associated with the formation of a complex [15, 16].

A more detailed analysis of the depicted curves reveals important features of another product of in-

terpolymer reactions between the macromolecules – hydrophilic interpolymer associate (HIA). The mechanism of formation of HIA, in accordance with the arguments reported in [10-12], is as follows.

The dimensions of polyacid and non-ionic polymer coils differ greatly, even when the medium is not very acidic. This is due to the well-known polyelectrolyte effect, which occurs until the ionization of the polyacid is suppressed caused by the low-molecular component. Therefore, for the formation of the classical interpolymer complex (IPC) in an alkaline or slightly acidic region, it is necessary that the energy needed to stabilize its bonds exceeds a certain critical value.

This value is determined by the work that must be done either against the forces of polyelectrolyte stretching of the coil formed by the ionic polymer or, on the contrary, against the forces of elastic compression of the coil formed by the non-ionic component. It is obvious that to form the classical IPC, a sufficiently large number of hydrogen bonds must be formed between two macromolecules. This could only be occurred when the coils they form are of comparable size. Consequently, in the acidic environment, the formation of IPC stabilized by hydrogen bonds is facilitated, since the size of the coil formed by the ionic coil is reduced due to the suppression of polyelectrolyte swelling. This conclusion is directly confirmed by the experimental data presented above (Figures 1-4) and by the theory developed in [16].

In contrast, in a weakly acidic or alkaline environment, the size of coils formed by ionic and non-ionic macromolecules are not comparable. In this case, a significant number of bonds could be formed only when a single coil of non-ionic polymer interacts with several polyacid molecules instantly (or vice versa). Therefore, in this case, the polyacid molecules (due to the fact that the coil they form is relatively larger in size) serve as a cross-linking agent for a non-ionic polymer. Since the energy of formation of hydrogen bonds is relatively low (these bonds are not strong enough), then a loose network is formed in the solution, the bonds of which are in dynamic equilibrium that disrupt constantly and appear again. This dynamic network, according to the reports in [10-12], is interpreted as HIA. HIA is a product of an interpolymer reaction, intermediate both with respect to the classical IPC and to a true solution containing non-interacting macromolecules, as well as with respect to a hydrogel with physical cross-linking nodes.

A schematic illustration of consecutive transitions from a solution containing non-interacting macromolecules to the classical IPC through HIA is depicted on Figure 5.
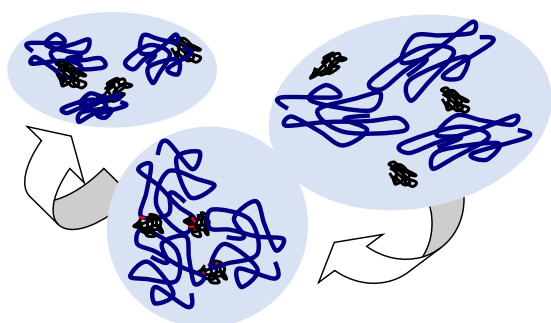
Figure 5 – A schematic illustration of sequential transitions in a system that allows the formation of HIA: non-interacting macromolecules–HIA–IPC

A comparison of the curves on Figures 2-4 demonstrates that their shape also changes markedly as the molecular weight of PAA increases. A detailed analysis of these curves allows to conclude that there are at least a number of intermediates in PVCL and PAA solution mixture. Moreover, as will be clear from the following, the transitions between such forms are of a stadial nature, which, in turn, allows to consider the environment in which the HIA is formed as a system with distributed memory.

In [10, 12], the following approximation was proposed for the dependence of the optical density of a polymer solution undergoing a phase transition.

$$D = \frac{D_0}{1 + \exp\left((pH - pH_0)/\tau_0\right)} \qquad (1)$$

where: D_0 – an extrapolation extremum of the optical density (i.e. the value that would be realized if the reaction between the polymers took place completely, but the reaction product did not precipitate); pH_0 – a parameter that determines the boundary of the area of existence of the complex by pH (this parameter is directly related to the critical pH value determined by the standard method, but differs slightly from it in numerical value); τ_0 – a parameter that determines the slope of the curve describing the transition from a solution of non-interacting polymers to a complex.

The type of curve (1) could be obtained, including, based on semi-phenomenological theory [12], parameters D_0, pH_0 and τ_0 are calculated based on the experimental data. However, it is seen that the type of this dependence coincides with the logistic curve which is often used in the theory of neural networks [17]. In other words, this curve could be used for approximate description of any type of phase transition, regardless of whether it corresponds to the phenomenological model [12] or not.

Curve (1) satisfies a first-order differential equation

$$\frac{dD}{dpH} = \frac{D^2}{D_0\tau_0} - \frac{D}{\tau_0} \qquad (2)$$

which could be obtained by directly differentiating (1) by a variable pH and expressing exponential factors through the function D in the equation (1) [19].

Equation (2) could be interpreted as the equation of the phase portrait of $D(pH)$ curves, which is assumed as the dependence of the derivative of some function on the values of this function. Such phase portraits were used, in particular, in [18] to analyze the swelling kinetics of hydrogels in the presence of copper ions.

If the phase portrait of the curve under consideration obeys equation (2), i.e. it allows parabola approximation, then this curve itself will be described by the equation (1) [18].

Figures 6-8 display phase portraits of the experimental curves illustrated in Figures 2-4, respectively.

The depicted phase portraits were obtained using numerical differentiation with an approximate equation:

$$\left.\frac{dy}{dx}\right|_n = \frac{1}{10\Delta x}\left(2y_{n+2} + y_{n+1} - y_{n-1} - 2y_{n-2}\right) \qquad (3)$$

The Figures show that the phase portraits of these curves allow (with acceptable accuracy) approximations by a set of parabola fragments.

It can be seen that the phase portraits of individual curves shown in Figures 2-4 are indeed described with satisfactory accuracy by parabolic dependence. This, in particular, indicates the applicability of equation (1) to describe a change in the transparency of the solution during the phase transition (at least when such a transition is the only one).

However, there are curves whose phase portraits differ significantly from the parabolic one, too. Nevertheless, each of the presented phase portraits could be divided into separate sections, each of which is approximated by parabolic dependencies with satisfactory accuracy.

Based on this, it can be concluded that there are several different phase transitions take place in the system under consideration, i.e. the transition from a solution containing non-interacting macromolecules to IPC has a stadial nature. In particular, the phase portraits displayed on Figures 6-7 clearly show that the transition under consideration occurs in two stages.
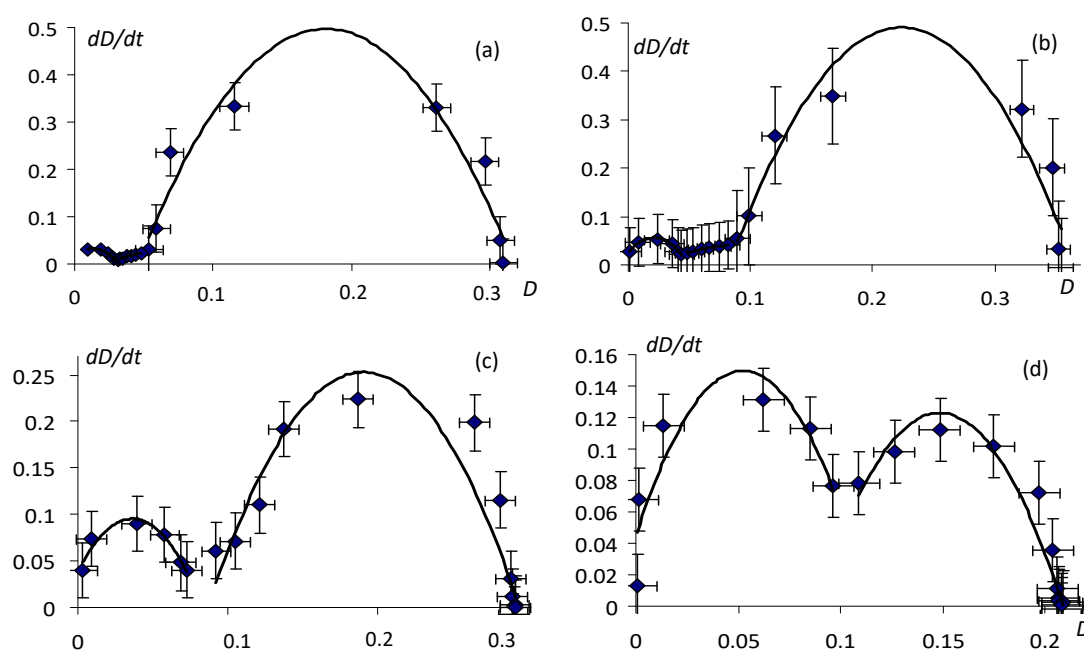
Figure 6 – Phase portraits of curves 1 (a), 2 (b), 3 (c) and 4 (d) shown in Figure 2

The two-stage phase transition fully corresponds to the scheme of Figure 5, specifically, the presence of an intermediate product of the interpolymer reaction – a hydrophilic interpolymer associate.

However, it can also be specified the case when the number of individual stages reaches three, which indicates the existence of not single, but two intermediate products. As will be clear from the following, even a system in which the phase transition occurs in two stages already possesses the properties with its inherent distributed memory (more specifically, such a system can become an analog of a neural network consisting of two neurons).

It should be emphasized that the method of phase portraits used to plot Figures 6-8 was originally developed in macromolecular chemistry to identify the stadial nature of the processes under consideration. Thus, it could be considered as experimentally proven that there are conditions under which the phase transition from the true solution of non-interacting macromolecules to the classical interpolymer complex may undergo through several different stages, some of which may not be determined in experiments, since the phase portrait method has a limited resolution, which depends both on the precision of optical measurements and on the possible superposition of one stage on another (the corresponding effect is also seen in above phase portraits).

It should also be emphasized that the nature of these stages, generally speaking, is not primarily determined by the nature of the interaction between macromolecules of the types under consideration.

Indeed, in fact, it is about a well-defined labile network structure, which could be considered as a complex system (in the philosophical meaning of the term).

As reported in [19-23], the behavior of complex systems, in which the structure of bonds can be transformed, is very non-trivial. It is emphasized that in the cited papers, extremely abstract network structures composed of formal elements, the only property of which is the formation of links, have been studied. Despite the fact that the elements in such grids are extremely simple, it was found that such objects are also characterized by pronounced phase transitions [22, 23]. Moreover, proofs of the existence of phase transitions in abstract grids, whose elements are endowed with the only property – the ability to form links with other elements of the system – can be obtained by direct calculation [24] without the use of numerical modeling methods used in such works as in [22, 23].

The results of work carried out in the study of complex network structures of various nature depict that there are conditions when in systems of this kind there are grids occur that differ from each other in structure, and differences in the nature of the structure could be associated with the occurrence of local inhomogeneities.

This conclusion could be used to justify the possibility of converting a hydrophilic interpolymer associate into a non-trivial information processing system.
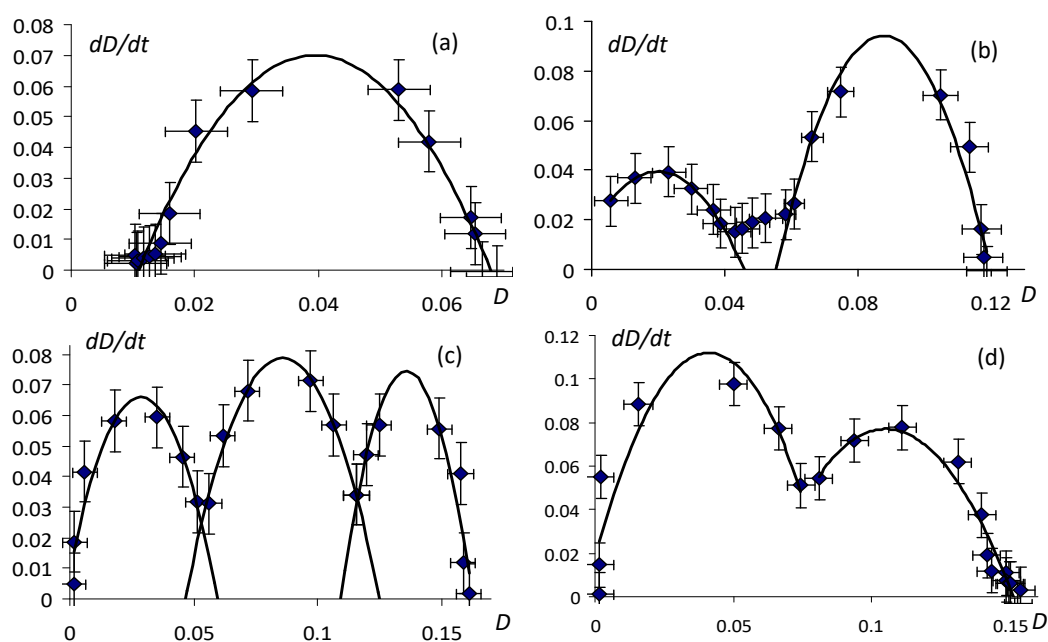
Figure 7 – Phase portraits of curves 1 (a), 2 (b), 3 (c) and 4 (d) shown in Figure 3
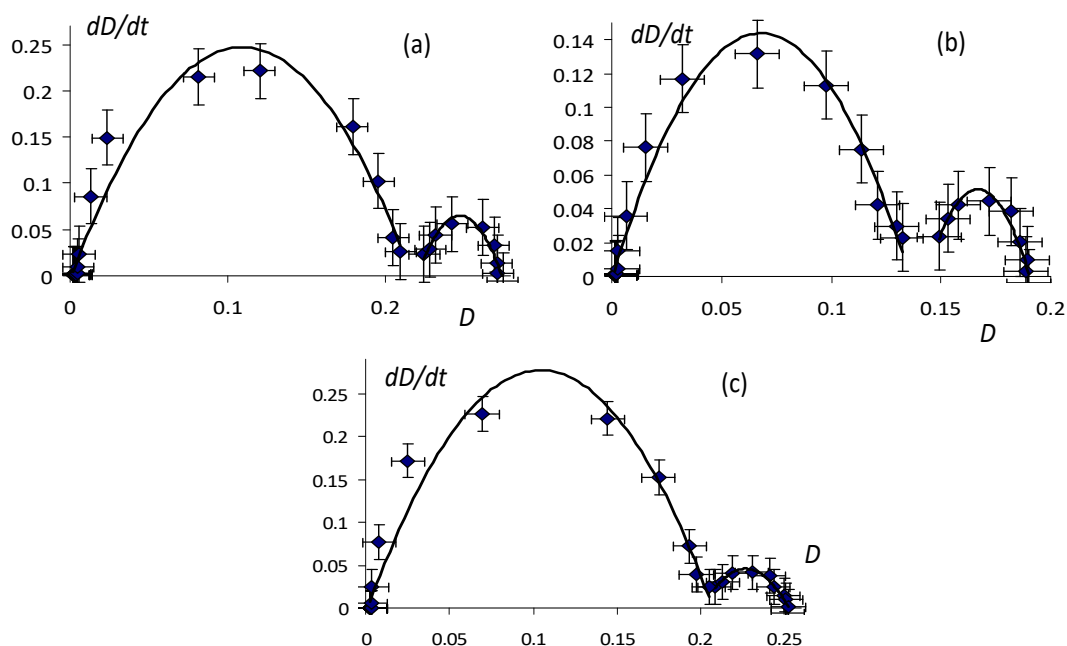
Figure 8 – Phase portraits of curves 1 (a), 2 (b) and 3 (c) shown in Figure 4

Transition from a dynamic network, i.e. from the hydrophilic interpolymer associate to the true interpolymer complex could be considered as a limiting case of "thickening of the grid" in some of its local regions. In this case, the density of bonds between two macromolecules at a local point reaches a maximum, and the links between these two macromolecules with others are terminated.

In other words, the true interpolymer complex can be considered as a limiting example of a hydro-

philic associate in some parts of which the degree of heterogeneity of the dynamic network has reached its maximum value (maximum bond density between two separate macromolecules upon all other bonds are broken). This understanding, as well as the results of the works cited above, suggests that in fact intermediate cases can be implemented in such a system, i.e. situations when the distribution of the density of bonds along the dynamic grid is uneven. Apparently, the transitions of this kind that demonstrate the experimental results described above.

Thus, it becomes clear that at least some phase transitions in the system under consideration are not related to a change in the nature of the chemistry of bonds between macromolecules, but to changes in the structure of the network itself. In other words, it is about the observed manifestations of changes in the network structure at local scales, but exceeding the size of individual macromolecular coil by their characteristic dimensions.

The existence of staged phase transitions, which, as shown by the experiments described above, can be very complex (the number of stages could be up to three and, possibly, more) allows to state that such a system itself can have distributed memory.

Provided that the phase transition has a stadial nature, then the solution containing a hydrophilic interpolymer associate can be considered as a neural network (Figure 9). In accordance with the scheme shown in Figure 9, the solution is conditionally divid-
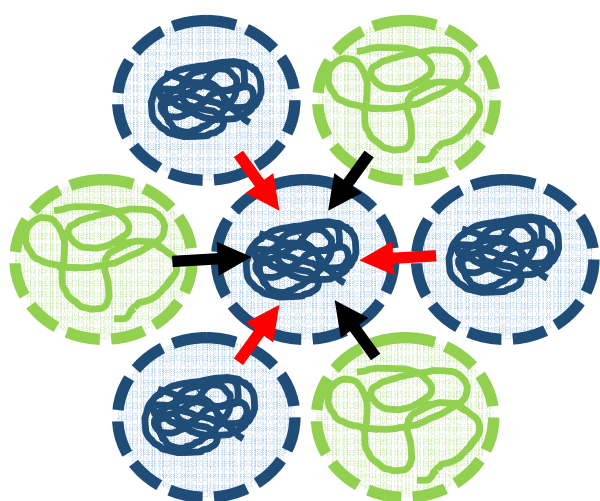
ed into regions, in each of which a phase transition occurs, and which corresponds to one of the stages discussed above. This stage corresponds to the transition from a hydrophilic interpolymer associate of the simplest type to the hydrophilic interpolymer associate, in which there are pronounced heterogeneities of the distribution of bond density.

As it was shown above, this stage is expressed for some conditions and can be interpreted as a transition from more homogeneous HIA to less homogeneous HIA, i.e., to the one in which a kind of nuclei of the interpolymer complex are formed, and more correctly, regions are formed in which the density of bonds between molecules of two interacting varieties is locally increased.

It is emphasized once again that, in accordance with the most general ideas about the nature of structural transitions in complex networks, any phase transition that does not change the nature of the interacting elements themselves can only be associated with structural transformations in the network itself. Thus, there is a transition associated with a local increase in the density of bonds and, accordingly, the density of swollen coils. Each of these sections can conditionally be considered as a neuron, and the output state of the neuron meets a logical zero is placed under the distribution corresponding to a more uniform grid, i.e. HIA of first type mentioned above, and the state corresponding to a logical unit is denser, i.e. HIA of second type.

Figure 9 – A solution containing HIA as an analog of a neural network
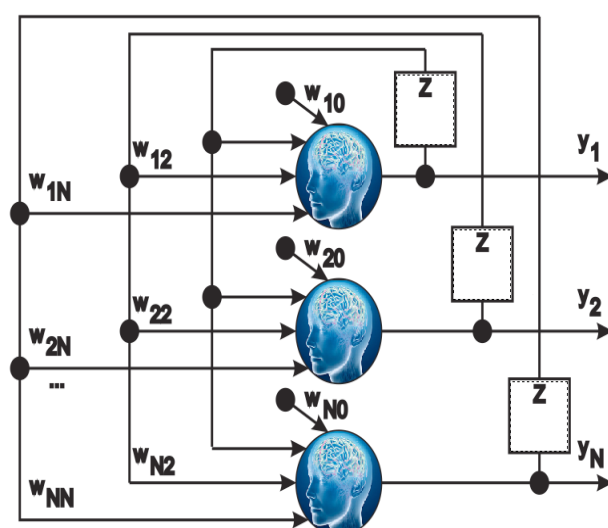
Figure 10 – Diagram of the Hopfield neuroprocessor

Obviously, there is a well-defined impact of neighboring regions on each other in the grid structure. Conditionally, such effect is shown by arrows on Figure 10. Therefore, this structure could be likened to a Hopfield neural network, in which all elements are covered by a feedback system (Figure 10). It is the fact that this system could be considered by analogy with the Hopfield neural network that proves that information can actually be written into a system of this type, that is, this system has distributed memory.

Conclusion

Thus, a solution of two interacting polymers in which hydrophilic interpolymer associates are formed is a direct analog of a neural network in a defined range of conditions. This object is able to evolve as a whole, which proves the possibility of implementing an alternative mechanism to the evolution considered in the framework of Darwinian theories.

The results obtained in this work could also be considered as a direct experimental confirmation of the concept of dialectical positivism. Specifically, it is about the interpretation of evolutionary processes in terms of understanding the information as a philosophical category, a paired category of matter.

From this point of view, the evolution of complex systems is complementary to the evolution of information objects. More precisely, qualitative-quantitative transitions that link different structural levels of the hierarchy of matter are complementary to structural levels that correspond to qualitative-quantitative transitions in the world of information entities.

We emphasize that it is about the evolution of the system as a whole. Even being composed of the same elements, it could experience transitions from quantity to quality, each of which can raise the level of information complexity, i.e. the emergence of the system of the new entities capable of processing the information qualitatively in different way than the components of the system elements.

As a result, the combination of such qualitative and quantitative transitions may well lead to a new state of the system, as a result of which it is converted into something qualitatively, that is different at the physical level. In other words, it turns into a kind of "filter" capable selecting the elements that are most relevant to its new state.

It is obvious that this kind of representation returns, including to the concept of Gaia J. Lovelock. More precisely, the results obtained allow to look at the problem of the origin of life from the point of view of J. Lovelock.

The primary is not the evolution of individual elements that later became components of the biosphere, the entire shell of the Earth evolved as a whole. Of course, a detailed consideration of these issues is beyond the scope of this work, however the results obtained in it already allow us to say that systems based on hydrophilic macromolecules can indeed evolve as a system whole and a well-defined structural memory occurs in them in a natural manner.

References

1   Avetisov V.A., Nechaev S.K. (2014) Fractal polymer globules: A new insight on prebiological evolution. Geochemistry International, 52(13), pp. 1252-1259. https://doi.org/10.1134/S0016702914130023.

2   Ruiz-Mirazo K., Briones C., de la Escosura A. (2017) Chemical roots of biological evolution: the origins of life as a process of development of autonomous functional systems. Open biology, 7(4), 170050. https://doi.org/ 10.1098/rsob.170050.

3   Higgs P.G. (2017) Chemical evolution and the evolutionary definition of life. Journal of Molecular Evolution, 84(5-6), pp. 225-235. https://doi.org/10.1007/s00239-017-9799-3.

4   Suleymenova K.I., Shaltykova D.B., Suleimenov I.E. (2013) Aromorphoses phenomenon in the development of culture: a view from the standpoint of neural net theory of complex systems evolution. European Scientific Journal, 9(19). https://doi.org/10.19044/esj.2020.v16n15.

5   Suleimenov I., Panchenko S. (2013) Non-Darwinists Scenarios of Evolution of Complicated Systems and Natural Neural Networks Based on Partly Dissociated Macromolecules. World Applied Sciences Journal, 24(9), pp. 1141-1147. https://doi.org/10.5829/idosi.wasj.2013.24.09.13272.

6   Chernavskiĭ D.S. (2000) The origin of life and thinking from the viewpoint of modern physics. Physics-Uspekhi, 43(2), pp. 151-176. https://doi.org/10.1070/PU2000v043n02ABEH000609.

7   Reutov V.P., Schechter A.N. (2010) How in the 20th century physicists, chemists and biologists answered the question: what is life? Physics-Uspekhi, 53(4), pp. 377-396. https://doi.org/ 10.3367/UFNe.0180.201004d.0393.

8   Suleimenov I., Massalimova A., Bakirov A., Gabrielyan O. (2018) Neural Networks and the Philosophy of Dialectical Positivism. In MATEC Web of Conferences (Vol. 214). EDP Sciences. https://doi.org/10.1051/matecconf/201821402002.

9   Suleimenov I.E., Gabrielyan O.A., Bakirov A.S., Vitulyova Y.S. (2019) Dialectical Understand-

ing of Information in the Context of the Artificial Intelligence Problems. In IOP Conference Series: Materials Science and Engineering (Vol. 630). Institute of Physics Publishing. https://doi.org/10.1088/1757-899X/630/1/012007.

10   Suleimenov I., Güven O., Mun G., Beissegul A., Panchenko S., Ivlev R. (2013) The formation of interpolymer complexes and hydrophilic associates of poly (acrylic acid) and non☐ionic copolymers based on 2☐hydroxyethylacrylate in aqueous solutions. Polymer International. 62, №. 9. pp. 1310-1315. https://doi.org/10.1002/pi.4422.

11   Suleimenov I.E., Shaltykova D.B., Mun G.A, Obukhova P.V., Panchenko S.V., Isembergenov N. (2013) Influence of Hydrophilic Interpolymer Associates on the Formation of Interpolymer Complexes. Advanced Materials Research. 749. pp. 60-64. https://doi.org/10.4028/www.scientific.net/AMR.749.60.

12   Suleimenov I., Shaltykova D., Sedlakova Z., Mun G., Semenyakin N., Kaldybekov D., Obukhova P. (2014) Hydrophilic interpolymer associates as a satellite product of reactions of formation of interpolymer complexes. Applied Mechanics and Materials, Vol. 467, pp. 58-63. https://doi.org/ 10.4028/www.scientific.net/AMM.467.58.

13 Laukkanen A., Wiedmer S.K., Varjo S., Riekkola M.L., Tenhu H. (2002) Stability and thermosensitive properties of various poly (N-vinylcaprolactam) microgels. Colloid and Polymer Science, 280(1), pp. 65-70. https://doi.org/10.1007/s003960200009.

14 Yanul N.A., Kirsh Y.E., Anufrieva E.V. (2000) Thermosensitive Water–Polymer Systems Studied by Luminescent Spectroscopy. Copolymers of N-vinylcaprolactam and N-vinylpyrrolidone. Journal of thermal analysis and calorimetry, 62(1), pp. 7-14. https://doi.org/10.1023/A:1010180624147.

15 Mun G.A., Nurkeeva Z.S., Khutoryanskiy V.V., Sergaziyev A.D. (2002) Interpolymer complexes of copolymers of vinyl ether of diethylene glycol with poly (acrylic acid). Colloid and Polymer Science, 280(3), pp. 282-289. https://doi.org/10.1007/s00396-001-0609-4.

16 Mun G.A., Suleimenov I.E., Yermukhambetova B.B., Vorob'eva N.A., Irmukhametova G.S. (2016) Features of the formation of interpolymer complexes of poly (carboxylic acids) and nonionic polymers in aqueous solutions in the presence of low-molecular-mass electrolytes. Polymer Science Series A, 58(6), pp. 944-955. https://doi.org/10.1134/S0965545X16060134.

17 Anthony M., Bartlett P.L. (2009) Neural network learning: Theoretical foundations. Cambridge university press.

18 Suleimenov I.E., Budtova T.V., Adilbekov S.A., Pereladov I.Yu., Bekturov E.A. (2004) Application of the method of phase portraits to the analysis of the kinetics of redistribution of metal ion concentrations in the polyelectrolyte hydrogel-multicomponent solution system. Polymer science. Series A, 46(8), pp. 797-805.

19 Wang X.F. (2002) Complex networks: topology, dynamics and synchronization. International Journal of Bifurcation and Chaos in Applied Sciences and Engineering, 12(05), pp. 885-916. https://doi.org/10.1142/S0218127402004802.

20 Albert R., Barabási A.L. (2002) Statistical mechanics of complex networks. Reviews of modern physics, 74(1), pp. 47-97. https://doi.org/10.1103/RevModPhys.74.47.

21 Gross T., Blasius B. (2008) Adaptive coevolutionary networks: a review. Journal of the Royal Society Interface, Vol. 5(20), pp. 259–271. https://doi.org/10.1098/rsif.2007.1229.

22 Solé R.V., Manrubia S.C., Luque B., Delgado J., Bascompte J. (1996) Phase transitions and complex systems: Simple, nonlinear models capture complex systems at the edge of chaos. Complexity, 1(4), pp. 13-26. https://doi.org/10.1002/cplx.6130010405.

23 Radin C., Sadun L. (2013) Phase transitions in a complex network. Journal of Physics A: Mathematical and Theoretical, 46(30), 305002. https://doi.org/10.1088/1751-8113/46/30/305002.

24 Suleimenov I.E., Mun G.A., Panchenko S.V., Tasbulatova Z., Nurtazin A. (2017) Phase Transitions in Communication Networks with Limited Elements of Valence. International Journal of Information and Electronics Engineering, 7(3), pp. 113-118. https://doi.org/10.18178/IJIEE.

H. Balouch[1*] iD , Z. Demirbag[2] iD , B.K. Zayadan[1] iD ,
A.K. Sadvakasaova[1] iD , K. Bolatkhan[1] iD , D. Gencer[2] iD , D. Civelek[2] iD

[1]Al-Farabi Kazakh National University, Almaty, Kazakhstan
[2]Karadeniz Technical University, Trabzon, Turkey
*e-mail: huma@comsats.org

Isolation, identification, and antimicrobial activity
of psychrophilic freshwater microalgae *Monoraphidium* sp.
from Almaty region

Abstract. Microalgae is one of the potential biotechnologically valuable groups of photosynthetic microorganisms and represent the most promising resource for new products and applications. In this study, our efforts were focused on identification, isolation, and characterization of psychrophilic microalgae from the underinvestigated extreme environment. Three new isolates were isolated from the frozen Big Almaty Lake, but only for one of them the attempt to clean from bacteria and fungus was successful and it was obtained in algologically and bacteriologically pure form. The taxonomy and phylogeny of the green microalgae, was examined based on morphological (light and scanning electron microscopy) and sequence-based approach using universal molecular markers of ITS region and rbcL gene. Morphological and molecular characterization showed that this green microalgae is *Monoraphidium* sp. (strain ZBD-06). The antibacterial activity of the isolate was determined as well and 60% methanol extract of *Monoraphidium* sp. was used for antibacterial activity by disk diffusion assay and minimum inhibitory concentration using eleven different types of pathogenic bacteria including Gram positive (*Bacillus subtilis* ATCC 6633, *Enterococcus faecalis* ATCC 29212, *Staphylococcus aureus* ATCC 25923, *Staphylococcus epidermidis* ATCC 12228) and Gram negative bacteria (*Escherichia coli* ATCC 25922, *Klebsiella pneumoniae* ATCC 13883, *Pseudomonas aeruginosa* ATCC 27853, *Proteus vulgaris* ATCC 13315, *Salmonella typhimurium* ATCC 14028, *Yersinia pseudotuberculosis* ATCC 911, and *Enterobacter cloacae* ATCC 13047). The zone of inhibition (10±2 mm in diameter with 10ul of extract and 20±2 mm in diameter with 30uL) was observed against *Klebsiella pneumoniae* ATCC 13883.

Key words: Almaty region, psychrophilic, microalgae, *Monoraphidium*, phylogenetic analysis, antimicrobial assay.

Introduction

Microalgae is one of the potential biotechnologically valuable groups of photosynthetic microorganisms and represent the most promising resource for new products and applications [1]. Recent decades have witnessed an increased appreciation of the role of microalgal diversity in ecosystem function and their significant value as source for important biological materials such as antibiotics, drugs, enzymes, herbicides, growth promoters and source of energy [2]. For transition toward a modern and sustainable bio-based economy, the researchers are harnessing the maximum potential of microalgae for providing solutions for addressing the diverse global challenges of the twenty-first century. Being instrumental for efficient nutrient recycling for modern agriculture and wastewater treatment systems [3], a viable alternative source of energy to replace the fossil fuels [4-5], valuable additive for food and animal feed products [6], serving as a raw material for amino acids, vitamins and productions of valuable bioactive compounds [7; 8], the unique attributes of microalgae has widened the scope of their utilization in nearly every research field.

Despite the widely acknowledged value of microalgae virtually in all fields of biotechnology, studies about their diversity, various ecological functions and properties from understudied environment are still scarce. Speculation that the number of still

undiscovered microalgal species exceeds such of known species has led researchers globally to search and collect new strains of microalgae, preserve, and explore their biotechnological potentials [9].

Owing to their extraordinary physiological, ecological, molecular and regulatory mechanisms, microalgae can be found in number of environments and are capable of surviving in extreme conditions [10]. Thus, the novel natural products with diverse biological activities, notably antibacterial, are expected to be obtained from microalgae, thriving in extreme conditions. It is important to understand the molecular and regulatory mechanism of such microalgae in order to use their biochemical, ecological, evolutionary and industrial potential. Therefore, over the past few decades, new strains of microalgae thriving in extreme conditions have been extensively studied through various culture-dependent and independent approaches in pursuit of novel biologically active molecules [11; 12].

The precise identification of microalgae is of great practical importance to unlock their possible biochemical potential and aid in understanding the basis of their biological activity. Studies of microalgae diversity have traditionally relied on morphological traits and various valuable and highly descriptive taxonomic identifiers, web-based guides, keys, manuals and manuscripts for microalgae [13-19]. Nevertheless, the misleading similarities of characteristic morphological features within microalgae do not enable a reliable identification of microalgae.

The recent advancement in molecular biology has revolutionized the taxonomic studies and offer a more consistently reliable and accurate method for identification. However, there is also a mounting evidence that sequence similarity-based approach alone is not superior to morphological taxonomy [20]. Therefore, reliable identification to species level can only be achieved using hybrid approaches, traditional taxonomic methods complemented with molecular diagnostic markers.

In the present study, investigations were focused on finding new strain of microalgae from extreme cold environment, able to demonstrate antimicrobial activity. Here we describe the discovery of a novel strain of *Monoraphidium* sp. The present study aims to report the morphological and molecular characterization of a psychrophilic green microalgae collected from glacial freshwater site, Big Almaty Lake in Almaty region of Kazakhstan, and examine the antibacterial activity of methanol extract of the isolate by performing disk diffusion and minimum inhibitory concentration (MIC) assays.

Materials and methods

Isolation and growth conditions. The microalgae was isolated from Big Almaty Lake by separating single microalgal cells from the mixed microbial suspension using capillary pipettes (repeated until single cell isolation) and cultivated in culture dishes containing BG-11 growth medium [21], with following composition (gL⁻¹): NaNO□, 1.5; K□HPO□, 0.04; MgSO□·7H$_2$O, 0.076; CaCl□·2H□O, 0.036; citric acid, 0.006; EDTA, 0.001; Na□CO□, 0.02; FeSO□, 0.006; trace elements solution: H□BO□, 2.86; MnCl□·4H□O 1.81; ZnSO□·7H□O, 0.222; CuSO$_4$·5H□O, 0.08; MoO□, 0.015; NaBO□.4H□O, 2.63; (NH□)□Mo□O□□·4H□O, 1; FeSO□.7H□O, 2.3; CaCl□·2H□O, 1.2; Co(NO□)□·2H□O, 0.02; EDTA, 10; and distilled water, 1.0 L.

To enumerate the growth of microalgae after successful direct isolation procedure and observable growth, the microalgae culture was transferred to separate 250-mL flask containing 100 mL of liquid BG-11 medium. The enrichment culture was kept at 22°C ±2 for about 20 days under fluorescent light with a photoperiod of 12 h, with shaker speed 100±10 rpm.

Later the microalgae were plated onto BG-11 agar medium (supplemented with antibiotics), which was placed at 22°C ±2 until single colonies of same size and similar appearance emerged. The isolate was further purified by selecting a single colony and re-streaked, followed by microscopic examination, and individual pure colony was placed in autoclaved liquid medium to obtain axenic monoculture.

Identification of microalgal species. Light microscopic examination. The preliminary morphological identification was done under a light microscope, with a system of image capturing (MicroOptix OPTIX C600, Austria). Morphological identification was carried out based on some prominent morphological features for differentiation such as cell size (length to width ratio) and shape, solitary or colonial, presence or absence of mucilage etc., mentioned in the guidelines of description keys, taxonomic literature, manuals, manuscript and photo gallery available for microalgae species identification [15; 19; 21-24].

Sample preparation for scanning electron microscopy. After determination of the genera according to the microscopic features, the SEM technique was carried out at Electron Microscope Laboratory, Gazi University, Ankara, Turkey. The cells were washed with phosphate buffered saline (PBS) to remove culture medium and then they were collected by centrifugation at 1000xg for 5 min. After that, cells were fixed with 5% glutaraldehyde, dehydrat-

ed in ascending order of 20, 40, 60, 80 and 100% ethanol. After critical point drying with CO□ (Polaron CPD 7501), samples were coated with gold in a Polaron SC 502 sputer coater. The coated specimen was observed with JEOL JSM 6060 LV at accelerating voltage 10kV and SEM images were digitally produced.

Molecular identification of algal species. For molecular identification, the microalgal cell pellet (approximately 30mg) was obtained from culture medium by centrifugation at 6,000 rpm for 10 min and genomic DNA of strain was extracted using Quick-DNA™ Fungal/Bacterial Miniprep Kit (Zymo Research, D6005), according to the manufacturer instructions. The quality and quantity of DNA samples were measured with the Spectropho-

tometer Thermo Scientific™ NanoDrop 2000. DNA extracts were stored at -20 °C. The ribosomal ITS region and rbcL gene sequences were amplified using the universal primer pair, listed in Table 1, chosen from published studies with microalgae from class Chlorophyceae.

The 50 µL PCR reaction mixture was composed of 27.75 µL of dH_2O, 10 µL of GoTaq 5X PCR buffer, 6 µL $MgCl_2$ 25 mM, 1 µL dNTPs 10 mM, 0.25 µL of GoTaq DNA polymerase (5 U/µL) (Promega, USA), 1 µL of each primer (10 µM) and 3.0 µl of DNA template (30-50 ng/µL). The PCR amplification protocol used for both markers was: 95 °C for 2 min, 35 cycles of 95 °C for 50 sec, primer-annealing temperature 49 °C for 30 sec and 72°C for 1 min, with a final extension at 72 °C for 10 min.

Table 1 – List of Primer Sequences used for amplification of rbcL and ribosomal ITS region of Isolate

Primer	Sequence (5′-3′)	Type	Source
ITS1	TCCGTAGGTGAACCTGCGG	Forward	[25]
ITS4	TCCTCCGCTTATTGATATGC	Reverse	
ITS1	AGGAGAAGTCGTAACAAGGT	Forward	[25]
ITS4	TCCTCCGCTTATTGATATGC	Reverse	
ITS5	GGAAGTAAAAGTCGTAACAAG	Forward	[25]
ITS4	TCCTCCGCTTATTGATATGC	Reverse	
rbcL	GCTGGWGTAAAAGATTAYCG	Forward	[26]
	TCACGCCAACGCATRAASGG	Reverse	

Each PCR product of about 600 bp was cloned using a pUCm-T cloning vector (Bio Labs) and cDNA of strain was sequenced in both directions by Sanger sequencing (Macrogen Europe, Amsterdam, Netherland). The resulting ITS1/ITS4, ITS5/ITS4 and rbcL forward and reverse DNA sequences of ZBD-06 18S were aligned using sequence alignment editor Bioedit version 6.0 and search for similar sequences was carried out with the Basic Local Alignment Search Tool in the GenBank database of the National Center for Biotechnology Information (NCBI). Fifteen sequences having the highest similarity to each query sequence were obtained and used for phylogenetic analyses with *Isochrysis galbana* strain (JX393298) as an outgroup (accession numbers of these sequences are indicated before the name of each strain on Figure 4). Multiple sequence alignment was carried out using the MUSCLE program with default parameters integrated in Molecular Genetics Analysis (MEGA) 6.06. The Phylogenetic tree was built by the

Neighbor-Joining method (Kimura-2-Parameter algorithm) using bootstrap value (n = 1000 replicates) to determine the statistical reliability of the obtained topologies.

The resulting sequences were deposited in the GenBank database for accession number. A living axenic culture of ZBD-06 was deposited in the Collection for Microalgae Cultures at the Biotechnology Lab, Al-Farabi Kazakh National University.

Antibacterial assay. Preparation of crude extract. The microalgae crude extract was obtained according to the method reported in previous study [27]. The cell density was counted with hemocytometer for quantifying the biomass and microalgal cells was harvested from 5 mL axenic monoculture by spun at 3500 rpm for 30 min. Subsequently, the pellet was washed with phosphate-buffered saline (PBS). In the next step, the solution was sonicated (twenty cycles of 30 s each) with a Soniprep Ultrasonicator (Sartorius Labsonic), and re-centrifuged at 3500 rpm for 30

min to remove cell debris. Afterwards, 60% methanol was added to the pellet in 1:5 w/w ratio of the initial biomass concentration. The resulting sample was re-centrifuged at 3500 rpm for 20 min. The obtained supernatant was utilized to assess the antimicrobial activity, and cell suspension density (number of algal cells in one mL) at the start of the extraction process.

Evaluation of antimicrobial activity. Antibacterial activity of microalgae crude extract against eleven bacterial strains, namely, Gram-positive (*Bacillus subtilis* ATCC 6633, *Enterococcus faecalis* ATCC 29212, *Staphylococcus aureus* ATCC 25923, *Staphylococcus epidermidis* ATCC 12228) and Gram-negative (*Escherichia coli* ATCC 25922, *Klebsiella pneumoniae* ATCC 13883, *Pseudomonas aeruginosa* ATCC 27853, *Proteus vulgaris* ATCC 13315, *Salmonella typhimurium* ATCC 14028, *Yersinia pseudotuberculosis* ATCC 911, and *Enterobacter cloacae* ATCC 13047) were examined by disk diffusion assay. Pure colonies of test bacteria were obtained from the Microbiology Laboratory, Karadeniz Technical University. Turkey. The Mueller-Hinton agar (pH 7.2-7.4) plates were inoculated with broth cultures diluted to 0.5 turbidity (~$1.5 \times 10\square$ cells·mL^{-1}). Discs containing 10 µL of methanol extract of the isolate were placed on filter paper disc on the surface of an agar plate, pre-inoculated with bacterial suspension to be tested. Paper discs with only methanol and antibiotic (rifampicin) were used as negative controls. Finally, the plates were incubated at 37 °C for 16-24 h. The inhibition zones were measured in mm. All experiments were carried out three times with similar results.

Determination of minimum inhibitory concentration (MIC). The crude extract were then added in serial dilution to Mueller-Hinton Broth culture in test tubes and bacterial strains were inoculated at the same concentration used for disk diffusion method. The tubes were incubated at 37°C for 24-48 h and then examined for bacterial growth. The MIC values were obtained from the lowest concentration of the extract where the tubes remained clear, indicating that the bacterial growth was completely inhibited at this concentration.

Results and discussion

Isolation of new strain of microalgae. Microalgal strain ZBD-06 was isolated from water samples collected from Big Almaty Lake (43°0506′ N 76°9850′ E), a natural alpine reservoir, located in the Trans-Ili Alatau mountains, on south of Almaty, a city in the southeastern region of Kazakhstan. The glacial water reservoir lake, extended approximately 1.6 km in length and 1 km in width, is used for drinking water needs of the Almaty city.

Figure 1 – Map and location of sampling site of the isolate – Big Almaty Lake

Six algological samples were taken from this lake, the water temperature at the time of sampling was + 2 °C, pH 7.3. Water samples were taken from the coast of lake directly from the surface and from the water column (depth – 20 cm).

As a result, 4 accumulative cultures were obtained from the selected samples, of which 2 microalgae cultures were isolated by successive reseeding. Various concentrations of mixture antibiotics from wide-spectrum antibiotics against Gram-positive and Gram-negative bacteria and antifungal antibiotics was used to clean the isolated cultures from bacteria, because the concomitant microflora reacted differently to different antibiotics. Thus by treatment with a mixture of antibiotics, only 1 strain of microalgae was obtained in a bacteriologically pure form.

Morphological characterization. The light microscopy and scanning electron microscopy visualization of single cell of microalgal strain ZBD-06 revealed the cell size (Figure 2) varying from 4-6 µm in length and 0.78-1.23 µm in diameter. Solitary cells were predominantly observed having croissant shape to crescent shape with varying degree of curvature,

rounded ends, occasionally appearing colonial in irregular arrangement. Solitary cells exhibited mucilage and wrinkled cell surface but no mucilaginous colonies were observed. Chloroplast occupied the majority of the cell volume. Such cell morphology shows that the ZBD-06 resembles the characterization of genus *Monoraphidium* and *Ankistrodesmus*.

However, the strain was preliminarily identified as member of the genus *Monoraphidium*, for demonstrating cells dimensions and shape variations similar to *Monoraphidium subclavatum* as described in previous studies [15; 21; 28]. Both genus, classified under the family Selenastraceae, are similar in morphology, however the *Ankistrodesmus* differs by having larger cell dimensions, more or less straight cells, joined by mucilage to form colonies of various shapes, while cells of *Monoraphidium* are distinguished from other genera in the family being strongly curved and lacking mucilage [23]. By assessment of all the morphological characteristic of the isolated microalgae, as illustrated in the microphotograph of the specimen under 40x magnifications (Figure 2) the suspected species was *Monoraphidium subclavatum*.
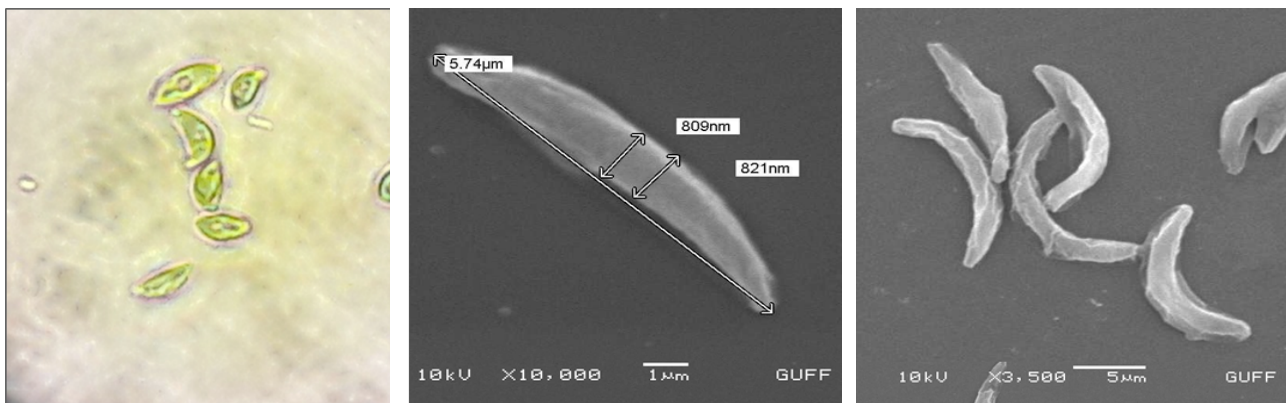
Figure 2 – The Light and Scanning Electron Microscope images of ZBD-06

Nevertheless, the morphological characteristics of the strain investigated in this study doesn't completely fit with the typical description of Monoraphidium at species level and, therefore, species-level identification could not be achieved based merely on morphological and ultrastructural characters. The identification results from the cell morphology were then verified by molecular identification through sequencing of the rbcL genes, ITS1-5.8S-ITS2 and 18S rDNA targeted region and alignment with sequences from the Genbank (NCBI).

Molecular identification and phylogenetic analysis. To perform the molecular identification of the

isolate, the desired DNA fragments (~600 – bp) of isolate, amplified with universal primers of rbcL gene and ITS region were compared with the similar sequences in the database using BLAST online (http://www.NCBI.nim.nih.gov/). The similarity searches of the obtained amplicon sequences in the GenBank database were observed for the universal primer sets of ITS1/ITS4 and ITS5/ITS4, whereas the amplicon sequences generated from rbcL could not retrieved any blast match.

The blast result of only first set of primer ITS1/ITS4 was supportive and useful in species discrimination, while second set of primer ITS1/ITS4 and ITS5/

ITS4 resulted in database mismatches with macro algae, uncultured microorganism and microalgae completely conflicting with morphological description. As the results with the second set of primers were not satisfactory to infer generic identity, therefore, the phylogenetic analysis was performed only with the first set of ITS/ITS4 primer. This reduced success in retrieving accurate sequence matches can be attributed to the fact that the number of well-described microalgae species are still not significantly represented in Genbank. The limitations in molecular identification of some microalgae at the species-level implied that further work is required to establish efficient DNA barcode markers for revealing sufficient heterogeneity for species identification, maximizing the gene database, as well as employing combination of molecular and morphological methods for accu-

rate identification of species with extreme morphological plasticity.

The fifteen sequence entries with highest similarity to the obtained sequence of isolate ITS region were observed and multiple alignment of the sequences were generated with the MUSCLE program. The phylogenetic tree was constructed with MEGA software version 6 [29] based on the evolutionary distances that were calculated by the Neighbor-Joining method [30] using Kimura-2-Parameter algorithm. Statistical evaluation of the tree topologies was performed by bootstrap analysis with 1000 re-samplings [31]. *Isochrysis galbana* strain (JX393298) was used as an outgroup. Figure 4 represents the Neighbour-Joining showing phylogenetic position of strain and related taxa based on ITS1-5.8S-ITS2 region sequence comparisons.
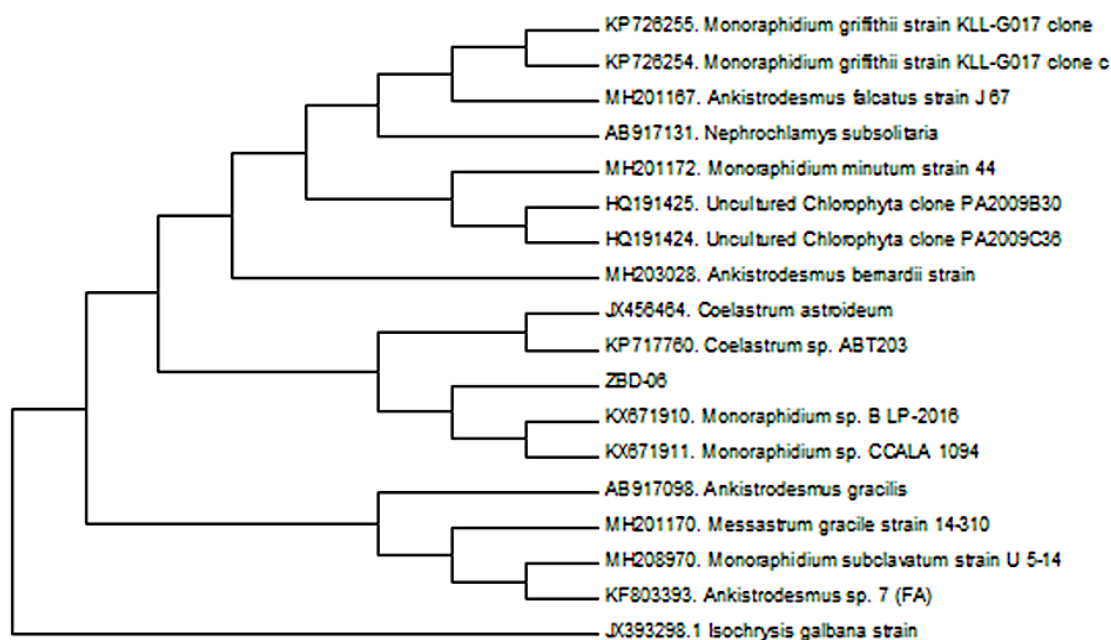
Figure 3 – Phylogenetic tree of the isolated microalgae and
the closely related strains based on ITS1-5.8S-ITS2 region sequence comparisons

Phylogenetic tree consisted of basically three major clusters and one outgroup, each of which mostly contained different species of genus *Monoraphidium* and *Ankistrodesmus*. The phylogram shows that the ZBD-06 strain is closely related to *Monoraphidium sp.* B LP-2016 (score = 911; ident. = 93.33%), *Monoraphidium sp.* CCALA 1094 (score = 900, ident. = 93.28%) isolated from ice-covered lakes on James Ross Island (northeastern Antarctic Peninsula) [32].

The clustering of *Monoraohidium* sp. from Almaty region with *Monoaphidium* sp. from Antarctic region determines the presence of closely related extermophilic species of microalgae in geographically far distinct location (continental level). The phylogram also depicts the relatedness of the newly isolated native strain to *Coelastrum astroideum* (JX456464), however, both strains are morphologically different [33]. Other closely related species were from the genus of *Ankistrodesmus* and *Monoraphidium*

representing a polyphyletic group [34]. The overall morphological features and sequence-based phylogenetic analysis of ZBD-06 with one of the primers of ITS1 region presented a good correlation and served as important molecular target for identification and taxonomical position of the isolate to great extent based on the availability of sequence database. The obtained molecular result suggests the consideration of ZBD-06 strain as *Monoraphidium* sp. that was also based on light and SEM microscopic observation and the genus belongs to the family *Selenastracaceae* (*Cholorophyceae*). The ITS sequence of the isolate was submitted with accession number of MT178772 in NCBI database, respectively. The relative phylogenetic position based on the ITS1/ITS4 primer sequence might not determine species-level resolution for this species, but when matched with the results of morphological studies, it provided more reliable identification of the isolate.

Antibacterial assay. In this study, the 60% methanol extract of ZBD-06 was tested for antimicrobial activity against eleven bacterial strains, including Gram-positive (*Bacillus subtilis* ATCC 6633, *Enterococcus faecalis* ATCC 29212, *Staphylococcus aureus* ATCC 25923, *Staphylococcus epidermidis* ATCC 12228) and Gram-negative (*Escherichia coli*

ATCC 25922, *Enterobacter cloacae* ATCC 13047, *Klebsiella pneumoniae* ATCC 13883, *Pseudomonas aeruginosa* ATCC 27853, *Proteus vulgaris* ATCC 13315, *Salmonella typhimurium* ATCC 14028, and *Yersinia pseudotuberculosis* ATCC 911). The bacterial cultures in petri plates were incubated along with filter paper discs containing 10 and 30 μL of methanol extract of specimen (initial cell number $5.0 \times 10\square$ cells/mL before extraction), for 16-24 h to determine the growth inhibitory effect in the form of inhibition zone.

The most susceptible microbes to specimen methanol extract were Gram-positive bacteria than Gram-negative bacteria. However, surprisingly the methanol extracts of *Monoraphidium* sp. ZBD-06 exhibited the notable antibacterial activity against *Klebsiella pneumoniae* ATCC 13883. The strain showed a positive response in an inhibition zone assay (10±2 mm with 10μl and 20±2 mm in diameter with 30μL) against Gram-negative bacteria *Klebsiella pneumoniae* ATCC 13883 (Figure 4, a and b). In order to confirm the antimicrobial action of strain, the Minimum Inhibitory Concentration (MIC) of the methanol extract was performed against the same bacterial isolate. The MIC value of the extract of ZBD-06 was observed at the first well (2-1).

(10 μL)   (30 μL)
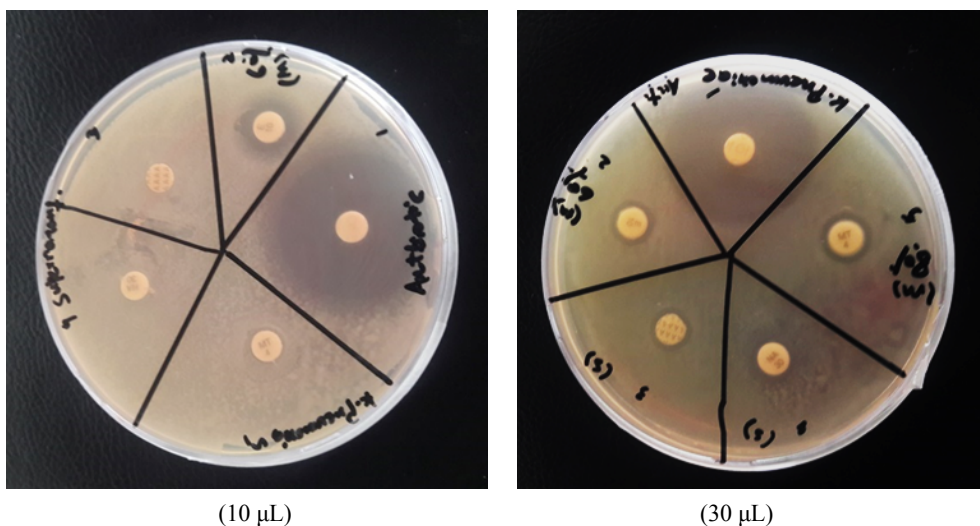
Figure 4 – The disk diffusion assay indicating antibacterial activity of methanol extract of *Monoraphidium* sp. ZBD-06

The results showed the potential presence of certain metabolites like phenols, flavonoids, terpenes or carbohydrates, which are responsible for antibacterial activity of the extract against Gram-negative bacteria. Earlier, the presence of phenols, tannins,

and anthraquinones was determined in the methanol crude extract of *Monoraphidium contortum* [35].One previous study on assessment of antimicrobial potential of marine green microalgae *Desmococcus* (*D.*) *olivaceus* and *Chlorella* (*C.*) *vulgaris*, revealed that

the solvent choice influence the physical and chemical properties of the extract, such as high phenol content was only found in methanol extract, and amount of falvonoids, terpenes, carbohydrates and alkaloids differed when extracted with different solvents such as ethanol, methanol and chloroform and diethyl ether extract [36].

The multilayered and complex cell envelope of the Gram-negative bacteria is one of the major obstacles, which restrict the entrance of antibacterial agents [37]. However, certain biomolecules can damage the bacterial membrane component, such as terpenoid and phenolic compounds [38]. Antibacterial action of *Monoraphidium* sp. ZBD-06 against *Klebsiella pneumoniae* is possibly related with presence of high content of key molecule, which was specific in action for growth inhibition of the bacterium. Taking into account the isolation of the strain from the freezing lake and continued growth at 24 °C retaining optimal functionality of their macromolecules suggests that adaptation to extreme environment (low temperature) in this strain confers a particular ability to produce unique antifreeze proteins, intracellular molecule or membrane structure to protect the cell from freezing damage, and bioactive compounds of potential antibacterial activity [39; 40]. Another possible explanation of the antimicrobial activity of the studied microalgal extract can be attributed to its potential contents of fatty acids, as the psychrophilic microalgae maintain their membrane fluidity at low temperature by incorporating a higher level of polyunsaturated fatty acids (PUFAs) in membrane lipids [41], thereby making them a potential source of polyunsaturated fatty acids for antibacterial product.

The obtained result invokes the necessity of further exploring this great potential and specific action of the *Monoraphidium* sp. strain ZBD-06 by screening biotechnologically appealing bioactive molecules, investigating its source in the cell (chloroplast, cytoplasm, mitochondria, etc.) and deciphering the main biosynthetic pathways of the bioactive molecules. Because antimicrobial activity against *Klebsiella pneumoniae* have, to our knowledge, not previously been reported for Monoraphidium genus, the identification of novel bioactive metabolites may be possible in this strain, which probably either independently or synergistically act together against the bacterium.

Conclusion

A new strain of green microalgae was isolated from the Big Almaty Lake. This strain was identified using scanning electron microscopy and molecular identification as *Monoraphidium* sp. ZBD-06. According to morphology, these are single cells having the shape of a croissant or the shape of a crescent with varying degrees of curvature, rounded ends. Cells of algae with mucus and a wrinkled cell surface, with chloroplast, which occupies most of the cell volume.

The molecular analysis of this study highlighted the on-going challenge in identification of microalgae strains due to lack of availability of taxonomically curated DNA databases. For improving success in accurate specific or infra-specific identification of microalgae strain, more systematic studies using combined approach of morpho-taxonomy and metabarcoding using different molecular markers and deposition of more taxonomically accurate reference barcodes in curated databases are needed.

A study of the antibacterial activity of this microalgae culture showed that the extract of a new strain of psychrophilic microalgae *Monoraphidium* sp. ZBD-06 can yield pharmaceutically promising bioactive substances provided with antibacterial activity useful against Gram-negative bacteria *Klebsiella pneumonia*. However, further studies are needed to better evaluate the presence of antibacterial compounds in the isolated microalgae, and potential effectiveness of the crude extract as the antibacterial agent. It is also expected that additional screening of this under-explored strain may reveal a novel antimicrobial substance that have not yet described and identify yet more useful characteristics for biotechnology.

References

1   Raja R., Hemaiswarya S., Kumar N.A., Sridhar S., Rengasamy R. (2008) A perspective on the biotechnological potential of microalgae. Crit Rev Microbiol., vol. 34, no. 3, pp. 77-88. https://doi.org/10.1080/10408410802086783.

2   Liu J., Sun Z., Gerken H. (2014) Recent advances in microalgal biotechnology. Potential applications of microalgae in wastewater treatments.

Published by OMICS Group eBooks, USA, ISBN: 978-1-63278-066-9.

3   Brennan L., Owende P. (2010) Biofuels from microalgae–a review of technologies for production, processing, and extractions of biofuels and co-products. Renew Sustain Energy Rev., vol. 14, no. 2, pp. 557–577. doi:10.1016/j.rser.2009.10.009.

4   Markou G., Nerantzis E. (2013) Microalgae for high-value compounds and biofuels production: a review with focus on cultivation under stress conditions. Biotechnol. Adv., vol. 31, no. 8, pp. 1532–1542. https://doi.org/10.1016/j.biotechadv.2013.07.011.

5   Priyadarshani I., Rath B. (2012) Commercial and industrial applications of micro algae–A review. Journal of Algal Biomass Utilization, vol. 3, no. 4, pp. 89-100.

6   Larkum A.W., Ross I.L., Kruse O., Hankamer B. (2012) Selection, breeding and engineering of microalgae for bioenergy and biofuel production. Trends in biotechnology, vol. 30, no. 4, pp. 198-205. https://doi.org/10.1016/j.tibtech.2011.11.003.

7   Muñoz-Ochoa M., Murillo-Álvarez J.I., Zermeño-Cervantes L. A., Martínez-Díaz S., Rodríguez-Riosmena R. (2010) Screening of extracts of algae from Baja California Sur, Mexico as reversers of the antibiotic resistance of some pathogenic bacteria. Eur. Rev. Med. Pharmacol. Sci, vol. 14, no. 9, pp. 739-747.

8   Pane G., Cacciola G., Giacco E., Mariottini G. L., Coppo E. (2015) Assessment of the antimicrobial activity of algae extracts on bacteria responsible of external otitis. Marine drugs, vol. 13, no. 10, pp. 6440-6452. https://doi.org/10.3390/md13106440.

9   Guiry, M.D. (2012) How many species of algae are there?. Journal of phycology, vol. 48, no. 5, pp. 1057-1063. https://doi.org/10.1111/j.1529-8817.2012.01222.

10   Pradhan J., Das S., Das B. K. (2014) Antibacterial activity of freshwater microalgae: A review. African Journal of Pharmacy and. Pharmacology, vol. 8, no. 32, pp. 809-818. https://doi.org/10.5897/AJPP2013.0002.

11   Sydney E.B., Schafranski K., Barreti B.R.V., Sydney A.C.N., Zimmerman J.F.D.A., Cerri M.L., Demiate I.M. (2019) Biomolecules from extremophile microalgae: from genetics to bioprocessing of a new candidate for large-scale production. Process Biochemistry, vol. 87, pp. 37–44. https://doi.org/10.1016/j.procbio.2019.09.012

12   Heidari F., Shariatmadari Z., Riahi H., (2019) Screening of Extremophile Microalgae Isolated from High Background Radiation Areas as Source of Bioactive Materials, Current Bioactive Compounds, vol. 15, pp. 1-8. https://doi.org/10.2174/1573407215666118121910451 81219104518.

13   Canter-Lund H., Lund J.W.G. (1995) Freshwater algae: Their microscopic world explored. Biopress Ltd., Bristol. 360 p. ISBN 0-948737-25-5.

14   Dillard, G.E. 1999) Common Freshwater Algae of the United States. An Illustrated Key to the Genera (Excluding the Diatoms). J. Cramer in der Gebr. Bomtraeger Verlagsbuchhandlung, Berlin-Stuttgart., pp.173, 298 Figs. DM 58. ISBN 3-443-50026-9.

15   Edward G.B., David C.S. (2010) Freshwater algae identification and use as bioindicators. A John Wiley & Sons, Ltd, 101. ISBN-13: 978-0470058145.

16   Huynh, M., Serediak, N. (2006) Algae identification field guide agriculture and agric food canada. Agri-Environment Services Branch, Majesty the Queen in Right of Canada, pp. 40. ISBN 9781100183077-1100183078

17   John D.M., Whitton B.A., Brook A.J. (2002) Freshwater algal flora of the British Isles: An identification guide to freshwater and terrestrial algae. Cambridge University Press. 702 p. ISBN 0□521□77051□3.

18   Shayler H.A. and Siver P.A. (2006) Key to Freshwater Algae: A web-based tool to enhance understanding of microscopic biodiversity. Journal of Science Education and Technology vol. 15, no. 3, pp. 298-303. https://doi.org/10.1007/s10956-006-9016-4.

19   Whitford L.A., Schumacher G.J. (1973) A manual of freshwater algae (p. 324). Raleigh: Sparks.

20   Stoykova P., Stoyneva-Gärtner M., Uzunov B., Gärtner G., Atanassov I., Draganova P., Borisova, C. (2019) Morphological characterization and phylogenetic analysis of aeroterrestrial Vischeria/Eustigmatos strains with industrial potential. Biotechnology & Biotechnological Equipment, vol. 33, no. 1, pp. 231-242. https://doi.org/10.1080/13102818.2018.1561212.

21   Hindák, F. (1970) A contribution to the systematics of the family Ankistrodesmaceae (Chlorophyceae). Archiv für Hydrobiologie Supplement – Algological Studies 1, pp. 7-32.

22   Komárková – Legnerová J., (1969) The systematics and ontogenesis of the genera Ankistrodesmus Corda and Monoraphidium gen. nov. In: Studies in Phycology (Fott B, ed). E Schweizerbart'sche Verlagsbuchhandlung (Nägele u. Obermiller) Stuttgart. pp. 75 – 144.

23   Ramos G.J.P., Bicudo C.E.D.M., Góes-Neto A. Moura C.W.D.N. (2012) Monoraphidium and Ankistrodesmus (Chlorophyceae, Chlorophyta) from

Pantanal dos Marimbus, Chapada Diamantina, Bahia State, Brazil. Hoehnea, vol. 39, no. 3, pp, 421-434. https://doi.org/10.1590/S2236-89062012000300006.

24 Ramos G.J.P., Bicudo C.E.D.M., Góes-Neto A. Moura C.W.D.N. (2014) New additions of coccoid green algae to the phycoflora of Brazil and the Neotropics. Acta Botanica Brasilica, vol. 28, no. 1, pp. 8-16. https://doi.org/10.1590/S0102-33062014000100002.

25 White T. J., Bruns T., Lee S.J.W.T., Taylor J. (1990) Amplification and direct sequencing of fungal ribosomal RNA genes for phylogenetics. PCR protocols: a guide to methods and applications, vol. 18, no. 1, pp. 315-322. https://doi.org/10.1016/b978-0-12-372180-8.50042-1.

26 Saunders G.W., Kucera H. (2010) An evaluation of rbcL, tufA, UPA, LSU and ITS as DNA barcode markers for the marine macroalgae. Cryptogam, Algol, vol. 31, no. 4, pp. 487–528.

27 Pane G., Cacciola G., Giacco E., Mariottini G.L., Coppo E. (2015) Assessment of the antimicrobial activity of algae extracts on bacteria responsible of external otitis. Marine drugs, vol. 13, no. 10, pp.6440-6452. https://doi.org/10.3390/md13106440.

28 Nygaard G. (1977) New or interesting plankton algae with a contribution on their ecology. Det Kongelige Danske Videnskabernes Selskab, Biologiske Skrifter, vol. 21, no. 1, pp. 1-107.

29 Tamura K., Stecher G., Peterson D., Filipski A., & Kumar S. (2013) MEGA6: molecular evolutionary genetics analysis version 6.0. Molecular biology and evolution, vol. 30, no. 12, pp. 2725-2729. https://doi.org/10.1093/molbev/mst197.

30 Saitou N, Nei M. (1987) The neighbor-joining method: a new method for reconstructing phylogenetic trees. Mol Biol Evol, vol. 4, no. 4, pp. 406–25. https://doi.org/10.1093/oxfordjournals.molbev.a040454.

31 Felsenstein J. (1985) Confidence limits on phylogenies: an approach using the bootstrap. Evolution, vol. 39, no. 4, pp. 783–91. https://doi.org/10.2307/2408678.

32 Nedbalová L., Mihál M., Kvíderová J., Procházková L., Řezanka T., & Elster J. (2017) Identity, ecology and ecophysiology of planktic green algae dominating in ice-covered lakes on James Ross Island (northeastern Antarctic Peninsula). Extremophiles, vol. 21, no. 1, pp. 187-200. https://doi.org/10.1007/s00792-016-0894-y.

33 Hentschke G.S., Prado J.F. (2012) Chlorococcales sl (Chlorophyceae) e Zygnematales (Zygne-matophyceae) em um açude do Balneário do Lérmen, Rio Grande do Sul, Brasil. Iheringia. Série Botânica., vol. 67, no. 1, pp. 59-74.

34 Krienitz L., Bock C., Dadheech P. K., Pro¨schold T. (2011) Taxonomic reassessment of the genus Mychonastes (Chlorophy-ceae, Chlorophy-ta) including the description of eight newspecies. Phycologia, vol. 50, no. 1, pp. 89–106. https://doi.org/10.2216/10-15.1.

35 Ferreira C.R.S., Gama F.S., Faustino S.M.M., Almeida S.S.M.S. (2017) Study of the Secondary Metabolites, Cytotoxic and Antioxidant Activity of the Methanolic Monoraphidium contortum Crude Extract. Journal of Chemical and Pharmaceutical Research, vol. 9, no. 6, pp. 327-331.

36 Ramar D., Rajendran N., Pichai S. (2016) Phytochemical and antimicrobial activity of green microalgae from Vellar Estuary, southeast coast of India. Journal of Coastal Life Medicine, vol. 4, pp. 374-376. https://doi.org/10.12980/jclm.4.2016J5-167.

37 Bergsson G., Arnfinnsson J., Steingrímsson Ó., & Thormar H. (2001) In vitro killing of Candida albicans by fatty acids and monoglycerides. Antimicrobial agents and chemotherapy, vol. 45, no. 11, pp. 3209-3212. https://doi.org/10.1128/AAC.45.11.3209–3212.2001.

38 Helander I.M., Alakomi H.L., Latva-Kala K., Mattila-Sandholm T., et al. (1998) Characterization of the action of selected essential oil components on Gram-negative bacteria. Journal of agricultural and food chemistry, vol. 46, no. 9, pp. 3590-3595. https://doi.org/10.1021/jf980154.

39 Jung W., Gwak Y., Davies P.L., Kim H.J., Jin E. (2014) Isolation and characterization of antifreeze proteins from the antarctic marine microalga Pyramimonas gelidicola. Mar Biotechnol, vol. 16, no. 5, pp. 502–12. https://doi.org/10.1007/s10126-014-9567-y.

40 Varshney P., Mikulic P., Vonshak A., Beardall, J., Wangikar P.P. (2015) Extremophilic micro-algae and their potential contribution in biotechnology. Bioresource technology, vol. 184, pp. 363-372. https://doi.org/10.1016/j.biortech.2014.11.040.

41 Spijkerman E., and Wacker A. (2011) Interactions between P-limitation and different C conditions on the fatty acid composition of an extremophile microalga. Extremophiles, vol. 15, no. 5, pp. 597–609. https://doi.org/ 10.1007/s00792-011-0390-3.

L. Sutuyeva[1*] iD , T.M. Shalakhmetova[1] iD , V. Trudeau [2] iD

[1] SRI of Biology and Biotechnology Problems. Almaty, Kazakhstan
[2] University of Ottawa, Ottawa, Canada
*e-mail: leila.sutuyeva@kaznu.kz

Histological structure of thyroid gland and level of thyroid hormones in tadpoles exposed to oil and petroleum products

Abstract. Growing global demand and growth in oil production and refining lead to an increase in environmental pollution by waste from these industries. Huge territories of Kazakhstan are influenced by the activities of the oil and oil refining industries. The consequence of this is the deterioration of ecosystems in the oil-producing regions, the decline in biodiversity and deterioration of public health. In this regard, there is a need in an informative bioindicator for studying the state of ecosystems of oil producing regions. The aim of this research was to evaluate the effects of oil and petroleum products exposure on the function of thyroid gland in tadpoles of local amphibian species. The study revealed that chronic exposure to water-soluble fraction of oil, o-xylene or diesel fuel causes hypertrophy and hyperplasia of the thyroid follicular cells, a decrease in the colloid volume in the follicles, as well as a decrease in the content of thyroid hormones in the tadpoles of the marsh frog (*Rana ridibunda*) and green toad (*Bufo viridis*), which indicates a suppression of thyroid function.

Key words: thyroid histostructure, thyroid hormones, water-soluble fraction of oil, petroleum products, amphibians, tadpoles.

Introduction

Deterioration of ecosystems, reduction of biodiversity and deterioration of human health is a well-known problem in the oil producing regions of Kazakhstan [1-2]. Oil spills on the water surface, as well as leak of chemical compounds of oil and petroleum products with the wastewater of enterprises through groundwater are dangerous to the aquatic environment. This poses a great risk to aquatic organisms, causing significant mortality among fish, amphibians and invertebrates [3]. Moreover, not only adults are sensitive to the action of pollutants, but also juveniles, larvae, and embryos, the death of which can lead to a decrease in biological resources. In this regard, it becomes relevant to study the toxic effects of oil and petroleum products on the growth and development of aquatic organisms. In this regard, amphibians are a convenient model system for assessing the state of both terrestrial and aquatic ecosystems under conditions of anthropogenic transformation and environmental pollution [4; 5]. For example, marsh frog (*Rana ridibunda*) and green toad (*Bufo viridis*) can serve as such objects, due to the wide distribution in Kazakhstan, including oil-producing regions [6-9].

It is known that the process of growth and development of vertebrates is controlled by thyroid hormones (TH) secreted by the thyroid gland [10; 11]. TH play a vital regulatory and conservative role in the development of many body systems of amphibians, like in all other vertebrate classes [12-14]. The main toxic components of oil, such as naphthenic acids (NA) and polycyclic aromatic hydrocarbons (PAHs) negatively affect the functioning of the endocrine system in amphibians. NAs can directly reduce the rate of metamorphosis in *X. tropicalis* and *R. pipiens*, and PAHs can significantly reduce the rate of metamorphosis in *X. laevis* [15; 16]. Since the thyroid gland stores produced TH extracellularly (in the follicles), changes in the histological structure of the thyroid gland are widely used to evaluate TH production during development and metamorphosis. Numerous studies of ontogenesis and activity of the thyroid gland in amphibians undergoing the process of metamorphosis confirmed the presence of a correlation between the activity of the thyroid gland and the duration of the larval period [11]. Histopathological changes in the thyroid gland are often the most

sensitive indicator of the adverse effects of chemicals on thyroid function [17]. It is believed that an increase in the follicular space of the thyroid gland, changes in follicular deformation and proliferation of follicular cells are associated with a decrease in the secretion of thyroid hormones [18; 19]. Unfortunately, there is a lack of knowledge on the functioning of the thyroid gland in developing amphibians of natural populations of Kazakhstan under oil pollution conditions. In this regard, the aim of our research was to study the effect of the chronic exposure to water-soluble fraction of crude oil (WSFO) and petroleum products (o-xylene or diesel fuel) on the thyroid gland of *R. ridibunda* and *B. viridis* tadpoles.

Materials and methods

In our previous studies, the analysis of WSFO showed a significant content of o-xylene [20], in connection with which it was decided to study its effect on the functioning of the thyroid gland. Diesel fuel was chosen as a toxicant due to its use as a fuel in water transport. The concentrations were chosen according to the MPC value for petroleum products in water [21].

Preparation of WSFO. 100 ml of oil was mixed with 900 ml of distilled water, then placed in a 1 L flask with a tightly closed stopper and stirred in the dark for 18 hours, avoiding violation of the integrity of the oil film and its emulsification. The resulting mixture was left at room temperature for 6 hours. Next, the water-soluble fraction was extracted using a separatory funnel and stored at 4 °C. Before using in experiments, the water-soluble fraction was warmed to room temperature (21-23 °C) [22; 23].

Obtaining of eggs and experimental design of chronic experiments. Eggs and tadpole care were carried out according to the previously described methodology [20; 24]. Briefly, to obtain eggs, fifteen sexually mature individuals of *R. ridibunda* and *B. viridis* (nine males and six females) were caught from reservoirs of oil-contaminated regions of Kazakhstan, and then delivered to the Ecotoxicology laboratory, Faculty of Biology and Biotechnology, al-Farabi KazNU. After acclimatization of amphibians to laboratory conditions, hormonal stimulation of spawning using hormonal mixture AMPHIPLEX [25] was performed. The larvae that developed to active feeding stage were placed in 18 L aquariums filled with 15 L of pure dechlorinated aerated water (24-26 °C). The tadpoles were divided into 4 groups of 15 tadpoles in each: control, 0.05 mg/L, 0.5 mg/L and 1.5 mg/L of WSFO or petroleum products in triplicate. Every

2 days, 50% of the water was replaced, after which a new dose of WSFO and petroleum products was introduced. At the end of the experiment, tadpoles that reached the stage of metamorphic climax were euthanized in a buffered anesthetic solution (3-aminobenzoic acid ethyl ester (MS-222; Sigma, USA), fixed in 10% formalin for histological examination or frozen in liquid nitrogen, and then stored at -80 °C until further TH analysis.

Histological and morphometric examination of the thyroid gland. After fixation, the material was washed in running tap water for 12 h, then dehydrated in a series of ascending alcohols, purified in xylene and placed in paraffin. Next, sections of 5 μm thickness were made on the MS-2 microtome. Sections were stained with hematoxylin and eosin and covered with Bio-Mount synthetic medium (Bio-Optica, Italy). During dehydration, pouring into paraffin and processing of paraffin sections, isopropyl alcohol was used [26]. Analysis of sections was carried out using a Leica DMLB2 light microscope with a Leica DFC 320 digital camera and microphotography at various magnifications: x200 and x400 were taken. Morphometric analysis of the obtained micrographs was carried out using special BioVision software (version 4.0). In this case, the follicle diameter and the height of the thyroid follicular cells were measured.

Determination of thyroid hormone content in tadpoles. Thyroid hormone extraction was performed based on a method developed by Brasfield et al. [27]. At the end of the chronic experiment, the tadpoles were frozen in liquid nitrogen immediately after euthanasia. Tissue manipulations were performed on ice. A homogenization buffer consisting of 1 mM 6-propyl-2-thiouracil (Sigma Aldrich, USA) in 95% ethanol was prepared before extraction and stored at -20 °C in a glass bottle. The tadpoles were weighed, ground in an equal amount of a homogenizing buffer and transferred to 16 mm x 100 mm glass tubes for cultivation. A second buffer volume equal to the tadpole volume was then added to the obtained homogenate before further homogenization using a Potter homogenizer. Then the samples were shaken for 1 min and kept on ice. Each sample was centrifuged at 2900 rpm at 4 °C for 10 minutes in a centrifuge. Next, the supernatant was transferred into a glass tube. The described procedure was repeated with the obtained precipitate. The resulting supernatant containing ethanol used in the extraction and thyroid hormones was combined with the first supernatant. Then this sample was evaporated in a stream of nitrogen in a water bath at 50 °C, so that the final volume was equal to the initial volume of the tadpole. The

extract was divided into 150 ml aliquots and stored at -80 °C until analysis. Thyroid hormones were quantified in an extract obtained from whole tadpoles using enzyme-linked immunosorbent assay kits (T3-BQ043T for triiodothyronine (T3) and T4-BQ044T for thyroxine (T4), BioQuant Inc., USA).

Statistical analysis. Data were analyzed for statistical significance using a one-way ANOVA followed by a Tukey test using SPSS software version 23 (IBM Inc., Chicago, USA) with α set to 0.05. Before analysis, the data were analyzed for homogeneity of variance using the Levene's test [28].

All work with the animals was carried out in full accordance with the requirements of scientific ethics and international standards, and regulatory legal acts of the Republic of Kazakhstan [29-33].

Results and discussion

Histological structure of the thyroid gland R. ridibunda and B. viridis under chronic exposure to WSFO and petroleum products. A microscopic examination of the thyroid gland of *R. ridibunda* and *B. viridis* tadpoles during chronic exposure to WSFO or petroleum products revealed pathological changes in the histological structure of the organ, such as a decrease in the volume of colloid in the follicles, hyperplasia and hypertrophy of thyrocytes.

The thyroid histostructure of *R. ridibunda* tadpoles in the control group was normal. Follicular cells formed a cuboudal epithelium. The nuclei of follicular cells were compacted and had an oval or round shape. The cytoplasm of these cells was acidophilic, homogeneous. Thyroid follicles contained an eosinophilic homogeneous colloid and were lined with a single layer of cuboidal follicular cells. Single foci of hyperplasia and hypertrophy of follicular cells, which may be present in the normal thyroid gland, were noted.

Changes during chronic exposure to WSFO, o-xylene, and diesel fuel were of a similar nature and were expressed in violation of the structure of the thyroid follicles. Moreover, the severity of pathological changes depended on the concentration of the active substance. Follicular cells under the influence of 0.05 mg/L WSFO, o-xylene or diesel fuel had a structure close to normal, however, cell hyperplasia and a decrease in the amount of colloid in some follicles were observed, which indicates atrophic processes in the thyroid gland.

Chronic exposure to 0.5 mg/L of WSFO or petroleum products caused a structural disorder of about 60% of thyroid tissue. Colloid was observed in only a few follicles and its amount was noticeably less compared to the control. The thyrocytes of most follicles were prismatic and hypertrophied.

With chronic exposure to 1.5 mg/L of WSFO, o-xylene or diesel fuel, more than 80% of the thyroid tissue of the *R. ridibunda* tadpoles underwent pathological changes. Hyperplasia of follicular cells was observed, manifested in the appearance of stratification of the glandular epithelium. Hypertrophied thyrocytes had a prismatic shape; in most follicles, a lack of colloid was noted.

A study of the histological structure of the thyroid gland of *B. viridis* tadpoles during chronic exposure to WSFO or petroleum products revealed similar changes. In the tadpoles of the control group, the structure of the thyroid gland was normal. The severity of pathological changes also had a dose-dependent nature. Under chronic exposure to low doses (0.05 mg/L) of WSFO, o-xylene, or diesel fuel, the histostructure of the thyroid of the *B. viridis* tadpoles slightly differed from the norm. Foci of hyperplasia and a decrease in the size of follicles were observed. Most thyrocytes had a cuboidal shape, but there were follicles lined with prismatic epithelium.

With chronic exposure to 0.5 mg/L of WSFO and petroleum products on the tadpoles of *B. viridis*, atrophy of the thyroid gland was observed. A decrease in the number of follicles containing colloid was observed, while their size was smaller compared to the control, which indicated a decrease in thyroid function. The follicular epithelium became stratified, which indicated hyperplasia of thyrocytes.

During chronic exposure to 1.5 ml/L of oil and petroleum products in most tadpoles exposed to high concentrations of oil and petroleum products, the thyroid gland was hypertrophied. A decrease in the volume of follicles was noted, as well as a thickening of the glandular epithelium due to hyperplasia and hypertrophy of follicular cells. At the same time, in tadpoles, which had the largest developmental delay, an almost complete atrophy of the thyroid gland was noted. In this case, small follicles with a small content or complete absence of a colloid were observed, lined with one or several layers of cuboidal thyrocytes.

To confirm the observed changes in the histostructure of the thyroid gland of *R. ridibunda* and *B. viridis* tadpoles, a morphometric study was carried out, which included measuring the diameter of the follicles and the height of follicular cells.

The results of a morphometric study of the thyroid gland of *R. ridibunda* and *B. viridis* are presented in table 1 and 2.

Table 1 – The follicles diameter and the follicular cells height of the thyroid gland of *R. ridibunda* tadpoles after chronic exposure to WSFO or oil products, μm

Concentration	WSFO	O-xylene	Diesel fuel
	follicles diameter		
Control	53.14±17.21	49.45±12.43	56.33±15.58
0.05 mg/L	51.2±23.11	47.91±16.30	53.27±21.18
0.5 mg/L	39.64±14.70**	38.39±11.46***	43.72±13.66**
1.5 mg/L	24.82±8.36***	28.47±10.52***	28.53±11.23***
	follicular cells height		
Control	6.22±1.10	5.83±1.32	5.92±1.81
0.05 mg/L	5.91±2.04	5.78±1.40	5.96±1.73
0.5 mg/L	3.27±1.41***	3.61±2.52**	3.44±1.30***
1.5 mg/L	2.85±1.10***	3.19±1.60***	3.03±1.51***
Note: *** – P≤0.001, ** – P≤0.01 compared to control			

As can be seen from the tables, the thyroid follicles diameter in the tadpoles of *R. ridibunda* and *B. viridis* exposed to chronic exposure to WSFO or petroleum products was significantly smaller compared to control. At the same time, high concentrations of oil and petroleum products (1.5 mg/L) had the most pronounced inhibitory effect, causing a 1.6-2.1 fold reduction in follicles compared to control values. Similarly, a decrease in the height of follicular cells was observed when exposed to WSFO or petroleum products. Changes in this parameter were more pronounced with increasing concentration of treatment compounds.

Table 2 – The follicles diameter and the follicular cells height of the thyroid gland of *B. viridis* tadpoles after chronic exposure to WSFO or oil products, μm

Concentration	WSFO	O-xylene	Diesel fuel
	follicles diameter		
Control	37.18±11.41	35.92±13.17	40.21±9.61
0.05 mg/L	38.56±13.20	33.56±12.22	39.44±12.10
0.5 mg/L	24.78±13.11**	27.63±9.81***	28.72±8.76**
1.5 mg/L	19.56±9.72***	22.45±10.12***	23.64±8.93***
	follicular cells height		
Control	5.44±1.31	5.56±1.07	5.29±1.26
0.05 mg/L	5.25±1.07	5.67±1.46	5.06±1.47
0.5 mg/L	3.09±1.14***	3.68±1.45**	3.26±1.09***
1.5 mg/L	2.62±1.18***	3.05±1.33***	2.77±1.05***
Note: *** – P≤0.001, ** – P≤0.01 compared to control			

Disruption of thyroid gland function in the tadpoles of *R. ridibunda* and *B.viridis* shown by histological examination was confirmed with morphometrical measurements. The analysis of morphometric data revealed notable reduction of thyroid follicles diameter and decrease of follicular cells height in both studied species. However, there was no significant difference between the species. It is generally accepted that histological examination of the thyroid gland is an important method for determining the ability of a chemical substance to affect the synthesis of thyroid hormones [18], as was shown on *X. laevis*, *X. tropicalis* and *R. rugosa* [34; 35]. Histopathological changes in the thyroid gland can be caused by various

chemicals [36; 37]. Typically, thyroid histopathology is characterized by a decrease in colloid, atrophy, gland hypertrophy, as well as cell hyperplasia and hypertrophy [17; 18]. A histomorphological study of the thyroid of *R. ridibunda* and *B. viridis* tadpoles under chronic exposure to WSFO or petroleum products showed a decrease in follicle size, hyperplasia and hypertrophy of thyrocytes. In tadpoles with the greatest developmental delay, thyroid atrophy was noted. According to foreign researchers, a decrease in the amount of colloid in the follicles indicates a predominance of secretion of thyroid hormones over their accumulation in the follicles of the thyroid gland. Thus, the size of the follicle may correlate with the level of thyroid hormones circulating in the blood [38]. In a study by Wang et al. [39] when studying the effect of copper on the growth and development of *B. gargarizans*, hyperplasia of follicular cells in the thyroid gland was detected. According to diagnostic criteria [18], follicular cell hyperplasia is associated with a decrease in the secretion of thyroid hormones in the thyroid gland. Similarly, in a recent study, exposure to lead also induced follicular cell hyperplasia and depletion of colloids in the thyroid gland. In addition, some follicles were markedly increased in thickness and height of the layer of epithelial cells, which led to an increase in the size of the thyroid gland [40]. It is known that the histological structure of the thyroid gland reflects its functional state, i.e. storage and release of thyroid hormones [41]. Therefore, the changes in the thyroid gland histostructure observed during chronic exposure to hypertension and petroleum products indicate a violation of the thyroid hormone homeostasis in tadpoles and, therefore, their effect on the growth and development of *R. ridibunda* and *B. viridis* tadpoles. This is confirmed by the fact that under the influence of WSFO or petroleum products a developmental delay, weight loss and a decrease in the body size of intoxicated tadpoles were found [20].

The content of hormones T3 and T4. The content of thyroid hormones in *R. ridibunda* tadpoles after chronic exposure to WSFO or petroleum products is shown on Figure 1. As can be seen in the figure, chronic exposure to 0.05 mg/L WSFO reduced the T4 content in tadpole by 1.2-fold. When exposed to 0.5 mg/L, the T4 content in the tadpoles was 1.5-fold lower compared to the control. Exposure to 1.5 mg/L WSFO caused a 1.8-fold decrease in T4 content. When exposed to 0.05 mg/L of o-xylene, the difference in the T4 content in the body of the tadpoles was insignificant. Compared with the control, when exposed to 0.5 and 1.5 mg/L of o-xylene, the T4 content was 1.2 and 1.4-fold lower, respectively. Simi-

larly, a chronic exposure of 0.05; 0.5 and 1.5 mg/L of diesel fuel led to a decrease in the content of T4 in the tadpoles of *R. ridibunda* by 1.2; 1.3 and 1.5-fold, respectively.
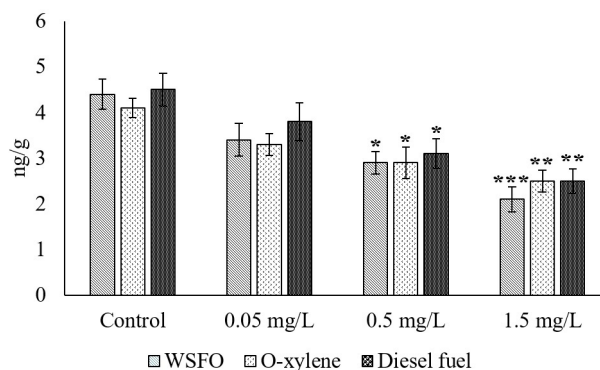
Figure 1 – The content of T4 hormone in *R. ridibunda* tadpoles after chronic exposure to WSFO, o-xylene or diesel fuel.
Note: *** – P≤0.001, ** – P≤0.01,
* – P≤0.05 compared to control

Similar changes in T4 content were observed in *B. viridis* tadpoles (Figure 2). Chronic exposure to 0.05 mg/L of WSFO caused a decrease in T4 content by 1.3-fold, 0.5 mg/L by 1.5-fold, 1.5 mg/L by 2.1-fold. With chronic exposure to 0.05 mg/L of o-xylene, a decrease in T4 content by 1.2-fold was noted. In the tadpoles exposed to 0.5 mg/L o-xylene, the T4 content was 1.4-fold lower than in the tadpoles of the control group. When exposed to 1.5 mg/L of o-xylene, the decrease was 1.6-fold. The impact of diesel fuel also led to a reduced T4 content in the *B. viridis* tadpoles: at 0.05 mg/L – 1.2-fold, at 0.5 mg/l – 1.5-fold, at 1.5 mg/L – 1.8-fold.
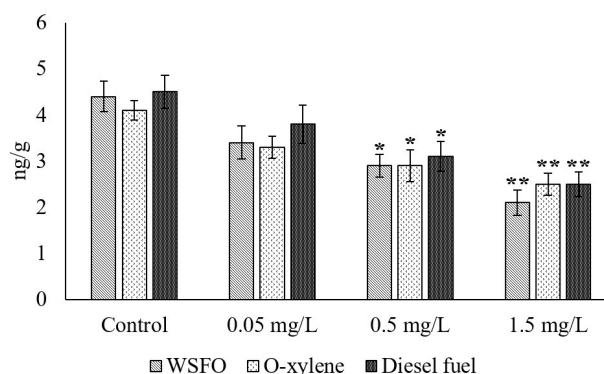
Figure 2 – The content of T4 hormone in *B. viridis* tadpoles after chronic exposure to WSFO, o-xylene or diesel fuel.
Note: *** – P≤0.001, ** – P≤0.01,
* – P≤0.05 compared to control

Analysis of the T3 content in *R. ridibunda* tadpoles showed significant changes (Figure 3). Expo-

sure to WSFO at a concentration of 0.05 mg/L caused a 1.5-fold decrease in T3 content.

Figure 3 – The content of T3 hormone
in *R. ridibunda* tadpoles after chronic exposure
to WSFO, o-xylene or diesel fuel.
Note: *** – P≤0.001, ** – P≤0.01,
* – P≤0.05 compared to control

Higher concentrations reduced the T3 content by 2.2-fold when exposed to 0.5 mg/L and by 3.2-fold when exposed to 1.5 mg/L. With chronic exposure to o-xylene at a concentration of 0.05 mg/L, the T3 content was 1.5-fold lower. Exposure to 0.5 mg/L of o-xylene led to a 1.8-fold decrease in the T3 content. When exposed to 1.5 mg/L of o-xylene, the decrease was 2.7-fold compared with the control. When exposed to diesel fuel at a concentration of 0.05; 0.5 and 1.5 mg/L, a decrease in the content of T3 in *R. ridibunda* tadpoles by 1.3-fold; 2.0-fold and 2.9-fold, respectively, was also observed.

The content of T3 in *B. viridis* tadpoles was reduced by 1.6-fold when exposed to 0.05 mg/L of WSFO (Figure 4). T3 content in 0.5 mg/L WSFO treated tadpoles was 2.5-fold lower than the control. The largest decrease of 3.8-fold was found when exposed to 1.5 mg/L of WSFO. Exposure to o-xylene led to a decrease in the T3 content in *B. viridis* tadpoles at 0.05 mg/L – 1.5-fold, at 0.5 mg/L – 2.4-fold, at 1.5 mg/L – 3.1-fold. Under chronic exposure to 0.05 mg/L diesel fuel, a 1.4-fold decrease in T3 content was observed. Exposure to higher concentrations (0.5 and 1.5 mg/L) caused a decrease in T3 content by 2.4 and 3.4-fold, respectively, compared with the control.

The ratio of the content of T3 to T4 in the body of tadpoles shows the completeness of the conversion of T4 into a more active form of the hormone – in T3. Studies have shown that the lowest ratio of triiodothyronine to thyroxine was in tadpoles exposed to high concentrations of WSFO or petroleum products (Figures 5 and 6).

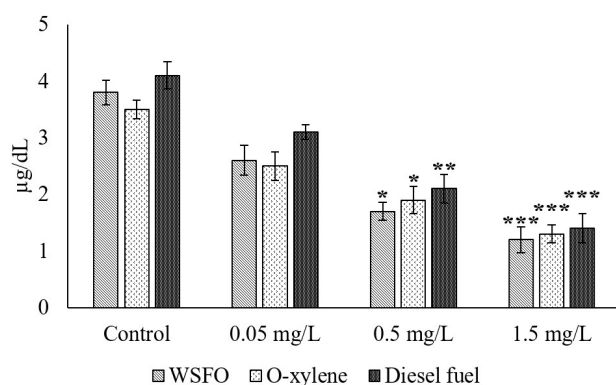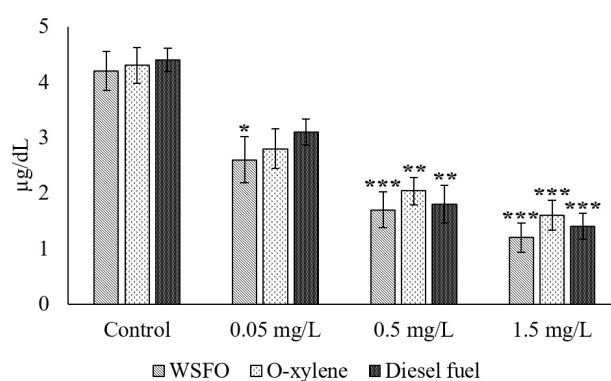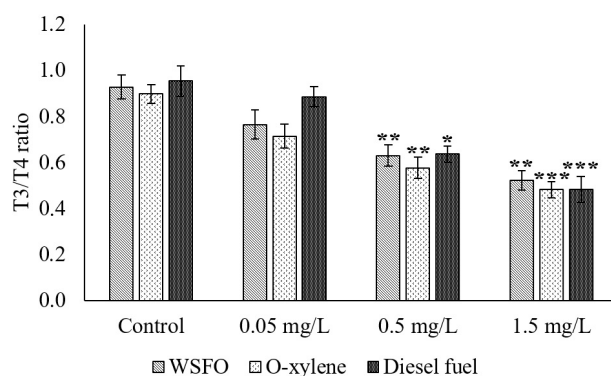**Figure 4** – The content of T3 hormone in *B. viridis* tadpoles
after chronic exposure to WSFO, o-xylene or diesel fuel.
Note: *** – P≤0.001, ** – P≤0.01,
* – P≤0.05 compared to control

Figure 5 – The content of T3 and T4 hormones ratio
in the *R. ridibunda* tadpoles after chronic exposure
to WSFO, o-xylene or diesel fuel.
Note: *** – P≤0.001, ** – P≤0.01,
* – P≤0.05 compared to control
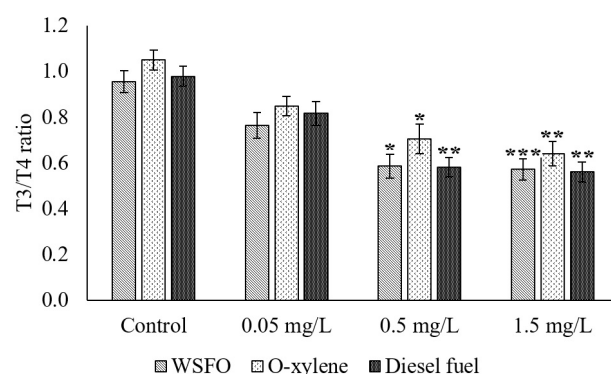
Figure 6 – The content of T3 and T4 hormones ratio
in the *B. viridis* tadpoles after chronic exposure
to WSFO, o-xylene or diesel fuel.
Note: *** – P≤0.001, ** – P≤0.01,
* – P≤0.05 compared to control

A study of the effects of various concentrations of WSFO and petroleum products revealed a significant

decrease in the content of T3 and T4 in *R. ridibunda* and *B. viridis* tadpoles compared to the control. The T3:T4 ratio, which reflects the rate of conversion of T4 to T3 [42], was the lowest among tadpoles exposed to high concentrations of WSFO or petroleum products. A lower T3: T4 ratio in tadpoles from groups exposed to 0.5 and 1.5 mg/L of WSFO or petroleum products may result from changes in the normal physiology of tadpoles by contaminants. Similar to the changes in histostructure of thyroid gland, difference in alteration of T3 and T4 levels between *R. ridibunda* and *B. viridis* tadpoles was insignificant.

Two possible normal physiological phenomena that pollutants might have acted, as Shi [12] suggested, are the incomplete conversion of all T4 to T3, as well as the conversion of T3 to reverse T3 (rT3) by the enzyme deiodinase 3. Both of these processes can lead to decrease in the concentration of T3 in relation to T4. These changes in the functional state of the thyroid gland are probably responsible for the delay in the metamorphosis of the tadpoles. An impaired metabolism of thyroid hormones can have other consequences for frogs, since thyroid hormones are necessary for normal, competent immunological function and growth, along with other metabolic processes. Thyroid hormones have similar functions in a large number of vertebrates, including regulation of growth and development. Thyroid hormones are crucial for amphibian metamorphosis [12] and have complex functions that control multiple events, such as tail resorption and development of the forelimbs. Metamorphosis changes in the absence of normal levels of thyroid hormones, although stopped metamorphosis can be resumed if thyroid hormones are introduced [43]. The endocrine destructive potential of these compounds is apparently quite stable in the environment since the ratio of T3/T4 changed significantly in the tadpoles of *R. sylvatica* exposed to water from ponds of wetlands located near reclaimed oil sands, and also changed the rate of metamorphosis depending on the age of the reclaimed wetlands [44]. Thus, it was shown that the study of histological structure and hormones of thyroid gland in tadpoles of amphibians may serve as an informative indicator of petroleum contamination.

Conclusion

Our results indicate a violation of the thyroid gland of the tadpoles of anuran amphibians in oil pollution conditions. Hypertrophy and hyperplasia of follicular cells, as well as a decrease in the volume of colloid in the follicles, found in the thyroid gland his-

tostructure of the tadpoles of amphibians, representatives of natural populations of Kazakhstan, indicate a violation of its function and TH homeostasis. As a result of the study, it was found that during chronic exposure to the water-soluble fraction of crude oil or petroleum products (o-xylene, diesel fuel), the content of triiodothyronine and thyroxine in the tadpoles of *R. ridibunda* and *B. viridis* decreases, which also indicates a suppression of thyroid function.

References

1   Environment and sustainable development in Kazakhstan. Overview. UNDP Kazakhstan Publication Series No UNDPKAZ 06 (2004) [Okruzhajush-haja sreda i ustojchivoe razvitie v Kazahstane. Obzor. Serija publikacij PROON Kazahstan. No UNDPKAZ 06], Almaty, 210 p.

2   Askarova M.A., and Mussagaliyeva A.N. (2014). The ecological situation in contaminated areas of oil and gas exploration in Atyrau region. Procedia. Social. Behav. Sci., vol. 120, pp. 455–459. https://doi.org/10.1016/j.sbspro.2014.02.124.

3   Wake H. (2005). Oil refineries: a review of their ecological impacts on the aquatic environment. Estuar. Coast. Shelf Sci., vol. 62, pp. 131–140. https://doi.org/10.1016/j.ecss.2004.08.013.

4   ENSR International (2004) Development of a standartized approach for assessing potential risks to amphibians exposed to sediment and hydric soils, ANSI Std., Z39.18.

5   Duellman, W. E., Trueb L. (1994). Biology of amphibians. London: John Hopkins University Press, 325 p. ISBN 978-0801847806.

6   Duysebaeva T.N., Berezovikov N.N., Brushko Z.K., Kubykin R.A., Khromov V.A. (2005). Marsh frog (Rana Ridibunda Pallas, 1771) in Kazakhstan: Range changing and recent distribution [Ozernaja ljagushka (Rana ridibunda Pallas 1771) v Kazahstane: izmenenie areala v HH stoletii i sovremennoe rasprostranenie vida], Contemp. Herpetol, vol. 3, pp. 29–59.

7   Duisebaeva T.N., Chirikova M.A., Winter Yu.A., Belyalov O.V., Kovalenke A.V. (2010) New data on the distribution of amphibians and reptiles in

Kazakhstan: a review of the first decade of the 21st century [Novye dannye po rasprostraneniju amfibij i reptilij v Kazahstane: obzor po pervomu desjatiletiju XXI vek]. Herpetological studies in Kazakhstan and in neighboring countries. Collection of articles dedicated to the memory of Paraskiv K.P., Almaty, pp. 84-99.

8   Duisebaeva T.N. (2012) Overview of the fauna of amphibians and reptiles of the Mangistau region [Obzor fauny amfibij i reptilij Mangistauskoj oblasti], Selevinia. vol. 20, pp. 59-65.

9   Kubykin R.A., Plakhov K.N. (2012) About the fauna of amphibians and reptiles of the Aral-Caspian watershed (based on the materials of expeditions of R. A. Kubykin in 1989-1990) [Kubykin R.A., Plahov K.N. O faune amfibij i reptilij Aralo-Kaspijskogo vodorazdela (po materialam jekspedicij R.A. Kubykina v 1989-1990 gg.)], Selevinia, vol. 20, pp. 66-76.

10   Yen P. (2001) Physiological and molecular basis of thyroid hormone action. Physiol. Rev., vol. 81, no. 3, pp. 1097–1142. https://doi.org/10.1152/physrev.2001.81.3.1097.

11   Brown D, Cai L. (2007). Amphibian metamorphosis. Dev. Biol., vol. 306, no. 1, pp. 20–33. https://doi.org/10.1016/j.ydbio.2007.03.021.

12   Shi Y. (2000). Amphibian Metamorphosis: From Morphology to Molecular Biology, New York: John Wiley & Sons, 288 p. ISBN 978-3540278931.

13   Power D., Llewellyn L., Faustino M., Nowell M., Bjornsson B., Einarsdottir I., Canario A., Sweeney G. (2001). Thyroid hormones in growth and development of fish. Comp. Biochem. Physiol., vol. 130, no. 4, pp. 447–459. https://doi.org/10.1016/s1532-0456(01)00271-x.

14   McNabb F. (1989). Development and aging of the thyroid in homeotherms. In: "Development, maturation and senescence of neuroendocrine systems: a comparative approach, (Schreibman M, Scanes C. eds)". New York: Academic Press, pp. 333–352.

15   Melvin S. D., Trudeau V. L. (2012). Growth, development and incidence of deformities in amphibian larvae exposed as embryos to naphthenic acid concentrations detected in the Canadian oil sands region. Environmental Pollution, vol. 167, pp. 178-183. https://doi.org/10.1016/j.envpol.2012.04.002.

16   Bryer P.J., Elliott J.N., Willingham E.J. (2006). The effects of coal tar based pavement sealer on amphibian development and metamorphosis. Ecotoxicology, vol. 15, pp. 241–247. https://doi.org/10.1007/s10646-005-0055-z.

17   Miyata K., Ose K. (2012). Thyroid hormone-disrupting effects and the amphibian metamorphosis assay. J. Toxicol. Pathol., vol. 25, pp. 1–9. https://doi.org/10.1293/tox.25.1.

18   Grim K.C., Wolfe M., Braunbeck T., Iguchi T., Ohta Y., Tooi O., Touart L., Wolf D.C., Tietge J. (2009). Thyroid histopathology assessments for the amphibian metamorphosis assay to detect thyroid-active substances. Toxicol. Pathol., vol. 37, pp. 415–424. https://doi.org/10.1177/0192623309335063.

19   Tebourbi O., Sakly M., Rhouma K.B. (2010). Subacute toxicity of p, p′-DDT on rat thyroid: hormonal and histopathological changes. Environ. Toxicol. Pharmacol., vol. 29, pp. 271–279. https://doi.org/10.1186/s12958-017-0259-0.

20   Sutuyeva L., Trudeau V., Shalakhmetova T. (2019). Mortality of Embryos, Developmental Disorders and Changes in Biochemical Parameters in Marsh Frog (Rana ridibunda) Tadpoles Exposed to the Water-Soluble Fraction of Kazakhstan Crude Oil and O-Xylene. Journal of Toxicology and Environmental Health, Part A, vol. 82, no. 3, pp. 200-215. https://doi.org/0.1080/15287394.2019.1576562.

21   Gorchev H. G., Ozolins G. (2011). WHO Guidelines for drinking-water quality. WHO Chron., vol. 38, pp. 104–108. https://doi.org/10.1016/S1462-0758(00)00006-6.

22   Anderson J. W., Neff J. M., Cox B. A., Tatem H. B., Hightower G. M. (1974). Characteristics of dispersions and water soluble extracts of crude and refined oils and their toxicity to estuarine crustaceans and fish. Mar. Biol., vol. 27, pp. 75-88.

23   Singer M. M., Aurand D., Bragin G. E., Clark J. R., Coelho G. M., Sowby M. L., Tjeerdema R. S. (2000). Standardization of the preparation and quantitation of water-accommodated fractions of petroleum for toxicity testing. Mar. Pollut. Bull., vol. 40, pp. 1007–1016. https://doi.org/10.1016/S0025-326X(00)00045-X.

24   Sutuyeva L.R., Shalakhmetova T.M. (2019) Morphological Deformities of Green Toad (Bufo viridis) Tadpoles Caused by Petroleum Products. Bulletin of L.N. Gumilyov ENU. Biological Sciences series, vol. 128, no. 3, pp. 100-118. https://doi.org/10.32523/2616-7034-2019-128-3-100-110.

25   Trudeau V. L., Somoza G. M., Natale G. S., Pauli B., Wignall J., Jackman P., Doe K., Schueler F. W. (2010). Hormonal induction of spawning in 4 species of frogs by coinjection with a gonadotropin-releasing hormone agonist and a dopamine antagonist. Reprod. Biol. Endocrinol., vol. 8, pp. 2–10. https://doi.org/10.1186/1477-7827-8-36.

26   Viktorov I.V., Proshin S.S. (2003). The use of isopropyl alcohol in histological methods: dehydration and filling of fabric in paraffin, processing

of paraffin wax [Primenenie izopropilovogo spirta v gistologicheskih metodah: obezvozhivanie i zalivka tkani v parafin, obrabotka parafinovyh srezov], Bulentinum, no. 7, pp. 119–120.

27 Brasfield S.M., Bradham K., Wells J.B., Talent L.G., Lanno R.P., Janz D.M. (2004). Development of a terrestrial vertebrate model for assessing bioavailability of cadmium in the fence lizard (Sceloporus undulatus) and in ovo effects on hatchling size and thyroid function. Chemosphere, vol. 54, pp. 1643-1651. https://doi.org/10.1016/j.chemosphere.2003.09.030.

28 Levene H. (1960). In Contributions to Probability and Statistics: Essays in Honor of Harold Hotelling, I. Olkin et al. eds., Stanford University Press, pp. 278-292.

29 Bayne K, Bayvel D, MacArthur Clark J, Demers G, Joubert C, Kurosawa TM, Rivera E, Souilem O, Turner PV. (2011). Harmonizing veterinary training and qualifications in laboratory animal medicine: a global perspective. ILAR J., vol. 52, pp. 393–403. https://doi.org/10.1093/ilar.52.3.393.

30 Council for International Organizations of Medical Sciences and International Council for Laboratory Animal Science. (2012). International guiding principles for biomedical research involving animals, 4 p.

31 Demers G, Brown M, Gauthier C, Rozmiarek H, Griffin G, Bedard M. (2013). International harmonization of guidance on the ethical review of proposals for the use of animals, and on the education and training of animal users in science. STAL, vol. 38, pp. 73–79.

32 Sanitary and epidemiological requirements for laboratories. (2012) Decree of the Government of the Republic of Kazakhstan No. 13 from January 10, 2012 [Sanitarno-jepidemiologicheskie trebovanija k laboratorijam].

33 Sarymsakova B.E., Rozenson R.I., Battakova J.E. (2007) Guidelines for research ethics: (guidelines) [Rukovodstvo po jetike nauchnyh issledovanij: (metodicheskie rekomendacii)], Astana, 98 p.

34 OECD (2007). Guidance document on amphibian thyroid histology. In: Series for Testing and Assessment, Environmental Health and Safety Publications. OECD, Paris, France.

35 Oka T., Miyahara M., Yamamoto J., Mitsui N., Fujii T., Tooi O., Kashiwagi K., Takase M., Kashiwagi A., Iguchi T. (2009). Application of metamorphosis assay to a native japanese amphibian species, Rana rugosa, for assessing effects of thyroid system affecting chemicals. Ecotoxicol. Environ. Saf., vol. 72, pp. 1400–1405. https://doi.org/10.1016/j.ecoenv.2009.03.012.

36 Helbing C.C., Ovaska K., Ji L. (2006). Evaluation of the effect of acetochlor on thyroid hormone receptor gene expression in the brain and behavior of Rana catesbeiana tadpoles. Aquat Toxicol., vol. 80, pp. 42–51. https://doi.org/10.1016/j.aquatox.2006.07.011.

37 Croteau M.C., Davidson M., Duarte-Guterman P., Wade M., Popesku J.T., Wiens S., Lean D.R., Trudeau V.L. (2009). Assessment of thyroid system disruption in Rana pipiens tadpoles chronically exposed to UVB radiation and 4-tert-octylphenol. Aquat Toxicol., vol. 95, pp. 81–92. https://doi.org/10.1016/j.aquatox.2009.05.013.

38 Chai L., Wang H., Deng H., Zhao H., Wang W. (2014) Chronic exposure effects of copper on growth, metamorphosis and thyroid gland, liver health in Chinese toad, Bufo gargarizans tadpoles. Chemistry and Ecology, vol. 30, no. 7, pp. 589-601, https://doi.org/10.1080/02757540.2014.894985.

39 Wang C., Liang G., Chai L., Wang H. (2016). Effects of copper on growth, metamorphosis and endocrine disruption of Bufo gargarizans larvae. Aquatic Toxicology, vol. 170, pp. 24–30. https://doi.org/10.1016/j.aquatox.2015.10.023.

40 Yang H., Liu R., Liang Z., Zheng R., Yang Y., Chai L., Wang H. (2019). Chronic effects of lead on metamorphosis, development of thyroid gland, and skeletal ossification in Bufo gargarizans. Chemosphere, vol. 236, pp 1242-1251. doi.org/10.1016/j.chemosphere.2019.06.221.

41 Opitz R., Hartmann S., Blank T., Braunbeck T., Lutz I., Kloas W. (2006). Evaluation of histological and molecular endpoints for enhanced detection of thyroid system disruption in Xenopus laevis tadpoles. Toxicol. Sci., vol. 90, pp. 337-348. https://doi.org/10.1093/toxsci/kfj083.

42 Picard-Aitken M., Fournier H., Pariseau R., Marcogliese D.J., Cyr D.G. (2007). Thyroid disruption in walleye (Sander vitreus) exposed to environmental contaminants: cloning and use of iodothyronine deiodinases as molecular biomarkers. Aquat. Toxicol., vol. 83, pp. 200-211. https://doi.org/10.1016/j.aquatox.2007.04.004.

43 Rot-Nikcevic I., Wassersug R.J. (2004) Arrested development in Xenopus laevis tadpoles: how size constrains metamorphosis. The Journal of Experimental Biology, vol. 207, pp. 2133-2145. https://doi.org/10.1242/jeb.01002

44 Hersikorn B.D., Smits J.E.G. (2011). Compromised metamorphosis and thyroid hormone changes in wood frogs (Lithobates sylvaticus) raised on reclaimed wetlands on the Athabasca oil sands. Environ. Pollut., vol. 159, pp. 596–601. https://doi.org/10.1016/j.envpol.2010.10.005.

M.O. Myrzabekova[1*] iD , S.B. Labeit[2] iD , R.Ye. Niyazova[1] iD

[1]al-Farabi Kazakh National University, Almaty, Kazakhstan
[2]Medical Faculty Mannheim, University of Heidelberg, Heidelberg, Germany
*e-mail: moldir.myrzabek@gmail.com

Features of miRNAs binding sites within the C2H2 ZNF family: a *Bos taurus, Eqqus caballus,* and *Ovies aries* comparative approach

Abstract. C2H2 zinc finger genes constitute the largest class of transcription factors in humans and one of the largest gene families in mammals. Using the MirTarget program, we predicted miRNA binding sites (BSs) in CDS, 5'UTR and 3'UTR mRNAs of the ZNF family transcription factors genes of *Bos (B.) taurus, Equus (E.) caballus, Ovis (O.) aries*. We studied interactions of 1025 *B.taurus* miRNAs with 315 mRNAs of zf-C2H2 transcription factors family genes. From established 442 BSs, 196 are located in CDS, 164 in 3'UTR, 82 in 5'UTR. The free binding energy values range from -83 to -127 kJ/mol. mRNAs of several genes have miRNA BSs with overlapping nucleotide sequences (clusters). The cluster of BSs of miR-11975, miR-11976 and miR-2885 were found in 5'UTR, 3'UTR and CDS mRNAs of *FEZF1, SP8, VEZF1, PRDM6, SP3, ZNF366, PRDM13, PRDM12, ZIC4* and *ZFP91* genes. Multiple BSs were predicted for miR-574 in mRNAs of *HIVEP2, KLF7, SNAI2, SP4, ZNF677, ZNF710, ZFP91* genes. We studied binding characteristics between 690 miRNAs and 257 mRNAs of *E.qaballus* zf-C2H2 TFs family genes. The free binding energy ΔG values varied between -87 and -129 kJ/mol. From established 60 BSs, 24 are located in CDS, 21 in 5'UTR, 15 in 3'UTR. The largest ΔG value determined for binding of miR-8996 with *PRDM16* mRNA equals to -129 kJ/mol. The interaction of 152 miRNAs with 223 mRNAs of *O.aries* zf-C2H2 transcription factors genes was identified. The free binding energy values varied in between -85 and -117 kJ/mol. 18 BSs were found in mRNAs of TFs genes, located in CDS and 3'UTR. Therefore, our data suggests that regulation of zf-C2H2 transcription factors by miRNAs may involve their coding regions, thus providing a novel level of complexity when decoding the complex mechanism of miRNA/mRNA interplay and when interpreting conserved motifs within ZF coding sequences.
Key words: miRNA, mRNA, gene, binding site, animal, transcription factor, ZNF.

Introduction

miRNAs are class of ~22-nucleotide "non-messenger" RNAs, generally conserved in evolution, that they have been important regulatory functions. miRNAs play a key role for the control of animal development and physiology [1; 2]. Recent studies demonstrated that animal genomes contain at least 500 genes encoding miRNAs, as well as thousands of genes are targets of miRNA action [3-7]. In animals, miRNAs have been shown suppress mRNA translation and decrease mRNA stability by binding sequences in 3'UTR [8; 9].

The largest family of transcription factors (TF) is zinc-coordinating-group. There are ~20 different types of zinc finger (ZNF) genes domains, the majority is the classical Cys2-His2 (C2H2) [10,11].

The C2H2-type ZNF family has over 700 members, many of which are unique to primates and have appear through gene duplication [12]. The ZNF TFs are known as the most abundant DNA-recognition domain and are stabilized by the coordinated binding of a zinc ion [13]. ZNFs is one of the largest gene families in mammals [14].

Nearly all of the miRNA binding sites which were identified are located in 3′ untranslated region (3′UTR) of target genes in animals. Some recent research has shown that miRNAs are also found in targeted coding sequence (CDS) regions of some species [15-17].

Currently, the effect of miRNAs on the expression of TFs genes in organisms is not sufficiently understood. More systematic and also genome-wide studies on the effects of miRNA on the expression of

transcription factors are currently a topical research theme. For example, the effects of miRNAs on animal gene expression of MYB TFs have been reported in [18]. In this study, we systematically studied miRNA binding motifs in all known C2H2 ZNFs genes, including comparisons of their conservation in three different mammalian species. Surprisingly, our results indicate that mRNA regulation may predominantly involve the ZF coding regions.

Materials and methods

Nucleotide sequences of zf-C2H2 family TFs genes of *B. taurus, E. caballus* and *O. aries* mRNAs were downloaded from Animal Transcription Factor Database (http://www.bioguo.org/AnimalTFDB/). Nucleotide sequences of miRNAs were downloaded from miRBase database (http://mirbase.org). The search for binding sites (BSs) of miRNAs in mRNAs of target genes was performed using the MirTarget program [19]. This program defines the following features of binding: a) the start of the initiation of miRNA binding to mRNAs; b) the localization of miRNA binding sites in 5'-untranslated regions (5'UTR), CDS and 3'UTR of mRNAs; c) the free energy of interaction miRNA and mRNA (ΔG, kJ/mol); and d) schemes of nucleotide interactions between miRNAs and mRNAs. The ratio $\Delta G/\Delta Gm$ (%) was determined for each site (ΔGm equals the free energy of miRNA binding with its perfect complementary nucleotide sequence). $\Delta G/\Delta Gm$ ratios were taken on the assumption that the members of miRNA family generally differ by no more than 1-2 nt; with a miRNA length of 22 nt, $\Delta G/\Delta Gm$ value is higher than 90%. With a larger difference in the number of mismatched nucleotides, the probability of two or more miRNAs to bind in one site increases. With a larger difference in the number of mismatched nucleotides, the probability of two or more miRNAs to bind in one site increases, which excludes the natural property of miRNA to interact selectively with mRNA of target gene. The MirTarget program identifies the positions of BSs on mRNA, beginning from the first nucleotide of mRNA's 5'UTR. The MirTarget program finds hydrogen bonds between adenine (A) and uracil (U), guanine (G) and cytosine (C), G and U, A and C. The distances between A and C are equal to those between G and C, A and U, G and U and equal to 1.02 nm [20]. G-C, A-U, G-U and A-C interactions form 3, 2, 1 and 1 hydrogen bonds. The miRNA binding sites for mRNA were taken with $\Delta G/\Delta Gm$ ratios equal and more than 85%.

Results and discussion

Characteristics of miRNAs binding to mRNAs of Bos taurus zf-C2H2 transcription factors genes. We studied interactions of 1025 *B. taurus* miRNAs with 315 mRNAs of zf-C2H2 transcription factors family genes. We established 442 binding sites: 196 are located in CDS, 164 in 3'UTR, 82 in 5'UTR. The free binding energy (ΔG) values ranged from -83 to – 127 kJ/mol. mRNAs of several genes have miRNA binding sites with overlapping nucleotide sequences (clusters) located in 5'UTR, CDS, or 3'UTR.

Table 1 presents results of the prediction of characteristics of miRNAs binding with mRNAs of *BCL11B, PRDM2, RREB1, SP4, ZNF628, ZNF710, ZNF142, ZNF236, ZNF687, ZNF652, ZNF467, ZFP91* genes.

Table 1 – Characteristics of miRNAs binding to mRNAs of *B. taurus* zf-C2H2 transcription factors genes

Gene	bta-miRNA	Start of site, nt	Region of mRNA	ΔG, kJ/mol	$\Delta G/\Delta G_m$ %	Length, nt
BCL11B	bta-miR-7865	465	5'UTR	-102	91	19
	bta-miR-1281	865		-93	96	17
	bta-miR-2885	2240	CDS	-108	91	19
	bta-miR-2388-3p	2467		-104	91	21
	bta-miR-2309	4516	3'UTR	-115	87	23
	bta-miR-1777b	4519		-113	90	20
	bta-miR-1777a	4520		-106	86	20
	bta-miR-11971	7367		-102	94	20
	bta-miR-1281	8096		-91	93	17

Table 1 continued

Gene	bta-miRNA	Start of site, nt	Region of mRNA	ΔG, kJ/mol	ΔG/ΔG$_m$ %	Length, nt
PRDM2	bta-miR-2450a	1235	CDS	-102	89	21
	bta-miR-2450b	1235		-108	88	23
	bta-miR-324	1606		-110	87	23
	bta-miR-6528	2997		-100	90	20
	bta-miR-3141	3002		-100	94	18
	bta-miR-6528	3285		-100	90	20
	bta-miR-7865	5719	3'UTR	-104	92	19
RREB1	bta-miR-2361	310	5'UTR	-89	93	20
	bta-miR-2359	312		-87	91	20
	bta-miR-1281	5424	CDS	-91	93	17
	bta-miR-2328-3p	6522	3'UTR	-113	91	21
	bta-miR-11972	7387		-115	89	21
	bta-miR-3141	8270		-98	92	18
SP4	bta-miR-2285ah-5p	122	5'UTR	-110	90	22
	bta-miR-1777a	123		-110	90	20
	bta-miR-2374	123		-110	90	21
	bta-miR-1281	214	CDS	-91	93	17
	bta-miR-376d	2949	3'UTR	-93	90	21
ZNF 628	bta-miR-2881	2322	CDS	-104	92	18
	bta-miR-2305	2331		-113	91	20
	bta-miR-1777a	2333		-110	90	20
	bta-miR-3957	2504		-102	91	20
	bta-miR-11981	2565		-119	87	23
	bta-miR-11976	2575		-119	89	21
	bta-miR-4444	3625		-93	94	18
	bta-miR-7865	3712		-104	92	19
	bta-miR-2899	4345		-98	92	18
	bta-miR-12030	4493		-110	93	19
ZNF710	bta-miR-128	322	5'UTR	-100	90	21
	bta-miR-7865	623		-102	91	19
	bta-miR-1777b	5760	3'UTR	-113	90	20
	bta-miR-1777a	5761		-110	90	20
	bta-miR-1296	6906		-110	90	22
	bta-miR-574	7086-7096		-113-115	87-93	19-24
	bta-miR-2304	7097		-96	90	20
ZNF142	bta-miR-2324	1772	CDS	-113	87	23
	bta-miR-8548	2412		-83	93	17
	bta-miR-12022	5731	3'UTR	-98	90	21
	bta-miR-10161-5p	5735		-106	88	23
	bta-miR-12032	5796		-106	89	21
	bta-miR-12054	6956		-96	94	18

Table 1 continued

Gene	bta-miRNA	Start of site, nt	Region of mRNA	ΔG, kJ/mol	ΔG/ΔG$_m$ %	Length, nt
ZNF236	bta-miR-2892	72	5'UTR	-119	89	22
	bta-miR-11975	77		-115	90	20
	bta-miR-411c-3p	2454	CDS	-100	89	22
	bta-miR-149-3p	3994		-117	90	22
	bta-miR-1224	4556		-106	89	21
	bta-miR-23b-3p	5810		-106	88	23
ZNF687	bta-miR-2305	1	5'UTR	-115	93	20
	bta-miR-3141	1		-100	94	18
	bta-miR-2882	438	CDS	-104	91	19
	bta-miR-2475	2269		-108	88	23
	bta-miR-2285ah-5p	2541		-110	90	22
ZNF652	bta-miR-2485	1582	CDS	-96	90	21
	bta-miR-149-3p	2026		-115	89	22
	bta-miR-1777b	2153		-117	93	20
	bta-miR-1777a	2154		-115	93	20
	bta-miR-11989	8441	3'UTR	-110	87	23
ZNF467	bta-miR-7865	16	5'UTR	-104	92	19
	bta-miR-6528	152		-102	92	20
	bta-miR-2305	158		-113	91	20
	bta-miR-1777b	1605	CDS	-117	93	20
	bta-miR-1777a	1606		-110	90	20
ZFP91	bta-miR-11976	177-189	CDS	-121-127	90-95	21
	bta-miR-11975	178-190		-115-121	90-95	20
	bta-miR-2885	180		-110	93	19
		189		-110	93	19
		192		-110	93	19
	bta-miR-574	1849-1870	3'UTR	-110-117	87-92	24
	bta-miR-11988	1895		-113	95	22

The mRNA of *BCL11B* gene has binding sites with miR-7865, miR-1281, miR-2885, miR-2388-3p, miR-2309, miR-1777b, miR-1777a, miR-11971. BSs of miR-7865, miR-2885 are localized in 5'UTR, of miR-2388-3p and miR-2309 are located in CDS, of others in 3'UTR. Cluster of mir-2309, mir-1777a and mir-1777b BSs is localized in 3'UTR with a total length of 24 nt. The largest ΔG value is determined for miR-2309 BS equal to -115 kJ/mol.

The mRNA of *PRDM2* gene has binding sites with miR-2450a, miR-2450b, miR-324, miR-6528, miR-3141, miR-7865. BSs of miRNAs are located in CDS and for miR-7865 in 3'UTR. Two clusters of binding sites are found in CDS, first cluster for miR-2450a and miR-2450b BSs with a total length of 23

nt and second cluster for miR-6528 and miR-3141 BSs also with a length of 23 nt. miR-6528 has two binding sites.

The mRNA of *RREB1* gene has binding sites with miR-2361, miR-2359 miR-1281, miR-2328-3p, miR-11972, miR-3141 located in 5'UTR, CDS, 3'UTR. We identified miRNA binding sites located with overlapping of nucleotide sequences. Cluster of miR-2361 and miR-2359 BSs with a length of 22 nt is localized in 5'UTR. Binding sites of miR-2361 and miR-2359 are located across two nucleotides in 5'UTR.

The mRNA of *SP4* gene has binding sites with miR-2285ah-5p, miR-1777a, miR-2374, miR-1281, miR-376d located in 5'UTR, CDS, 3'UTR. miR-

1777a and miR-2374 BSs are located with overlay in 5'UTR.

The mRNA of *ZNF628* gene has the largest number of binding sites with ten miRNAs: miR-2881, miR-2305, miR-1777a, miR-3957, miR-11981, miR-11976, miR-4444, miR-7865, miR-2899, miR-12030. All BSs are located in CDS. miR-2881, miR-2305 and miR-1777a have overlapping binding sites which form a cluster. Binding sites of miR-11981 and miR-11976 also form a cluster. In this case it is important the location of binding sites mainly in protein coding part of mRNA. The greater free binding energy is determined for miR-11976 equal to-127 kJ/mol.

The mRNA of *ZNF710* gene has binding sites with miR-128, miR-7865, miR-1777b, miR-1777a, miR-1296, miR-574, miR-2304 located in 3'UTR and 5'UTR. Cluster of BSs is found for miR-1777b and 1777a in the 3'UTR. miRNAs BSs are located with overlapping of 19 nt. miR-574 has polysites in 3'UTR, located through two nucleotides. Binding sites of miR-574 and miR-2304 form a cluster, located from 7094 to 7118 nt.

The mRNA of *ZNF142* gene has binding sites with miR-2324, miR-8548, miR-12022, miR-10161-5p, miR-12032, miR-12054 located in CDS and 3'UTR. Binding sites of miR-12022 and miR-10161-5p form a cluster in 3'UTR, located from 5731 to 5758 nt.

The mRNA of *ZNF236* gene has binding sites with miR-2892, miR-11975, miR-411c-3p, miR-149-3p, miR-1224, miR-23b-3p located in 5'UTR and 3'UTR. In 5'UTR binding sites of miR-2892 and miR-11975 are located with overlapping of five nucleotides.

The mRNA of *ZNF687* gene has binding sites of five miRNAs: miR-2305, miR-3141, miR-2882, miR-2475, miR-2285ah-5p located in 5'UTR and 3'UTR. miR-2305 and miR-3141 BSs are located with an overlay in 5'UTR.

mRNAs of *ZNF652, ZNF467* genes have binding sites with miR-2485, miR-149-3p, miR-1777b, miR-1777a, miR-11989, miR-7865, miR-6528, miR-2305 located in CDS, 3'UTR, 5'UTR. Binding sites of miR-1777b and miR-1777a in CDS mRNA of *ZNF652, ZNF467* genes form a cluster with overlapping of 19 nucleotides.

miR-11976, miR-11975, miR-2885, miR-574, miR-11988 bind in mRNA of *ZFP91* gene. Polysites of miR-11976, miR-11975 and miR-2885 form a cluster with a total length of 34 nt, located across three nucleotides. miR-11976, miR-11975 and miR-2885 bind with ΔG values equal to -127 kJ/mol, -115 kJ/mol and -110 kJ/mol. Described miRNAs also form a cluster with mRNA of *MYB* transcription factors [18]. Also found polysites for miR-574 in 3'UTR mRNA of *ZFP91* gene, located through two nucleotides. The great free binding energy is equal to -127 kJ/mol.

The role of some studied miRNAs is given in Table 2.

Table 2 – Information on role of bta-miRNAs

miRNA	Role of miRNA	A source of information
miR-122	HCV pathogenesis	PMID:29769341
miR-1281	apoptosis	PMID:31884421
miR-149	muscle protein synthesis (MPS) and anabolism	PMID:28341051
mir-1777a	mastitis resistance	PMID:22084936
miR-2304	I. MODULATION OF HOST IMMUNE RESPONSE	PMID:23504566
miR-2361	BHV-1 pathogenesis	PMID:31176405
miR-2881	myotube MPS and anabolism	PMID:28341051
miR-2885	liver diseases	PMID:24428929
miR-2899	energy metabolism; mastitis resistance	PMID:31208329; PMID:31096910
miR-34a	II. ENERGY METABOLISM IN SKELETAL MUSCLE; MAMMARY METABOLISM	PMID:31208329; PMID:30639019

miR-574 has multiple sites in mRNAs of *HIVEP2, KLF7, SNAI2, SP4, ZNF677, ZNF710, ZFP91* genes (Table 3). In all mRNAs of genes miR-574 has poly-sites, located mainly in 3'UTR through two nucleotides. In mRNA of *ZFP91* gene miR-574 has eleven, in *KLF7* ten, in mRNA of *HIVEP2, SNAI2* genes six binding sites. miR-574 has five binding sites in mRNA of *ZNF710* gene, three – in *ZNF677* gene, one binding site in *SP4* gene. The largest ΔG value is determined for BSs in mRNA of *KLF7* gene equal to -121 kJ/mol.

Table 3 – Characteristics of miR-574 binding with 3'UTR mRNA of *B. taurus* zf-C2H2 transcription factor genes

Gene	Start of site, nt	ΔG, kJ/mol	ΔG/ΔG$_m$%
HIVEP2	9694-9704	-113-119	87-94
KLF7	1324-1342	-113-121	87-95
	1352	-110	87
SNAI2	1059-1069	-113	87-93
SP4	1849	-117	92
ZNF677	2419-2423	-113-115	88-90
ZNF710	7086-7096	-113-115	87-93
ZFP91	1849-1870	-110-117	87-92

A previous study demonstrated that in the case of human miR-574-5p, interaction with it target mRNAs involves many binding sites located across two nucleotides [21]. miR-574 is of particular interest because the change in its expression detected in various pathologies. Thus, miR-574-3p is a potential therapeutic and prognostic biomarker in human colorectal cancer cells, it's up-regulation had prohibited the cell proliferation of human colorectal cancer cells *in vitro* and increased the apoptosis level [22]. miR-574-3p expression levels were decreased in spinal chordoma patients [23]. miR-574 has been found to be upregulated in several types of cancers, including human osteosarcoma, lung cancer, bladder cancer and prostate cancer [24-27].

In mRNAs of *REPIN1, ZNF592, ZNF771* genes the cluster of miR-1777b and 1777a binding sites were found (Table 4). In all genes binding sites are located through one nucleotide in 3'UTR mRNA of *REPIN1*, *ZNF592* genes, in 5'UTR mRNA of *ZNF771* gene.

In mRNA of *ZNF699* gene binding sites of miR-3432 and miR-3432a are located with overlay, BSs of miR-3432b across one nucleotide.

Table 4 – Characteristics of miRNAs binding with mRNAs of *REPIN1, ZNF592, ZNF771 B. taurus* zf-C2H2 transcription factor genes

Gene	bta-miRNA	Start of site, nt	Region of mRNA	ΔG, kJ/mol	ΔG/ΔG$_m$ %	Length, nt
REPIN1	bta-miR-1777b	3209	3'UTR	-113	90	20
	bta-miR-1777a	3210		-113	91	20
ZNF592	bta-miR-1777b	4903	3'UTR	-117	93	20
	bta-miR-1777a	4904		-110	90	20
ZNF771	bta-miR-1777b	14	5'UTR	-115	92	20
	bta-miR-1777a	15		-110	90	20
	bta-miR-34a	1011	CDS	-104	89	22
ZNF699	bta-miR-3432	4180	3'UTR	-106	91	22
	bta-miR-3432a	4180		-106	91	22
	bta-miR-3432b	4181		-98	90	21

The cluster of binding sites of miR-11975, miR-11976 and miR-2885 were found in 5'UTR, 3'UTR and CDS of mRNAs of *FEZF1, SP8, VEZF1, PRDM6, SP3, ZNF366, PRDM13, PRDM12, ZIC4* and *ZFP91* genes (Table 5).

In mRNAs of *SP8* and *VEZF1* genes miRNAs have polysites located across three nucleotides. In mRNA *of SP8* gene was predicted seven binding sites of miR-11975, six BSs of miR-11976 and three BSs of miR-2885. In 5'UTR mRNA of *VEZF1* gene predict-

ed six binding sites of miR-11976, four BSs of miR-11975 and two BSs of miR-2885 in 5'UTR. The starts of miR-11976, mir-11975 binding sites in mRNAs of *PRDM6, SP3, SP4, ZNF366* genes are located across one nucleotide. In mRNAs of *PRDM12, PRDM13, ZIC4* genes mir-11976 and mir-2885 BSs are located with overlay. The largest free binding energy were characterized for miR-11976 and varied between -127-(-119) kJ/mol, for miR-11975 – (-121-(-115)) kJ/mol and for miR-2885 – (-110-(108)) kJ/mol.

Table 5 – Characteristics of miRNAs binding with mRNAs of *B.taurus FEZF1, SP8, VEZF1 PRDM6, SP3, ZNF366, PRDM13, PRDM12, ZIC4, ZFP91*zf-C2H2 transcription factor genes

Gene	bta-miRNA	Start of site, nt	Region of mRNA	ΔG, kJ/mol	$\Delta G/\Delta G_m$ %	Length, nt
FEZF1	bta-miR-11976	1331	CDS	-119	89	21
	bta-miR-2885	1349		-108	91	19
SP8	bta-miR-11975	511-528	CDS	-115	90	20
	bta-miR-11976	512-527		-127	95	21
	bta-miR-2885	512		-110	93	19
		515		-110	93	19
		524		-108	91	19
VEZF1	bta-miR-11976	11-26	5'UTR	-119	89	21
	bta-miR-11975	18-27		-117	92	20
	bta-miR-2885	11		-108	91	19
		26		-110	93	19
PRDM6	bta-miR-11976	678	CDS	-119	89	21
	bta-miR-11975	679		-117	92	20
SP3	bta-miR-11976	882	CDS	-121	90	21
	bta-miR-11975	883		-121	95	20
ZNF366	bta-miR-11976	969	CDS	-121	90	21
	bta-miR-11975	970		-115	90	20
		1246		-117	92	20
PRDM13	bta-miR-11976	1215	CDS	-121	90	21
	bta-miR-2885	1215		-110	93	19
	bta-miR-11975	1216		-115	90	20
PRDM12	bta-miR-11976	1035	CDS	-119	89	21
	bta-miR-2885	1035		-108	91	19
ZIC4	bta-miR-11976	3946	CDS	-119	89	21
	bta-miR-2885	3946		-108	91	19
ZFP91	bta-miR-11976	177-189	CDS	-121	90	21
	bta-miR-11975	178-190		-115	90	20
	bta-miR-2885	180	CDS	-110	93	19
		189		-110	93	19
		192		-110	93	19

Characteristics of miRNAs binding with mRNAs of Equus qaballus zf-C2H2 transcription factor genes. To detect miRNAs targeted by genes of zf-C2H2 TFs family we studied binding characteristics between 690 miRNAs and 257 mRNAs of *E. qaballus* zf-C2H2 TFs family genes. The free binding energy ΔG values were varied between -87 and -129 kJ/mol. Was established 60 binding sites: 24 located in CDS, 21 in 5'UTR, 15 in 3'UTR. The largest ΔG value determined for binding of miR-8996 with *PRDM16* mRNA equal to -129 kJ/mol. Each of mRNAs of *HIVEP3, PLAGL2, PRDM15, ZNF592* genes have BSs for three miRNAs located in 5'UTR, 3'UTR and CDS (Table 6).

Table 6 – Characteristics of miRNAs binding with mRNAs of *E. caballus* zf-C2H2 transcription factor genes

Gene	miRNA	Start of site, nt	Region of mRNA	ΔG, kJ/mol	ΔG/ΔG$_m$ %	Length, nt
EGR3	eca-miR-568	2708	3'UTR	-87	91	20
FEZF2	eca-miR-8953	297	CDS	-98	90	21
GLIS3	eca-miR-9000	75	5'UTR	-119	90	23
HIVEP2	eca-miR-23a	3632	CDS	-102	92	21
HIVEP3	eca-miR-9181	5213	CDS	-108	91	21
	eca-miR-122	7110		-102	89	22
	eca-miR-8984	11837	3'UTR	-98	90	20
IKZF1	eca-miR-8915	4842	3'UTR	-119	87	24
IKZF4	eca-miR-1597	384	5'UTR	-106	89	22
IKZF5	eca-miR-8941	935	CDS	-96	90	20
KLF12	eca-let-7a	4232	3'UTR	-96	87	22
	eca-let-7f	4232		-98	90	22
KLF7	eca-miR-703	5825	3'UTR	-96	90	21
LOC100052677	eca-miR-9140	2136	CDS	-123	87	25
LOC100060110	eca-miR-27b	649	CDS	-100	90	21
LOC100629880	eca-miR-9004	6238	3'UTR	-102	89	22
PLAGL2	eca-miR-432	676	5'UTR	-108	88	23
	eca-miR-7667	727		-113	88	23
	eca-miR-8969	2538	CDS	-104	91	21
PRDM15	eca-miR-135b	2237	CDS	-100	87	23
	eca-miR-135a	2238		-98	87	23
	eca-miR-135b	2238		-102	89	23
PRDM16	eca-miR-7035	5628	3'UTR	-117	86	25
	eca-miR-8996	6349		-129	87	25
WIZ	eca-miR-8931	7515		-113	90	22
ZFP64	eca-miR-769a-5p	1847	CDS	-113	93	22
	eca-miR-769b	1847		-108	91	22
ZFP69B	eca-miR-9167	2294	5'UTR	-119	86	25
ZFX	eca-miR-544b	6514	3'UTR	-96	90	22
ZKSCAN2	eca-miR-7045	301	5'UTR	-121	88	23
ZKSCAN4	eca-miR-141	839	CDS	-102	91	22
ZKSCAN5	eca-miR-197	1451	CDS	-108	89	22

Gene	miRNA	Start of site, nt	Region of mRNA	ΔG, kJ/mol	ΔG/ΔG$_m$ %	Length, nt
ZMAT3	eca-miR-8957	1043	5'UTR	-115	86	25
ZNF142	eca-miR-9121	2971	CDS	-115	86	25
ZNF214	eca-miR-539	936	CDS	-100	89	22
ZNF215	eca-miR-9031	5677	5'UTR	-117	87	25
ZNF324	eca-miR-1379	357	CDS	-123	87	24
	eca-miR-8984	2788	3'UTR	-98	90	20
ZNF333	eca-miR-7045	718	5'UTR	-121	88	23
	eca-miR-493b	1836	CDS	-108	89	22
ZNF34	eca-miR-9005	3807	5'UTR	-117	86	25
ZNF408	eca-miR-9159	4680	3'UTR	-100	89	22
ZNF423	eca-miR-143	2670	CDS	-100	90	21
ZNF445	eca-miR-9115	243	5'UTR	-117	90	24
ZNF45	eca-miR-8945	1888	CDS	-106	88	23
ZNF512	eca-miR-8917	1897	CDS	-108	88	23
ZNF514	eca-miR-8917	218	5'UTR	-110	90	23
ZNF521	eca-miR-9039	399	CDS	-108	88	23
ZNF544	eca-miR-186	1380	5'UTR	-100	89	22
ZNF592	eca-miR-493a	145	5'UTR	-110	91	22
	eca-miR-764-3p	220		-108	91	22
	eca-miR-197	6289	3'UTR	-110	91	22
ZNF614	eca-miR-9163	482	5'UTR	-115	87	24
ZNF615	eca-miR-9000	51	5'UTR	-123	94	23
ZNF618	eca-miR-9164	14187	3'UTR	-102	92	20
ZNF710	eca-miR-9124	2168	5'UTR	-108	88	23
ZNF75D	eca-miR-876-5p	1074	CDS	-100	90	22
ZNF79	eca-mir-9024	1759	5'UTR	-115	86	25
ZSCAN23	eca-miR-211	2324	5'UTR	-102	89	22
ZSCAN29	eca-miR-149	299	5'UTR	-113	88	23

Each of mRNAs of *KLF12, PRDM16, ZFP64, ZNF324, ZNF333* genes have BSs for two miRNAs. mRNAs of other genes have BSs with one miRNA. miR-9000 has BSs in 5'UTR mRNA of *GLIS3* and *ZNF615* genes. miR-8984 has binding sites in 3'UTR mRNA of *HIVEP3* and *ZNF324* genes. let-7a and let-7f BSs located with overlay in mRNA of *KLF12* gene in 3'UTR. miR-135b and miR-135a binding sites are located across one nucleotide in CDS mRNA of *PRDM15* gene. miR-769a-5p and miR-769b have by one BS located in CDS mRNA of *ZFP64* gene. miR-7045 has BSs in mRNAs of *ZKSCAN2* and *ZNF333* genes located in 5'UTR. miR-197 also has BS in mRNA of *ZKSCAN5* and *ZNF592* genes located in CDS and 3'UTR. miR-8917 has BSs in mRNA of *ZNF512* and *ZNF514* genes located in CDS and 5'UTR.

Characteristics of miRNAs binding with mRNAs of Ovis aries zf-C2H2 transcription factor genes. The interaction of 152 miRNAs with 223 mRNAs of *O. aries* zf-C2H2 transcription factors genes was identified. The free binding energy ΔG values were varied between -85 and -117 kJ/mol. Was found 18 binding sites: 9 located in CDS and 9 in 3'UTR (Table 7).

Table 7 – Characteristics of miRNAs binding to mRNAs of *O. aries* zf-C2H2 transcription factor genes

Gene	miRNA	Start of site, nt	Region of mRNA	ΔG, kJ/mol	$\Delta G/\Delta G_m$ %	Length, nt
BCL11A	oar-miR-544-3p	1184	CDS	-91	90	21
IKZF1	oar-miR-493-5p	3712	3'UTR	-98	88	22
KLF12	oar-miR-106a	3777	3'UTR	-98	90	21
	oar-miR-23b	969	CDS	-85	91	18
	oar-miR-544-5p	9302	3'UTR	-93	90	21
LOC101110699	oar-miR-1193-3p	752	CDS	-104	89	22
LOC101111419	oar-miR-543-5p	4458	CDS	-91	90	19
LOC101119987	oar-miR-27a	1133	CDS	-100	89	21
MTF1	oar-miR-106a	2630	3'UTR	-96	88	21
PRDM1	oar-let-7d	2784	CDS	-93	90	20
SNAI2	oar-miR-654-5p	196	CDS	-117	87	24
ZFP62	oar-miR-493-5p	4087	3'UTR	-98	88	22
ZIC3	oar-miR-30d	2946	3'UTR	-91	90	19
ZNF236	oar-miR-3959-3p	2362	CDS	-100	89	22
ZNF331	oar-miR-3955-3p	3104	3'UTR	-96	90	21
ZNF541	oar-miR-410-5p	325	CDS	-110	88	23
ZNF606	oar-miR-329a-5p	4099	3'UTR	-102	89	22
	oar-miR-329b-5p	4098	3'UTR	-106	89	23

The largest ΔG value determined for miR-8996 binding with mRNA of *SNAI2* gene and equal to -117 kJ/mol (Table 7). *KLF12* mRNA have binding sites for three miRNAs: oar-miR-106a, oar-miR-23b and oar-miR-544-5p. *ZNF606* mRNA have binding sites for oar-miR-329a-5p and oar-miR-329b-5p. Other genes have BSs for one miRNA with $\Delta G/\Delta G_m$ values more than 85.

The possible schemes of interaction of miRNA and mRNA nucleotides are shown in Figure 1. The schemes show the following advantages of the Mir-Target program, taking into account that: almost of miRNA nucleotides in the interaction with mRNA; the formation of non-canonical pairs G-U and A-C that do not change the double-stranded conformation of the miRNA complex with mRNA, since the distances between G-U and A-C are equal to the distances between G-C and A-U; an important criterion for binding miRNA to mRNA is the free energy of interaction; the localization of the miRNA binding site in 5'UTR, CDS and 3'UTR of mRNA.

The schemes demonstrate a total complementarity between nucleotides. For example, of the 23 nucleotides of eca-miR-135b, all nucleotides formed a double-stranded helical structure with mRNA. We can see three pairs of G-U and two pairs of A-C non-canonical pairs interaction between nucleotides of eca-miR-135b and eca-PRDM15 mRNA.

The level of miRNA interaction with mRNA is given by the size of free energy of their binding. By this indicator several miRNAs were identified. The largest ΔG value -123 kJ/mol is character for eca-miR-9000 binding with *ZNF615* mRNA. Bta-miR-1777b binds to mRNA of *ZNF592* gene with ΔG value equal to -117 kJ/mol, which is 90% of maximum free binding energy, which indicates the strong binding of these miRNAs and more efficient suppression of *ZNF615* and *ZNF592* proteins synthesis.

An amino acid sequence of oligopeptide is encoded by the nucleotides of three clusters which located between conserved oligopeptides PGSSA-FSLTSSS and AAAAASSSPFAN of SP8 protein presented in Table 8.

The bta-miR-11975 binding sites in the mRNAs of *SP8* genes are located in CDS and encode the AAAAAAA oligopeptide in the first and third reading frames. Bta-miR-11976 binding sites in *SP8* gene also encode this oligopeptide in the first and third reading frames. The bta-miR-2885 BS in CDS encodes AAAAAAA in the third reading frame.

bta-BCL11B, bta-miR-7865, 465, 5'UTR, -102, 91
5' – CC**U**CCCC**C**CGCCCU**U**CCUG – 3'
    |||||||| ||||||||||
3' – GG**G**AGGGG**A**–CGGGA**G**GGAC – 5'
	bta-ZNF710, bta-miR-1296, 6906, 3'UTR, -110, 90
	5' – GGAGGUG**AG**GCCAUGGGCCC**CAG** – 3'
	    ||||||||||| ||||||||||
	3' – CCUCUAC**CU**CGGU–CCCGGG**AU**U – 5'

bta-ZNF652, bta-miR-11989, 8441, 3'UTR, -110, 87
5' – **A**CACUGAG**A**AGCC**G**CAUCCCUGAG – 3'
    ||||| |||||||||||||
3' – **C**GUGA–UC**C**UCGA**U**GUAGGGACCC – 5'
	bta-ZNF592, bta-miR-1777b, 4903, 3'UTR, -117, 93
	5' – CCCCGC**U**GCCCCAC**U**GCCCCC – 3'
	    ||||||| |||||||||||
	3' – GGGGCG**G**–GGGGUG**G**CGGGGG – 5'

eca-PRDM15, eca-miR-135b, 2238, CDS, -100, 87
5' – **C**CACACAGGA**G**UGAA**G**AGCCA**C**G – 3'
    ||||||||||||||||||||||
3' – **A**GUGUAUCCU**U**ACUU**U**UCGGU**AU** – 5'
	eca-ZNF615, eca-miR 9000, 51, 5'UTR, -123, 94
	5' – CACUGC**A**CCACUGGGCC**G**GCCCCU – 3'
	    |||||||||||||||||||| ||
	3' – GUGACG**C**GGUGACCCAGU**C**GG–GA – 5'

oar-LOC101119987, oar-miR-27a, 1133, CDS, -100, 89
5' – GC**A**GGAACCU**G**GCCACUGUG**GG** – 3'
    |||| |||||||||||||||
3' – CG**C**C–UUGAA**U**CGGUGACAC**UU** – 5'
	oar-PRDM1, oar-let-7d, 2784, CDS, -93, 90
	5' – **UC**AC**A**GCAACCCACUACCUCU – 3'
	    |||| ||||||||||||||
	3' – **GA**UA–CGUUGGAUGAUGGAGA – 5'

Note. Gene, miRNA, site, region of mRNA, characteristics of binding. The bold type indicates the non-canonical interactions U-G, A-C.

Figure 1 – Schemes of miRNAs interaction with mRNAs of *B. taurus,*
E. caballus, O. aries zf-C2H2 family transcription factors genes

Table 8 – The variability of amino acid sequences of ZNF family proteins containing oligopeptide AAAAAAA encoded by the binding sites of miRNAs in CDS mRNAs of genes

Gene	miRNA	Start of site, nt	Region of transcription factor containing oligopeptide AAAAAAA
SP8	bta-miR-11975	511-522	PGSSAFSLTSSS**AAAAAAA**AAAAASSSPFAN[1]
		525-528	PGSSAFSLTSSS**AAAAAAA**AAAAASSSPFAN[3]
	bta-miR-11976	512-518	PGSSAFSLTSSS**AAAAAAA**AAAAASSSPFAN[1]
		521-527	PGSSAFSLTSSS**AAAAAAA**AAAAASSSPFAN[3]
	bta-miR-2885	512-515	PGSSAFSLTSSS**AAAAAAA**AAAAASSSPFAN[3]
		524	PGSSAFSLTSSS**AAAAAAA**AAAAASSSPFAN[3]
PRDM6	bta-miR-11976	678	SSSTSASSASSC**AAAAAAA**AAAALAGLSALP[1]
	bta-miR-11975	679	SSSTSASSASSC**AAAAAAA**AAAALAGLSALP[1]
ZFP91	bta-miR-11976	177	SRVLRGGRDRGR**AAAAAAA**AAAAVSRRRKAE[1]
		180-189	SRVLRGGRDRGR**AAAAAAA**AAAAVSRRRKAE[2]
	bta-miR-11975	178-190	SRVLRGGRDRGR**AAAAAAA**AAAAVSRRRKAE[3]
	bta-miR-2885	180-192	SRVLRGGRDRGR**AAAAAAA**AAAAVSRRRKAE[2]
Note: Indexes show reading frames – 1, 2, 3.			

In the mRNA of *PRDM6* gene cluster of bta-miR-11976 and bta-miR-11975 BSs encodes AAAAAAA in the first reading frame, which are located between conserved oligopeptides SSSTSAS-SASSC and AAAALAGLSALP.

In the mRNA of *ZFP91* gene three clusters also encode polyA between oligopeptides SRVLRG-GRDRGR and AAAAVSRRRKAE.

Recent studies have revealed that aberrant expression of zinc finger proteins contributes to progression in multiple cancers, including tumorigenicity, metastasis and chemoresistance [28-30]. *PRDM2* gene has a large role in human cancers such as neuroblastoma [31], hepatoma [32], and breast cancer [33]. A significant decrease of *PRDM2* gene expression is observed in high-grade gliomas [34]. *BCL11B* mRNA

is essential for growth of αβ T cells and most of γδ T cells [35]. Oncogenic properties of *ZFP91* is revealed in experiments. Where is found overexpression of *ZFP91* in a screening-type of study in leukemic cells and neoplastic blood cell lines [36]. Overexpression has been connected to cancer pathogenesis in melanoma, pancreatic, breast and lung cancers [37], colon cancer and endometrial cancer cell lines and stomach cancer cell lines [38]. Overexpression of *ZFP91* gene is observed in many types of cancer. Therefore, it is possible to bind the cluster into the protein encoding part has an important role to suppress the expressions of this gene. Also miRNA binds to a complementary sequence in the 3′ untranslated region (3′UTR) of its target mRNA and expression of this mRNA is silenced. The *ZNF628* known to be essential for normal growth and development, found in mammals, conserved, seems to be functionally important [39]. Was identified to have significant association with Alzheimer's disease [40]. This *in silico* research indicates that some miRNAs can regulate gene family by targeting their coding regions, thus providing an important and novel perspective for decoding the complex mechanism of miRNA/mRNA interplay. Overall, miRNA binding sites in coding regions show bigger regulation than 3′UTR and 5′UTR binding.

Conclusion

In this paper, we identified the features of interactions of 1025 *B. taurus* miRNAs with 315 ZNFs genes mRNAs, 690 miRNAs and 257 mRNAs of *E. qaballus* ZNFs genes mRNAs and 152 miRNAs with 223 mRNAs of *O. aries* zf-C2H2 transcription factors genes. Using the MirTarget program, we predicted miRNA BSs in the CDS, 5'UTR and 3'UTR mRNAs of genes. It has been found that some miRNAs may bind to mRNA of more than one target gene. For example, bta-miR-1777b and bta-miR-1777a have BSs in mRNAs of *BCL11B, SP4, ZNF 628, ZNF710, ZNF652, ZNF467, REPIN1, ZNF592* and *ZNF771* genes. miR-574 has polysites in 3'UTR mRNA of *B. taurus* zf-C2H2 transcription factor genes. On the basis of the miRTarget program, the organization of binding sites was established in arranged located sites with overlapping nucleotide sequences. The cluster organization of miRNA BSs, together with the free energy of miRNA interaction with mRNA, causes competition between miRNAs to bind to mRNA. Since hundreds of miRNAs have now been identified in various farm animal species, more systematic and genome-wide studies will be required on the effect of miRNAs. This will address how the expression of transcription factors is regulated during a diverse range of biological processes by the fast growing miRNA signal networks.

References

1   Ambros V. (2004) The functions of animal microRNAs. Nature, vol. 431, no.7006, pp. 350–355. https://doi.org/10.1038/nature02871.

2   Reinhart B., Weinstein E., Rhoades M., Bartel B., et al. (2002) MicroRNAs in plants. Genes Dev., vol. 16, no. 17, pp. 2313. https://doi.org/10.1101/gad.1004402.

3   Bartel D. (2004) MicroRNAs: Genomics, biogenesis, mechanism, and function. Cell, vol. 116, no. 2, pp. 281–297. https://doi.org/10.1016/s0092-8674(04)00045-5.

4   Berezikov E., Guryev V., van de Belt J., Wienholds E., et al. (2005) Phylogenetic shadowing and computational identification of human microRNA genes. Cell, vol. 120, no. 1, pp. 21–24. https://doi.org/10.1016/j.cell.2004.12.031.

5   Bentwich I., Avniel A., Karov Y., Aharonov R., et al. (2005) Identification of hundreds of conserved and nonconserved human microRNAs. Nat. Genet., vol. 37, no. 7, pp. 766–770. https://doi.org/10.1038/ng1590.

6   Lim L., Lau N., Garrett-Engele P., Grimson A., et al. (2005) Microarray analysis shows that some microRNAs downregulate large numbers of target mRNAs. Nature, vol. 433, no. 7027, pp. 769–773. https://doi.org/10.1038/nature03315.

7   Lewis B., Burge C., Bartel D. (2005) Conserved seed pairing, often flanked by adenosines, indicates that thousands of human genes are microRNA targets. Cell, vol. 120, no. 1, pp.15–20. https://doi.org/10.1016/j.cell.2004.12.035.

8   Wu L, Fan J. (2006) MicroRNAs direct rapid deadenylation of mRNA. Proc Natl Acad Sci USA., vol. 103, no. 11, pp. 4034-4039.

9   Standart N., Jackson R. (2007) MicroRNAs repress translation of m7Gppp-capped target mRNAs in vitro by inhibiting initiation and promoting deadenylation. Genes Dev., 2007, vol. 21, no. 16, pp.1975-82.

10   Krishna S., Majumdar I., Grishin N. (2003) Structural classification of zinc fingers: survey 597 and summary. Nucleic Acids Res., vol. 31, no. 2, pp. 532-50. https://doi.org/ 10.1093/nar/gkg161.

11 Matthews J., Sunde M. (2002) Zinc fingers--folds for many occasions. IUBMB

Life., vol. 54, no. 6, pp. 351-355. https://doi.org/10.1080/15216540216035.

12 Joseph R., Aimee L., Jalkanen A., Heck C., et al. (2018) Sequences encoding C2H2 zinc fingers inhibit polyadenylation and mRNA export in human cells. Sci Rep., vol. 8, no. 16995. https://doi.org/10.1038/s41598-018-35138-4.

13 Ding G., Lorenz P., Kreutzer M., Li Y., et al. (2009) Sys ZNF: The C2H2 zinc finger gene database. Nucleic Acids Res., vol. 37, no. 267-73. https://doi.org/10.1093/nar/gkn782

14 Huang S., Wu S., Ding J., Lin J., et al. (2010) MicroRNA-181a modulates gene expression of zinc finger family members by directly targeting their coding regions. Nucleic Acids Res., vol. 38, no. 20, pp. 7211–7218. https://doi.org/10.1093/nar/gkq564

15 Duursma A., Kedde M., Schrier M., Carlos le Sage., et al (2008) miR-148 targets human DNMT3b protein coding region. RNA., vol. 14, no. 5, pp. 872-877. https://doi.org/10.1261/rna.972008

16 Forman J., Legesse-Miller A., Coller H. (2008) A search for conserved sequences in coding regions reveals that the let-7 microRNA targets Dicer within its coding sequence. Proc. Natl Acad. Sci. USA., vol. 105, no. 39, pp. 14879-14884. https://doi.org/10.1073/pnas.0803230105

17 Tay Y., Zhang J., Thomson A., Lim B., et al. (2008) MicroRNAs to Nanog, Oct4 and Sox2 coding regions modulate embryonic stem cell differentiation. Nature, vol. 455, no. 7216. pp. 1124-1128. https://doi.org/10.1038/nature07299

18 Myrzabekova M., Niyazova R., Ivashchenko A. (2019) Features of bindings of miRNA with genes of MYB family transcription factors of B. taurus, E. caballus, O. aries. Experimental biology, vol. 4, no. 81, pp. 25-32. https://doi.org/10.26577/eb-2019-4-b3

19 Ivashchenko A., Berillo O., Pyrkova A., Niyazova R., et al. (2014) MIR-3960 binding sites with mRNA of human genes. Bioinformation, vol. 10, no. 7, pp. 423-427.

20 Kool T. (2001) Hydrogen bonding, base stacking, and steric effects in DNA replication. Annu Rev Biophys Biomol Struct., vol. 30, no. 22, pp. 1–22, https://doi:org/ 10.1146/annurev.biophys.30.1.1

21 Atambaeva Sh., Niyazova R., Berillo O., Ivashchenko A. (2015) The features of binding sites mir-574-5p and mir-574-3p with target genes of mRNA. [Osobennosti saitov svyazyvaniya miR-574-5p i miR-574-3p s mRNA genov mishenei], Biology, vol. 1, no. 63, pp. 349-354

22 Li Wen., Wu Yan., Gao B., Wang Chao., et al. (2019) MiRNA-574-3p inhibits cell progres-sion by directly targeting CCND2 in colorectal cancer. Bioscience Reports, vol. 39, no. 12. https://doi.org/10.1042/BSR20190976.

23 Zou M., Guo K., Lv G., Huang W., et al. (2018) Clinicopathologic implications of CD8(+)/Foxp3(+) ratio and miR-574-3p/PD-L1 axis in spinal chordoma patients. Cancer Immunol Immunother., vol. 67, no. 2, pp. 209–224. https://doi.org/10.1007/s00262-017-2080-1

24 Xu H., Liu X., Zhou J., Chen X., et.al. (2016) miR-574-3p acts as a tumor promoter in osteosarcoma by targeting SMAD4 signaling pathway. Oncol Lett., vol.12, no. 6, pp. 5247–5253. https://doi.org/10.3892/ol.2016.5355

25 Xu H, Liu X, Zhao J. (2014) Down-regulation of miR-3928 promoted osteosarcoma growth. Cell PhysiolBiochem., vol. 33, no. 5, pp. 1547–1556. doi: https://doi.org/10.1159/000358718.

26 Mei Q., Li F., Quan H., Liu Y., et al. (2014) Busulfan inhibits growth of human osteosarcoma through miR-200 family microRNAs in vitro and in vivo. Cancer Sci., vol. 105, no. 7, pp.755–762. https://doi.org/10.1111/cas.12436.

27 Shi Y., Massagué J. (2003) Mechanisms of TGF-beta signaling from cell membrane to the nucleus. Cell, vol. 6, no. 13, pp.685–700.https://doi.org/10.1016/S0092-8674(03)00432-X.

28 Jen J., Lin L., Chen T., Liao S., et al. (2016) Oncoprotein ZNF322A transcriptionally deregulates alpha-adducin, cyclin D1 and p53 to promote tumor growth and metastasis in lung cancer. Oncogene, vol. 35, no. 18, pp. 2357-69. https://doi.org/10.1038/onc.2015.296

29 Yang L., Hamilton S., Sood A., Kuwai T., et al. (2008) The previously undescribed ZKSCAN3 (ZNF306) is a novel "driver" of colorectal cancer progression. Boyd Cancer Research, vol. 68, no. 11, pp. 4321-30.

30 Lai K., Chen J., He M., Ching A., et al. (2014) Wong Overexpression of ZFX confers self-renewal and chemoresistance properties in hepatocellular carcinoma. Int J Cancer., vol. 135, no. 8, pp.1790-9.

31 Fong C., White P., Peterson K., Sapienza C., et al. (1992) Loss of heterozygosity for chromosomes 1 or 14 defines subsets of advanced neuroblastomas. Cancer Research, vol. 52, pp. 1780-1785.

32 Simon D., Knowles B., Weith A. (1991), Abnormalities of chromosome 1 and loss of heterozygosity on 1p in primary hepatomas. Oncogene, vol. 6, pp. 765-770

33 Abbondanza C.., De Rosa C., D'Arcangelo A., Pacifico M., et al. (2012) Identification of a func-

tional estrogen-responsive enhancer element in the promoter 2 of PRDM2 gene in breast cancer cell lines. J Cell Physiol., vol. 227, no. 3, pp. 964-75. https://doi.org/ 10.1002/jcp.22803.

34 Zhang C., Zhu Q., He H., Jiang L., et al. (2016) RIZ1: a potential tumor suppressor in glioma. BMC Cancer., vol. 16, no. 26, pp. 990. https://doi.org/10.1186/s12885-016-2067-x

35 Wakabayashi Y., Watanabe H., Inoue J., Takeda N., et al. (2003) Bcl11b is required for differentiation and survival of alphabeta T lymphocytes. Nat Immunol., vol. 4, no. 6, pp. 533-9.

36 Unoki M., Okutsu J., Nakamura Y. (2003) Identification of a novel human gene, ZFP91, involved in acute myelogenousleukemia. Oncol., vol. 22, no. 6, pp. 1217-23.

37 Xiao G., Fu J. (2011) NF-κB and cancer: a paradigm of Yin-Yang. Cancer Research, vol. 1, no. 2, pp.192-221.

38 Lee J., Lee J., Lee K., Hong Ys., et al. (2008) Therapeutic agent for cancer, inflammation and autoimmune disease containing inhibitor of Zinc Finger Protein 91. US Patent 20: 080,248,024.

39 Chen G., Muramatsu H., Ichihara-Tanaka K., Muramatsu T. (2004) ZEC, a zinc finger protein with novel binding specificity and transcription regulatory activity. Gene, vol. 340, no. 1, pp. 71-81.

40 Kim J., Song P., Lim H., Lee J., et al. (2014) Gene-based rare allele analyses identified a risk gene of Alzheimer's disease. Plos One, vol. 9, no. 10, https://doi.org/10.1371/journal.pone.0107983.

M.M. Yermagambetova[1,2] iD , A.B. Kusmangazinov[1,2] iD ,

M.S. Kurmanbayeva[2*] iD , M. Höhn[3] iD

[1]Institute of Plant Biology and Biotechnology, Laboratory of Molecular Genetics, Almaty, Kazakhstan
[2]Al-Farabi Kazakh National University, Almaty, Kazakhstan
[3]Szent Istvan University, Department of Botany and Soroksár Botanical Garden, Budapest, Hungary
*e-mail: kurmanbayevakz@gmail.com

Study of changes in anatomical structures of young needles *Picea schrenkiana* Fisch et C.A. Mey and shoots of *Haloxylon* bunge species in Kazakhstan

Abstract. The work is devoted to the anatomical study of five populations of the forest-forming species *Picea schrenkiana*, which grows in the Trans Ili Alatau range of Northern Tian Shan Mountains, and three species of the desert tree *Haloxylon*, which grows in three regions of Kazakhstan. As the study was taken young needles of *P. schrenkiana* and shoots of *Haloxylon* species. In this study, anatomical analyses of young needles from five populations of *P. schrenkiana* and shoots from three *Haloxylon* species were performed to identify and describe anatomical features in search of distinctive features that could be used to determine the characteristics of these species. In the cross-section of *P. schrenkiana* needles, all five populations have a rectangular shape, and the tissue types and their location are similar in all populations. Study of the young needles of *P. schrenkiana* revealed the presence of the epidermis, hypodermis, stomata, mesophyll, resin ducts, endodermis and vascular bundles all of the five populations. The area of the vascular bundles varies from 141.4 ± 1.9 to 182.7 ± 1.4 μm². Comparatively, all indicators were the same, which means that the origins of all five populations are similar to each other. As a result, the anatomical structure of *P. schrenkiana* needles corresponds to the structure of coniferous plants. In the study of three species of *Haloxylon*, more precisely *Haloxylon aphyllum, Haloxylon persicum, Haloxylon ammodendron*, differences were found in the section of each species. This is possible due to the fact that they grow in three different regions and different environmental conditions. And it proves that the environmental conditions of the place where these species grow affects the anatomy and structure of plants.

Key words: *Picea schrenkiana, Haloxylon aphyllum*, *Haloxylon persicum, Haloxylon ammodendron,* scanning electron microscopy, anatomical signs, vegetative organs of plants.

Introduction

Despite the fact that the territory of Kazakhstan is vast, it has little forest resources. Forests cover only 4-6% (12.4 million hectares) of the total area. The country has the third largest forest area in Eastern Europe and Central Asia. Forests are unevenly distributed across the country: forest cover is generally 4.57 %, and in some administrative regions 16% in Eastern Kazakhstan prevails compared to 0.1% in Western Kazakhstan, in particular in Almaty, coniferous plantations range from 10-13 %, and deciduous – 12 % and are located in tracts on the inclination of the southern and Eastern mountains. Also, the forests are dominated by saxaul forests, which occupy 49.8 % of the area, and shrub plantations – 24.1%, located mainly in the desert and steppe zones.

The problem of preserving forest genetic resources for current and future generations is becoming increasingly important. Due to the rapid development of scientific and technological progress, the threat of extinction of plant diversity and, above all, forests has increased dramatically. The role of woody vegetation in maintaining the quality of the environment is well known, but even more so in its utilitarian value.

The distribution of ecosystems is subject to the law of latitudinal zoning on the plains and high-altitude zoning in the mountains. On the plains, forest-steppe, steppe and desert ecosystems are major zonal associations.

Mountain ecosystems are much more complex and diverse than on the plain. In the Jungar and Trans-Ili Alatau, most of the forest area is covered with forests of Shrenk spruce, or Tianshan spruce with the inclusion of Siberian fir and Semyonov fir. Desert ecosystems are formed by rare-coniferous forests of arid regions and consist of white saxaul, black saxaul, and desert shrubs on sandy and takyrovid habitats [1]. The flora of Kazakhstan includes 68 species of tree species, 266 species of shrubs, 433 species of semi-shrubs and semi-herbs, 2598 species of perennial grasses, 849 species of annual grasses [2].

Pinaceae include overall 225 species in 11 common genera (*Abies, Cathaya, Cedrus, Keteleeria, Nothotsuga, Picea, Pinus, Pseudolarix, Pseudotsuga* and *Tsuga*) distributed worldwide [3]. Hart [4] divided the family *Pinaceae* into two groups: first group with the presence of resin canals in the seeds and cleavage polyembryony supported the monophyly of *Abies, Cedrus, Keteleeria, Pseudolarix* and *Tsuga* and second group which the presence of resin canals in the secondary xylem and leaves having an endodermis with thickened Casparian strips supported the monophyly of *Cathaya, Larix, Picea, Pinus* and *Pseudotsuga* [5]. Francis [6] identified four subsystems from the pine family in the generally accepted classification [7], based on the morphological structure of the vegetative and reproductive organs: *Pinoideae (Pinus), Piceoideae (Picea), Laricoideae (Cathaya, Larix and Pseudotsuga),* and *Abietoideae (Abies, Cedrus, Keteleeria, Nothotsuga, Pseudolarix* and *Tsuga)*. In Kazakhstan there are 4 genera and 7 species of *Pinaceae* [8].

One of the most common coniferous genus in this family is *Picea* A. Dietr. Farjon [3] identified 34 species of *Picea* in its list of conifers, of which 24 grow in Asia, eight in North America and two in Europe. It is a very homogeneous genus, and therefore it is difficult to work with it from a taxonomic point of view because species have a relatively narrow range of morphological features and ecological preferences [5; 9-11].

In Kazakhstan, 2 species from the genus are present: *P. obovata* Ledeb. and *P. schrenkiana* Fisch et C. A. Mey [8; 12]. The object of our study is the Shrenk's spruce (*Picea schrenkiana*), which occupies relatively small areas in the mountainous regions of Kyrgyzstan and Kazakhstan, but nevertheless plays a huge water-regulating, soil -, water- and avalanche-protective role [13; 14]. The dwarf form of the Schrenk's spruce (*P. schrenkiana* Fisch et C. A. Mey. f. prostrata K. Isakov) is included in the Red book of Kazakhstan [15] and the world IUCN [16], as it is

rare. Outwardly, *P. schrenkiana* resembles *P. obovata,* from which it differs by a longer needling with bare young shoots and larger cones [12].

P. schrenkiana occurs between 1300 and 3000 (-3600) m a.s.l., especially on Northern slopes and in cool ravines. It grows on various mountain soils, usually in stony places with seeping water from snowmelt (eternal snow at high altitudes). The climate is cold continental. It forms usually pure forests, but is sometimes mixed with *Abies sibirica* (*A. sibirica* subsp. semenovii with *Picea schrenkiana* subspecies. tianschanica), on lower elevations with *Ulmus* and *Populus* along streams [16].

P. schrenkiana is a perennial tree up to 40 m high with a narrow cylindrical crown. The bark is dark grey, the branches are often hanging, the young branches are bare. Leaves (needles) are 4-sided, sharp, 2-3.5 cm long. The leaves of many coniferous plants live for several years. For example, *P. schrenkiana* has a leaf life span of 26-28 years. They are adapted to insufficient water supply, especially in winter, and sharp fluctuations in summer and winter temperatures. Therefore, the leaves of most conifers have a xeromorphic structure: they are hard, small, with a small evaporating surface [17]. We looked at young needles anatomy from 5 populations of *Picea schrenkiana*.

Chenopodiaceae Vent. family of more than 100 related and about 1600 species of large family. The family includes herbaceous, shrubby, and even woody plants. A representative of the main tree belonging to the *Chenopodiaceae* family *Haloxylon* Bunge. There are 5 species of saxaul growing all over the world [2]. In Kazakhstan, you can find 3 species of saxaul, this is *Haloxylon aphyllum* (Minkw.) Iljin, *Haloxylon persicum* Bunge ex Boiss. et Buhse and *Haloxylon ammodendron* (C.A. Mey.) [8].

The main forest-forming representative of the desert and semi-desert zones of Kazakhstan is the saxaul tree. Especially in the Ili-Balkhash region of the country, the number of saxaul forests prevails. There is also a shrub 1.5 m high or a woody species that reaches up to 12 m. Branch consists of young fragile shoots. The leaves of the saxaul are reduced, formed by a small colorless film, and the functions of photosynthesis are performed by green shoots consisting of chlorophyll [18].

Desert plants that grow in arid conditions for many years usually have a high convergent adaptation over time and have similar internal structure, morphology, and physiological characteristics. The relative *Haloxylon* has many similarities in the morphological structure of leaves, stems, and fruits.

There is a difference in the types of life forms and environmental conditions of growth. 3 species found in Kazakhstan are halophyte and psammophyte adapted to salty and alkaline soil cover [19].

According to scientists, biomorphology are megaphanerophytes desert with differentiated shoots, deprived of saxaul. The main morphological differences are their leaves, shoots fall in the summer. Fallen plant parts form the main layer of soil cover. The loss of leaves and branches is characteristic of the black saxaul, so it is characterized as a portable ecological plant. Characteristic features of xerophyte, halophyte and mesophyte black saxaul, growing in semi-desert grove and sandstones. Black saxaul, which are halophytes, growing in the old river valleys, takyric soils in reinforced sands. The psammophyte white saxaul, which grows in the sandy deserts and sandstones. In turn, the Zaisan saxaul grows in Eastern Kazakhstan, on eroded soils, clay, and saline soils.

As you know, the generally recognized feature that arose in the course of an evolutionary process adapted to the dry state of the environment is the reduction of the sheet board. The mesophyll layer of vegetation increases, especially stem tissues develop strongly, so the soil resists drought. With increasing density and layers of columnar tissues, the area of photosynthetic organs is significantly reduced. On the other hand, in a small area of a flat surface, photosynthetic plants must provide themselves with plastic substances. This is influenced by the colonial parenchyma developing on both sides of the escape. Since columnar tissue is the most productive type of tissue and the tissue that makes the main contribution to the process of photosynthesis [18; 20].

Thus, the aim of our research is to study the anatomical structure of the young needles of *P. schrenkiana* and green shoots of *Haloxylon* species in Kazakhstan.

Materials and methods

Plant material of Picea schrenkiana Fisch et C.A. Mey. The object of the study is five populations of *Picea schrenkiana* Fisch et C.A. Mey., including the dwarf form (*P. schrenkiana* Fisch et C. A. Mey. f. prostrata K. Isakov) were collected to study the anatomical structure of needles in Trans Ili Alatau range of Northern Tian Shan Mountains (Figure 1).
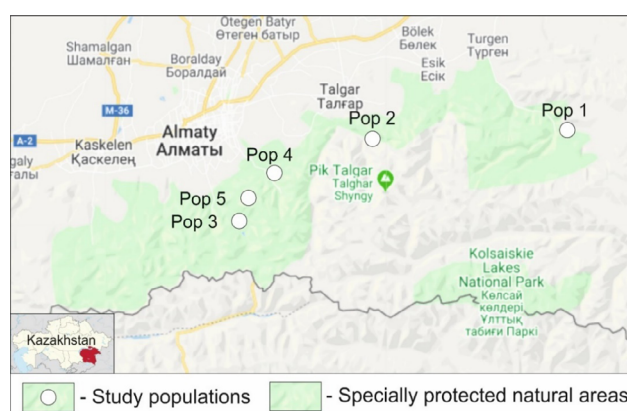
Figure 1 – Location of the collected
Picea schrenkiana populations

Young needles of *P. schrenkiana* were collected randomly (Figure 2), with the distance between plants of not less than 100 meters.
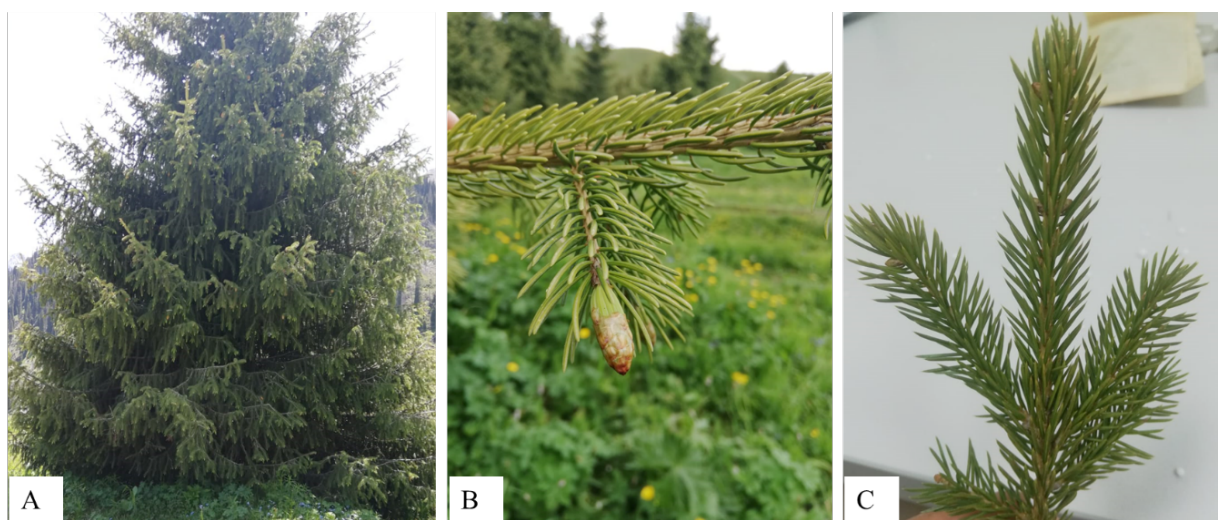
Figure 2 – Young needles of collected *Picea schrenkiana*. Note: A – general view, B, C – young needles of *P. schrenkiana*

GPS coordinates of the collected populations are given in Table 1. For the study, 3 samples were taken from each population.

Plant material of Haloxylon species. The second object of the study is representatives of the genus *Haloxylon* from the family *Chenopodiaceae* – *Haloxylon aphyllum*, *Haloxylon persicum* and *Haloxylon ammodendron*, living on the territory of Kazakhstan, collected from three regions of Kazakhstan. *Haloxylon aphyllum* was collected from the Western Kazakhstan, *Haloxylon persicum* was collected from the South-East of Kazakhstan and *Haloxylon ammodendron* was collected from the East of Kazakhstan.

Table 1 – The information on five populations of *Picea schrenkiana* collected in Northern Tian Shan Mountains in South-East of Kazakhstan

Species	Population	Geographic coordinates	Altitude (m a.s.l)	Place of collection
P. schrenkiana Fisch. et C. A. Mey.	Pop 1	N 43.23639 E 77.76528	1694	Turgen gorge
	Pop 2	N 43.2215 E 77.30733	1730	Talgar gorge
	Pop 3	N 43.08083 E 76.99314	2160	Big Almaty gorge
	Pop 4	N 43.16275 E 77.07678	1919	Kim Asar gorge
P. schrenkiana Fisch et C. A. Mey. f. prostrata K. Isakov	Pop 5	N 43.12857 E 77.01357	2830	Big Almaty gorge, Tri brata rocks
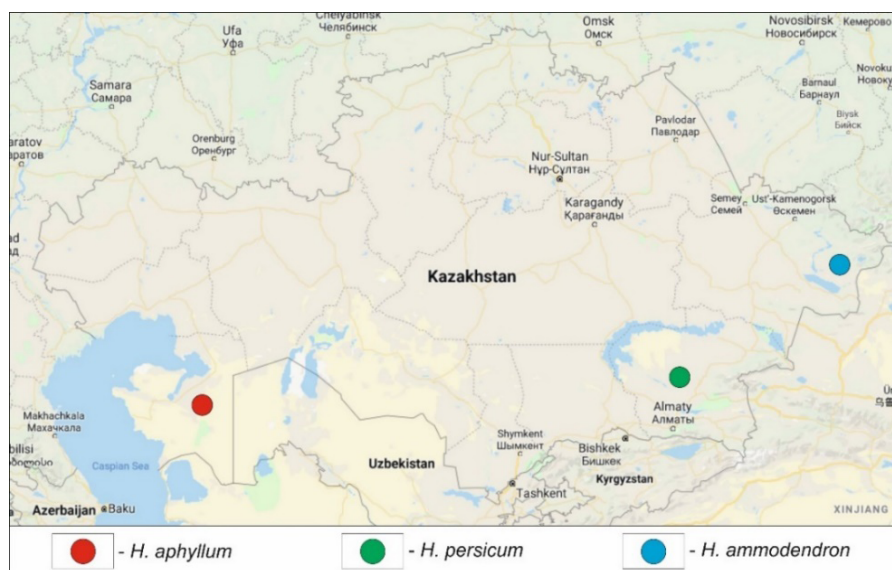
Figure 3 – Map of *Haloxylon,* collected from three regions

Young, annual, green shoots of three species of saxaul were collected from three regions of Kazakhstan.

Methods of research. The route reconnaissance surveys in the mountains of the Northern Tien Shan of the Almaty region, five populations of *P. schrenkiana* were found: Pop 1 – Turgen gorge, Pop 2 – Talgar gorge, Pop 3 – Big Almaty gorge, Pop 4 – Kim Asar gorge, Pop 5 – Big Almaty gorge, Tri brata rocks. Also, as a result of route – reconnaissance surveys, three *Haloxylon* species were collected from three regions of Kazakhstan. *Haloxylon aphyllum* was collected from the Ustyurt plateau, *Haloxylon persicum* was collected from the

Balkhash area, *Haloxylon ammodendron* was collected from the Zaisan basin. For further morpho-anatomical studies, herbarium and fixed specimens were collected. Preservation of plants was carried out according to the method of Strasburger-Fleming [21]. Anatomical preparations are made in accordance with generally accepted methods Prozina M.N. (1960), Permyakov A.I. (1988), Barykina R.P. (2004) [21-23]. Anatomical sections of the needles of *P. schrenkiana* and young green shoots of *Haloxylon* were made using the microtome MZP-01

"Technom". The thickness of the anatomical sections was 10-15 μm. Temporary preparations were enclosed in glycerin. Microphotographs of the anatomical sections were taken on an MC 300 microscope with a CAM V400/1.3M video camera. Measurements of micropreparations were carried out on an MCX100 microscope with a 519CU 5.OM CMOS Camera. The statistical processing of morphometric indicators was carried out using the Microsoft Office Excel 2003 program based on the G.F. Lakin (1990) [24].
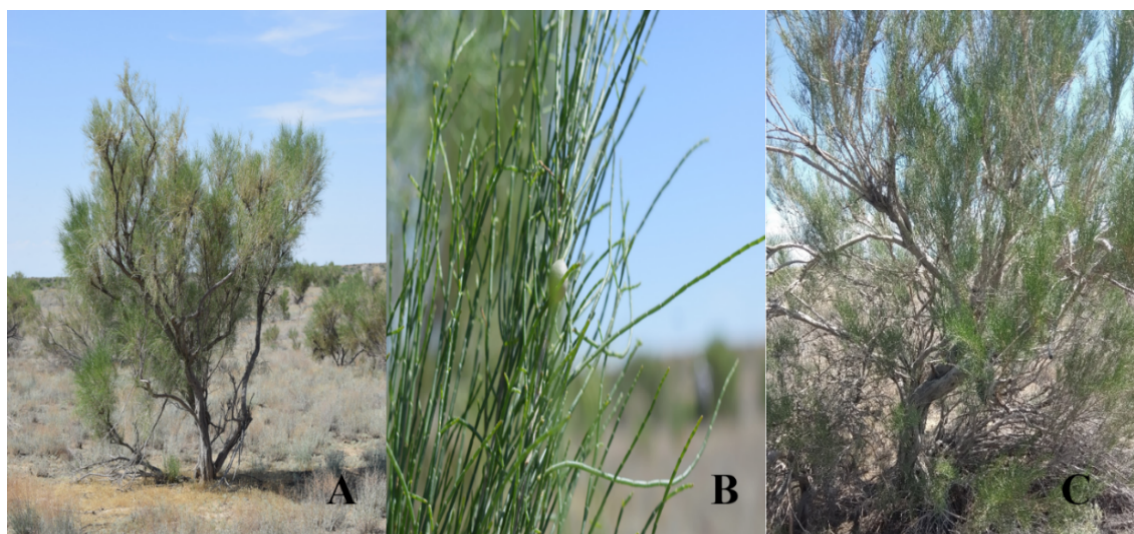
Figure 4 – Photos of *Haloxylon*. Note: A-*Haloxylon persicum*,
B-young shoots of *Haloxylon persicum*, C-*Haloxylon ammodendron*

Table 2 – The information of *Haloxylon* collected in three region of Kazakhstan.

Genus	Names of species	Geographic coordinates	Altitude (m a.s.l.)	Place of collection
Haloxylon Bunge	*Haloxylon aphyllum* (Minkw.) Iljin	N 43.31897 E 54.48114	163	West Kazakhstan, The Ustyurt plateau
	Haloxylon persicum Bunge ex Boiss. et Buhse	N 44.41077 E 76.45582	410	South-East Kazakhstan, The Balkhash area
	H.ammodendron (C.A. Mey.) Bunge	N 48.13066 E 84.30375	444	East Kazakhstan, Zaisan basin

Results and discussion

Results of anatomical studies of P. schrenkiana. The results of anatomical studies, cross sections were made from each population with a thickness of 10-15 μm. In the cross-section of *P. schrenkiana* needles, all five populations have a rectangular shape, and the tissue types and their location are similar in all populations.

In the next stage of research, the internal structure of needles from each population was studied. The needles are covered with primary integumentary tissue – the epidermis, the cells of which are tightly closed together and arranged in a row, without intercellular spaces (Figure 5). The width of the epidermal cells significantly exceeds the height. The outer wall of epidermal cells kutinized. There is a well-devel-

oped hypodermic layer under the epidermis. Under the hypodermis is a mesophyll consisting of homogeneous cells. The cell walls sometimes grow into the cell cavity, forming folds (folded parenchyma). This significantly increases the area of the cytoplasm layer adjacent to the wall with chloroplasts, and, consequently, the assimilating surface. Stomata are located on the entire surface of the leaf. Their closing cells are located at the hypodermic level, under the nearly stomato cells. Stomata cells are very large, with strongly thickened outer walls. The stomatal apertures leads to a sub-stomatal air cavity surrounded by mesophyll cells. The mesophyll is homogeneous, folded. Folds occur due to the ingrowth of the inner layers of the shell into the cell cavity, which thus acquires a lobed shape. Due to the folds, the surface of the wall layer

of the cytoplasm containing chloroplasts increases. Mesophyll cells are tightly connected, the intercellular spaces between them are very small.

Characteristic of coniferous plants in needles, the vascular bundle is surrounded by an endodermis. On the radial walls of the endodermis cells, there are lignified thickenings – Caspari spots. Along the centers are vascular bundles consisting of xylem and phloem. Between the endodermis and the vascular bundles is a transfusion tissue consisting partly of dead cells of irregular shape with bordered pores that transmit water from the xylem of the conducting bundle to the folded parenchyma, and partly of living parenchymal cells that transmit organic substances produced by the chlorenchyma to the phloem of the vascular bundle.
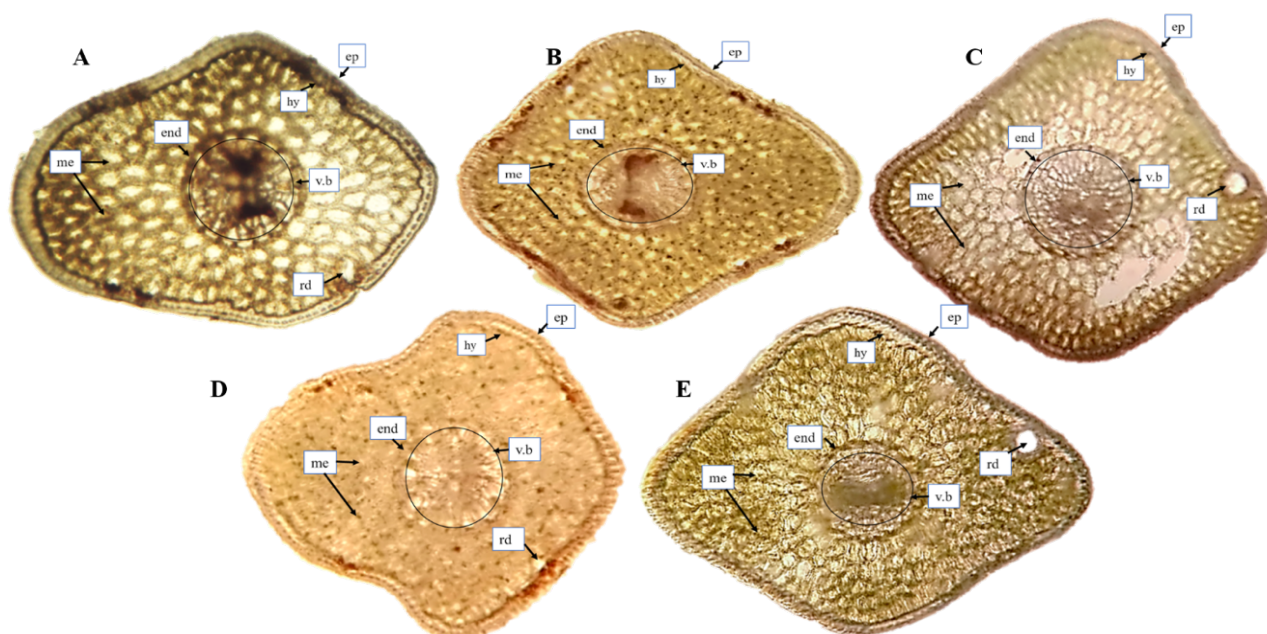
Figure 5 – Cross section (CS) of 5 population of *P. schrenkiana* (A – Pop 1, B – Pop 2, C – Pop3, D – Pop 4, E – Pop 5).
Note: ep – epidermis, hy – hypodermis, end – endodermis, v.b – vascular bundle, rd – resin duct, me – mesophyll

All conifers in the folded parenchyma have a large resin ducts running along the needles and covered with a cover of mechanical fibers (sclerenchyma). The number and location of resin ducts play an important diagnostic role in determining species based on the anatomical structure of needles. In our case, all populations of *P. schrenkiana* had resin ducts. Resin ducts that penetrate the folded parenchyma are lined inside with thin-walled cells that secrete resin inside, and outside they have a lining of thick-walled cells (Figure 5).

As a result of statistical processing of morphometric indicators, the thickness of the epidermis varied from 15.7 ± 2.2 μm (Pop 1) to 34.8 ± 0.9 μm (Pop 3). The epidermis is well protected from the effects of adverse environmental factors by a thick layer of wax coating. Moreover, in many species, the raid is so thick that the needles acquire a blue hue. The thickness of the hypodermis ranges from 7.8 ± 1.7 μm to 22.9 ± 4.4 μm. The area of the vascular bundles varies from 141.4 ± 1.9 to 182.7 ± 1.4 μm². And shows that the area of the vascular bundles in popula-

tion 3 is greater than 20-40 μm² compared to other populations. The thickness of the endodermis ranged from 11.7 ± 2.2 μm to 14.4 ± 1.1 μm. When studying the anatomical structure of needles, it was found that needles of the Pop 1 have a less thick thickness of the epidermis. The size of the vascular bundles in individuals in Pop 3 is larger than in other populations (Figure 6).
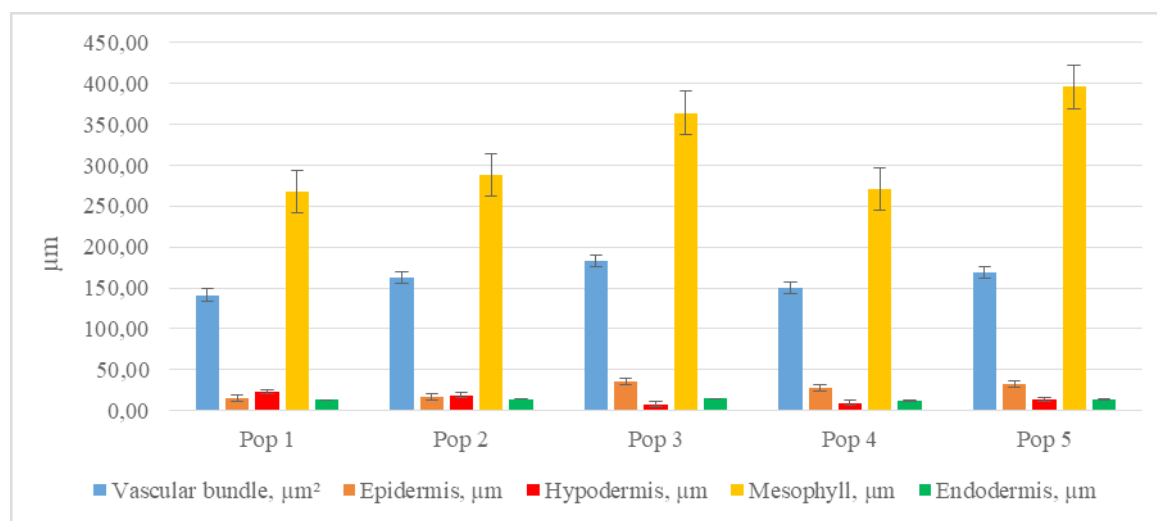
Figure 6 – The data of anatomical structure of needles in 5 populations of *Picea schrenkiana*

The anatomical structure of *P. schrenkiana* needles corresponds to the structure of coniferous plants. It should be noted that the anatomy of the leaves of all populations is clearly traced by the characteristic coniferous and xerophytic features. Some anatomical features, such as the shape of the cross section, the thickness of the epidermis, the location, nature and number of resin ducts, and the distribution of stomata can be key features for distinguishing species.

Results of anatomical studies of Haloxylon species. To identify anatomical similarities and differences between the black saxaul, white saxaul, and Zaisan saxaul, a horizontal segment was developed from the young green shoots of the saxaul. According to the obtained anatomical analyses, the cross section of young saxaul consists of the cuticle, the epidermis layer, calcium oxalate salts, the sclerenchyma, the cambium layer, the conducting layer, the primary shell, the central circle, and the conducting bundles. In the context of each type of saxaul, there is a difference. The diagram shows the average value of 3 segments. We measured the diameter of the shoots, the thickness of cuticle, thickness of epidermis, length of the primary shell, the diameter of the central circle and the volume of the vascular bundle.

The average diameter of the young shoot of *Haloxylon ammodendron* and *Haloxylon aphyllum* ex-ceeds 600 μm, and the diameter of the shoot of *Haloxylon persicum* is 515.48±23.4 μm. In the Balkhash district of Almaty region, there is a high temperature compared to other areas of the environmental survey. Due to the lack of moisture in the white saxaul (*Haloxylon persicum*), the greatest narrowing of shoots was observed. *Haloxylon ammodendron* and *Haloxylon aphyllum* are succulent, succulents. Since the cuticle does not give the plant excessive evaporation, its thickness is important, the study found that the cuticle thickness of *Haloxylon persicum* was 6 mm thicker than *Haloxylon ammodendron* and *Haloxylon aphyllum*. Therefore, because of the thin layer of the cuticle of the white saxaul, the transpiration process is intense and indicates the cause of the thin escape. The thickness of the epidermis also has the lowest index in the white saxaul, where 18.14±3.5μm is respectively the highest index in the black saxaul 27.56±3.5 μm. The thickness of the primary cortex, on the contrary, in the Zaisan saxaul is thick 114.19±2.6 μm, in the white saxaul 107.40±6.7 μm, in the black saxaul 103.65±15.5 μm. The average cylinder diameter in the black saxaul and Zaisan saxaul was 300 μm, and in the white saxaul 215.33±23.3 μm. The volume of the conducting beam located in the phloem and xylem was about 40% in the black saxaul and Zaisan saxaul, and in the white saxaul the values are 2 times less.
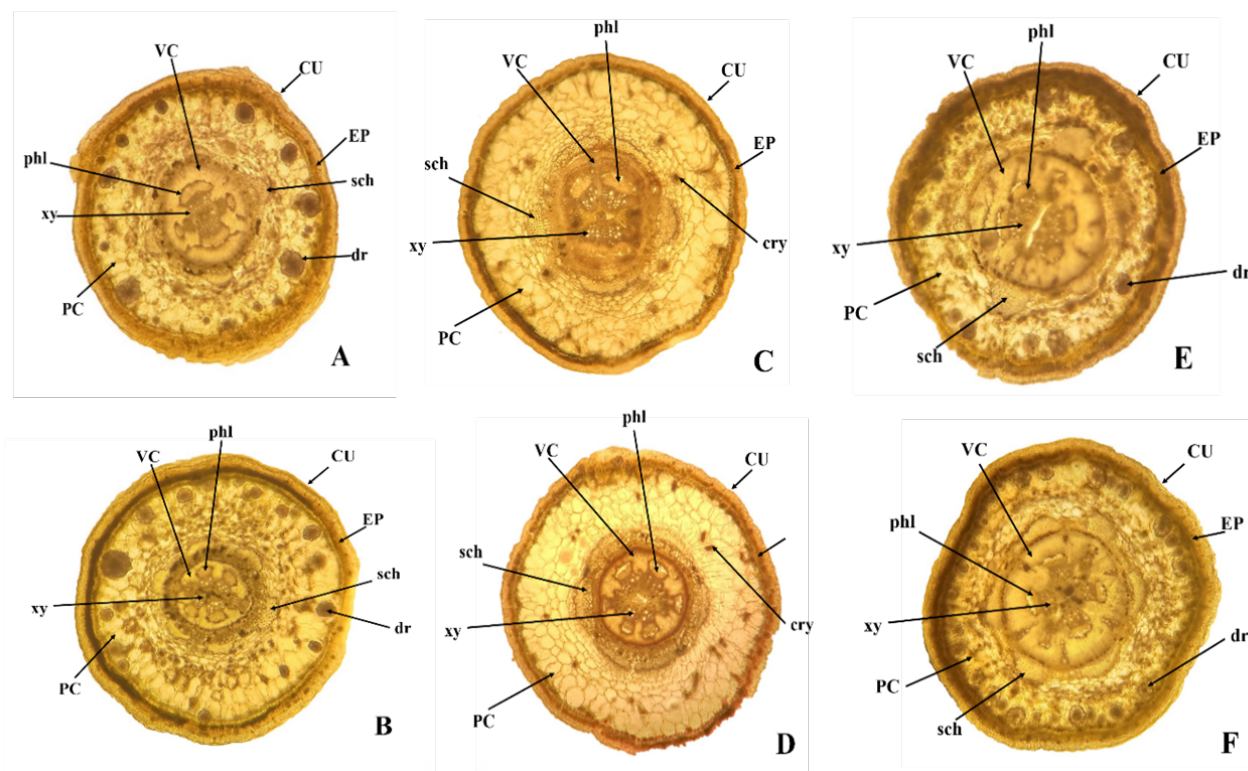
Figure 7 – *Haloxylon persicum (A,B), H.ammodendron (C,D)* және *Haloxylon aphyllum (E,F)*
comparative anatomy of annual shoots. CU-cuticle, EP-epidermis, VC-conducting cylinder,
PC-primary cortex, xy-xylem, phl-phloem, sch-sclerenchyma, dr-druses of salts, cry-calcium oxalate crystals
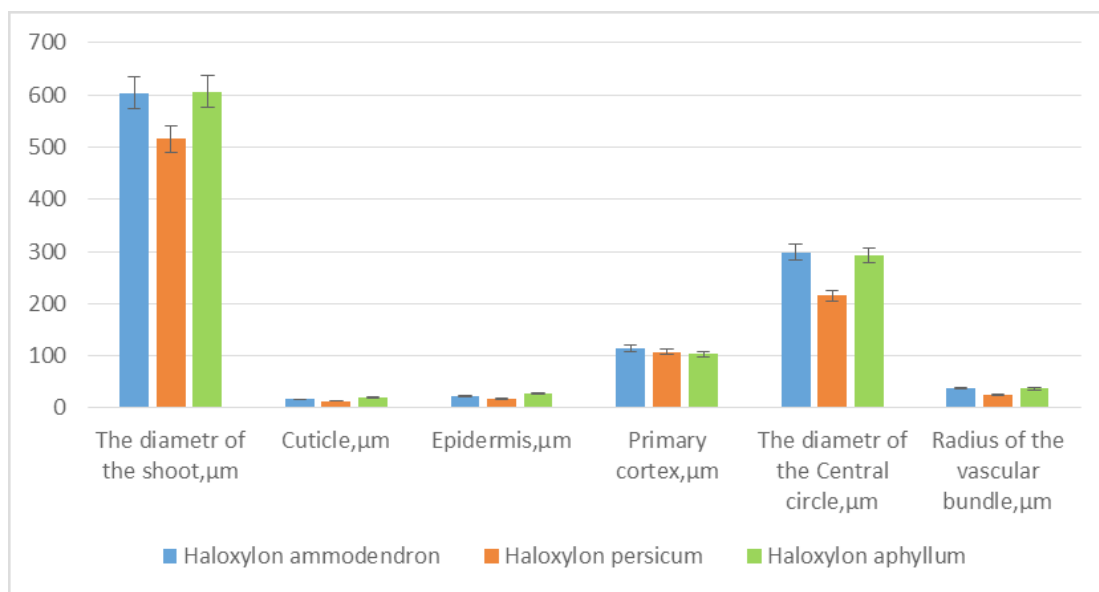
Figure 8 – Data from anatomical analysis of three species of saxaul

In the black saxaul, the crystals are located in the lower part of the epidermis. But the crystal concentrates are crushed in comparison with the crystals of white saxaul. Scientists have developed the concept that these crystals are crystals of calcium oxalate salts [25].

In the anatomical structure of saxaul shoots, a large number of crystals indicates that it grows in a salty area. The mineralization of groundwater can withstand up to 40 g/L and since sodium belongs to the group of alkaline plants [26], the crystals contain more black saxaul than white saxaul.

Conclusion

In conclusion, it should be noted that the anatomy of the needles of all populations is clearly traced by the characteristic coniferous and xerophytic features. Certain anatomical features, such as the shape of the cross section, the location of the subcutaneous tissue, the location, nature, and number of resin ducts, and the distribution of stomata may be key features for distinguishing species. Anatomical data is useful for the systematic study of conifers, and this study has provided potential results for systematic and phylogenetic studies of *Picea*. Similar studies on other species will help clarify the phylogenetic relationships between populations in each species and between species [27].

The following conclusions were made during the analysis of the anatomical structure of the saxaul. The morphometric index of the *Haloxylon ammodendron* and *Haloxylon aphyllum* plants is much higher than that of *Haloxylon persicum*. The anatomical structure of the saxaul species, the location of the phloem and xylem are similar. The location of the crystal salts can be clearly seen from the horizontal section. In the Zaisan saxaul, salt crystals are located in the center of the shell. The shapes are round, small crystals in the form of eggs. In the white saxaul, the crystals are large, several crystals form a druze. The crystals are located in the lower part of the epidermis. Thus, according to the results of studies, it is possible to determine the type of plants by their anatomical sections, by the presence and location of crystals of calcium oxalate and other salts. These results can be used to find out under what environmental conditions this plant grew.

Acknowledgements

References

1   Radionov A. (2013). The states of forest genetic resources in the SEC region, the Republic of Kazakhstan country report, Ankara, FAO, 131 p.

2   Pavlov N. (1960). Flora of Kazakhstan [Flora Kazahstana], Alma-Ata: AS KazSSR, vol. 3, 477 p.

3   Farjon A. (2001). World Checklist and Bibliography of Conifers. 2nd ed., Kew Royal Botanical Garden, 309 p.

4   Hart J.A. (1987). A cladistic analysis of conifers: preliminary results. J. Arnold Arboretum, vol. 68, pp. 269-307.

5   Ghimire B., Lee C., Yang J., Heo K. (2015). Comparative leaf anatomy of some species of Abies and Picea (Pinaceae). Acta Bot. Bras., vol. 29, no. 3, pp. 346-353. https://doi.org/10.1590/0102-33062014abb0009.

6   Frankis M.P. (1988). Generic inter-relationships in Pinaceae. Notes from the Royal Botanic Garden, Edinburgh, vol. 45, pp. 527-548.

7   Farjon A, Rushforth K.D. (1990). A classification of Abies Miller (Pinaceae). Notes from the Royal Botanic Garden, Edinburgh, vol. 46, pp. 59-79.

8   Abdulina S.A. (1998) Checklist of vascular plants of Kazakhstan [Spisok sosudistyh rastenij Kazahstana]. Ed. by R.V. Kamelin, Almaty, 187 p.

9   Wright J.W. (1955). Species cross ability in spruce in relation to distribution and taxonomy. Forest Science, vol. 1, pp. 319-340.

10   Taylor R.J, Patterson T.F. (1980). Biosystematics of Mexican spruce species and populations. Taxon., vol. 29, no. 4, pp. 421-469.

11   Rehfeldt G.E. (1994). Adaptation of Picea engelmannii populations to the heterogeneous environments of the Intermountain West. Can. J. Botany, vol. 72, pp. 1197-1208.

12   Baitenov M.S. (2001). Flora of Kazakhstan [Flora Kazahstana]. Genus complex of flora. Almaty, Gylym, vol. 2, p. 17.

13   Kozhevnikova N.D. (1983). Biology of the Schrenk spruce (Picea schrenkiana Fisch et. Mey [Biologija Eli Shrenka (Picea schrenkiana Fish et. Mey)]. Summary of thesis, Moscow, 41 p.

14   Magnuszewski M., Nowakowska J. A., Zasada M., Orozumbekov A. (2014). Genetic characteristic of schrenk spruce (Picea schrenkiana) in the altitudal and geographical gradient in kyrgyz part of Tien-Shan mountains, Sylwan, vol. 158, no. 5, pp. 361-369.

15   The Red Book of Kazakhstan (plants) [Krasnaja kniga Kazahstana (rastenija)] (2014). Astana, vol. 2, 452 p.

16   The IUCN Red List of Threatened Species. Version 2019-3. http://www.iucnredlist.org. Downloaded on 10 December 2019.

17   Pavlov N. (1956). Flora of Kazakhstan [Flora Kazakhstana], Alma-Ata, AS KazSSR, vol. 1, p. 66.

18   Zhaglovskaya A., Aidosova S., Akhtayeva N., Mamurova A., Yesimova D. (2015). Anatomical and Morphological Stem Features of two Haloxylon Species (Chenopodiaceae Vent.) of Drought Stress, Kazakhstan. Biosciences, Biotechnology Research Asia, vol. 12, pp.1965-1974. https://doi.org/10.13005/bbra/1863.

19   Li C., Shi X., Mohamad O.A., Gao J., Xu X., Xie Y. (2017). Moderate irrigation intervals facilitate establishment of two desert shrubs in the Taklimakan Desert Highway Shelterbelt in China. PLoS One, vol. 12, no. 7. https://doi.org/10.1371/journal.pone.0180875

20   Li Y., Ma X., Zhao J., Xu J., Shi J., Zhu X-G., et al. (2015) Developmental Genetic Mechanisms of C4 Syndrome Based on Transcriptome Analysis of C3 Cotyledons and C4 Assimilating Shoots in Haloxylon ammodendron. PLoS One, vol. 10, no. 2. https://doi.org/10.1371/journal.pone.0117175.

21   Baryikina R.P. et al. (2004) Reference book on botanical microtechnology. Basics and methods [Spravochnik po botanicheskoy mikrotehnike. Osnovyi i metodyi], p. 312.

22   Prozina M.N. (1960). Botanical microtechnics. [Botanicheskaja mikrotehnika]. Moscow, Vysshaja shkola, 207 p.

23   Permyakov A.I. (1988) Microtechnics [Mikrotehnika]. MSU Publ., p. 58.

24   Lakin G.F. (1990) Biometrics [Biometriya]. Moscow, Vysshaja shkola, p. 352.

25   Al Sahli A., Doaigey A., El Sheikha A., El-Zaidy M. (2015). Anatomical adaptations of two Haloxylon species for drought tolerance. Bothalia, vol. 45. pp. 47-57.

26   Rodin L.E. (1963). Vegetation of the deserts of Western Turkmenistan [Rastitel'nost' pustyn' Zapadnoj Turkmenii], pp. 89-124.

27   Turuspekov Y., Abugalieva S. (2015) Plant DNA barcoding project in Kazakhstan. Genome. vol. 58, no. 5, p. 290.

N. Favarisova [iD] , A. Kusmangazinov [iD] , D. Karelova [iD] ,

M. Yermagambetova [iD] , S.I. Abugalieva* [iD]

Institute of Plant Biology and Biotechnology, Almaty, Kazakhstan
*e-mail: absaule@yahoo.com

Optimization of PCR conditions for *Agriophyllum, Haloxylon* and *Salsola* microsatellite markers

Abstract. Microsatellites or Simple Sequence Repeat (SSR) are among the most informative and popular types of molecular markers for assessment of genetic diversity, population structure, construction of genetic maps, phylogenetics, phylogeography, systematics, etc. Hence, for reliable inference of results, optimization of various conditions involved in polymerase chain reaction (PCR) is a pre-requisite. The usage of the essential PCR components in optimal concentrations, as well as PCR conditions, determines the success of amplification. The present study was carried out to optimize conditions of PCR for further assessment of the genetic diversity of eight species in genera *Agriophyllum*, *Haloxylon,* and *Salsola* that belong to the *Chenopodiaceae* Vent. family. The list of species includes *Agriophyllum squarrosum*, *Agriophyllum minus*, *Haloxylon aphyllum*, *Haloxylon persicum*, *Haloxylon ammodendron, Salsola arbuscula*, *Salsola arbusculiformis*, and *Salsola chiwensis*. These selected species are widespread in desert regions of Kazakhstan and have great importance for sand dunes fixing, animal feeding, and other purposes.
Key words: *Haloxylon*, *Agriophyllum*, *Salsola*, polymerase chain reaction, microsatellite markers.

Introduction

Climate change poses a challenge to the ecological environment, and dune migration may pose a severe hazard to settled and agricultural areas and are considered as one of the main factors causing desertification. Desertification has a notable impact on human economic and political stability, and in the long term, will threaten human survival and development. Global warming is increasing the prevalence of drought, drying up waterholes, and relocating local species. High temperatures increase the number of wildfires, which may alter landscapes eliminating trees and shrubs that are growing. Understanding of these vulnerabilities of desert plants and their communities can then be developed into technologies for conservation and restoration of the flora in dry regions. "At the heart of these complex problems are several key principals: (1) recognizing changes in plant species and communities and whether or not climate is the root cause, (2) understanding species vulnerabilities under climate change, (3) accurate prediction of the movement of plant communities to plan for the future, and (4) mitigating these changes by fostering regeneration or assisting the dispersal of appropriately adapted plant materials" [1].

In Kazakhstan, the most territory is the steppe (26%), semidesert (14%), and desert (up to 44%) areas. The prolonged droughts and strong winds in such areas are common, which affects the yield of agricultural land. The territory of the country is almost entirely part of the arid zone, and its two-thirds already subject to varying degrees of desertification [2].

The major representatives of wild flora in the desert are herbaceous plants, subshrubs, shrubs, and subtrees. In spring, a variety of ephemeris (up to 150 species) blooms in the deserts for a few weeks. Later on, after drought stress and increasing mean daily temperatures, xerophytes, and psammophytes dominate the landscapes, among others, many scrub species of the genera *Calligonum*, *Ammodendron* or *Aristida* [3]. One of the special features of sandy deserts is sites of saxaul thickets, mainly black saxaul (*Haloxylon aphyllum* Minkw.) Iljin and white saxaul (*Haloxylon persicum* Bunge ex Boiss. et Buhse), which are usually interspersed with *Tamarix, Salsola, Artemisia,* and many other plant species.

Haloxylon, Salsola, and Agriophyllum, belonging to *Chenopodiaceae* Vent. (*Amaranthaceae* Juss.) family of flowering plants, are represented by several species that grow in Kazakhstan and have importance for dunes fixing, animal feeding, water conservation, and other purposes. Plants of genus *Haloxylon* Bunge are psammophytic shrubs or small trees. Saxaul has a strong root system fixed in the sands, which can reach up to 8 m in height and, in exceptional cases, even more. Both black and white saxaul constitute the principal arboreal cover of the cold continental deserts of Central Asia, while white saxaul is a rain-fed shrub distributed on sand dunes. The former is a ground-water phreatophyte mainly found on alluvial terraces [4; 5]. Saxaul has an important role as a fodder plant, also used as firewood by local herders [6]. Black and white saxaul have a habitat-forming role, pasture protective, and economically importance. *Haloxylon ammodendron* (C.A. Mey.) Bunge is widely distributed across a range of habitats, including gravel desert, clay desert, fixed and semi-fixed sand, and saline land in Asian and African deserts [7]. For Kazakhstan, it is a rare species with habitat forming, soil protective, pasture protective significance.

Agriophyllum comprises six West and Central Asian species of annual herbs and belongs to the subfamily *Corispermoideae* [8]. Two species, *Agriophyllum squarrosum* (L.) Moq. and *Agriophyllum minus* Fisch. et C.A. Mey. grow in Western and South-eastern Kazakhstan [9]. Sand rice (*A. squarrosum)* is an annual shrub-like plant adapted to mobile dunes in the desert and semi-desert regions of Central Asia [10]. Sand rice has evolved many strategies to adapt to dune surface environment, including rapid root growth after germination, long hypocotyl, and pronounced drought and heat tolerance. It is a good candidate species for domestication to provide a food crop resilient to future climate change [10].

Salsola is a genus of the subfamily Salsoloideae in the family Chenopodiaceae. A common name of various members of this genus and related genera is saltwort, for their salt tolerance. *Salsola arbuscula* Pall. and *Salsola chiwensis* M.Pop. have great environmental importance since they perform sand-fixing and rock-strengthening functions. *S. arbuscula* is a widespread species in the desert regions of Central Asia [11]. *S. chiwensis* is listed in the Red Book of Kazakhstan (2014) as a rare endangered species (category II) occurring in the limited areas and suffers from livestock grazing [12]. *S. arbuscula*, *S. gemmascens* Pall., and *S. rigida* Pall. were used to improve and create long-term pastures in the sandy desert [13]. Also, *S. arbuscula* is used as a year-round feed by camels as well as winter feed by other animals. It is also applied as a fuel, for tanning leathers, and dye for wool.

Due to overgrazing and overexploitation for fuel during the past fifty years, the once-dominant saxaul and other desert species vegetation have considerably degraded [14]. It is important to develop and continue strategies for the conservation of plant genetic resources, combating desertification, measures to restore desert fertility, the reintroduction of rare and endangered native plant species. It is necessary to study the biodiversity of the desert plant species both on inter- and intraspecific levels in terms of preservation strategy and reintroduction of valuable and endangered species. For assessment the genetic diversity, phylogenetic relationships, for molecular taxonomy of wild species there is many various classes of widely used molecular markers, such as RAPD or Random Amplified Polymorphic DNA [15; 16], ISSR or Inter Simple Sequence Repeats [17], IRAP or retrotransposons [18], SSR or Simple sequence repeats [19-21], AFLP or Amplified Fragment Length Polymorphism [22; 23], SNP or Single Nucleotide Polymorphism [24; 25], DNA barcoding markers [9; 26-31]. Among listed markers, SSR markers, or microsatellites, are considered to be one of the most informative and reliable classes of PCR based DNA markers for genetic diversity studies, to estimate gene flow and crossing over rates, in evolutionary studies, above all to infer intraspecific genetic relations. Microsatellites have been the most widely used markers for genotyping plants over the past 20 years because they are highly informative, codominant, multi-allele genetic markers that are experimentally reproducible and transferable among related species. However, for reliable inference of the results of these studies, the optimization of various conditions involved in PCR amplification is a pre-requisite. The utilization of the essential PCR components in optimal concentrations, as well as conditions of amplification, determines the success of amplification.

High amplification success within and between genera in many groups of animals and plants indicates a great potential to use microsatellites and their flanking regions as a source of single- or low-copy nuclear sequences, as suggested by Zhang & Hewitt [32]. Sometimes flanking regions are highly conserved across taxa, allowing cross-species amplification of microsatellite loci from primers developed from other species in the same genus or even family. Since the flanking region of SSR loci are evolutionary well conserved, computational prediction of such

loci has practical significance. Such SSR loci can cater yo the need for molecular markers even in the absence of whole-genome sequence data. Thus, in cases when microsatellite markers have not been developed for a particular plant species a good alternative would be the use of a set of primers to obtain cross-species transferability. Barbará et al. [33] discussed the implications of these findings and close with an outlook on potential alternative sources of cross-species transferable markers. The potential for successful cross-species transfer appears highest in species with long generation times, mixed or outcrossing breeding systems, and where genome size in the target species is small compared to the source [33]. In the transferability or cross-amplification procedure, PCR primers developed for a studied (source) species are used to amplify microsatellites from closely [34; 35] or sometimes quite distantly related species [36].

SSRs can be developed from specific species and potentially used for related species, which lack the source of genome sequences to develop species-specific SSRs. Many reports are describing SSR markers that successfully developed and used for the genetic diversity studies of other species or genera of *Chenopodiaceae* (*Amaranthaceae*) family [7; 37; 38]. The aim of this study was the optimization of PCR conditions for microsatellite analysis to analyze the genetic diversity of desert plant species of three genera *Agriofillum*, *Haloxylon*, and *Salsola* in the family *Chenopodiaceae* using cross-species and cross-genus transferability.

Materials and methods

Plant materials. The objects of this study were wild desert species of three genera *Haloxylon*, *Salsola,* and *Agriophyllum,* which belong to Chenopodiaceae family: *Haloxylon persicum* Bunge ex Boiss. & Buhse, *Haloxylon aphyllum (Minkw.)* Iljin*, Haloxylon ammodendron* (C.A.Mey.) Bunge ex Fenzl*., Salsola arbuscula* Pall.*, Salsola arbusculiformis* Drobow, *Salsola chiwensis* M.Pop.*, Agriophyllum squarrosum* (L.) Moq and *Agriophyllum minus* Fisch. &Mey.

Three populations of *A. squarrosum* and one population of *A. minus* were sampled in Moyynkym Sands in Zhambyl region on South-east Kazakhstan [9]. Three *Salsola* species were collected in Mangistau region of Western Kazakhstan (by Dr. A. Imanbayeva, Mangyshlak Experimental Botanical Garden), populations of three *Haloxylon* species both in Western (by Dr. A. Imanbayeva) and south-eastern parts of Kazakhstan.

The samplings of the wild species plant material were done in the framework of the Program 0237 (2015-2017) and project AP05131621 (2018-2020) supported by MES RK [27] and the International collaborative project REF: 2016YFE0203400 (2018-2020) by Chinese Ministry of Science and Technology.

Young leaves of collected plant material dried in silica gel were used for DNA extraction.

DNA extraction. The total genomic DNA was isolated from the dry leaf tissues using CTAB (cetyl trimethylammonium bromide buffer) method [39].

The quality and concentration of extracted DNA was assessed on NanoDrop 2000 spectrophotometer (Thermo Fisher Scientific, USA) and observed for its intactness using 1% agarose gel electrophoresis.

The DNA concentration for all samples was normalized to 10-50 ng/µl for further analysis.

PCR amplification. PCR amplification using different SSR primer pairs for each above-mentioned species was performed in a thermal cycler Veriti (Thermo Fisher Scientific, USA). A temperature gradient was used via six innovative VeriFlex™ Blocks for precise control over PCR conditions optimization for each template-primer pair combination.

Presently, different software packages are available to calculate the melting temperature (T_m) as well as the annealing temperature (T_a) for a particular PCR reaction using particular Taq polymerase. Tm is a temperature at which half of the DNA strand denatured or opened.

In many cases, a known simple formula for Tm that usually works is:

$$T_m = 4 (G + C) + 2 (A + T)$$

Commonly, the appropriate annealing temperature is 5-7 °C lower than T_m. Still, it is just an assumption not correctly work all the time. Most of the time, this value is not optimal, and it is necessary to determine Ta empirically. Thus, it should be matched for a particular primer pair for particular conditions to get appropriate bands. For the most primers, the T_a between 55 °C to 65 °C should be ideal for PCR reaction, deviation of Ta above or below this range can cause non-specific bindings or reaction failure. If the T_a is too high, the primer can not bind properly to the template DNA. On the other side, if the annealing temperature is too low, it facilitates more bindings, more bands, and non-specific amplification during the PCR reaction.

Below is the information on primers and polymerase chain reaction conditions for three plant genera.

A. squarrosum and *A. minus*. Eighteen EST-SSR markers were selected from the list of 6150 SSR primer sequences derived from RNA_seq data of *A. squarrosum* genome reported by Zhang et al. [37]. Information on chosen primers concerning forward and reverse primers sequences, repeated motif, and expected size of amplified products are given in Table 1.

Primers had tri- (8), tetra- (5), and pentanucleotide (3) simple repeat motifs. There were compound repeats, which are composed of two successive sets of perfect repeats, such as $(CA)_6(AAT)_5$ and $(TTG)_6(TTC)_6$ (Table 1).

Table 1 – SSR markers developed for *A. squarrosum* [37] used in this study

Primer	F & R primers sequence (5'- 3')	Motif	Expected size (bp)*	Expected T_a (°C)**	T_a (°C)***
Ags02	F: AGCATCGGATGTGAGGAATC R: TCCTTCAACTCCTCCGTGTC	$(CAT)_6$	237	54-60	54
Ags03	F: AGGGAAATCAAGGGCTAGGA R: ATCCGACCTCTTACACGACG	$(CTT)_6$	280	54-60	60
Ags05	F: CTATGCCCATTCGTCATCCT R: GGCCGTTAGCTGAGTTGAAG	$(TCC)_6$	280	54-60	48
Ags07	F: AGGAGCAGCAGTAGAGGCAG R: CAACAGAAAAGAAGGCGGAG	$(AGC)_7$	242	54-60	54
Ags09	F: CAAGTTTTAATCTTTTAGCACCCTTT R: CCCCCTTTTCCCTCTTTCTA	$(AGA)_7$	280	54-60	54
Ags10	F: TTGGCTGTGGTTTGCATTTA R: AGAAGGCGTGAGCAATCTGT	$(GAT)_7$	280	54-60	54
Ags11	F: CCAATGCAGTGAATGTGGAG R: TCCTCTTTCTGGCCTTCTGA	$(CAG)_8$	217	54-60	54
Ags13	F: TTGGGAGTAGGGAAAAGAGGA R: GGAGGAGATGGTTGAAGCAC	$(TTG)_8$	275	54-60	48
Ags21	F: TCCTTCCCCTCTCACCTTCT R: TGTTTGGGAGGAGAAACTGG	$(TGTA)_5$	125	54-60	57
Ags22	F: AGTGGTGTTTGTTGCTGCTG R: ACTCCCTCACCCCTCACTCT	$(CTTT)_5$	124	54-60	54
Ags23	F: CAATGGGGTTTGAGCATTTC R: TTCCGGATGAATGATGGAAT	$(ATTA)_6$	254	50-56	54
Ags24	F: AAAGACAGGTCGTGAGTGGG R: AAAAACAGGTCTGATCCCCC	$(AGAT)_6$	108	54-60	51
Ags25	F: ACAACAAAATTGCCGAGGAC R: CGCCTCTCCCTCTTCTTTTT	$(AATC)_6$	279	48-54	42
Ags26	F: GAATTTTGATCGAAAAGGCG R: TCTCTCTCCTCCATTGCCAC	$(TTATT)_5$	185	48-54	54
Ags27	F: TTGGGCTACAACATTGGTGA R: GGCAGGTTACAACCTTTGGA	$(CCACT)_5$	182	54-60	45
Ags28	F: ACCAGCACCAAAACCTATGC R: ATAGCTGCTTCACGGTCGTC	$(AACCA)_5$	246	54-60	48
Ags29	F: TAAGTTCATCCTTGGCCCAT R: CCTCTTGCTGGACATGTGTTT	$(CA)_6(AAT)_5$	270	54-60	42
Ags30	F: TTGAGAGGGCTTGTTTGACA R: ACAATAACGACAACCCCAGC	$(TTG)_6(TTC)_6$	250	54-60	51

* – Zhang et al. [37]; ** – Expected T_a (°C) calculated by formula; *** – T_a (°C) – Annealing temperature, optimized in this study

All PCR reactions were performed in total 16 μl volumes, including 4 mM of each dNTP, 2mM of MgCl$_2$, 6.4 mM of primer mix (forward + reverse), 1.6 U of Taq polymerase and 10 ng of DNA.

The reactions were performed with an initial denaturation step at 94 °C for 3 min, followed by 40 cycles of 94 °C for 30 sec, T$_a$ °C for 45 sec and 72 °C for 1.5 min. The final extension step was at 72 °C for 10 min. Annealing temperature (T$_a$) for in-dividual primer pairs and a common concentration of reagents in a PCR reaction mix were determined empirically using Veriflex.

H. persicum, H. aphyllum, H. ammodendron. Ten primer pairs developed for *H. ammodendron* [7] were used for PCR optimization for further genetic diversity studies of this and other saxaul species. Table 2 contains the information on primers used in this study.

Table 2 – Characteristics of SSR primers developed for *H. ammodendron* [7] in this study for three *Haloxylon* species

Primer	Forward and reverse primers sequences (5′-3′)	Expected size (bp)[1]	Expected T$_a$ (°C)[2]	T$_a$ (°C)[3]	Alleles number[4]
Hal27760	F: AACTGCTGGGGATGGGAATG R: CAGCCCAATACTGCCCCTTT	242	62	58	7
Hal32182	F: AAAGGAGCAGAGTGAGTGCA R: TGCCTGCCTTTGTGTAGTGT	249	62	58	3
Hal42802	F: AACCCTAGAAAGCTTCGCCC R: TTTGGGAAAGCAGCGGAGAT	280	60	43	4
Hal45535	F: AACATCAACAGCGCCCACTA R: GGCCTATGATGCTGCACTCT	212	60	43	5
Hal47234	F: AACACAACATCCGCACCTCA R: GGATTTGGGTACGGGTCAGG	277	60	43	2
Hal60072	F: TGCACACACAGTTGCACTTG R: TGGGGTTTTGGGAGGAGAGA	268	60	62	3
Hal62940	F: TAACAACCGTGGCTGAAGCA R: GCGCGATGATGCCTTCTTTT	214	60	62	3
Hal63650	F: AAGAAGGTGGTGGTGGTTGG R: GCGGACGGTTGAAATTCACC	270	62	62	5
Hal64839	F: AAGAGGAAGACGAGGGTGGT R: TTGCGGAAGGAAAGTGGGAG	271	60	59	3
Hal65094	F: CTTGGAGCAGTGCCCTAGTG R: TTTGACTTCGGCGGCTACAT	277	60	53	3

Note: 1 – Long et al. [7]; 2 – Expected Ta (°C) calculated by formula; 3 – Ta (°C) – Annealing temperature, optimized in this study; 4 – Alleles number observed in this study

PCR was performed in a volume of 20 μL, containing genomic DNA (about 50 ng), 0.1 μM of each primer, 2 U Taq DNA polymerase (Fermentas, USA), 0.2 mM of each dNTP, MgCl$_2$ (1.5, 2.0 or 2.5 mM).

The PCR program consisted of denaturing the template DNA at 94 °C for 4 min, followed by 35 cycles, each at 94 °C for 30 s, T$_a$ for 45 sec, and 72 °C for 1 min, followed by 72 °C for 10 min. The annealing temperature for each primer pair was selected due to the gradient PCR conditions.

S. arbuscula, S. arbusculiformis and *S. chiwensis.* Eleven SSR markers developed for other plant genera/species in the *Chenopodiaceae* family [7; 37; 38] were used for *Salsola* species.

The common reaction mixture (10 μl) contained 3.7 μl ddH$_2$O, 1 μl Taq buffer, 1 μl dNTP, 1.2 μl MgCl$_2$, 2 μl primer, 0.1 μl Taq polymerase and 50 ng of genomic DNA.

The PCR was performed with an initial denaturation step at 94 °C for 3 min, followed by 35 cycles of 94 °C for 30 sec, T$_a$ °C for 45 sec and 72 °C for 1.5 min. The final extension step was at 72 °C for 10 min. The annealing temperature was individually optimized for each primer pair and varied from 43 °C to 58 °C.

Electrophoresis. The PCR products of wild species DNA were separated on 6% denaturing polyacrylamide gel (PAG) in 0.05M Tris-EDTA-borate

buffer, pH 8.0. The gel solution was applied to the assembled gel plates (0.35 mm thick) using the TV400-DGGE Sequencing electrophoresis apparatus (Scie-Plas, UK). The gels were stained with ethidium bromide, and SSR patterns images were captured using the GelDoc XR gel documentation system (Bio-Rad, USA). The size of the fragments was estimated based on a 100 bp ladder (Fermentas, USA).

Results and discussion

Considering the limited information on the new studied primers, and cross transferability of primers for related genera, the T_a for several sets of primer pairs was selected empirically as the result of gradient PCR on VeriFlex™ Blocks of Verity™ (Thermo Fisher Scientific, USA).

A. squarrosum and *A. minus.* Eighteen SSR primer pairs developed for *A. squarrosum* reported by Zhang et al. [37] with available information on the expected size of PCR product (Table 1) were used to optimize PCR amplification for two *Agriophyllum* species in our conditions. Figure 1 shows an example of PCR patterns of *Agriophyllum* samples as a result of T_a optimization for Ags21.

As shown in Table 1, T_a for primers with trinucleotide motifs was expected in the range of 54-60 °C. Due to the gradient, T_a for *A. squarrosum* and *A. minus* samples was different for three groups: 48 °C, 54 °C, or 60 °C, respectively. T_a for four primers with tetranucleotide repeated motif, was 42 °C for Ags25, 51 °C for Ags 24, and

54 °C for primers Ags22, and Ags23, and 57 °C Ags21, respectively. PCR product sizes were coincided with expected sizes for primers Ags03, Ags05, Ags11, Ags13, Ags16, Ags21, Ags25, Ags26, Ags27, and Ags29.
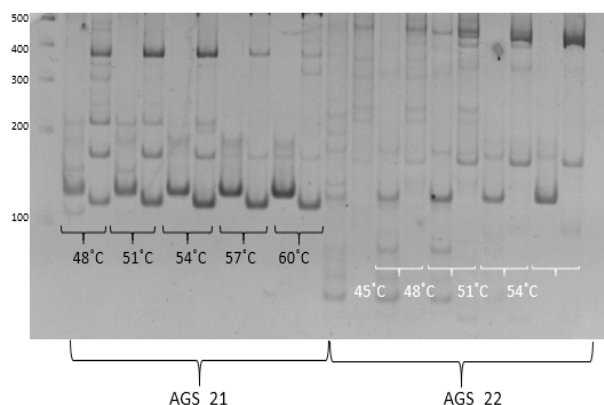
Figure 1 – Optimization of annealing temperature for Ags21 primers pair for *A. squarrosum* and *A. minus*

The optimized conditions were used for SSR analysis of populations of *A. squarrosum* and *A. minus* collected in the south-eastern region of Kazakhstan. Figure 2 represents SSR patterns on marker *Ags*26 of individuals representing different populations of these two species amplified on the 54 °C.

These conditions revealed distinguishing the species and individuals inside populations or species later on.
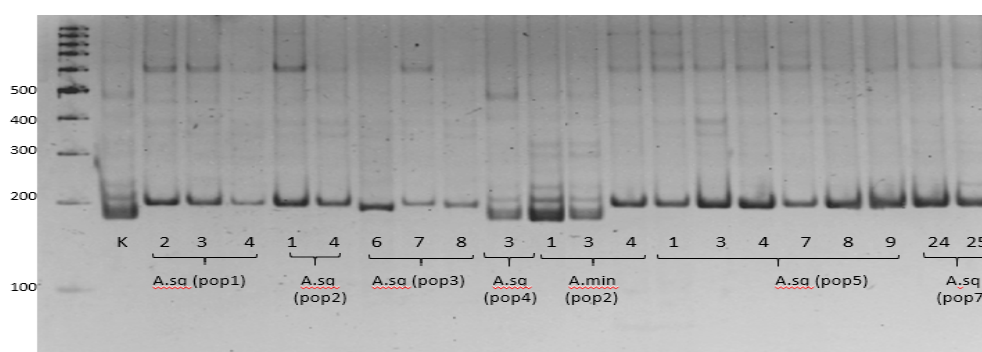
Figure 2 – SSR patterns of individuals of *A. squarrosum* and *A. minus* populations from Kazakhstan on SSR marker *Ags26*.
Note: M – 100 bp Molecular weight marker (Thermo Fisher Scientific), *A.sq – A. squarrosum, A.min – A.minus*

H. persicum, H. aphyllum, H. ammodendron. *H. persicum, H. aphyllum,* and *H. ammodendron* are closely related species in the genus *Haloxylon* of *Chenopodiaceae* (*Amaranthaceae* Juss.).

Several studies were conducted on genetic diversity studies of these species using molecular markers [40-42]. Few SSR markers have been reported for *Haloxylon* species, and their genetic

background is still poorly understood [42]. In this study, ten primer pairs of EST-SSR developed for *H. ammodendron* [7] were used for PCR optimization (Table 2) for further genetic diversity studies of intra- and interspecific diversity of three *Haloxylon* species. To optimize PCR conditions for these primers, the annealing temperature was set either to 40 °C, 43 °C, 46 °C, 50 °C, 53 °C, 56 °C, 59 °C or 62 °C (Figure 3).

a)

b)

*2, 5 – individuals of populations 2 (2-8) and
5 (5-3) of H. aphyllum*
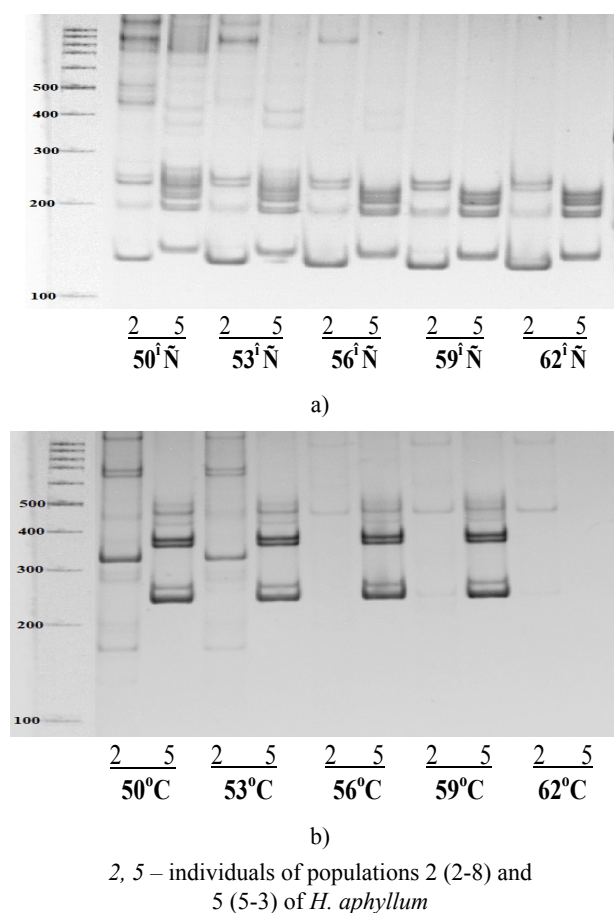
Figure 3 – Annealing temperature optimization using gradient PCR conditions (50-62 °C) on SSR primers *Hal64839* (a) and *Hal 65094 (b)* for *H. aphyllum*

The optimized annealing temperature for ten primer pairs allowed amplifying appropriate PCR products for three saxaul species and observing both intra- and interspecific diversity (data not presented). Figure 4 demonstrates the microsatellite patterns of individuals from populations of *H. ammodendron* and *H. aphyllum* on microsatellite markers *Hal65094* and *Hal64839,* which produced clear amplification of expected sized.

Preliminary data have shown from 2 to 7 alleles per locus while studying populations of three saxaul

genera from Kazakhstan (Table 2). Intra- and interspecific diversity of saxaul species will be determined.

Salsola. Transferability of SSR primers developed for other genera. Several reports described the development of microsatellite markers for use in genetic studies in different related genera and cross-genus transferability SSR primers [19; 42-45].

EST-SSR markers derived from transcribed regions of the DNA produce a higher rate of transferability, but less polymorphism [44]. Many EST-SSR primers were shown to be useful in discriminating different genera or species within a particular genus and genomes of the tribe *Triticeae* of the *Poaceae* [43]. Microsatellite markers derived from the functional parts of the bread wheat genome may be successfully used both in cultivated wheat and its wild relatives belonging to *Triticum-Aegilops* species for comparative genomics. Based on wheat genomic SSR markers, the transferability from wheat to rye was found to be only 17%; while, based on EST-SSR markers, the transferability from wheat to 18 *Triticum-Aegilops* species was found as 84% [43], and from Tall fescue (*Festuca arundinacea* Schreb.) to seven grass species was found to be nearly 92% [45].

As for genera of *Chenopodiaceae*, McGray et al. [19] reported that six of twenty SSR primer pairs previously developed for *Beta vulgaris* were found to be useful in molecular classification of five genetically distinct *Salsola* taxa [19]. The transferability (1.8%) of the SSR markers from the other related genera to genus *Haloxylon* was considerably low, suggesting a larger genetic divergence between taxa [42].

As no novel SSR loci have been reported for Salsola genus, in this study, we tested primers developed for the related species from the same family, namely for *Beta vulgaris, A. squarrosum,* and *H. ammodendron*. The PCR protocols were optimized using a particular primer pair is to change the T_a or the concentration of $MgCl_2$. PCR products with the usage of all studied primers pairs were successfully amplified. The information on the results of PCR amplification of Salsola species at varying annealing temperatures is given in Table 3.

Cureton et al. suggested T_a for sugar beet primer pairs (Bmb3 and Bmb4) used in this study [39] as 55 °C and 43 °C. In our study, the better T_a for Bmb3 and Bmb4 was 46 °C and 50 °C, respectively. McGray et al. [19] showed the successful usage of 6 out of 17 SSR *Beta* primer pairs in good amplification with yielding scorable PCR products and further genetic analysis of 5 Salsola taxa in California: *S. tragus, S. paulsenii, S. kali ssp. austroafricana, S. p. lax,* and Type C [19]. The authors reported that Bmb3 primers worked for all five taxa and revealed polymorphism within 5 species of *Salsola*, while Bmb4 failed to amplify *Salsola's* DNA.

populations of black saxaul.
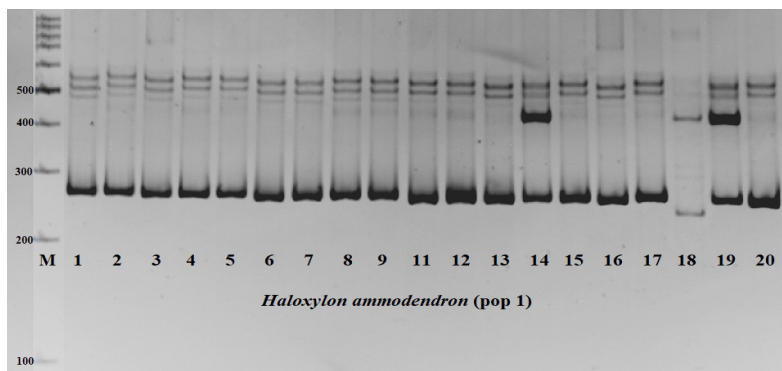
a)
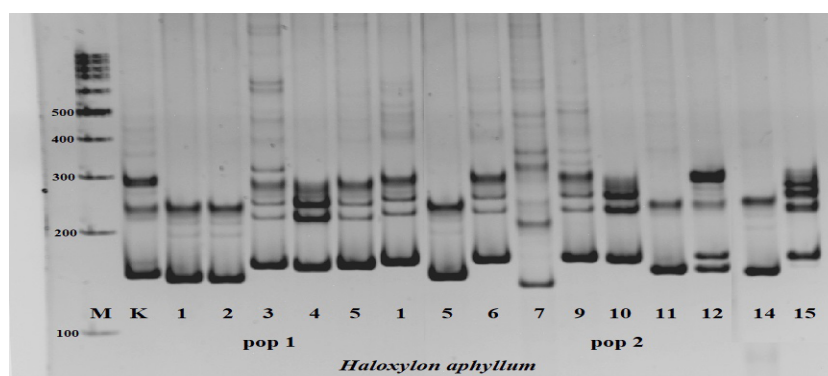
b)

Figure 4 – SSR patterns of individuals of *H. ammodendron* on SSR marker *Hal65094* (a) and
H. aphyllum (populations 1 and 2) on SSR marker *Hal64839* (b). Note: M – 100 bp Molecular weight marker
(Thermo Fisher Scientific), 1-20 – individuals of the population

Table 3 – Characteristics of SSR primers developed for *Beta vulgaris* (Bmb), *A. squarrosum* (Ags), and *H. ammodendron* for three Salsola species (*S. arbuscula, S. arbusculiformis*, and *S. chiwensis* in this study

Primer	F & R primers sequence (5'- 3')	Motif	Exp. size (bp)	T_a (ºC)	T_a (ºC)***	MgCl$_2$ (µl)	Alleles N
Bmb3	F: CGGTTGCAAGTCGATAAGGT R: CCGGTTGAACAGCAGAACAGG	(CA)$_{42}$	261*	55* 43**	46	3.6	4
Bmb4	F: CCTCTTTATTTCACGAGGTCCC R: CCCAGATTGAAATCAGGATCG	(CA)$_{13}$	212	55*	50	2.9	
Ags3	F: AGGGAAATCAAGGGCTAGGA R: ATCCGACCTCTTACACGACG	(CTT)$_6$	280	N/A	58	1.2	3
Ags9	F: CAAGTTTTAATCTTTTAGCACCTTT R: CCCCCTTTTCCCTCTTTCTA	(AGA)$_7$	280	N/A	46	1.2	3
Ags29	F: TAAGTTCATCCTTGGCCCAT R: CCTCTTGCTGGACATGTGTTT	(CA)$_6$(AAT)$_5$	270	N/A	46	1.2	3
Hal34975	F: AACTCGCCCATTATTGCACG R: AGAGGGTCAACGTCGTCAAC	N/A	235	N/A	43	1.0	2
Hal42802	F: AACCCTAGAAAGCTTCGCCC R: TTTGGGAAAGCAGCGGAGAT	N/A	280	N/A	43	1.0	3

Table 3 continued

Primer	F & R primers sequence (5'- 3')	Motif	Exp. size (bp)	T$_a$ (ºC)	T$_a$ (ºC)***	MgCl$_2$ (µl)	Alleles N
Hal45535	F: AACATCAACAGCGCCCACTA R: GGCCTATGATGCTGCACTCT	N/A	212	N/A	43	1.0	2
Hal47234	F: AACACAACATCCGCACCTCA R: GGATTTGGGTACGGGTCAGG	N/A	277	N/A	43	1.0	3
Note: * – Cureton et al.[39]; ** – McGray, 2008 [19]							

Determining the optimal concentration of different MgCl$_2$ concentrations (even for different primers from the same region of a given template) may have a large impact on the success of the PCR. For Bmb3 primers, two different MgCl$_2$ concentrations were reported to be optimal – 1.5 mM [39] and 3.6 mM [39], while no information was given on this matter for Bmb4 primers [19; 39]. In our case, the concentration 3.6 mM for Bmb4 was more suitable for the better PCR product yield, and less smearing on the gel. Examples of the SSR patterns of individuals of *S. arbusculiformis* on SSR marker *Ags*9 and *Bmb*3 are presented on Figure 5.

Salsola arbuscula, pop.2, K=1-18, *AGS-9* (Size=280), T=46°C
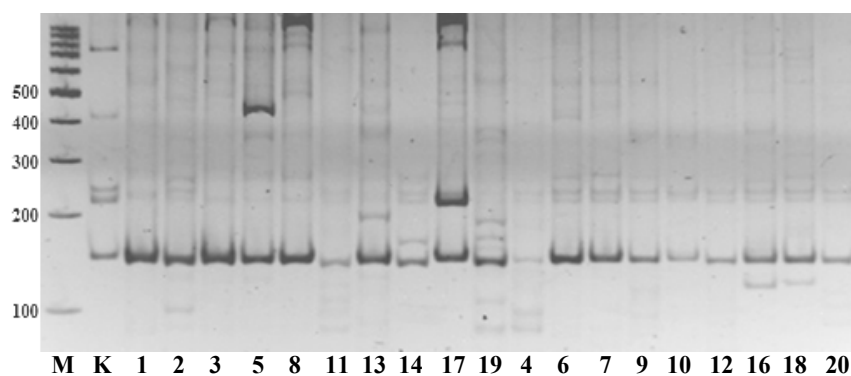
a)
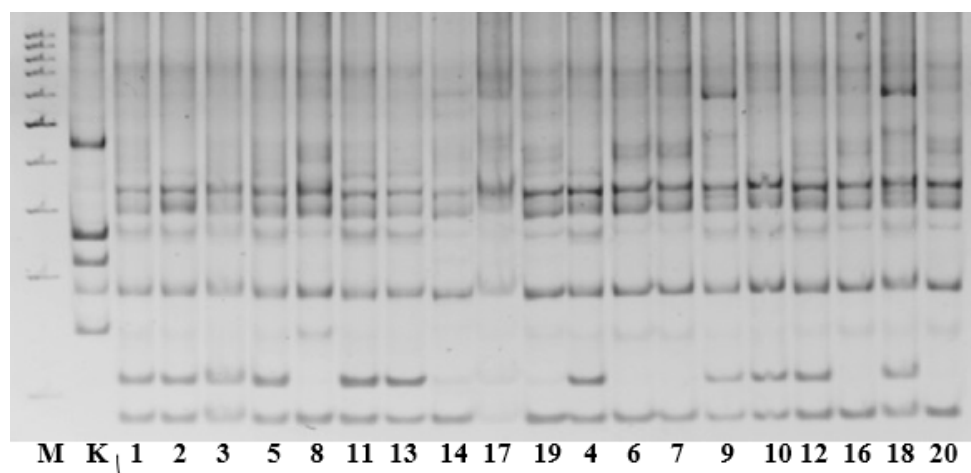
b)

Figure 5 – SSR patterns of individuals of *S. arbusculiformis* on SSR markers
*Ags*9 (a) and *Bmb*3 (b). Note: M – 100 bp Molecular weight marker (Thermo Fisher Scientific, USA),
K – individual #18 of the population 1 of *S. arbuscula*

Expected sizes of PCR products for other related species are given in Table 3: for Ags3, Ags 9, and Ags29 primers (for sand rice) – according to Zhang et al. [37], and for Hal34975, Hal42802, Hal45535, and Hal47234 (for saxaul) according to Long et al. [7]. Preliminary data showed more than 2 alleles per locus when study focused on *S. arbusculiformis.*

Obtained data showed that all nine primer pairs have their high cross-genera transferability and usefulness in differentiating three *Salsola* taxa – *S. arbuscula, S. arbusculiformis* and *S. chiwensis.*

Optimized PCR conditions for the annealing temperature and MgCl$_2$ concentration are reliable to analyze the genetic diversity both between and within eight species of *Agriophyllum, Haloxylon,* and *Salsola* collected in Kazakhstan to the date. The obtained information is important in terms of the development of optimized PCR conditions as a prerequisite for the successful application of SSR markers in population genetics of studied species.

Conclusion

Investigation on the level and pattern of genetic diversity of populations of the rare and valuable species using microsatellite markers is crucial for understanding the structure of the population and assessing the strategies for biodiversity preservation. SSR markers are reliable, informative markers with codominant nature are widely used in molecular genetic studies. An important limitation, however, regarding the use of microsatellites is the prior need for optimization of PCR conditions for each SSR marker.

The annealing temperatures and MgCl$_2$ concentrations were individually optimized for each primer pair for samples of *Agriophyllum, Haloxylon,* and *Salsola.*

Since little information was found in the literature on microsatellite markers for the Salsola genus, we tested the cross-genera transferability of SSR markers previously developed for other members of the Chenopodiaceae family, including *Beta vulgaris, Agriophyllum squarrosum,* and *Haloxylon ammodendron.* PCR conditions for representatives of the other two genera, *Agriophyllum* and *Haloxylon* were also tested in this study. The optimization of PCR conditions for studied Salsola species indicated their good cross-genera transferability via the successful amplification and will be used in population structure analyses.

Acknowledgments

References

1   Finch D.M. (2012) Climate change in grasslands, shrublands, and deserts of the interior American West: a review and needs assessment. Gen. Tech. Rep., vol. 285, pp. 139. https://doi.org/10.2737/RMRS-GTR-285.

2   The Sixth National report of biological diversity in the Republic of Kazakhstan, Astana, 2018.

3   Kurochkina L.Ya. (2003) Psammofit desert shrub. Botanical geography of Kazakhstan and Central Asia (within the desert region) [Psammofit-nokustarnikovye pustyni. Botanicheskaja geografija Kazahstana i Srednej Azii (v predelah pustynnoj oblasti)], Nauka: St. Petersburg, pp. 83-92. ISBN 5-201-11116-5.

4   Buras A., Wucherer W., Zerbe S., Noviskiy Z., Muchitdinov N. (2012) Allometric variability of Haloxylon species in Central Asia. Forest Ecol Manag., vol. 274, pp. 1-9. https://doi.org/10.1016/j.foreco.2012.02.023.

5   Zhaglovskaya A., Chlachula J., Thevs N., Myrzagaliyeva A., Aidossova S. (2017) Natural Regeneration Potential of the Black Saxaul Shrub forests in Semi-Deserts of Central Asia – the Ili River Delta Area, SE Kazakhstan. Pol J Ecol., vol. 65, no. 3, pp. 352-368. https://doi.org/10.3161/15052249PJE2017.65.3.004.

6   Shomurodov H.F., Khasanov F.O. (2014) Fodder plants of the Kyzyl Kum Desert. Arid Ecosystems, vol. 4, no. 3, pp. 208–213. https://doi.org/10.1134/S2079096114030093.

7   Long Y., Zhang J., Tian X., Wu S., et al. (2014) De novo assembly of the desert tree Haloxylon ammodendron (CA Mey.) based on RNA-Seq

data provides insight into drought response, gene discovery and marker identification. BMC genomics, vol. 15, no. 1, pp. 1-11. https://doi.org/10.1186/1471-2164-15-1111.

8   Kadereit G., Gotzek D., Jacobs S., Freitag H. (2005) Origin and age of Australian Chenopodiaceae. Org Divers Evol., vol. 5, no. 1, pp. 59–80. https://doi.org/10.1016/j.ode.2004.07.002.

9   Genievskaya Y., Abugalieva S., Zhubanysheva A., Turuspekov Y. (2017) Morphological description and DNA barcoding study of sand rice (Agriophyllum squarrosum, Chenopodiaceae) collected in Kazakhstan. BMC Plant Biol., vol. 17, no. 1, pp. 177. https://doi.org/10.1186/s12870-017-1132-1.

10   Chen G., Zhao J., Zhao X., Zhao P., et al. (2014) A psammophyte Agriophyllum squarrosum (L.) Moq.: a potential food crop. Genet Resour Crop Ev., vol. 61, no. 3, pp. 669-676. https://doi.org/10.1007/s10722-014-0083-8.

11   Grebennikov K.A. (2016) Features of the current distribution and state of populations of Salsola arbuscula Pall., Chenopodiaceae in the vicinity of Baskunchak lake [Osobennosti sovremennogo rasprostranenija i sostojanija populjacij soljanki derevcevidnoj (Salsola arbuscula Pall., Chenopodiaceae) v okrestnostjah ozera Baskunchak], Astrakhan herald of ecological education, vol. 35, no. 1, pp. 42-45.

12   Red Book of Kazakhstan. Plants [Krasnaja kniga Kazahstana. Rastenija], 2014, vol. 2, no. 1. Astana, JSC ArtPrintXXI, 52 p.

13   Toderich K.N., Popova V.V., Aralova D.B., Gismatulina L.G., et al. (2016) Halophytes and salt-resistant plants as animal feed at the farm level in Karakalpakstan [Galofity i soleustojchivye rastenija v kachestve korma zhivotnyh na urovne fermerskih hozjajstv v Karakalpakstane], Tashkent, 58 p.

14   Simonett O., Novikov O. (2010) Land Degradation and Desertification in Central Asia. In: Report, Central Asian Countries Initiative for Landscape Management. Final Report for the Swiss GEF Council Member, 19 p.

15   Ryan F.J., Ayres D.R. (2000) Molecular markers indicate two cryptic, genetically divergent populations of Russian thistle (Salsola tragus) in California. Can. J Botany, vol. 78, no. 1, pp. 59-67. https://doi.org/10.1139/b99-160.

16   Turuspekov Y., Adams R., Kearney C. (2002) Genetic diversity in three perennial grasses from the Semipalatinsk nuclear testing region of Kazakhstan after long-term radiation exposure. Biochem Syst Ecol., vol. 30, no. 9, pp. 809-817. https://doi.org/10.1016/S0305-1978(02)00021-2.

17   Ayres D., Ryan F.J., Grotkopp E., Bailey J., Gaskin J. (2009) Tumbleweed (Salsola, section Kali) species and speciation in California. Biol Invasions, vol. 11, no. 5, pp. 1175-1187. https://doi.org/10.1007/s10530-008-9380-5.

18   Boronnikova S.V., Kalendar R.N. (2010) Using IRAP markers for analysis of genetic variability in populations of resource and rare species of plants. Russ J Genet., vol. 46, no. 1, pp. 44-50. https://doi.org/10.1134/S1022795410010060.

19   McGray H.G., Ayres D.R., Sloop C.M., Lee A.K. (2008) Beta SSR loci cross-amplify in five Salsola taxa. Mol Ecol Resour., vol. 8, no. 3, pp. 608-611. https://doi.org/10.1111/j.1471-8286.2007.02014.x.

20   Ravishankar K.V., Bommisetty P. (2013) Simple Sequence Repeats Amplification. Microsatellites. Methods in Molecular Biology (Methods and Protocols), vol. 1006, pp. 133-138. https://doi.org/10.1007/978-1-62703-389-3_9.

21   Omasheva M., Flachowsky H., Ryabushkina N., Pozharskiy A., et al. (2017) To what extent do wild apples in Kazakhstan retain their genetic integrity? Tree Genet Genomes, vol. 13, no. 3, p. 52. https://doi.org/10.1007/s11295-017-1134-z.

22   Abdel-Hamid A.M.E. (2016) Characterization of four Salsola species and their genetic relationship by AFLP. Pak J Bot., vol. 48, no. 3, pp. 1183-1187.

23   Almerekova S., Lisztes-Szabo Z., Mukhitdinov N., Kurmanbayeva M., Abidkulova K., Sramko G. (2018) Genetic diversity and population genetic structure of the endangered Kazakh endemic Oxytropis almaatensis Bajt. (Fabaceae). Acta Botanica Hungarica, vol. 60, no. 3-4, pp. 263-278. https://doi.org/10.1556/034.2018.1.

24   Schroeder H., Fladung M. (2010) SSR and SNP markers for the identification of clones, hybrids and species within the genus Populus. Silvae Genet., vol. 59, no. 6, pp. 257-263. https://doi.org/10.1515/sg-2010-0036.

25   Turuspekov Y., Abugalieva S., Ermekbayev K., Sato K. (2014) Genetic characterization of wild barley populations (Hordeum vulgare ssp. spontaneum) from Kazakhstan based on genome wide SNP analysis. Breeding Sci., vol. 64, no. 4, pp. 399-403. https://doi.org/10.1270/jsbbs.64.399.

26   Akhani H., Edwards G., Roalson E. H. (2007) Diversification of the Old World Salsoleae s.l. (Chenopodiaceae): Molecular phylogenetic analysis of nuclear and chloroplast data sets and a revised classification. Int J Plant Sci., vol. 168, no. 6, pp. 931-956. https://doi.org/10.1086/518263.

27 Turuspekov Y., Abugalieva S. (2015) Plant DNA barcoding project in Kazakhstan. Genome, vol. 58, no. 5, p. 290.

28 Wen Z.B., Zhang M.L., Zhu G.L., Sanderson S.C. (2010) Phylogeny of Salsoleae s.l. (Chenopodiaceae) based on DNA sequence data from ITS, psbB–psbH, and rbcL, with emphasis on taxa of northwestern China. Plant Syst and Evol., vol. 288, no. 1-2, pp. 25-42. https://doi.org/10.1007/s00606-010-0310-5

29 Abugalieva S., Volkova L., Genievskaya Y., Ivaschenko A., et al. (2017) Taxonomic assessment of Allium species from Kazakhstan based on ITS and matK markers. BMC Plant Biol., vol. 17, no. 2, pp. 51-60. https://doi.org/10.1186/s12870-017-1194-0.

30 Almerekova Sh., Mukhitdinov N., Abugalieva S. (2017) Phylogenetic study of the endemic species Oxytropis almaatensis (Fabaceae) based on nuclear ribosomal DNA ITS sequences. BMC Plant Biol., vol. 17, suppl. 1, pp. 19-27. https://doi.org/10.1186/s12870-017-1128-x.

31 Turuspekov Y., Genievskaya Y., Baibulatova A., Zatybekov A., et al. (2018) Phylogenetic taxonomy of Artemisia L. species from Kazakhstan based on matK analyses. Proceedings of the Latvian Academy of Sciences. Section B., vol. 72, no. 1, pp. 29-37. https://doi.org/10.1515/prolas-2017-0068.

32 Zhang D.X., Hewitt G.M. (2003) Nuclear DNA analyses in genetic studies of populations: practice, problems and prospects. Mol Ecol., vol. 12, no. 3, pp. 563–584. https://doi.org/10.1046/j.1365-294X.2003.01773.x.

33 Barbara T., Palma-Silva C., Paggi G.M., Bered F., et al. (2007) Cross-species transfer of nuclear microsatellite markers: potential and limitations. Mol Ecol., vol. 16, no. 18, pp. 3759-3767. https://doi.org/10.1111/J.1365-294X.2007.03439.X.

34 Raveendar S., Lee G.A., Jeon Y.A., Lee Y.J., et al. (2015). Cross-amplification of Vicia sativa subsp. Sativa microsatellites across 22 other Vicia species. Molecules, vol. 20, no. 1, pp. 1543-1550. https://doi.org/10.3390/molecules20011543.

35 Yan Z., Wu F., Luo K., Zhao Y., et al. (2017) Cross-species transferability of EST-SSR markers developed from the transcriptome of Melilotus and their application to population genetics research. Sci Rep-UK, vol. 7, no. 1, pp. 1-11. https://doi.org/10.1038/s41598-017-18049-8.

36 González-Martínez S., Robledo-Arnuncio J., Collada C., Díaz A., et al. (2004) Cross-amplification and sequence variation of microsatellite loci in Eurasian hard pines. Theor Appl Genet., vol. 109, no. 1, pp. 103-111. https://doi.org/10.1007/s00122-004-1596-x.

37 Zhang J., Zhao P., Zhao J., Chen G. (2018) Synteny-based mapping of causal point mutations relevant to sand rice (Agriophyllum squarrosum) trichomeless mutant by RNA-sequencing. Journal Plant Physiol., vol. 231, pp. 86-95. ttps://doi.org/10.1016/j.jplph.2018.09.003.

38 Cureton A.N., Burns M.J., Ford-Lloyd B.V., Newbury H.J. (2002) Development of simple sequence repeat (SSR) markers for the assessment of gene flow between sea beet (Beta vulgaris ssp. maritima) populations. Mol. Ecol. Notes, vol. 2, no. 4, pp. 402-403. https://doi.org/10.1046/j.1471-8286.2002.00253.x.

39 Doyle J.J., Doyle J.L. (1987). A rapid DNA isolation procedure for small quantities of fresh leaf tissue. Phytochem. Bulletin, vol. 19, no. 1, pp. 11-15.

40 Sheng Y, Zheng W., et al. (2004) Population genetic structure of a dominant desert tree, Haloxylon ammodendron (Chenopodiaceae), in the southeast Gurbantunggut desert detected by RAPD and ISSR markers (in Chinese with English Abstract). Acta Bot Sin., vol. 46, no. 6, pp. 675-681.

41 Wang X.M., Yang D.Y., Tian Y.Z., Zhang B.W., et al. (2009) Inter-simple sequence repeats analysis of Haloxylon ammodendron from seeds carried back by "Shenzhou No.4" spaceship (in Chinese with English Abstract). Journal of Northwest University, vol. 39, pp. 259-263.

42 Suo Z., Jia Z., Lu Q., Pan B., et al. (2012) Distinguishing Haloxylon persicum and H. ammodendron (Haloxylon Bunge, Amaranthaceae) using DNA Marker. AASRI Proc., vol. 1, pp. 305-310. https://doi.org/10.1016/j.aasri.2012.06.047.

43 Bandopadhyay R., Sharma S., Rustgi S., Singh R., et al. (2004) DNA polymorphism among 18 species of Triticum-Aegilops complex using wheat EST-SSRs. Plant Sci., vol. 166, no. 2, pp. 349-356. https://doi.org/10.1016/j.plantsci.2003.09.022.

44 Kuleung C., Baenziger P.S., Dweikat I. (2004) Transferability of SSR markers among wheat, rye, and triticale. Theor Appl Genet., vol. 108, no. 6, pp. 1147–1150. https://doi.org/10.1007/s00122-003-1532-5.

45 Saha M.C., Mian M.A.R., Eujayl I., Zwonitzer J.C., et al. (2004) Tall fescue EST-SSR markers with transferability across several grass species. Theor Appl Genet., vol. 109, no. 4, pp. 783-791. https://doi.org/10.1007/s00122-004-1681-1.

A.N. Akimniyazova[1*] iD , D.E. Aisina[1] iD , A. Bolshoy[2] iD , A.T. Ivashchenko[1] iD

[1]SRI of Biology and Biotechnology problems, Almaty, Kazakhstan
[2]Department of Evolutionary and Environmental Biology, University of Haifa, Haifa, Israel
*e-mail: akimniyazova@gmail.com

Prediction of miRNAs interaction
with gastrointestinal tract cancer candidate genes

Abstract. miRNAs play an important role in regulating the expression of prevailing number of genes in the human genome. The vast majority of miRNAs are involved in the development of several diseases. Of the more than six thousand human miRNAs, only miR-619-5p has more than 200 genes with which it interacts fully complementary. These genes include several genes involved in the development of cancer of the gastrointestinal tract, which is a rare property among other miRNAs. It is required to establish the features of miR-619-5p and other miRNAs binding with candidate genes of gastrointestinal tract cancer. The location of miRNA binding sites in mRNA, the free energy of miRNA-mRNA interaction, the miRNA-mRNA nucleotide interaction scheme, and other quantitative characteristics of the miRNA-mRNA interaction were determined using the MirTarget programme. The overwhelming number of miRNAs binding sites, including miR-619-5p, are located in the 3'UTR of *CYP2W1, KIAA1456, SLC26A2, SPATA13* and *UQCRB* genes mRNA. In the mRNA of these genes, in addition to the miR-619-5p binding sites, the binding sites of seven, twenty, nine, five and four miRNAs were detected, respectively. In mRNA of these genes, clusters of miRNAs binding sites from two and three binding sites were identified. The identified miRNAs binding sites are conserved in mRNA of orthologous primates genes, which indicates the evolutionarily early emergence of a link between miRNAs and their target genes. Schemes of interaction between miRNA and mRNA nucleotides show high efficiency in determination the quantitative characteristics of this interaction. The important role of non-canonical nucleotide pairs, which increase the free energy of the interaction between miRNA and mRNA, is shown. The revealed associations of miRNA and *CYP2W1, KIAA1456, SLC26A2, SPATA13* and *UQCRB* target genes allow us to recommend them as markers in the development of methods for the diagnosis of the gastrointestinal tract cancer.

Key words: cancer, gene, mRNA, miRNA, miR-619-5p, target genes, associations.

Inroduction

In recent years, it has been identified that miRNAs are fully complementary to mRNA target genes [1-5]. It has been shown that such miRNAs bind to 5'UTR [3; 4; 6; 7], CDS [1; 3; 4-9] and 3'UTR [10-13]. The miRNA target genes perform many functions. It is shown that 201 target genes of miR-619-5p might serve as transcription factors, kinases, participants in metabolic processes associated with the development of various diseases, etc. [5-9]. In this work, the target genes of miR-619-5p that are involved in the development of cancer of the gastrointestinal tract are considered: *CYP2W1, KIAA1456, SLC26A2, SPATA13, UQCRB*. The *CYP2W1* gene involved in the development of stomach cancer [14;

15], small and large intestine [16-21], colorectal cancer [22-30]. The *KIAA1456* gene is associated with colorectal cancer [31]. A change in the expression of the *SLC26A2* gene in colorectal cancer was detected [32-34]. *SPATA13* [35] and *UQCRB* [36; 37] genes participate in the development of colorectal cancer. The interest in such miRNAs is determined by several factors: what function do related genes perform; whether these miRNAs can perform the function of siRNA; whether these genes are targets of other miRNAs; whether miRNAs interactions with mRNAs of orthologous genes persist, etc. A comparison of the interactions of miR-619-5p and other miRNAs with mRNAs of these genes will help to understand their participation in the development of gastrointestinal tract cancer.

Materials and methods

The nucleotide (nt) sequences of candidate genes of gastrointestinal tract cancer were downloaded from GenBank (http://www.ncbi.nlm.nih.gov). The nucleotide sequences of mRNA genes of *Chlorocebus sabaeus* (Csa)*, Homo sapiens* (Hsa)*, Macaca mulatta* (Mml)*, Pan troglodytes* (Ptr) and *Pongo abelii* (Pab) were downloaded from NCBI (http://www.ncbi.nlm.nih.gov). The nucleotide sequences of 2,565 miRNAs were taken from miRBase, and 3,707 miRNAs from a previous study [38].

The MirTarget program (created at al-Farabi Kazakh National University by Prof. A.Yu. Pyrkova and Prof. A.T. Ivashchenko) [39] defines the following features of miRNA binding to mRNAs: (a) the start of the initiation of miRNA binding to mRNAs; (b) the localization of miRNA binding sites in 5'UTRs, CDSs and 3'UTRs of the mRNAs; (c) the free energy of interaction between miRNA and the mRNA (ΔG, kJ/mole); and (d) the schemes of nucleotide interactions between miRNAs and mRNAs. The ratio $\Delta G/\Delta Gm$ (%) was determined for each site (ΔGm equals the free energy of miRNA binding with its fully complementary nucleotide sequence). The MirTarget program looks for hydrogen bonds between adenine (A) and uracil (U), guanine (G) and cytosine (C), G and U, and A and C [40; 41]. The MirTarget program identifies the positions of the binding sites on the mRNA, beginning with the first nucleotide of the mRNA's 5'UTR. The characteristics of the interaction between miRNA and mRNA reflect the intermolecular interactions of their molecules and were calculated for given parameters without their variation. Consequently, the results have no statistical scatter. Other factors that may have influenced these interactions have not been studied. The subject of changing the concentration ratio of miRNA and mRNA was not incorporated into the current study, since this aspect is of independent interest. For any other pathology, other candidate genes should be used, and other miRNA binding sites should be determined. The MirTarget program determines single miRNA binding sites in mRNA, and miRNA binding sites in clusters (arranged in series with overlapping of nucleotide sequences of the same or several miRNAs) [9].

Results and discussion

Table 1 shows the quantitative characteristics of the interaction of miRNA with candidate genes mRNA of gastrointestinal tract cancer. The characteristics of the interaction of miR-619-5p with mRNA of the five candidate genes are identical. Other miRNAs were associated with the mRNAs of each gene. The mRNA of the *CYP2W1* gene had targets for seven miRNAs, with miR-4739 binds with more free energy than miR-619-5p. The binding sites of the four miRNAs formed a cluster from 2160 nt to 2219 nt with a length of 59 nt. The total length of the binding sites of these miRNAs was 88 nt, which is 1.5 times the length of the cluster. This compaction of binding sites leads to competition between miRNAs for binding in the cluster.

The mRNA of *KIAA1456* gene had 21 binding sites from which two clusters of two miRNAs and three clusters of three miRNAs were formed (Table 1). miR-5096 binds completely complementary to the mRNA of the *KIAA1456* gene. Therefore, the expression of this gene is under the strong control of miRNA.

In the mRNA of the *SLC26A2* gene, 10 miRNAs binding sites were located (Table 1). Three clusters of two binding sites significantly reduced the proportion of binding sites in the total length of mRNA. miR-1285-5p and ID01237.3p-miR had a common start of binding sites, i.e., there is a clear competition between them for binding to the *SLC26A2* gene mRNA.

The mRNA of the *SPATA13* gene had six miRNAs binding sites, of which two binds with miR-619-5p. Binding sites of ID03024.5p-miR together with miR-619-5p formed a cluster (Table 1).

The mRNA of the *UQCRB* gene also had only one cluster including the miR-619-5p binding site (Table 1). Single binding sites of another three miRNAs characterized by a $\Delta G/\Delta Gm$ value of 88% to 98%.

For each of the five genes, miR-619-5p binding sites were included in the cluster. In the mRNA of the *CYP2W1* gene, the cluster consisted of ID01811.5p-miR, miR-5095, miR-619-5p and ID00913.5p-miR binding sites. The cluster of ID01334.5p-miR and miR-619-5p binding sites was present in the mRNA of the *KIAA1456* gene. In the mRNA of the *SLC26A2* gene, the cluster consisted of the miR-5585-3p and miR-619-5p binding sites. The binding sites of ID03024.5p-miR and miR-619-5p formed a cluster in the mRNA of the *SPATA13* gene. In the mRNA of the *UQCRB* gene, the cluster consisted of the binding sites ID00913.5p-miR and miR-619-5p. The ability of miR-619-5p to form associations with each of the five candidate genes is hardly accidental. In addition to the ability of miR-619-5p strongly suppress the expression of these genes; this miRNA excludes other miRNAs from regulating the expression of five candidate genes. In tumor cells, miR-619-5p always

synthesized more significantly than in normal cells [42-46].

Of the 50 binding sites, 45 sites were localized in 3'UTR, four sites in the CDS and one site in the 5'UTR. Clusters from only 2-3 binding sites, while clusters of binding sites consisting of more than ten miRNAs binding sites identified in mRNA of other genes.

Table 1 – The characteristics of miRNAs interaction with mRNA of colorectal cancer genes

Gene	miRNA	Start of site, nt	Region mRNA, nt	ΔG, kJ/mole	ΔG/ΔGm,%	Length miRNA, nt
CYP2W1	ID03126.5p-miR	39	CDS	-117	93	22
	miR-7110-5p	1546	3'UTR	-108	91	21
	miR-4739	1739	3'UTR	-125	87	25
	ID01811.5p-miR	2160	3'UTR	-113	90	22
	miR-5095	2170	3'UTR	-106	91	21
	miR-619-5p	2176	3'UTR	-121	100	22
	ID00913.5p-miR	2196	3'UTR	-117	92	23
	miR-5096	2248	3'UTR	-108	96	21
KIAA1456	ID00442.5p-miR	1751	CDS	-104	91	21
	ID01334.5p-miR	2522	3'UTR	-110	90	22
	miR-619-5p	2536	3'UTR	-121	100	22
	ID02199.5p-miR	2611	3'UTR	-113	90	23
	miR-1303	2621	3'UTR	-106	91	22
	miR-1285-5p	2768	3'UTR	-102	91	21
	miR-1273a	3875	3'UTR	-121	92	25
	miR-1273c	3877	3'UTR	-113	93	22
	miR-1273g-3p	3897	3'UTR	-106	91	21
	ID01815.5p-miR	4037	3'UTR	-106	89	23
	ID01334.3p-miR	4132	3'UTR	-115	92	22
	ID02017.3p-miR	4133	3'UTR	-115	90	22
	MiR-1972	4137	3'UTR	-113	91	22
	miR-5096	5137	3'UTR	-113	100	21
	miR-619-5p	5196	3'UTR	-117	96	22
	ID01836.5p-miR	5286	3'UTR	-113	90	23
	miR-1285-5p	5302	3'UTR	-102	91	21
	ID01360.3p-miR	8419	3'UTR	-104	91	21
	ID00367.5p-miR	8422	3'UTR	-115	93	22
	miR-1273g-3p	8429	3'UTR	-106	91	21
	ID02991.3p-miR	8854	3'UTR	-89	91	21
SLC26A2	ID01697.5p-miR	124	5'UTR	-108	93	20
	ID01838.5p-miR	4438	3'UTR	-119	95	24
	miR-1285-3p	4442	3'UTR	-110	95	22
	miR-7851-3p	4495	3'UTR	-108	91	22
	miR-619-5p	5066	3'UTR	-121	100	22
	miR-619-5p	5202	3'UTR	-110	91	22
	miR-5585-3p	5209	3'UTR	-113	96	22
	ID02175.3p-miR	5257	3'UTR	-110	91	22
	miR-1285-5p	5308	3'UTR	-102	91	21
	ID01237.3p-miR	5308	3'UTR	-113	88	24
SPATA13	ID01412.5p-miR	3846	CDS	-113	91	22

Table 1 continued

Gene	miRNA	Start of site, nt	Region mRNA, nt	ΔG, kJ/mole	ΔG/ΔGm,%	Length miRNA, nt
	ID02484.3p-miR	4057	CDS	-104	91	21
	ID03024.5p-miR	5010	3'UTR	-110	91	22
	miR-619-5p	5020	3'UTR	-121	100	22
	miR-619-5p	5155	3'UTR	-117	96	22
	miR-6510-5p	5931	3'UTR	-110	90	22
UQCRB	miR-619-5p	1269	3'UTR	-121	100	22
	ID00913.5p-miR	1289	3'UTR	-115	90	23
	miR-5096	1343	3'UTR	-110	98	21
	miR-5585-3p	1412	3'UTR	-108	93	22
	ID00695.3p-miR	2233	3'UTR	-127	88	24

Particular evidence for the adequacy of the Mir-Target program is in the interaction between miRNA and mRNA nucleotides. Figure 1 shows the interaction patterns of several miRNAs with mRNA nucleotides of the five studied genes. In the interaction scheme of miR-619-5p with mRNA of the *CYP2W1* gene, all nucleotides bind complementarily, which reflects the absolute affinity of miRNA and mRNA. For other miRNAs, in many cases, the interaction of miRNA with mRNA occurs with the formation of non-canonical A – C and G – U pairs. This interaction is weaker than in the case of canonical pairs; however, the nucleotide interaction stacking in each of the antiparallel RNA strands is preserved.

CYP2W1; miR-619-5p; 2176; -121; 100; 22
5'-GGCUCAUGCCUGUAAUCCCAGC-3'
    ||||||||||||||||||||||
3'-CCGAGUACGGACAUUAGGGUCG-5'

CYP2W1; ID00913.5p-miR; 2196; -117; 92; 23
5'-**G**CACUUUGGGAG**G**CCGAGGCAGG-3'
    ||||||||||||| |||||||||
3'-**U**GUGAAACCCUC**U**CGCUCCGUCC-5'

KIAA1456; ID00367.5p-miR; 8422; -115; 93; 22
5'-UCUGUCACCCAGG**C**UGGAGGGC-3'
    ||||||||||||| |||||||
3'-AGACAGUGGGUCC**A**ACCUCCCC-5'

KIAA1456; ID01334.3p-miR; 4132; -115; 92; 22
5'-AGG**C**GUGAGCCACCGCGCCCGG-3'
    |||||||||||||||||| ||
3'-UCC**A**CACUCGGUGGCGCGUUCC-5'

SLC26A2; ID01237.3p-miR; 5308; -113; 88; 24
5'-**C**CUGGGUGACAGAGC**G**AGACUCC**G**-3'
    ||||| ||||||||||||||| |||
3'-**A**GACCAACUGUCUCG**U**UCUGUGG**U**-5'

SLC26A2; ID01838.5p-miR; 4439; -113; 90; 24
5'-**G**AGA**G**GGUCUCACUGUGUUGC**C**CA-3'
    ||||||||||||||||||||||
3'-**U**UUCCUCAGAGUGACACAACG**A**GU-5'

SPATA13; ID00913.5p-miR; 5040; -113; 88; 23
5'-**G**CACUUUGGGAG**G**CC**A**AGGCAGG-3'
    |||||||||||| |||||||||
3'-**U**GUGAAACCCUC**U**CGCUCCGUCC-5'

UQCRB; ID00913.5p-miR; 1289; -115; 90; 23
5'-**G**CACUUUGGGAG**G**CCGAGGC**G**GG-3'
    ||||||||||||| ||||||||
3'-**U**GUGAAACCCUC**U**CGCUCCG**U**CC-5'

KIAA1456; miR-1273a; 3875; -121; 92; 25
5'-**G**AGACAGAGUCU**C**GCU**C**UGUCGCCC-3'
    |||| ||||||||||||||||||
3'-**U**UCUUUCUCAGA**A**CGA**A**ACAGCGGG-5'

KIAA1456; miR-1273c; 3877; -113; 93; 22
5'-GACAG**A**GUCUCG**C**UCUGUCGCC-3'
    ||||| ||||||||||||||||
3'-CUGUC**C**CAGAGC**A**AA**A**CAGCGG-5'

KIAA1456; miR-5096; 5137; -113; 100; 21
5'-GCCUGACCAACAUGGUGAAAC-3'
    |||||||||||||||||||||
3'-CGGACUGGUUGUACCACUUUG-5'

SLC26A2; miR-5585-3p; 5209; -113; 96; 22
5'-**G**CCUGUAGUCCCAGCUA**C**UCAG-3'
    ||||||||||||||||||||||
3'-**U**GGACAUCAGGGUCGAU**A**AGUC-5'

UQCRB; miR-5096; 1343; -110; 98; 21
5'-GCCUG**G**CCAACAUGGUGAAAC-3'
    ||||| ||||||||||||||||
3'-CGGAC**U**GGUUGUACCACUUUG-5'

UQCRB; miR-5585-3p; 1412; -108; 93; 22
5'-ACCUGUA**A**UCCCAGCUA**C**UCGG-3'
    ||||||||||||||||||||||
3'-UGGACAUC**A**GGGUCGAU**A**AGU**C**-5'

Note: Gene; miRNA; start of binding site (nt); the free energy, ΔG (kJ/mole); the ΔG/ΔGm (%); length of miRNA (nt). In bold type highlighted the non-canonical A-C and G-U pairs of nucleotide

Figure 1 – The schemes of miRNAs interaction in 3'UTR mRNAs of candidate genes

One way of proving the stability of miRNA and target gene associations is identification of these associations in orthologous genes. We found that in the orthologous genes of *CYP2W1*, the bond between ID03126.5p-miR and orthologous genes of several primates is conservative, which is reflected in the identity of the LGLLGLWG oligopeptide in orthologous proteins of primates (Figure 2).

The oligopeptides prior to the binding site in the *Hsa* and *Ptr* are different from other primates. The oligopeptides located after the binding site are more variable in the studied objects.

The miR-619-5p binding sites in the mRNA of the five studied genes are conservative. The flanking nucleotide sequences are variable (Figure 3).

The oligonucleotides located up to the conservative binding site of mir-619-5p are very variable. With the 3'-end, after a conserved oligonucleotide, nucleotide variability is also high.

```
MALLLLLFLGLLGLWGLLCACAQD Hsa
MALLLLLFLGLLGLWGLLRACARD Ptr
MALLLLLLLGLLGLWGLLRACARD Pab
MALLLLLLLGLLGLWGLLRACTRD Nle
MALLLLLLLGLLGLWGLLRAYARD Mml
MALLLLLLLGLLGLWGLLRAYARD Csa
```

Figure 2 – Regions of orthologous *CYP2W1* proteins containing the LGLLGLWG oligopeptide encoded by ID03126.5p-miR binding sites

```
CTGACCCGGTGCGGTGGCTCATGCCTGTAATCCCAGCACTTTGGGAGGCCGAGGCAGGCG CYP2W1
TAGGCTGAGCATGGTGGCTCATGCCTGTAATCCCAGCACTTTGGGAGGCCAAGGCAGAAG KIAA1456
TCGGCCAGGTGCAGTGGCTCATGCCTGTAATCCCAGCACGTTGGGAGGCCGAGGCGGGTG SLC26A2
AAGGCTGGGTGCTGTGGCTCATGCCTGTAATCCCAGCACTTTGGGAGGCCAAGGCAGGTG SPATA13
TTGGCAAGGCATGGTGGCTCATGCCTGTAATCCCAGCACTTTGGGAGGCCGAGGCGGGTA UQCRB
```

Figure 3 – The regions of mRNA nucleotide sequences of orthologous genes containing miR-619-5p binding sites

Conclusion

As a result of the research, the following conclusions can be drawn. The overwhelming number of miRNA binding sites, including miR-619-5p, are located in the 3'UTR. In the mRNA of *CYP2W1, KIAA1456, SLC26A2, SPATA13* and *UQCRB* target genes, in addition to the miR-619-5p binding sites, the binding sites of seven, twenty, nine, five and four miRNAs detected, respectively. In the mRNA *CYP2W1, KIAA1456, SLC26A2, SPATA13* and *UQCRB* target genes, there are clusters of miRNA binding sites from only two or three binding sites. Established miRNA binding sites conserved in mRNA of orthologous primates' genes. Schemes of interaction between miRNA and mRNA nucleotides show the important role of non-canonical A-C and G-U pairs that were not previously taken into account by other researchers, but they increase the free energy of interaction of miRNA and mRNA. The revealed associations of miRNA and *CYP2W1, KIAA1456, SLC26A2, SPATA13* and *UQCRB* target genes allow us to recommend them as markers in the development of methods for the diagnosis of the gastrointestinal tract cancer.

Acknowledgments

References

1   Davis E., Caiment F., Tordoir X., Cavaillé J., Ferguson-Smith A., Cockett N., et al. (2005) RNAi-mediated allelic trans-interaction at the imprinted Rtl1/Peg11 locus. Curr Biol., vol. 15, no. 8, pp. 743-749. https://doi.org/10.1016/j.cub.2005.02.060.

2   Ivashchenko A., Berillo O., Pyrkova A., Niyazova R., Atambayeva Sh. (2014) The properties of binding sites of miR-619-5p, miR-5095, miR-5096, and miR-5585-3p in the mRNAs of human genes. BioMed Research Int., vol. 2014, pp. 1-8. https://doi.org/10.1155/2014/720715.

3   Wang J., Li Z., Liu B., Chen G., Shao N., Ying X., et al. (2016) Systematic study of cis-anti-sense miRNAs in animal species reveals miR-3661 to target PPP2CA in human cells. RNA, vol. 22, no. 1, pp. 87-95. https://doi.org/10.1261/rna.052894.115.

4   Yurikova O.Yu., Aisina D.E., Niyazova R.E., Atambayeva Sh.A., Labeit S., Ivashchenko A.T. (2019) The Interaction of miRNA-5p and miRNA-3p with the mRNAs of orthologous Genes. Molecular biology, vol. 53, no. 4, pp. 692-704. https://doi.org/10.1134/S0026898419040189.

5   Atambayeva S., Niyazova R., Ivashchenko A., Pyrkova A., Pinsky I., Akimniyazova A., et al. (2017) The Binding Sites of miR-619-5p in the mRNAs of Human and Orthologous Genes. BMC Genomics, vol. 18, no. 1, pp. 428. https://doi.org/10.1186/s12864-017-3811-6.

6   Kondybayeva A.M., Akimniyazova A.N., Kamenova S.U., Ivashchenko A.T. (2018) The characteristics of miRNA binding sites in mRNA of ZFHX3 gene and its orthologs. Vavilov journal of Genetics and Breeding, vol. 22, pp. 438-444. https://doi.org/10.18699/VJ18.380.

7   Aisina D.E., Niyazova R.E., Atambayeva S.A., Imyanitov E.N., Ivashchenko A.T. (2017) Characteristics of interaction of miRNA with mRNA of E2F transcription factors family genes. International Journal of Biology and Chemistry, vol. 2, no. 10, pp. 10-18.

8   8.Kondybayeva A., Akimniyazova A., Kamenova S., Duchshanova G., Aisina D., Goncharova A., Ivashchenko A. (2019) Prediction of miRNA interaction with mRNA of stroke candidate genes. Neurological Sciences, pp. 1-10. https://doi.org/10.1007/s10072-019-04158-x

9   Aisina D., Niyazova R., Atambayeva S., Ivashchenko A. (2019) Prediction of clusters of miRNA binding sites in mRNA candidate genes of breast cancer subtypes. PeerJ, vol. 7, e8049. https://doi.org/10.7717/peerj.8049.

10   Ivashchenko A., Berillo O., Pyrkova A., Niyazova R. (2014) Binding Sites of miR-1273 Family on the mRNA of Target Genes. BioMed Res Int., 2014, pp. 620530. https://doi.org/10.1155/2014/620530.

11   Lytle J.R., Yario T.A., Steitz J.A. (2007) Target mRNAs are repressed as efficiently by microRNA-binding sites in the 5′ UTR as in the 3′ UTR. Proc. Natl Acad. Sci., vol. 104, no. 23, pp. 9667-9672. https://doi.org/10.1073/pnas.0703820104.

12   Lee I., Ajay S.S., Yook J.I., Kim H.S., Hong S.H., Kim N.H., et al. (2009) New class of microRNA targets containing simultaneous 5'-UTR and 3'-UTR interaction sites. Genome Res., vol. 19, no. 7, pp. 1175-1183. https://doi.org/10.1101/gr.089367.108

13   Ivashchenko A.T., Issabekova A.S., Berillo O.A. (2013) MiR-1279, miR-548j, miR-548m, and miR-548d-5p binding sites in CDSs of paralogous and orthologous PTPN12, MSH6, and ZEB1 genes.

14   Wang Y., Liu Y., Tang T., Luo Y., Stevens M.F.G., Cheng X., et al. (2019) The antitumour activity of 2-(4-amino-3-methylphenyl)-5-fluorobenzothiazole in human gastric cancer models is mediated by AhR signalling.J Cell Mol Med., vol. 24, no. 2, pp. 1750-1759. https://doi.org/10.1111/jcmm.14869

15   Aung P.P., Oue N., Mitani Y., Nakayama H., Yoshida K., Noguchi T., et al. (2006) Systematic search for gastric cancer-specific genes based on SAGE data: melanoma inhibitory activity and matrix metalloproteinase-10 are novel prognostic factors in patients with gastric cancer. Oncogene, vol. 25, no. 17, pp. 2546-2557. https://doi.org/10.1038/sj.onc.1209279

16   Guo J., Johansson I., Mkrtchian S., Ingelman-Sundberg M. (2016) The CYP2W1 enzyme: regulation, properties and activation of prodrugs. Drug Metab Rev., vol. 48, no. 3, pp. 369-378. https://doi.org/10.1080/03602532.2016.1188939.

17   Guo J., Thiess S., Johansson I., Mkrtchian S., Ingelman-Sundberg M. (2016) Membrane topology and search for potential redox partners of colon cancer-specific cytochrome P450 2W1.FEBS Lett., vol. 590, no. 3, pp. 330-339. https://doi.org/10.1002/1873-3468.12063.

18   Choong E., Guo J., Persson A., Virding S., Johansson I., Mkrtchian S., et al. (2015) Developmental regulation and induction of cytochrome P450 2W1, an enzyme expressed in colon tumors. PLoS One, vol. 10, no. 4, pp. e0122820. https://doi.org/10.1371/journal.pone.0122820.

19   Travica S., Pors K., Loadman P.M., Shnyder S.D., Johansson I., Alandas M.N., et al. (2013) Colon cancer-specific cytochrome P450 2W1 converts duocarmycin analogues into potent tumor cytotoxins. ClinCancer Res., vol. 19, no. 11, pp. 2952-2961. https://doi.org/10.1158/1078-0432.CCR-13-0238.

20   Stenstedt K., Hallstrom M., Johansson I., Ingelman-Sundberg M., Ragnhammar P., Edler D. (2012) The expression of CYP2W1: a prognostic marker in colon cancer.Anticancer Res., vol. 32, no. 9, pp. 3869-3874.

21   Gomez A., Karlgren M., Edler D., Bernal M.L., Mkrtchian S., Ingelman-Sundberg M. (2007) Expression of CYP2W1 in colon tumors: regulation by gene methylation. Pharmacogenomics, vol. 8, no. 10, pp. 1315-1325. https://doi.org/10.2217/14622416.8.10.1315.

22   Liang L., Zeng J.H., Qin X.G., Chen J.Q., Luo D.Z., Chen G. (2018) Distinguishable Prognostic Signatures of Left- and Right-Sided Colon Can-

cer: a Study Based on Sequencing Data.Cell PhysiolBiochem., vol. 48, no. 2, pp. 475-490. https://doi.org/10.1159/000491778.

23 Beyerle J., Holowatyj A.N., Haffa M., Frei E., Gigic B., Schrotz-King P., et al. (2020) Expression patterns of xenobiotic-metabolizing enzymes in tumor and adjacent normal mucosa tissues among patients with colorectal cancer: the colocare study. Cancer Epidemiol Biomarkers Prev., vol. 29, no. 2, pp. 460-469. https://doi.org/10.1158/1055-9965.EPI-19-0449.

24 Chung F.F., Mai C.W., Ng P.Y., Leong C.O. (2016) Cytochrome P450 2W1 (CYP2W1) in Colorectal Cancers.CurrCancer Drug Targets, vol. 16, no. 1, pp. 71-78. https://doi.org/10.2174/1568009616888151112095948.

25 Stenstedt K., Hallstrom M., Lédel F., Ragnhammar P., Ingelman-Sundberg M., Johansson I., et al. (2014) The expression of CYP2W1 in colorectal primary tumors, corresponding lymph node metastases and liver metastases. Acta Oncol., vol. 53, no. 7, pp. 885-891. https://doi.org/10.3109/0284186X.2014.887224.

26 Stenstedt K., Travica S., Guo J., Barragan I., Pors K., Patterson L., et al. (2013) CYP2W1 polymorphism: functional aspects and relation to risk for colorectal cancer. Pharmacogenomics, vol. 14, no. 13, pp. 1615-1622. https://doi.org/10.2217/pgs.13.136.

27 Tan B.S., Tiong K.H., Muruhadas A., Randhawa N., Choo H.L., Bradshaw T.D., et al. (2011) CYP2S1 and CYP2W1 mediate 2-(3,4-dimethoxyphenyl)-5-fluorobenzothiazole (GW-610, NSC 721648) sensitivity in breast and colorectal cancer cells. Mol Cancer Ther., vol. 10, no. 10, pp. 1982-1992. https://doi.org/10.1158/1535-7163.MCT-11-0391.

28 Gomez A., Nekvindova J., Travica S., Lee M.Y., Johansson I., Edler D., et al. (2010) Colorectal cancer-specific cytochrome P450 2W1: intracellular localization, glycosylation, and catalytic activity. MolPharmacol., vol. 78, no. 6, pp. 1004-1011. https://doi.org/10.1124/mol.110.067652.

29 Chung F.F., Mai C.W., Ng P.Y., Leong C.O. (2016) Cytochrome P450 2W1 (CYP2W1) in Colorectal Cancers. Curr Cancer Drug Targets, vol. 16, no. 1, pp. 71-8. https://doi.org/10.2174/1568009616888151112095948.

30 Edler D., Stenstedt K., Ohrling K., Hallström M., Karlgren M., Ingelman-Sundberg M., et al. (2009) The expression of the novel CYP2W1 enzyme is an independent prognostic factor in colorectal cancer – a

pilot study. Eur J Cancer., vol. 45, no. 4, pp. 705-712. https://doi.org/10.1016/j.ejca.2008.11.031.

31 Flanagan J.M., Healey S., Young J., Whitehall V., Trott D.A., Newbold R.F., et al. (2004) Mapping of a candidate colorectal cancer tumor-suppressor gene to a 900-kilobase region on the short arm of chromosome 8. Genes Chromosomes Cancer., vol. 40, no. 3, pp. 247-260. https://doi.org/10.1002/gcc.20039.

32 Inoue A., Okamoto K., Fujino Y., Nakagawa T., Muguruma N., Sannomiya K., et al. (2015) B-RAF mutation and accumulated gene methylation in aberrant crypt foci (ACF), sessile serrated adenoma/polyp (SSA/P) and cancer in SSA. P.Br J Cancer., vol. 112, no. 2, pp. 403-412. https://doi.org/10.1038/bjc.2014.545.

33 Pitule P., Vycital O., Bruha J., Novak P., Hosek P., Treska V., et al. (2013) Differential expression and prognostic role of selected genes in colorectal cancer patients. Anticancer Res., vol. 33, no. 11, pp. 4855-4865.

34 Yusa A., Miyazaki K., Kimura N., Izawa M., Kannagi R. (2010) Epigenetic silencing of the sulfate transporter gene DTDST induces sialyl Lewisx expression and accelerates proliferation of colon cancer cells. Cancer Res., vol. 70, no. 10, pp. 4064-4073. https://doi.org/10.1158/0008-5472.CAN-09-2383.

35 Kawasaki Y., Sagara M., Shibata Y., Shirouzu M., Yokoyama S., Akiyama T. (2007) Identification and characterization of Asef2, a guanine-nucleotide exchange factor specific for Rac1 and Cdc42. Oncogene., vol. 26, no. 55, pp. 7620-7267. https://doi.org/10.1038/sj.onc.1210574.

36 Kim H.C., Chang J., Lee H.S., Kwon H.J. (2017) Mitochondrial UQCRB as a new molecular prognostic biomarker of human colorectal cancer. ExpMol Med., vol. 49, no. 11, pp. e391. https://doi.org/10.1038/emm.2017.152.

37 Lascorz J., Bevier M., Schönfels W.V., Kalthoff H., Aselmann H., Beckmann J., et al. (2012) Polymorphisms in the mitochondrial oxidative phosphorylation chain genes as prognostic markers for colorectal cancer.BMC Med Genet., vol. 13, pp. 31. https://doi.org/10.1186/1471-2350-13-31.

38 Londin E., Loher P., Telonis A.G., Quann K., Clark P., Jing Y., et al. (2015) Analysis of 13 cell types reveals evidence for the expression of numerous novel primate- and tissue-specific microRNAs. PNAS USA, vol. 112, no. 10, pp. 1106-1115. https://doi.org/10.1073/pnas.1420955112.

39 Ivashchenko A., Berillo O., Pyrkova A., Niyazova R., Atambayeva Sh. (2014) MiR-3960 bind-

ing sites with mRNA of human genes. Bioinformation, vol. 10, no. 7, pp. 423–427.

40   Lemieux S., Major F. (2002) RNA canonical and non-canonical base pairing types: a recognition method and complete repertoire. Nucleic Acids Res., vol. 30, pp. 4250-4263. https://doi.org/10.1093/nar/gkf540

41   Garg A., Heinemann U. (2018) A novel form of RNA double helix based on G·U and C·A+ wobble base pairing. RNA, vol. 24, pp. 209-218. https://doi.org/:10.1261/rna.064048.117

42   Kim D.H., Park S., Kim H., Choi YJ., Kim SY., Sung KJ., Sung YH., Choi CM., Yun M., Yi YS., Lee CW., Kim SY., Lee JC., Rho JK. (2020) Tumor-derived exosomal miR-619-5p promotes tumor angiogenesis and metastasis through the inhibition of RCAN1.4. Cancer Lett., vol. 475, pp. 2-13. https://doi.org/10.1016/j.canlet.2020.01.023.

43   Chen G., Gu Y., Han P., Li Z., Zhao JL., Gao MZ. (2019) Long noncoding RNA SBF2-AS1 promotes colorectal cancer proliferation and invasion by inhibiting miR-619-5p activity and facilitating HDAC3 expression. J Cell Physiol., vol. 234, no. 10, pp. 18688-18696. https://doi.org/10.1002/jcp.28509.

44   Shkurnikov M.Y., Makarova Y.A., Knyazev E.N., Fomicheva K.A., Galatenko A.V., Nyushko K.M., Galatenko V.V., Vechorko V.I., Alekseev B.Y. (2017) Plasma Level of hsa-miR-619-5p microRNA Is Associated with Prostatic Cancer Dissemination beyond the Capsule. Bull Exp Biol Med., vol. 163, no. 4, pp. 475-477. https://doi.org/10.1007/s10517-017-3831-x. PMID:28853076

45   Qiu G., Zhang XB., Zhang SQ., Liu PL., Wu W., Zhang JY., Dai SR. (2016) Dysregulation of MALAT1 and miR-619-5p as a prognostic indicator in advanced colorectal carcinoma. OncolLett., vol. 12, no. 6, pp. 5036-5042. https://doi.org/10.3892/ol.2016.5312.

46   Knyazev E.N., Fomicheva K.A., Mikhailenko D.S., Nyushko K.M., Samatov T.R., Alekseev B.Y., Shkurnikov M.Y. (2016) Plasma levels of hsa-miR-619-5p and hsa-miR-1184 differ in prostatic benign hyperplasia and cancer. Bull Exp Biol Med., vol. 161, no. 1, pp. 108-11. https://doi.org/10.1007/s10517-016-3357-7.

E. Altınöz* (iD) , E.M. Altuner (iD)

Kastamonu University, Kastamonu, Turkey,
*e-mail: altinozedaa@gmail.com

Responses of some *Escherichia coli* clinical isolate strains with multiple drug resistance and overexpressed efflux pumps against efflux pump inhibitors

Abstract. Antibiotics are compounds, which inhibit the growth of or destroy microorganisms. But for some reason, microorganisms may develop resistance to antibiotics. One of the reasons for resistance to antibiotics is efflux pumps. By means of these pumps, microorganisms export antibiotics into the bacterial cell; consequently, they cannot inhibit the growth of or destroy bacteria. This situation decreases the spectrum of antibiotic activity and increases the antibiotic resistance. Thus, microorganisms could develop multiple drug resistance against not only the antibiotic used, but also for many other antibiotics and rapidly spread in the environment. Antibiotic resistance has become a major global issue, new antibiotics and efflux pump inhibitor studies are continuing rapidly. The aim of the present study is to observe the response of some *Escherichia coli* clinical isolate strains with multiple drug resistance and overexpressed efflux pumps against efflux pump inhibitors to use these strains for further studies. Ethidium bromide (EtBr)-agar cartwheel method was firstly used to identify *E. coli* strains with overexpressed efflux pumps by transferring inoculum of all strains to EtBr containing agars, and overexpressed efflux pumps were determined by exposing agar plates to UV light. Verapamil, phenyl arginine beta naphthylamide (PAβN) and thioridazine hydrochloride were used as efflux pump inhibitors (EPIs), and the lowest concentration of EPIs, which inhibit the growth of *E. coli* strains were determined by minimal inhibition concentration (MIC) test. Responses of microorganisms against efflux pump inhibitors were determined with a microplate-based assay, by using EPIs below their MIC values. According to the results of this study, effects of verapamil and thioridazine were observed to be more effective than PAβN. As a result, 98.41% of *E. coli* strains used in the study was found to be affected by Verapamil, where 96.82% by thioridazine and only 38.09% were affected by PAβN inhibitor.

Key words: multiple drug resistance, antibiotics, efflux pumps, efflux pump inhibitors, *E.coli*.

Introduction

Antibiotics are compounds, which inhibit the growth of or destroy microorganisms, thus are used to treat and prevent infections [1-3]. But for some reason, microorganisms in time develop resistance to antibiotics. One of the reasons for resistance to antibiotics is efflux pumps.

Efflux pumps were first described in 1980, as it was observed that tetracyclines were exported out of the cell [4; 5]. Efflux pumps, are known as active pumping systems, which are membrane transport proteins and remove toxic substances from inside to the outside of the cell [6-8]. These transport proteins are known to be found in all Gram-positive and Gram-negative bacteria, prokaryotic organisms and in eukaryotic cells as well [9; 10].

Efflux pump systems can be specific to a single compound or can transport a group of compounds, such as detergents, disinfectants, cancer drugs, antibiotics, antimicrobial peptides, biocides and certain dyes, and this situation causes multiple drug resistance (MDR) [11]. Efflux pumps classified as 5 superfamily; ABC (ATP Binding Cassette); MATE (Multidrug and Toxic Efflux), MF (Major Facilitator), RND (Resistance-nodulation-division) and SMR (Small Multidrug Resistance) [10; 12]. Acr AB-Tol C, AcrEF-TolC, EmrB and EmrD efflux pumps, which are examples of some of these superfamilies, are found commonly in *E.coli* [9; 10; 13-21].

Some compounds are known to inhibit the activity of efflux pumps. The efflux pump inhibitors used in Gram-negative bacteria are Phenyl Arginine Beta Naphthylamide (PAβN) (against RND pump), Carbonyl Cyanide m-Chlorophenyl Hydrazone (CCCP) (against RND, MFS and MATE pumps), 1-(1-Naphthylmethyl) Piperazine (NMP) (against RND pump), Verapamil (against MFS and ABC pumps), Paroxetine (against MFS and RND pumps), Milbemycin (against ABC pump), Biricodar (against VX-710-MFS and ABC pumps), Timkodar (against VX-853-MFS and ABC pumps) and Thioridazine (against EmrE family belonging to small multidrug resistance (SMR) pump) [22-34].

The aim of the present study is to observe the response of some *Escherichia coli* clinical isolate strains with multiple drug resistance and overexpressed efflux pumps against efflux pump inhibitors to facilitate the use of these strains for further studies.

Materials and methods

Objects of study. Eleven clinical isolate multi drug resistant *Escherichia coli* strains were chosen after screening of 100 isolates, and one standard strain (*E. coli* ATCC 25922) were used in the present study. All clinical *E. coli* isolates and the standard ATCC strain were taken from the Kastamonu University, Department of Biology, Microbiology and Biochemistry Laboratory culture collection. The clinical isolates were previously isolated from different clinical resources and identified by BD Phoenix system (Becton Dickinson, USA). All microorganisms were activated in LB Broth (Merck, Germany) and Tryptic Soy Broth (TSB) (Merck, Germany). Single pure colonies were obtained by transferring *E. coli* strains to LB Agar and TSB Agar. The bacterial identification and susceptibility testing for all clinical *E. coli* isolates were done by BD Phoenix system (Becton Dickinson, USA). Single colonies were transferred into sterile saline solution (0.9%) and adjusted to 0.5 McFarland standard to standardize the inocula used in the study to contain about 10^8 cfu/mL [35; 36].

Ethidium bromide-agar cartwheel method. TSB agar plates containing ethidium bromide (EtBr) (Merck, Germany) ranging between 0 and 2.5 mg/L (0, 0.5, 1, 1.5, 2 and 2.5 mg/L) prepared by serial dilution were used to identify *E. coli* strains with overexpressed efflux pumps as defined by Martins et al. (2010) previously [37]. Inoculum of all strains was transferred to EtBr containing agars and incubated at 37ºC for 24 h. After incubation, microorganisms presenting overexpressed efflux pumps were distinguished from others by exposing TSB agar plates to UV light. The EtBr-agar cartwheel method [37] was applied as two replicates for each *E. coli* strain (Figure 1).

Minimal inhibition concentration (MIC) test for efflux pump inhibitors. Verapamil (Sigma Aldrich, USA), phenyl arginine beta naphthylamide (PAβN) (Sigma Aldrich, USA) and thioridazine hydrochloride (Sigma Aldrich, USA) were used as efflux pump inhibitors (EPI). To identify the lowest concentration of EPIs that inhibits the growth of *E. coli* strains minimal inhibition concentration (MIC) test was used. EPI stock solutions were prepared as 512 µg/mL and a serial microdilution was applied in 96-well microplates containing Mueller Hinton Broth (Merck, Germany) to obtain a range of EPI concentrations (0.5-256 µg/mL) [37]. The MIC values were defined as the lowest concentration of EPI inhibiting visible *E. coli* growth. All tests were conducted in triplicate [38].

Efflux pump inhibitor-based microplate assay. One milliliter of Mueller Hinton Broth (MHB) was pipetted into each wells of a 24-well microplate. Antibiotic discs (Cefixime (CFM)-5µg, Ceftazidime (CAZ)-10µg, Ceftriaxone (CRO)-30µg, Cefepime (FEP)-30µg, Aztreonam (ATM)-30µg, Ampicillin (AMP)-10µg, Amoxicillin-Clavulanate (AMC)-30µg, Ciprofloxacin (CIP)-5µg, Norfloxacin (NOR)-10µg, Piperacillin-Tazobactam (TZP)-36µg, Gentamicin (CN)-10µg, Trimethoprim-Sulfamethoxazole (SXT)-25µg, Ertapenem (ETP)-10µg, Oxoid) were distributed to the wells of the plate and the plate incubated at 37°C during 1 h, to allow the diffusion of the antibiotic to the medium. After the incubation, the EPIs were also distributed to the corresponding wells of the microplate at half of their MIC values (MIC/2). The wells were inoculated with 0.1 mL of the *E. coli* suspensions. The microplate was incubated for 24 h at 37ºC. All tests were conducted in triplicate [37].

Statistical analysis. One-way analysis of variance (ANOVA), which is a parametric method was performed (P = 0.05) to determine whether difference between replicates is significant or not. R Studio, version 3.3.2 was used for statistical analysis [39].

Results and discussion

In the first part of the study, according to the BD Phoenix data the clinical *E.coli* isolates presenting multidrug resistance were selected and transferred to TSB agar plates containing EtBr to select strains presenting overexpressed efflux pumps (Figure 1).

According to the results, eleven *E. coli* strains and one standard strain were selected for the study (Table 1).
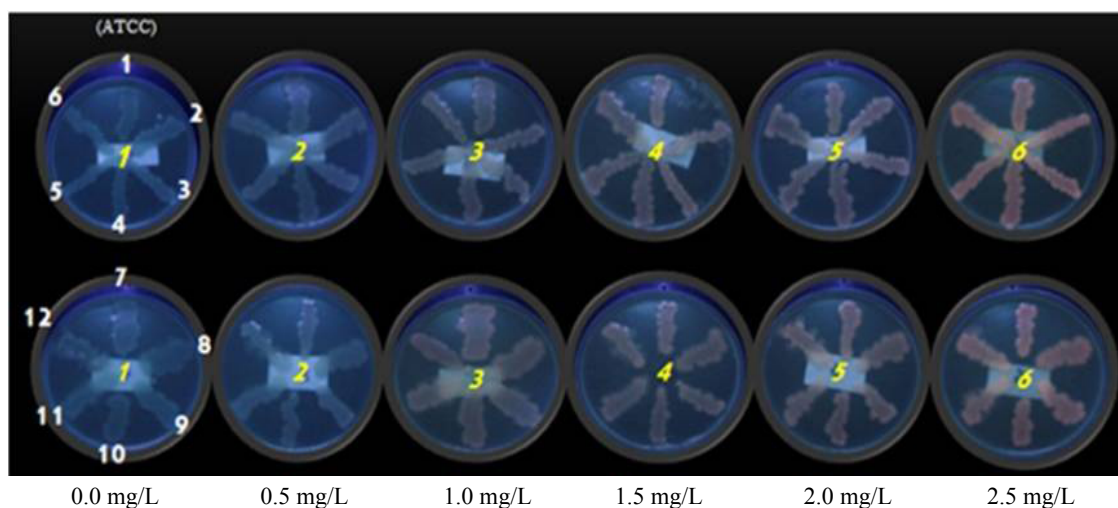
| 0.0 mg/L | 0.5 mg/L | 1.0 mg/L | 1.5 mg/L | 2.0 mg/L | 2.5 mg/L |

Figure 1 – The efflux capacities of twelve *E. coli* strains for different EtBr concentrations

Table 1 – Susceptibility test results (MIC values (µg/mL) for clinical *E. coli* isolates (bacteria 2 to 12)

Antibiotics	Bacte-ria 2	Bacte-ria 3	Bacte-ria 4	Bacte-ria 5	Bacte-ria 6	Bacte-ria 7	Bacte-ria 8	Bacte-ria 9	Bacteria 10	Bacteria 11	Bacteria 12
Gentamicin	< = 1 (S)	2 (S)	2 (S)	< = 1 (S)	< = 1 (S)	2 (S)	2 (S)	> 4 (R)	2 (S)	< = 1 (S)	< = 1 (S)
Ertapenem	< = 0.25 (S)	< = 0.25 (S)	< = 0.25 (S)	< = 0.25 (S)	< = 0.25 (S)	< = 0.25 (S)	< =0.25 (S)	< = 0.25 (S)	< = 0.25 (S)	> 1 (R)	< = 0.25 (S)
Cefixime	< = 0.5 (S)	> 2 (R)	< = 0.5 (S)	< = 0.5 (S)	1 (S)	< = 0.5 (S)	> 2 (R)	> 2 (R)	> 2 (R)	< = 0.5 (S)	> 2 (R)
Ceftazidime	< = 1 (S)	4 (I)	< = 1 (S)	< = 1 (S)	< = 1 (S)	< = 1 (S)	2 (I)	> 8 (R)	> 8 (R)	< = 1 (S)	> 8 (R)
Ceftriaxone	< = 1 (S)	> 4 (I)	< = 1 (S)	< = 1 (S)	< = 1 (S)	< = 1 (S)	> 4 (R)	> 4 (R)	> 4 (R)	< = 1 (S)	> 16 (R)
Cefepime	< = 1 (S)	2 (I)	< = 1 (S)	< = 1 (S)	< = 1 (S)	< = 1 (S)	4 (I)	> 8 (R)	< = 1 (S)	2 (I)	> 8 (R)
Aztreonam	< = 1 (S)	4 (I)	< = 1 (S)	< = 1 (S)	< = 1 (S)	< = 1 (S)	2 (I)	> 16 (R)	8 (R)	< = 1 (S)	> 16 (R)
Ampicillin	> 8 (R)	> 8 (R)	> 8 (R)	< = 2 (S)	> 8 (R)	> 8 (R)	> 8 (R)	> 8 (R)	> 8 (R)	< = 2 (S)	> 8 (R)
Amoxicillin-Clavulanate	16/2 (R)	4/2 (S)	16/ 2 (R)	4/2 (S)	8/2 (R)	> 32/2 (R)	> 32/2 (R)	> 32/2 (R)	> 32/2 (R)	4/2 (S)	16/2 (R)
Piperacillin-Tazobactam	< = 4/4 (S)	< = 4/4 (S)	< = 4/4 (S)	< = 4/4 (S)	< = 4/4 (S)	> 16/4 (R)	> 16/4 (I)	8/4 (S)	< = 4/4 (S)	< = 4/4 (S)	< = 4/4 (S)
Trimethoprim-Sulfamethox-azole	< = 1/19 (S)	> 4 / 76 (R)	< = 1/ 19 (S)	> 4 / 76 (R)	> 4 / 76 (R)	> 4 / 76 (R)	> 4 / 76 (R)	< = 1/ 19 (S)	< = 1/ 19 (S)	< = 1/ 19 (S)	< = 1/ 19 (S)
Ciprofloxacin	< = 0.25 (S)	> 1 (R)	> 1 (R)	> 1 (R)	> 1 (R)	< = 0.25 (S)	> 1 (R)	> 1 (R)	0.5 (I)	< = 0.25 (S)	< = 0.25 (S)
Norfloxacin	< = 0.5 (S)	> 2 (R)	> 2 (R)	> 2 (R)	> 2 (R)	< = 0.5 (S)	> 2 (R)	> 2 (R)	1 (I)	< = 0.5 (S)	< = 0.5 (S)
Note: (S): Susceptible (R): Resistance, (I): Intermediate Resistance.											

The Petri dishes having number 1 were negative controls, which contained no EtBr. Starting from number 2 to number 6 the EtBr concentration was increasing from 0.5 mg/L to 2.5 mg/L. The plates having number 1 presented no fluorescence under UV, as expected. All *E. coli* strains, except standard strain (bacteria number 1), on plate number 2 removed 0.5 mg/L EtBr to outside of the cell by their efflux pumps. A noticeably light pinkish fluorescence appeared for the standard strain, which indicates that this strain cannot efflux EtBr, although the concentration is as low as 0.5 mg/L. All *E. coli* strains, except the 5th strain, on plate number 3, which contained 1.0 mg/L EtBr, started to display a pinkish fluorescence under UV light. In Petri dishes numbered 4 to 6 a gradually increasing fluorescence was observed.

The susceptibility test results for clinical *E. coli* isolates (bacteria 2 to 12) are given in Table 1. In addition, the responses of clinical *E. coli* isolates against EPIs in combination with antibiotics are given in Tables 2-5.

To observe the responses of clinical *E. coli* isolates against EPIs in combination with antibiotics, only the antibiotics, against which each *E. coli* strain was found to be resistant and intermediate resistant were tested. The antibiotics, against which each *E. coli* strain was observed to be susceptible were not used. According to the data given in Table 2 four different results given as follows can be observed.

– Positive growth for no EPI;
– Negative growth for no EPI;
– Positive growth for EPI and antibiotic combination and
– Negative growth for EPI and antibiotic combination.

A positive growth for no EPI is an expected result, considering the antibiotics used in EPI test are the antibiotics against which each *E. coli* strain are resistant. However, the data presented in Table 2 presents negative growth in some antibiotics with no EPI, in contrary to the expectations, since the strains were resistant to those antibiotics. The reason for this observation can be explained with the final concentration of antibiotic in each well. Since the antibiotic preloaded disks were used in the EPI test, the final concentration of antibiotic in each well was a the same with the antibiotic loaded on each disk, thus the concentration of antibiotic in each well could be higher than their MIC value.

As a result of this there may be a negative control. For these results, in a negative growth in EPI-antibiotic combination, it cannot be possible to understand, whether this negative growth was due to the activity of antibiotic or EPI. For such results, a further research should be conducted by adjusting the final antibiotic concentration to be lower than the MIC values.

In addition to that, in negative growths for some antibiotics with no EPI, the final concentration of the antibiotic used was not higher than the MIC value. For such cases, a further fractional inhibitory concentration (FIC) test should also be conducted to observe, whether an additive or a synergistic interaction is present between the EPI and antibiotic, or not.

A positive growth for EPI and antibiotic combination means that the EPI used in the EPI-antibiotic combination did not block the efflux pump, thus the bacteria could export the antibiotic out of the cell and as the bacteria is resistant to that antibiotic they could still survive. On the other hand, a negative growth for EPI and antibiotic combination can be interpreted as the EPI used in the EPI-antibiotic combination blocked the efflux pump, as a result of that bacteria couldn't export the antibiotic out of the cell and survive.

Table 2 clearly shows that bacteria 2 is resistant against AMP within the concentration tested, but using AMP in combination with verapamil and thioridizin HCl killed bacteria 2. According to Table 2, bacteria 3 was found to be resistant against NOR, CFM and ATM within the concentration tested. Using NOR and ATM in combination with verapamil and thioridizin HCl killed bacteria 3, where PAβN with CFM also killed bacteria 3.

Table 2 also presents that bacteria 4 is resistant against AMP, CIP and NOR, and verapamil and thioridizin HCl in combination with these antibiotics killed this strain, where only AMP and PAβN combination inhibited the growth of bacteria 4. Verapamil and thioridizin HCl, which were used in combination with CIP, NOR and SXT against bacteria 5, were observed to kill this strain too.

Table 3 shows the responses of clinical *E. coli* isolates against EPIs in combination with antibiotics for bacteria 6, 7 and 8. According to Table 3, bacteria 6, 7 and 8 was observed to be resistant against AMP; AMC, TZP, AMP and SXT; and CFM, CAZ, CRO, AMP, AMC, CIP and SXT respectively. But, verapamil and thioridizin HCl, which were used in combination with AMP for bacteria 6, and in combination with AMC, TZP, AMP and SXT for bacteria 7, were killed these two strains. Similar results were also observed for CFM, CAZ, CRO, AMP, AMC, CIP and SXT, and Verapamil and Thioridizin HCl combinations. In addition, the combined use of CFM, CAZ, CRO and AMC, and PaβN were also killed bacteria 8.

Table 2 – Responses of clinical *E. coli* isolates against EPIs in combination with antibiotics (bacteria 2 to 5)

Part 1

Variants	Bacteria 2		Bacteria 3								
No EPI	AMP (+)	AMC (-)	AMP (-)	NOR (+)	CIP (-)	CFM (+)	CAZ (-)	CRO (-)	FEP (-)	ATM (+)	SXT (-)
Vera-pamil	AMP (-)	AMC (-)	AMP (-)	NOR (-)	CIP (-)	CFM (-)	CAZ (-)	CRO (-)	FEP (-)	ATM (-)	SXT (-)
Thio-ridizin HCL	AMP (-)	AMC (-)	AMP (-)	NOR (-)	CIP (-)	CFM (-)	CAZ (-)	CRO (-)	FEP (-)	ATM (-)	SXT (-)
PAβN	AMP (+)	AMC (-)	AMP (-)	NOR (+)	CIP (-)	CFM (-)	CAZ (-)	CRO (-)	FEP (+)	ATM (+)	SXT (-)
Note: (+) Bacterial growth, (-) No bacterial growth											

Part 2

Variants	Bacteria 4				Bacteria 5		
No EPI	AMP (+)	AMC (-)	CIP (+)	NOR (+)	CIP (+)	NOR (+)	SXT (+)
Verapamil	AMP (-)	AMC (-)	CIP (-)	NOR (-)	CIP (-)	NOR (-)	SXT (-)
Thioridizin HCL	AMP (-)	AMC (-)	CIP (-)	NOR (-)	CIP (-)	NOR (-)	SXT (-)
PAβN	AMP (-)	AMC (-)	CIP (+)	NOR (+)	CIP (+)	NOR (+)	SXT (+)
Note: (+) Bacterial growth, (-) No bacterial growth							

Table 4 presents the responses of clinical *E. coli* isolates against EPIs in combination with antibiotics for bacteria 9 and 10. According to the results, bacteria 9 was observed to be resistant against CN, CFM, CAZ, CRO, FEP, ATM, AMP, AMC, CIP and NOR, where bacteria 10 was resistant against CFM, CAZ, CRO, ATM, AMP and AMC.

As it was observed for previous strains, verapamil and thioridizin HCl combined with all antibiotics tested were killed bacteria 9 and 10, except for CRO and ATM against bacteria 9. Only combinations of verapamil, and CRO and ATM killed bacteria 9, but this strain was found to be resistant against the combinations of CRO and ATM, and thioridizin HCl. Also, bacteria 9 was observed to be susceptible against a combination of PaβN and AMC, where this is also true for a combination of PaβN and CAZ against bacteria 10.

Lastly, Table 5 shows the responses of clinical *E. coli* isolates against EPIs in combination with antibiotics for bacteria 11 and 12. Bacteria 11 was observed to be susceptible against all antibiotics within the concentration tested, but bacteria 12 found to be resistant against CFM, CRO, FEP, ATM, AMP and AMC. All antibiotics combined with verapamil,

except CRO, were killed bacteria 12. In addition, bacteria 12 was observed to be susceptible against all antibiotics combined with thioridizin HCl, except ATM. Bacteria 12 was also found to be susceptible against the combination of CFM and PaβN.

According to the results, the combinations of verapamil and antibiotics were observed to inhibit bacterial growth with 98.41%, where this value for thioridazine HCl and antibiotic combinations was 96.82% and 38.09% for PAβN (Figure 2).

According to some previous studies [22-34] PAβN, verapamil and thioridazin HCl are active EPIs for *E. coli* strains.

Özer [40], previously conducted a research to present the inhibition potential of PAβN on *E. coli* efflux pumps. In this study, bisbenzimidine, a fluorescent stain for DNA, was used in combination with some efflux pump inhibitors including PAβN. As a result, it was proved that PAβN inhibited the efflux of bisbenzimidine, thus the florescence is higher in bisbenzimidine – PAβN combination. In addition, Çetinkaya [41], also tested the efflux pump inhibition activity of PAβN in ciprofloxacin resistant *E. coli* strains and proved that increasing concentrations of PAβN decreased the MIC values for ciprofloxacin.

Table 3 – The responses of clinical *E. coli* isolates against EPIs in combination with antibiotics (bacteria 6 to 8)

	Bacteria 6				Bacteria 7				Bacteria 8									
	AMP	CIP	NOR	SXT	AMC	TZP	AMP	SXT	CFM	CAZ	CRO	FEP	ATM	AMP	AMC	TZP	CIP	SXT
No EPI	(+)	(-)	(-)	(-)	(+)	(+)	(+)	(+)	(+)	(+)	(+)	(-)	(-)	(+)	(+)	(-)	(+)	(+)
Vera-pamil	(-)	(-)	(-)	(-)	(-)	(-)	(-)	(-)	(-)	(-)	(-)	(-)	(-)	(-)	(-)	(-)	(-)	(-)
Thiori-dizin HCL	(-)	(-)	(-)	(-)	(-)	(-)	(-)	(-)	(-)	(-)	(-)	(-)	(-)	(-)	(-)	(-)	(-)	(-)
PAβN	(+)	(-)	(-)	(-)	(+)	(+)	(+)	(+)	(-)	(-)	(-)	(-)	(-)	(+)	(+)	(-)	(+)	(+)

Note: (+) Bacterial growth, (-) No bacterial growth

Table 4 – The responses of clinical *E. coli* isolates against EPIs in combination with antibiotics (bacteria 9 and 10)

	Bacteria 9										Bacteria 10						
	CN	CFM	CAZ	CRO	FEP	ATM	AMP	AMC	CIP	NOR	CRO	CAZ	ATM	AMP	AMC	CIP	NOR
No EPI	(+)	(+)	(+)	(+)	(+)	(+)	(+)	(+)	(+)	(+)	(+)	(+)	(+)	(+)	(+)	(-)	(-)
Vera-pamil	(-)	(-)	(-)	(-)	(-)	(-)	(-)	(-)	(-)	(-)	(-)	(-)	(-)	(-)	(-)	(-)	(-)
Thiori-dizin HCL	(-)	(-)	(-)	(+)	(-)	(+)	(-)	(-)	(-)	(-)	(-)	(-)	(-)	(-)	(-)	(-)	(-)
PAβN	(+)	(+)	(+)	(+)	(+)	(+)	(+)	(-)	(+)	(+)	(+)	(-)	(+)	(+)	(+)	(-)	(-)

Note: (+) Bacterial growth, (-) No bacterial growth

Table 5 – The responses of clinical *E. coli* isolates against EPIs in combination with antibiotics (bacteria 11 and 12)

	Bacteria 11		Bacteria 12						
No EPI	ETP (-)	FEP (-)	CFM (+)	CAZ (-)	CRO (+)	FEP (+)	ATM (+)	AMP (+)	AMC (+)
Verapamil	ETP (-)	FEP (-)	CFM (-)	CAZ (-)	CRO (+)	FEP (-)	ATM (-)	AMP (-)	AMC (-)
Thioridizin HCL	ETP (-)	FEP (-)	CFM (-)	CAZ (-)	CRO (-)	FEP (-)	ATM (+)	AMP (-)	AMC (-)
PAβN	ETP (-)	FEP (-)	CFM (-)	CAZ (+)	CRO (+)	FEP (+)	ATM (+)	AMP (+)	AMC (+)
Note: (+) Bacterial growth, (-) No bacterial growth									
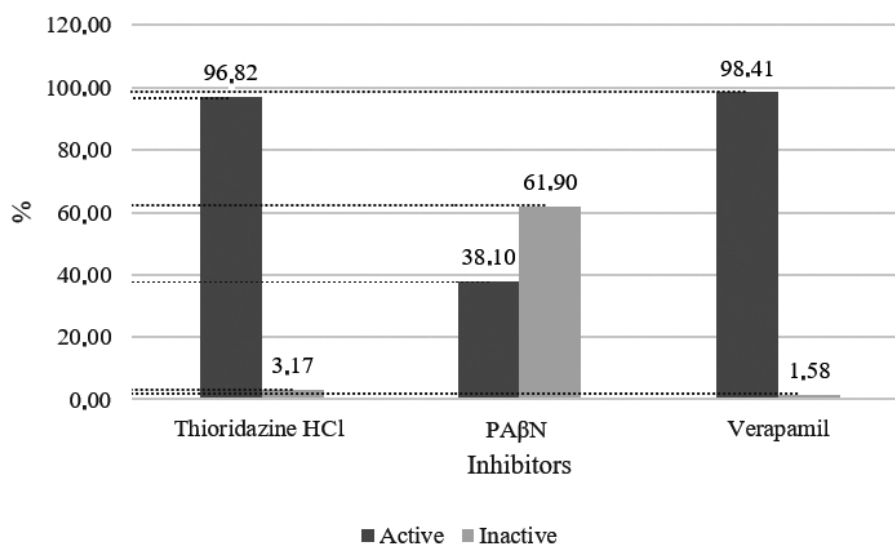
Figure 2 – The efflux capacities of twelve *E. coli* strains for different EtBr concentrations

The study conducted by Çoban et al. [42] also showed that PAβN decreased the MIC values 4 folds in *E. coli* strains presenting high fluoroquinolone resistance. Nevertheless, in the same study two-fold increase in MIC values was noted, when verapamil was used as an efflux inhibitor.

The responses of clinical *E. coli* isolates against EPIs in combination with antibiotics are given in Tables 3-5

Martins et al. [37] used two clinical *E. coli* isolates presenting multi drug resistance and as a result they proved that PAβN used in combination with tetracycline inhibit the growth of bacteria in both *E. coli* strains. Contrariwise, in only one *E. coli* strain thioridazine in combination with tetracycline inhibited the bacterial growth.

Dal [43], used *E. coli* ATCC 25922 as a control strain as we did in our study, and the result showed that the MIC values for ciprofloxacin gentamicin, erythromycin, chloramphenicol, trimethoprim and tetracycline did not affected from using in combination with efflux pump inhibitors, PAβN and 1-(1-naphthylmethyl) piperazine (NMP). According to Dal [43] any decrease was not observed in MIC values for *E. coli* ATCC 25922, because the MIC values were too low already, when compared to the other strains used. Since the *E. coli* ATCC 25922 strain was susceptible against all antibiotics used in this study with very low MIC values, there was no use to try any EPI – antibiotic combinations for *E. coli* ATCC 25922 in EPI test.

As a result, this study clearly presents that bacteria could have been developed resistance to antibiotics in time, which could cause severe problems for public health. In some of our previous studies we have used several multidrug resistant microorganisms, such as *Enterococcus faecalis*, *Enterococcus faecium* [44], *Acinetobacter baumannii*, *Proteus vulgaris* and *Streptococcus pneumoniae* [45; 46]. Time by time we observed an increase both in the number of multi drug resistant microorganisms and the resistance profiles of each strain. The results of the present study clearly indicate that one of the approaches to break their resistance against antibiotics is to use efflux pump inhibitors [47]. One of the approaches to break their resistance against antibiotics is to use efflux pump inhibitors. Studies presenting responses of multi drug resistant clinical isolated strains against EPIs could change the point of view in fight against such dangerous microorganisms [47-49]. Thus, this study extended our knowledge about the EPI use in multi drug resistant *E. coli* strains, which may be used in further researches searching for new efflux pump inhibitors to block efflux pumps present in *E. coli*. Present study also puts forward the responses of some clinical *E. coli* isolates against standard and commercially available EPIs, namely verapamil, phenyl arginine beta naphthylamide (PAβN) and thioridazine hydrochloride in combination with antibiotics, because in such researches the activities of EPI candidate molecules are needed to be compared with standard and commercially available EPIs.

Conclusion

As it was mentioned previously, antibiotics, which are used to treat and prevent infections, are compounds that inhibit the growth of or destroy microorganisms. But microorganisms may develop resistance to antibiotics. One of the reasons for resistance to antibiotics is efflux pumps. Thus, observing the responses of clinical isolated strains with multiple drug resistance and overexpressed efflux pumps against efflux pump inhibitors has great importance, in order to propose further studies about microorganisms with multiple drug resistance and overexpressed efflux pumps.

In the study, ethidium bromide-agar cartwheel method was firstly used to identify *E. coli* strains with overexpressed efflux pumps by transferring inoculum of all strains to EtBr containing agars, and overexpressed efflux pumps were determined by exposing agar plates to UV light. Verapamil, PAβN and thioridazine hydrochloride were used as efflux pump in-

hibitors (EPIs), and the lowest concentration of EPIs, which inhibit the growth of *E. coli* strains was determined by MIC test. Lastly, responses of microorganisms against efflux pump inhibitors were determined with a microplate-based assay, by using EPIs below their MIC values. The results of this study clearly presented that the combinations of Verapamil and antibiotics were observed to inhibit bacterial growth with 98.41%, where this value for Thioridazine HCl and antibiotic combinations was 96.82% and 38.09% for PAβN.

As a conclusion, it can be proposed that verapamil, thioridazine HCl and PAβN were observed to inhibit efflux pumps in our multi drug resistant clinical *E .coli* isolates at different levels with antibiotic combinations. In addition it can also be concluded that Verapamil and Thioridazine HCl inhibitors are more effective than PAβN inhibitors.

References

1   Kohanski M.A., Dwyer D.J., Collins J.J. (2010) How antibiotics kill bacteria: from targets to networks. Nat. Rev. Microbiol., vol. 8, no. 6, pp. 423-435. https://doi.org/10.1038/nrmicro2333.

2   Cheesman M.J., Ilanko A., Blonk B., Cock I. E. (2017) Developing new antimicrobial therapies: are synergistic combinations of plant extracts/compounds with conventional antibiotics the solution?. Pharmacogn. Rev., vol. 11, no. 22, pp. 57-72. https://doi.org/10.4103/phrev.phrev_21_17.

3   Lee G., Bishop P. (2012) Microbiology and infection control for health professionals. Australia: Pearson Higher Education. ISBN 9781486019144.

4   Al-Bahry S.N., Al-Mashani B.M., Al-Ansari A.S., Elshafie A.E., Mahmoud, I.Y. (2013) Escherichia coli tetracycline efflux determinants in relation to tetracycline residues in chicken. Asian Pac. J. Trop. Med., vol. 6, no. 9, pp. 718-722. https://doi.org/10.1016/S1995-7645(13)60125-X.

5   Blanco P., Hernando-Amado S., Reales-Calderon J.A., Corona F., Lira F., Alcalde-Rico M., Bernardini A., Sanchez M.B., Martinez, J.L. (2016). Bacterial multidrug efflux pumps: much more than antibiotic resistance determinants. Microorganisms, vol. 4, no. 1, p. 14. https://doi.org/10.3390/microorganisms4010014.

6   Soto S.M. (2013) Role of efflux pumps in the antibiotic resistance of bacteria embedded in a biofilm. Virulence, vol. 4, no. 3, pp. 223-229. https://doi.org/10.4161/viru.23724.

7   Moreira M.A.S., Souza E.C.D., Moraes C.A.D. (2004) Multidrug efflux systems in Gram-

negative bacteria. Braz. J. Microbiol., vol. 35, no. 1-2, pp. 19-28. http://dx.doi.org/10.1590/S1517-83822004000100003.

8 Yüce A. (2001) Mechanisms of gaining resistance to antimicrobial drugs. Klimik journal [Antimikrobik ilaçlara direnç kazanma mekanizmaları. Klimik dergisi], vol. 14, no. 2, pp. 41-46.

9 Bambeke V.F., Balzi E., Tulkens P.M. (2000) Antibiotic efflux pumps. Biochem. Pharmacol., vol. 60, no. 4, pp. 457-470. https://doi.org/10.1016/S0006-2952(00)00291-4.

10 Webber M.A., Piddock L.J.V. (2003) The importance of efflux pumps in bacterial antibiotic resistance. J. Antimicrob. Chemother., vol. 51, no. 1, pp. 9-11. https://doi.org/10.1093/jac/dkg050.

11 Zarakolu P. (2003) Active pump systems as resistance mechanisms in microorganisms. J. Hosp. Infect. [Mikroorganizmalarda direnç mekanizması olarak aktif pompa sistemleri. Hastane İnfeksiyonları Dergisi], pp. 131-136.

12 Lomovskaya O., Warren M.S., Lee A., Galazzo J., Fronko R., Lee M.A.Y., Blais J., Cho D., Chamberland S., Renau T., Leger R., Hecker S., Watkins W., Hoshino K., Ishida H., Lee V. (2001) Identification and characterization of inhibitors of multidrug resistance efflux pumps in Pseudomonas aeruginosa: novel agents for combination therapy. Antimicrob. Agents Chemother., vol. 45, no. 1, pp. 105-116. https://doi.org/10.1128/AAC.45.1.105-116.2001.

13 Li X.Z., Nikaido H., Poole K. (1995) Role of mexA-mexB-oprM in antibiotic efflux in Pseudomonas aeruginosa. Antimicrob. Agents Chemother., vol. 39, no. 9, pp. 1948-1953. https://doi.org/10.1128/aac.39.9.1948.

14 Nikaido H. (1998) Antibiotic resistance caused by gram-negative multidrug efflux pumps. Clin. Infect. Dis., vol. 27, no. Suppl_1, pp. S32-S41. https://doi.org/10.1086/514920.

15 Nikaido H. (2001) Preventing drug access to targets: cell surface permeability barriers and active efflux in bacteria. Semin. Cell Dev. Biol., vol. 12, no. 3, pp. 215-223. https://doi.org/10.1006/scdb.2000.0247.

16 Gülay Z. (2001) Antibiotic resistance mechanisms and solution suggestions: Resistance to beta-lactams and carbapenems. J. Hosp. Infect. [Antibiyotiklere direnç mekanizmaları ve çözüm önerileri: Betalaktamlara ve karbapenemlere direnç. Hastane İnfeksiyonları Dergisi], no. 5, pp. 210-229.

17 Kaatz G.W., Seo S.M. (1995) Inducible NorA-mediated multidrug resistance in Staphylococcus aureus. Antimicrobial agents and chemotherapy., vol. 39, no. 12, pp. 2650-2655. https://doi.org/10.1128/AAC.39.12.2650.

18 Gill M.J., Brenwald N.P, Wise R. (1999) Identification of an Efflux Pump Gene, pmrA, Associated with Fluoroquinolone Resistance in Streptococcus pneumoniae. Antimicrob. Agents Chemother., vol. 43, no. 1, pp. 187-189. https://doi.org/10.1128/AAC.43.1.187.

19 Poole K. (2000) Efflux-mediated resistance to fluoroquinolones in gram-negative bacteria. Antimicrob. Agents Chemother., vol. 44, no. 9, pp. 2233-2241. https://doi.org/10.1128/AAC.44.9.2233-2241.2000.

20 Lin J., Michel L.O., Zhang Q. (2002) CmeABC functions as a multidrug efflux system in Campylobacter jejuni. Antimicrob. Agents Chemother., vol. 46, no.7, pp. 2124-2131. https://doi.org/10.1128/AAC.46.7.2124–2131.2002.

21 Pumbwe L., Piddock L.J. (2002) Identification and molecular characterisation of CmeB, a Campylobacter jejuni multidrug efflux pump. FEMS Microbiol. Lett., vol. 206, no. 2, pp. 185-189. https://doi.org/10.1111/j.1574-6968.2002.tb11007.x.

22 Bambeke V.F., Pagès J.M., Lee V.J. (2006) Inhibitors of bacterial efflux pumps as adjuvants in antibiotic treatments and diagnostic tools for detection of resistance by efflux. Recent pat. Anti-infect. Drug Discov., vol. 1, no. 2, pp. 157-175. https://doi.org/10.2174/157489106777452692.

23 Li X.Z., Nikaido H. (2009) Efflux-mediated drug resistance in bacteria. Drugs, vol. 69, no. 12, pp. 1555-1623. https://doi.org/10.2165/11317030-000000000-00000.

24 Tegos P.G., Haynes M., Strouse J.J., Khan Md.T.M., Bologa G.C., Oprea I.T., Sklar A.L. (2011) Microbial efflux pump inhibition: tactics and strategies. Curr. Pharm. Des., vol. 17, no.13, pp. 1291-1302. https://doi.org/10.2174/138161211795703726.

25 Aygül A. (2015) The importance of efflux systems in antibiotic resistance and efflux pump inhibitors in the management of resistance. Mikrobiyol. Bul. [Antibiyotik direncinde dışa atım sistemlerinin ve dirençle mücadelede dışa atım pompa inhibitörlerinin önemi. Mikrobiyooji Bülteni], vol. 49, no. 2, pp. 278-291.

26 Opperman T.J., Nguyen S.T. (2015) Recent advances toward a molecular mechanism of efflux pump inhibition. Front. Microbiol., no. 6, pp. 421. https://doi.org/10.3389/fmicb.2015.00421.

27 Pagès J.M., Masi M., Barbe J. (2005) Inhibitors of efflux pumps in Gramnegative bacteria. Trends. Mol. Med., vol. 11, no. 8, pp. 382-389. https://doi.org/10.1016/j.molmed.2005.06.006.

28 Bohnert J.A., Kern W.V. (2005) Selected arylpiperazines are capable of reversing multidrug resistance in Escherichia coli overexpressing RND efflux pumps. Antimicrob. Agents Chemother., vol. 49, no. 2, pp. 849-852. https://doi.org/10.1128/AAC.49.2.849-852.2005.

29 Yang X., Domalaon R., Lyu Y., Zhanel G., Schweizer F. (2018) Tobramycinlinked efflux pump inhibitor conjugates synergize fluoroquinolones, rifampicin and fosfomycin against multidrug-resistant Pseudomonas aeruginosa. J. Clin. Med., vol. 7, no. 7, pp. 158. https://doi.org/10.3390/jcm7070158.

30 Loo T.W., Clarke D.M. (2001) Defining the drug-binding site in the human multidrug resistance P-glycoprotein using a methanethiosulfonate analog of verapamil, MTS-verapamil. J. Biol. Chem., vol. 276, no. 18, pp. 14972-14979. https://doi.org/10.1074/jbc.M100407200.

31 Gadhe C.G., Cho S.J. (2013) Investigation of Binding Modes of the Verapamil and Curcumin into Human P-glycoprotein (P-gp). J.Chosun Nat. Sci., vol. 6, no. 4, pp. 205-210. https://doi.org/10.13160/ricns.2013.6.4.205.

32 Porto C.E.D., Maia P.P., Freitas D.F.D., Araújo R.C.C., Siqueira M.E.P.B.D., Martins I., Santos-Neto Á.J.D. (2012) Liquid-phase microextraction for simultaneous chromatographic analysis of three antidepressant drugs in plasma. Quim. Nova., vol. 35, no. 1, pp. 72-76. https://doi.org/10.1590/S0100-40422012000100014.

33 Abongwa M., Martin R.J., Robertson A.P. (2017) A brief review on the mode of action of antinematodal drugs. Acta Vet., vol. 67, no. 2, pp. 137-152. https://doi.org/10.1515/acve-2017-0013.

34 Mullin S., Mani N., Grossman T.H. (2004) Inhibition of antibiotic efflux in bacteria by the novel multidrug resistance inhibitors biricodar (VX-710) and timcodar (VX-853). Antimicrob. Agents Chemother., vol. 48, no. 11, pp. 4171- 4176. https://doi.org/10.1128/AAC.48.11.4171-4176.2004.

35 Canli K., Akata I., Altuner E.M. (2016) In vitro antimicrobial activity screening of Xylaria hypoxylon. Afr. J. Tradit. Complement. Altern. Med., vol. 13, no. 4, pp. 42-46. https://doi.org/10.21010/ajtcam.v13i4.7.

36 Canli K., Yetgin A., Akata I., Altuner E.M. (2016) In vitro antimicrobial screening of Aquilaria agallocha roots. Afr. J. Tradit. Complement. Altern. Med., vol. 13, no. 5, pp. 178-181. https://doi.org/10.21010/ajtcam.v13i5.23.

37 Martins M., Couto I., Viveiros M., Amaral L. (2010) Identification of efflux mediated multi-drug resistance in bacterial clinical isolates by two simple methods. In: Antibiotic resistance protocols. Humana Press, pp. 143-157. https://doi.org/10.1007/978-1-60327-279-7_11.

38 Canli K., Yetgin A., Akata I., Altuner E.M. (2017) Antimicrobial activity and chemical composition screening of Anacyclus pyrethrum root. Indian J. Pharm. Educ. Res., vol. 51, no. 3s, pp. 244-248. https://doi.org/10.5530/ijper.51.3s.22.

39 Core R Team (accessed at September 15, 2019) "R: A language and environment for statistical computing." R-project.org. https://www.R-project.org/.

40 Özer C. (2013) Determination of antimicrobial resistance via efflux pump in bacteria by using microdilution method and bis-benzimide. Master Thesis Ege University Institute of Health Sciences [Bakterilerde dışa atım pompası yolu ile antimikrobiyal direnç gelişimini saptamada mikrodilüsyon yöntemi ve bisbenzimidin kullanımı. Yüksek Lisans Tezi Ege Üniversitesi Sağlık Bilimleri Enstitüsü]. İzmir, Turkey.

41 Çetinkaya E. (2007) In vitro investigation of the effects of the efflux pump inhibitors to the resistance inhibition of multidrug resistant gram negative and gram positive bacteria. Specialization Thesis, Ondokuz Mayıs University Faculty of Medicine, Department of Microbiology and Clinical Microbiology [Çok ilaca dirençli gram negatif ve gram pozitif bakterilerin direnç inhibisyonuna efluks pompa inhibitörlerinin etkilerinin in vitro araştırılması. Uzmanlık Tezi, Ondokuz Mayıs Üniversitesi Tıp Fakültesi Mikrobiyoloji ve Klinik Mikrobiyoloji Anabilim Dalı]. Samsun, Turkey.

42 Çoban A.Y., Birinci A., Ekinci B., Durupınar B. (2004) Investigation of the effects of efflux pump inhibitors on ciprofloxacin MIC values of high level fluoroquinolone resistant Esherichia coli clinical isolates. Mikrobiyol. Bul. [Yüksek düzey florokinolon dirençli Esherichia coli klinik izolatlarında effluks pompa inhibitörlerinin siprofloksasin MİK değerleri üzerine etkilerinin araştırılması. Mikrobiyoloji Bülteni] no. 38, pp. 21-25.

43 Dal T. (2009) The role of AdeABC efflux pump in multi-drug resistance Acinetobacter baumannii clinical isolates. Specialization Thesis, Marmara University Medical Faculty Medical Microbiology Department [Acinetobacter baumannii'nin klinik izolatlarının çoklu ilaç direncinde AdeABC aktif pompasının rolü. Uzmanlık Tezi, Marmara Üniversitesi Tıp Fakültesi Tıbbi Mikrobiyoloji Anabilim Dalı] İstanbul, Turkey.

44 Karaca B., Cihan A.Ç., Akata I., Altuner E.M. (2020) Anti-Biofilm and antimicrobial activi-

ties of five edible and medicinal macrofungi samples on some biofilm producing multi drug resistant Enterococcus strains. Turkish J. A. F. Sci. Tech., vol. 8, no. 1, pp. 69-80. https://doi.org/10.24925/turjaf.v8i1.69-80.2723.

45 Canli K., Yetgin A., Benek A., Bozyel, M.E., Altuner E.M. (2019) In vitro antimicrobial activity screening of ethanol extract of Lavandula stoechas and investigation of its biochemical composition. Adv. Pharmacol. Sci., vol. 2019, pp. 3201458. https://doi.org/10.1155/2019/3201458.

46 Canli K., Bozyel M.E., Yetgin A., Akata I., Altuner E.M. (2017) In vitro antimicrobial activity screening of Salvia fruticosa against wide range of microorganisms, multi drug resistant (MDR) bacteria and investigation of biochemical composition, Abstract Book of Japan – Turkey international symposium on pharmaceutical and biomedical sciences, Trabzon, Turkey, p.18.

47 Altinoz E., Altuner E.M. (2019) Antibiotic resistance and efflux pumps. Int. J. Inn. Res. Rev., vol. 3, no. 2, pp. 1-9.

48 Sharma A., Gupta V.K., Pathania R. (2019) Efflux pump inhibitors for bacterial pathogens: From bench to bedside. Indian J. Med. Res., vol. 149, no. 2, pp. 129-145. https://doi.org/10.4103/ijmr.IJMR_2079_17.

49 Kourtesi C., Ball A.R., Huang Y.Y., Jachak S.M., Vera D.M.A., Khondkar P., Gibbons S., Hamblin M.R, Tegos, G.P. (2013) Microbial efflux systems and inhibitors: approaches to drug discovery and the challenge of clinical implementation, Open Microbiol. J., vol. 7, no. 1, pp. 34-52. doi: 10.2174/1874285801307010034.

A. Bigaliev[1*] , L. Rihvanov[2], B. Bekmanov[3] , A. Zamuraeva[4] ,

L. Adilova[5] , A. Kozhahmetova[1]

[1]Al-Farabi Kazakh National University, Almaty, Kazakhstan
[2]Tomsk State Research Technical University, Tomsk, Russian
[3]Institute of General genetics and cytology, Almaty, Kazakhstan
[4]National Stock Company Medical University, Nur-Sultan, Kazakhstan
[5]S.Asfendiyarov National Medical University, Almaty, Kazakhstan
*e-mail: aitkhazha@gmail.com

Study of genetic effects of radiation pollution from contaminated territories on biota and human

Abstract. An important element of the set of works to determine the degree of impact of radiation contaminated territory on the environment and public health is the conduct of ecological-genetic and medical-biological research in the region. Current publication is based on the results of scientific research to analyze the current state of the habitat in radiation-contaminated territories. Genetic impact of the combined effect of radiation and non-radiation factors, unlike other mutagens, have not been studied sufficiently, and the results of this kind of research are rather contradictory. Industrial factors, the forceful action of full elementary evolutionary processes (mutational process, migration, isolation, etc.), can lead to qualitative transformations of the gene pool of populations. The study of chromosomal aberrations in natural populations and the human body acquires a special practical and theoretical significance related to the influence of factors of the changing habitat. Research data obtained using modern physico-chemical (AA-spectrometry, radiology), cytological and molecular-genetic methods are presented wuth a complex of test systems in order to fully assess the effectiveness of the combined action of radiation and non-radiation factors. Observations in the field and lab facilitate establishing a previously unknown fact that complexes of soil animals with chronic irradiation with doses of 0.5-20 mSv/day experience clearly recorded oppression. Especially sensitive are earthworms *Eisenia fetida*. The quantitative dependence of the spectrum of structural and numerical aberrations of chromosomes was studied. The frequency of cells with chromosome aberrations averages 2.4%. Both structural (93.6%) and numerical aberrations (6.4%) of chromosomes were revealed. Among the cells with chromosome structure disorders, chromosomal type aberrations (67.04%) prevailed over chromatid (32.95%), which indicates a predominant radiation exposure.

Key words: cytogenetic, ecology, chromosome, population, molecular genetic, radiation genetic, earthworms, polyheta.

Introduction

In the past decade and a half, the concept of radiation-induced genome instability has been shaped and intensively studied. According to the literature, this phenomenon is the emergence of de novo multiple genetic changes (gene or chromosomal) non-clonal in approximately 10-30% of descendants of irradiated cells that survived after irradiation [1-3]; observed after irradiation not only at high, but also so-called low doses (200 cSv or less) of radiation [4; 5].

Today the problem of assessing the environmental hazard and the genetic efficacy of the combined action of low doses of mutagens, such as natural radionuclides and heavy metals, have a complex effect on living objects. The genetic effects of the combined action of these factors, unlike other mutagens, have been studied insufficiently, and the results of such studies are rather contradictory so-called anthropogenic factors, intensifying the action of all elementary evolutionary processes (mutational process, migration, isolation, etc.), can lead to qualitative transformations of the gene pool of populations [4; 6; 7]. Therefore, it

becomes necessary to study the effects of chronic exposure to ionizing radiation on natural populations in order to fully assess the effectiveness of the combined effect of radiation and non-radiation factors that are difficult to reproduce in the laboratory. The study of chromosomal aberrations in natural populations of organisms acquires a special significance in connection with the influence of factors of a changing habitat.

The growing development of the extractive industry in Kazakhstan requires further intensification of studies of migration patterns in natural ecosystems of heavy natural and artificial radionuclides, as well as the biological effects of ionizing radiation at the population and biogeocenotic levels.

The purpose of this publication – based on the results of scientific research to analyze the current state of the habitat in radiation-contaminated territories, namely, to give an ecological-genetic assessment of the consequences of radiation effect on biota and human.

Materials and methods

Conducted conventional cytogenetic (micronucleus analysis [8-11] in peripheral blood cells of humans). Cytogenetic analysis and photography were performed under a microscope (MicroOptix, Austria, 2013) [12]. In persons living in settlements adjacent to the source of pollution was carried out in clinics from the phalanx of the upper extremities (fingers), observing the principles of antiseptics. Blood smears were made on the prepared glasses according to the method for micronuclear analysis. Statistical processing of the results was carried out by conventional methods of biostatistics in biology and medicine [11; 13]. Molecular genetic RAPD-PCR analysis [14; 15].

A set of reagents QIAamp DNA Mini Kit (Qiagen, USA) was used for genomic DNA extraction.

Quantitative and qualitative assessment of the isolated DNA was performed using DNA photometer (Biofotometer Plus, Eppendorf, Germany) and electrophoretic analysis. PCR mixture with Taq polymerase, PCR Master Mix (Thermo Scientific, Lithuania) was used for DNA amplification of the studied and control samples. Amplification was performed automatically on the programmable amplifier Master cycler nexus Gradient (Eppendorf, Germany) using the Hot-start PCR method. Polymerase chain reaction was performed with ten-membered oligonucleotide primers synthesized in RSE Institute of General genetics and Cytology (Kazakhstan) on synthesizer ASM-800 of Bioset (Russia). The PCR reaction was carried out in the following temperature regime: initial denaturation at 94 °C for 2 min, 40 cycles consisting of four stages, including 45 sec at 92 °C, 30 sec at 37 °C, 15 C at 45 °C and 2 min at 72 °C. The reaction is performed during 10-minute elongation stage at 72 °C. Negative reaction control (contamination test) contained a reaction mixture without DNA addition.

Results and discussion

The content of γ-emitting radionuclides and radioactivity of the test objects. Observations and experiments in environment made it possible to establish a previously unknown fact that, under chronic irradiation with doses, such as 0.5-20 mSv/day, the complexes of soil animals undergo clearly recorded inhibition [11]. Particularly sensitive are earthworms [16].

As a result of determining the total level of total radioactivity of the test objects under study, the background level of β-radiation was detected in representatives of the ringed worms – *Nereis diversicolor* and *Eisenia fetida* (Table 1).

Table 1 – The total level of β-radiation test objects

Sample title	β-radiation, 1 / min * cm^2 (SD± SE)	Sample title	β-radiation, 1 / min * cm^2 (SD± SE)	Sample title	β-radiation, 1/ min * cm^2 (SD± SE)
Abramus brama	0.88±0.003	*Unio pictorum*	0.86±0.004	*Nereis diversicolor*	1.24±0.005
Sander lucioperca	1.41±0.007	*Dreisena polymorha*	0.86±0.003	*Eisenia fetida (Earworms)*	8.81±0.021
Sander bersh	1.42±0.007	*Nereis diversicolor*	6.24±0.021	*LD (limited Dose)*	5

Basically, the results on the content of γ-emitting radionuclides in test objects correlate with this indicator. Only in this case, the results of all measurements are higher or close to the Limiting Dose (LD) with the exception of Cesium-137 (Table 2).

Table 2 – The content of γ-emitting radionuclides in test objects

Sample	The activity of radionuclides			
	Bk/kg		(SD± SE)	
	Cs-137	Ra-226	Th-232	K-40
Abramus brama	64.5±0.5	155±0.4	119±0.5	1296±12.3
Sander lucioperca	63±0.4	123±0.4	70±0.4	1124±12.4
Sander bersh	65±0.4	164±0.5	124±0.4	1300±11.9
Unio pictorum	109±0.5	31±0.3	43±0.4	625±9.9
Dreisena polymorha	76±0.3	32±0.5	45±0.4	624±9.8
Nereis diversicolor	111±0.5	100±0.3	100±0.3	850±9.8
Eisenia fetida	125±0.4	185±0.6	169±0.5	1332±12.5
Nereis diversicol	89±0.5	29±0.4	40±0.3	594±12.3
Limiting Dose	370	32	45	700

According to the data presented in the Table 2, the activity of Cesium-137 in all test objects is significantly lower than LD. The activity of Potassium-40 in mollusks and gadflies is less than the LD, while in other organisms it is much higher. The activity of Radium-226 and Tilura-232 in the tissues of the *Sander bersh, Dreisena polymorha* are within the LD. Therefore, of all studied fish species, pike perch accumulates less radionuclides, although as an active predator, this species should receive more radionuclides from food. Apparently, low activity are associated with the presence of the molecular mechanism for removing radionuclides from the body. Among invertebrates, the number of studied radionuclides (except for cesium) is significantly higher than the LD. In species more closely contacting with the soil and the ground: the *Eisenia fetida* earthworm and the polychaetes (*Nereis diversicolor*). Apparently, this is due to the subsidence and accumulation of radionuclides at the bottom and in the coastal soil, from which they enter the body of the above species with food. The presence of high activity of Radium-226 in the studied objects is explained by the presence of this isotope in all mountain and sedimentary rocks. Accordingly, this radionuclide always accompanies the pollution of the mining industry. Being in a dissolved state in water, radium forms the so-called secondary materials, which is part of the salts of lead, calcium, barium, etc. Referring to the group of alkaline earth metals, radium is an analogue of the elements of biological accumulators of copper and magnesium. Thorium-232 and Potassium-40 are low-toxic radionuclides, but at high activity that were found in invertebrate test objects, these isotopes contribute to the irradiation of organisms. Thus, on the basis of data on the content of radioisotopes in the body of hydro species, one can judge about the unfavorable radiation situation in the waters of the Northern Caspian. Of particular concern are the large concentrations of radionuclides in earthworms, which indicates that the soil in the studied area is radioactively contaminated. Accordingly, it can be assumed that radionuclides enter the food products of the region's population not only with commercial fish, but also along the following chain: soil – plants – livestock – meat and dairy products. It is these groups of organisms that can be recommended as bio indicators of radioactive contamination of the soil.

The effect of radiation on the body of animals and humans. Assessing the impact of factors that pollute the human environment, genetic consequences should be included. Among the factors leading to chromosome abnormalities, ionizing radiation is of particular importance, since all types of radiation cause chromosomal aberrations in human germ cells and somatic cells [17].

Cytogenetic analysis in rodents. Catching rodents big gerbil and small *R. opimus* was carried out

with live bait from adjacent to the tailing dump areas and were taken as control from the Balkhash zone. Following the standard (conventional) methods cytological preparations for chromosome analysis and samples for DNA extractions were conducted accordingly (molecular genetic research).

To establish the mutagenic potential, a test was used to account for chromosomal and genomic mutations in bone marrow cells. The obtained data on the assessment of the potential mutagenic hazard of contamination of the tailing dump and surrounding areas with oil and petroleum products using as a test object of big gerbil (*R. opimus*), showed that in all four points of the rodents studied, there are changes in both the frequency of aberrant cells and types of chromosomal abnormalities.

Cytogenetic studies of large gerbils (*R.opimus*). The karyotype of the great gerbil (*R. opimus*) consists of 40 chromosomes (Figure 1). 8th chromosome is a large submetacentric or metactntrics. 15 pairs of chromosomes gradually decrease in size and form are submetacentric or metacentric. One pair of chromosomes is the smallest in size and morphologically they are acrocentric chromosomes.
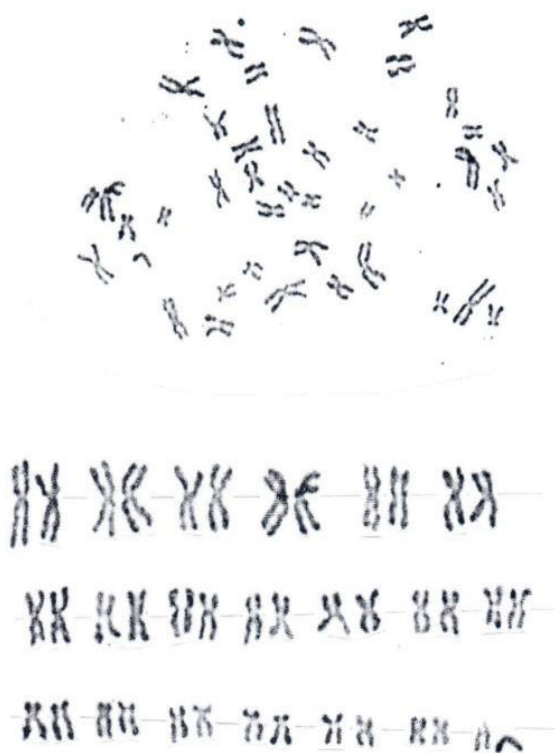

Figure 1 – Karyotype of a *big gerbil* (2n=40)

The maximum values of the studied cytogenetic parameters were observed in heavily polluted areas. In animals caught near the tailing dump, the frequency of chromosomal aberrations in the bone marrow of the gerbil is (5.03±13)% at t=3.83; p<0.003, which exceeds the spontaneous level by 2.5 times. Rodents living in the neighborhood, in the adjacent territory to the tailing dump really detect individual variability in cytogenetic damage. The level of cytogenetic disorders in *R. opimus*, living in the surrounding area, 1.5 times lower than in rodents from the tailings. In the studied animals of the adjacent territory at a distance of 500 m (place 1, 2), the frequency of metaphase cells with aberrations was (4.97±1.21)% at (t=2.58; p<0.01), 2,3 times higher than spontaneous level, and points 3.4 (1000 m) – (4.05±1.02)% at (t=2.01; p<0.05), 1.5 times higher than the level of spontaneous chromosomal mutations.

The quantitative and qualitative composition of cytogenetic disturbances revealed in this work according to dislocation from the source of pollution in the studied points testifies to the presence of strong clastogenic effects of pollutants here. The studied mutagenic factors radionuclides, heavy metals and others are the cause of the high frequency of chromosomal mutations of *R. opimus* in the surveyed areas. However, it is difficult to say which of these mutagenic environmental factors caused the observed changes [18]. However, the revealed level of genetic disorders in wild rodents with appropriate extrapolation can be considered as the real maximum mutagenic effect of environmental factors in relation to people living in these areas [19-21].

Figure 2 – Chromosome of metaphase cell with terminal deletion in *big gerbil*
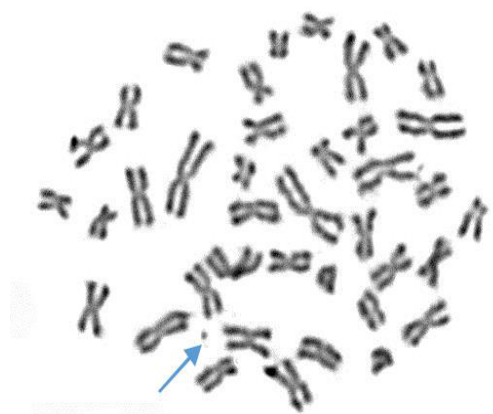
Figure 3 – Metaphase cell
with diploid set of chromosomes (2n=38)

Chromosomal rearrangements play an important role in karyotype divergence and population adaptation in many animal and plant species, and there are differing views on the role of chromosomal polymorphism in natural populations.

Micronuclear test. We examined the inhabitants of the settlements adjacent to the source of pollution of the coastal zone of the Caspian sea, using a micronuclear test. Table 3 presents the results of micronuclear test of people living in settlements: the city of Aktau and towns: Mangistau-1 village, Mangystau-5 village, Baskuduk village and Akshukur village.

Table 3 – The amount of blood examined erythrocytes with micronuclei in patients

Place of observation	Quantity of patients	Number of analyzed erythrocytes, in thousands	Erythrocytes with micronuclea	
			Absolute number	% (SD± SE)
Control group	35	482.4	2	0.415±0.01
Industrial chemistry metallic plant, Aktau city	10	1819.622	2029	3.693± 0.35
Baskuduk village	5	1180.5	1037	1.224±0.07
Mangystau-5 village	5	1158.9	1057	1.2250.06
Akshukur village	11	2368.3	1797.2	4.2560.03
Mangistau-1 village	6	1235.6	1225	1.513±0.06

As follows from Table 3, the maximum frequency of cytogenetic disorders in persons living in the area of the Aktau (uranium enterprises) was detected in the age group up to 60 years and ranges from 0.199 – 0.287, which is slightly lower than the age group over 60 years – from 0.189 to 0.201, and the minimum frequency in children is 0.102.

According to this test similar results were obtained from residents of other settlements adjacent to the source of pollution (total residents – 33). In particular, residents of Baskudyk village have the highest frequency of cells with disorders MN found in children under the age of 5 years (0.236-0.244), and in the age group of 31-40 years it is slightly lower (0.175-0.193).

A sufficiently high frequency of cells with MN in the blood of the examined residents of Mangystau – 5 in the age group 30-45 years and ranges from 0.208-0.221, and in persons over 45 years within 0,197 was revealed. In persons living in the village of Akshukyr, the number of cells with MN is: in the group over 60 years in the range 0.163-0.184; in the

age of 50 years-from 0.196 to 0.204; in the group of 20-23 years-from 0.213 to 0.25; in children-0.228. The number of erythrocytes with micronuclei in the blood of the examined art. Mangistau-1, up to 30 years ranges from 0.196-0.255, and in the group over 50 years – from 0.184-0.198.

Many authors [8; 9; 11; 14] evaluated the micronucleus test as a convenient method of screening substances, allowing to quickly determine the presence or absence of cytogenotoxicity and mutagenicity of various compounds. Comparison of the results of this study with the literature data indicates the adequacy of the results obtained by us, that is, the induction of pollutants, in our case radionuclides and chemical contaminants, in human peripheral blood cells leads to violations of genome stability.

As follows from the analysis, a clear dependence of cytogenetic disorders on the micronucleus test (MN) from the age of the examined is not observed. In turn, there is an increase in the frequency of cells with cytogenetic disorders (MN), depending on the location of the village from the source of pollution,

in particular, the tail of the Koshkar-Ata. Thus, the greatest frequency is found in persons living in the area GHS Aktau and towns have Baskuduk, Akshukur that corresponds to the data of radiation ecological surveys of these territories.

Molecular genetic analysis of the population living in Mangystau region by DNA repair genes XRCC1 and XRCC3. To analyze the state of re-

pair systems of the organism in the inhabitants of Mangystau region, polymorphism of genes XRCC1 Arg194Trp (rs1799782) and XRCC3 Trp241Met (rs861539) were studied. A group of people living in Almaty region was used as a control. The results of electrophoretic analysis of restriction products after PCR-analysis are presented on Figures 4 and 5.
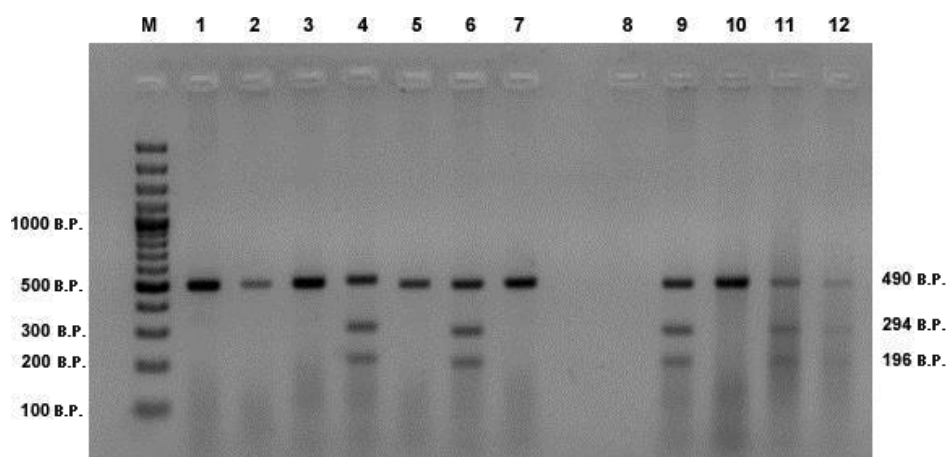
Figure 4 – Electrophoresis products in a polymorphic restriction site 194Arg/ Trp
of the XRCC1 gene. Note: M: molecular DNA marker. Homozygotes by normal allele XRCC1
194 Arg/Arg – 1, 2, 3, 5, 7, 10 heterozygotes XRCC1 194 Arg/Trp – 4, 6, 9, 11, 12
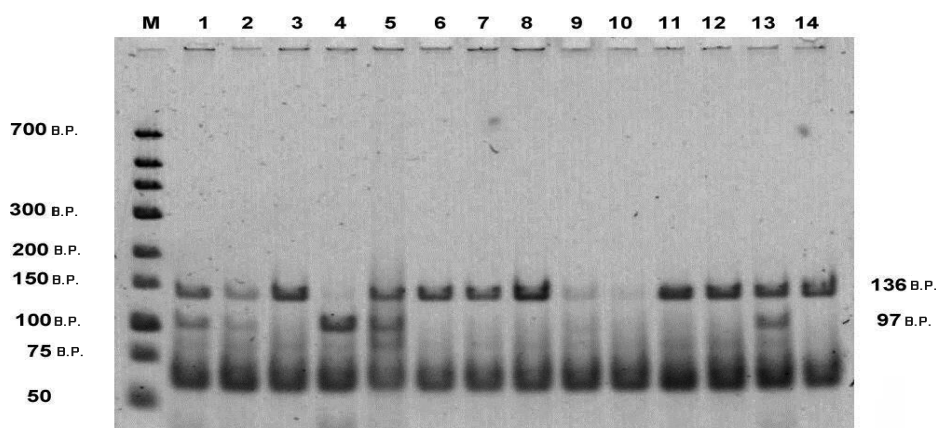
Figure 5 – Electrophoresis products of the restriction in the polymorphic site 241
Thr/Met XRCC3 gene. Note: M: molecular DNA marker. Homozygotes by normal allele
XRCC3 241 Thr/Thr– 3, 6, 7, 8, 9, 11, 12, 14 heterozygotes XRCC3 241 Thr/Met – 1, 2, 5, 13
homozygotes by mutant allele XRCC3 241 Met / Met – 4

The research method "case-control" is an effective method for epidemiological assessment of the relative effect (hazard ratio). The most important and crucial point of this study is the formation of groups for analysis.

As a criterion, we considered living in an ecologically unfavorable region of Kazakhstan near the Koshkar-Ata tailing dump.

The case study group was formed from representatives living in the Mangystau region (95 people) (Table 4).

Table 4 – Frequencies of polymorphic alleles of XRCC1 Arg194Trp and XRCC3 Trp241Met genes

gene	Alleles of gene	Allele frequency			
		Group "case"	Group "control"	Data NCBI/NIH	
				Asian Populations	European Populations
XRCC1 Arg194Trp	Arg	0.95	0.951	0.761 – 0.711	0.948 – 0.908
	Trp	0.205	0.049	0.239 – 0.289	0.052 – 0.092
XRCC3 Trp241Met	Thr	0.874	0.837	0.942 – 0.889	0.571 – 0.500
	Met	0.126	0.163	0.058 – 0.110	0.429 – 0.500

The mean age in this group was 35.16±1.16 years. The gender composition of the experimental group is 85% of women and 15% of men. The selection of the control group was based on the analysis of the database of biological samples (personal data and clinical examination data) of the laboratory of molecular genetics of the Institute of General genetics and Cytology, Almaty, Kazakhstan. Clinical material from these people was collected in 2008-2014 in the course of scientific projects of the Institute of genetics and Cytology, Almaty, Kazakhstan. Blood and DNA samples are stored in the Biological bank at -20 °C and -80 °C. The control group included healthy individuals living in ecologically favorable areas of Almaty region. The control population of conditionally healthy donors was selected in the maximum possible accordance with the personal data of the surveyed group according to age and gender criteria. A total of 92 peripheral blood samples were collected for the control group. The mean age in the control group was 36.99±1.02 years. The gender composition of the control group is 78% women and 22% men. The Student's t-test was used to determine the statistical significance of the differences in the studied samples. The differences were considered to be significant, starting with $p<0.05$, that is, when the probability of differences was equal to or greater than 95%. The analysis of the experimental and control cohorts showed that the differences of the compared values in Table 4 are not statistically significant, since in all cases $p>0.05$.

According to international experts, the threshold dose for deterministic (acute, immediate) effects is 0.2 Gr. Therefore, at lower doses, the only type of radiological consequences are stochastic (remote) effects – oncological and hereditary diseases. Considering the range of such small doses, it is more correct to speak of low radiation levels (LRL), implying not only the absolute value of the dose, but also the low intensity of radiation exposure – a low dose rate [4; 5].

All information about the long-term effects of LRL in humans was obtained either by extrapolation of experimental data on animals, or as a result of direct radiation-epidemiological studies. The main source of the latter is the data of acute single exposure of high dose rate in atomic catastrophes (Hiroshima and Nagasaki, Chernobyl, Fukushima, and other). The quantitative parameters of the probability of development of the stochastic effects of an LRL are characterized by a number of important radiobiological parameters. However, due to the lack of specific data, these effects have not been accurately determined to date and remain a subject of discussion.

If we consider that the human genome contains up to 100,000 genes, then the potential number of possible mutations, as well as various radiation genetic disorders, can be enormous, especially since there are no specific radiation mutations. Irradiation only increases the likelihood of the manifestation of all categories of hereditary disorders that occur in natural conditions – Mendelian, chromosomal and multifactorial [15].

In the process of evolution of the species under consideration, such a mechanism in humans has reached a maximum, ensuring the leveling of genetic effects in LRL. Without a doubt, the validity of the proposed mechanism needs experimental confirmation. The latest data on the assessment of the minimum significance of radiation genetic risk and provide grounds for a confident conclusion that this risk, as a factor taken into account when regulating LRL has firmly shifted to a much less significant place compared to radiation-carcinogenic risk. In this regard, there are two independent, albeit interrelated research aspects of radiobiology: basic research – the study of the effects of ionizing radiation at the molecular and cellular levels and applied – recording effects at the organismic and population levels to assess radiation safety [22].

It is important to keep in mind that it is impossible to evaluate the response of the whole organism in the field of an LRL under the conditions of a variety of other factors, based solely on radiobiological knowledge of the effects at previous levels of biological organization. The fact is that with the modern possibilities of registering the most diverse indicators of the action of radiation, the dose ranges at the cellular and organismic levels are very different. If this is not taken into account, then there are conclusions about the harm to human health of radiation in the range of so-called "ultra-low" doses. Knowledge of the effects of radiation on humans with an LRL (low exposure levels – up to 100 background levels) are given by radiation epidemiological studies.

Information on the effect of LRL for the population of Kazakhstan needs to develop a separate program in relation to the specific conditions of uranium mining activities, guaranteeing the technical conditions of radiation safety, ensuring compliance with radiation hygiene standards for external and incorporated exposure to different types of ionizing radiation. This program should be based on the data of modern scientific studies, taking into account the limits of applicability and significance for radiation safety of a person of relevant results at the molecular and cellular levels. The relevance of such a work program is evidenced by the materials of the 55th session of UNSCEAR, held from May 21 to 25, 2007 in Vienna (Austria) [13]. As was noted at this session, the exposure of occupational groups and the risk to the population of adjacent areas in the mining industry is a particular problem today, when very large amounts of waste rock are formed, containing even low concentrations of ^{238}U and ^{232}Th and their decay products. Although, on average, radiation doses of miners are insignificant, amounting to several micro-Sieverts(mSv) per year, in some cases they can reach several milli-Sieverts, which already represents a radiation risk [17; 24]. Japanese scientists studied the chromosomes in the blood leukocytes of people exposed to the atomic bombardment of Hiroshima and Nagasaki, and showed that chromosomal rearrangements are characteristic of human leukocytes even after at least three decades after the explosion.

When conducting cytogenetic analysis of leukocytes of people who received radiation, it turned out that all irradiated people had leukocytes, among which more than 10% had chromosomal rearrangements [6; 24-26]. The results of epidemiological and experimental studies indicate the induction of genome instability in the offspring of parents exposed to ionizing radiation. This genomic instability is primarily manifested by an increase in the rate of mutation and an increase in the risk of tumor and other pathologies in the offspring [8; 17]. Studies of many scientists have shown that the phenomenon of genomic instability is found in populations of distant descendants irradiated. At the same time, the appearance of different types of chromosomal aberrations in cells and an increase in the overall level of chromosome abnormalities are noted. It was revealed experimentally that prolonged low-intensity irradiation can cause a significant increase in the number of cells with chromosomal aberrations and reciprocal chromosomal translocations not only in the exposed but also in their descendants of the first [16; 25; 26], and especially the second generation. To date, cytogenetic studied the patterns of action of a wide variety of gene toxically agents and accumulated a sufficiently large amount of factual material on the dynamics of the yield and diversity of types of chromosomal aberrations, which are difficult to replicate double-stranded DNA breaks. The work of many scientists [16; 26] is devoted to the study of new molecular mechanisms of the formation of cytogenetic damage.

Conclusion

On the basis of data on the content of radioisotopes in the body of hydro species (fish's, mollusk's, polychaetes), one can judge about the unfavorable radiation situation in the waters of the Northern Caspian. Of particular concern are the large activity of radionuclides in body of polyhaetes and earthworms, which indicates that the soil in the studied area is radioactively contaminated. It is these groups of organisms that can be recommended as bio indicators of radioactive contamination of the soil.

The studied mutagenic factors radionuclides, heavy metals and others are the cause of the high frequency of chromosomal mutations of wild mouse (*R. opimus*) in the surveyed areas. The level of cytogenetic disorders in *R. opimus*, living in the surrounding area, 1.5 times lower than in rodents from the tailings. In the studied animals of the adjacent territory at a distance of 500 m (places 1, 2), the frequency of metaphase cells with aberrations was (4.97 ± 1.21)% at $(t=2.58; p<0.01)$, 2,3 times higher than spontaneous level, and points 3.4 (1000 m) – (4.05 ± 1.02)% at $(t=2.01; p<0.05)$, 1.5 times higher than the level of spontaneous chromosomal mutations [18]. However, the revealed level of genetic disorders in wild rodents with appropriate extrapolation can be considered as the real maximum mutagenic effect of environmental factors in relation to people living in these areas.

As next test-system for examined the inhabitants of the settlements adjacent to the source of pollution of the coastal zone of the Caspian sea was used a micro-nuclear test. Was obtained the maximum frequency of cytogenetic disorders in people living in the area of the Aktau (uranium enterprises) was detected in the age group up to 60 years and ranges from 0.199 – 0.287, which is slightly lower than the age group over 60 years – from 0.189 to 0.201, and the minimum frequency in children is 0.102. According to micronuclear test similar results were obtained from residents of other settlements adjacent to the source of pollution (total residents – 33). In particular, residents of Baskudyk village have the highest frequency of cells with disorders (MN) found in children under the age of 5 years (0.236-0.244), and in the age group of 31–40 years it is slightly lower (0.175-0.193). A sufficiently high frequency of cells with MN in the blood of the examined residents of Mangystau – 5 in the age group 30–45 years and ranges from 0.208-0.221, and in persons over 45 years within 0,197 was revealed. In persons living in the village of Akshukyr, the number of cells with MN is: in the group over 60 years in the range 0.163-0.184; in the age of 50 years-from 0.196 to 0.204; in the group of 20-23 years-from 0.213 to 0.25; in children – 0.228. The number of erythrocytes with micronuclei in the blood of the examined art. Mangistau-1, up to 30 years ranges from 0.196-0.255, and in the group over 50 years – from 0.184-0.198.

The results of molecular genetic investigation by electrophoretic analysis of restriction products after PCR-analysis the state of repair systems of the organism in the inhabitants of Mangystau region polymorphism of genes XRCC1 Arg194Trp (rs1799782) and XRCC3 Trp241Met (rs861539) was obtained. The study of the distribution of genotypes in people living near radiation-contaminated areas of Western Kazakhstan showed that the distribution of the mutaion genotype (TRP/TRP) gene XRCC1 Arg194 total-1.7%, and the gene XRCC1 arg 399GLn(English/English) – 8.6%, XRCC3Thr 241Met – (Met/Met)-7% and XPD751GLn – 5.2%-contaminated areas of Western Kazakhstan showed that the distribution of the mutaion genotype (TRP/TRP) of the gene XRCC1 Arg194 total – 1.7,%, and the gene XRCC1 arg 399gln(ENG/ENG) – 8.6%, xrcc3thr 241met – (Met/ Met) – 7% and XPD751GLn – (GLn/Gln) – 5.2%. The research method "case-control" is an effective method for epidemiological assessment of the relative effect (hazard ratio). The most important and crucial point of this study is the formation of groups

for analysis. As a criterion, we considered living in an ecologically unfavorable region of Kazakhstan near Koshkar-Ata tailing dump. In order to explain the possible causes of surprising interspecific quantitative differences in the manifestation of radiation-genetic consequences.

References

1   Preston J.K., Dean B.J., Galloway S. (1987) Mammalian in vivo cytogenetic assays. Analysis of chromosome aberrations in bone marrow cells. Mytat. Res., vol. 189, pp. 157-165.

2   Dubinin N.P., et al. (1990) Human genetic fund and environmental mutagens [Genofond cheloveka i mutageny okruzhajushhej sredy]. Materials of AS USSR. Report 1, pp. 19-31.

3   Rihvanov L.P. (2009) Radioactive elements in the environment and problems of radioecology [Radioaktivnye jelementy v okruzhajushhej srede i problemy radiojekologii]. Tomsk Polytechnic University Publ., 428 p.

4   Jablokov A.V. (2013) Non-appropriacy of the official concept of radioprotection in low dose impact field [Neadekvatnost' oficial'noj koncepcii radiacionnoj zashhity v oblasti vlijanija malyh doz]. Materials of IV international conference. Tomsk, June 4-8, pp. 580-587.

5   Mosse I., Dubovic B., Kostrova L., Molophei V. (2006) Melanin can be used for people protection against chronic irradiation and low radiation doses. 4th International Workshop on Space Radiation Research and 17th Annual NASA Space Radiation Health Investigators' Workshop, Book of Abstracts, Dubna, p. 81.

6   Bigaliev A.B. (2017) Ecological genetics, Qazaq University Publ., 346 p.

7   Rihvanov L.P. (2013) Radioactivity and radioactive elements in biosphere, possible ecological consequences [Radioaktivnost' i radioaktivnye jelementy v biosferei vozmozhnye jekologicheskie posledstvija]. Materials of IV international conference. Tomsk, June 4-8, pp. 440-447.

8   Loomis D.P., Shy C.M., Allen J.W., Saccomanno G. (1990) Micronuclei epithelial cells from sputum of uranium workers. Scand J Work Environ and Health, vol. 16, no. 5, pp. 355-362.

9   Montero R., Serrano L., Davila V., Segura Y., Arrieta A., Fuentes R., Abad I., Valencia L., Sierra P., Camacho R. (2003) Metabolic polymorphism and the micronucleus frequency in buccal epithelium of adolescents living in an urban environment. Environ. Mol. Mutagen., vol. 42, no. 3, pp. 216-222.

10 Lloyd D.C., Edwards A.A., Moquet, J.E., Guerrero-Carbajal Y.C. (2000) The role of cytogenetics in early triage of radiation casualties. Appl. Radiat. Isot., vol. 52, pp. 1107-1112.

11 MacGregor J.T., Heddie J.A. Hite F., Tice R.R. (1987) Guide lines for the conduct of micronucleus assays in mammalian bone marrow erythrocytes. Mutat. Res. Genet. Toxicol. Test, vol. 189, no. 2, pp. 103-112.

12 Zang K.D., Back E. I. (1968) Quantitative studies on the arrangement of human metaphase chromosomes. Individual features in the association pattern of the acrocentric chromosomes of normal males and females. Cytogenetics, vol. 6, pp. 455-470.

13 Levan A., Fregda K., Sandberg A.A. (2006) Nomenclature for centric position on chromosomes. Hereditas, vol. 52, pp. 201-220.

14 Mac Key B.E., Mac Gregor J.N. (1979) The Micronucleus test: statistical design and analysis. Mutat. Res., vol. 64, no. 2, pp. 195-201.

15 Mosse I.B. (2012) Genetic effects of ionizing radiation – some questions with no answers. Env. Radioactivity, vol. 112, no. 1, pp. 70-75.

16 Bigalyev A.B., Shalabaeva K.Z., Kulumbetov A.K., Jiyenbekov A.K., Adylova L.M., Kozhahmetova A.N., Myrzakhan A.G., Ishanova N.E. (2017). Ecology-genetical evaluation of radiation and chemical pollution (associated with heavy metals) on biota and man. International Journal of advanced research. vol. 5, no. 10, pp. 819-825.

17 Catana A., et al. (2012) Genetic polymorphism of DNA repair gene ERCC2/XPD (Arg 156 Arg) (A22541C) and lung cancer risk in Northern Romania. Revista Română de Medicină de Laborator. vol. 20, no. 2, pp. 157-161.

18 Hagmar L., Stromberg U., Bonassi S., Hansteen I.L., Knudsen L.E., Lindholm C., Norppa H. (2004) Impact of types of lymphocyte chromosomal aberrations on human cancer risk: results from Nordic and Italian cohorts, Cancer Research, vol. 64, no. 6, pp. 2258-2263.

19 Ecological and genetic assessment of the impact of the Koshkar-Ata tailing dump on the health of the population of adjacent territories. Annual scientific report. (2016). Almaty, 119 p.

20 Kadyrzhanov K.K., Lucashenko S.N., Gluschenko V.N., Kijatkina N.G., Morenko V.S., Silachyov I.Y., Poleshko A.N., Sadykov N.R., Zirojan V. (2005) Over all investigation of the influence on environment from Koshkar-Ata tailing pond and rehabilitation measure, ISTC Science Workshops at the International Conference on contamination Soil, Con Soil, Bordeaux Convention Centre France, pp. 55-59.

21 Luckey T.D. (1999) Nature with ionizing radiation: a provocative hypothesis, Nutrition and cancer, vol. 34, pp. 1-11.

22 Beljaeva N.N., Muhambetova L.H., Petrova I.V., Hripach L.V., Shamarin A.A., Jurchenko V.V., Zhurkov V.S. (2003) Medical and biological assessment criteria of environmental pollution impact on human health [Mediko-biologicheskie kriterii ocenki vlijanija zagrjaznenija okruzhajushhej sredy na zdorov'e naselenija], Hyg. Sanit., no. 6, pp. 77-79.

23 Hagmar L., Stromberg U., Bonassi S., Hansteen I.L., Knudsen L.E., Lindholm C., Norppa H. (2004) Impact of types of lymphocyte chromosomal aberrations on human cancer risk: results from Nordic and Italian cohorts, Cancer Research, vol. 64, no.6, pp. 2258-2263.

24 Bigaliev A.B., Sintjurina A. (2009) Features of radionucleide accumulation by hydrobionts and coastal inhabitants of Northern-Caspian region [Osobennosti akkumuljacii radionuklidov gshidrobiontami i obitateljami pribrezhnoj zony Severo-kaspijskogo regiona], KazNU Herald, Series Ecology, vol. 1, no. 24, pp. 97-100.

25 Shametov A.K., Kozhahmetova A.N., Bigaliev A.B. (2014) Reconnaissance and radioecological study of environmental objects of Koshkar-Ata tail storage. Biological sciences. Fundamental research, no. 12, pp. 1938-1941.

26 Kundakbaeva G.B., Svjatova G.S., Abil'dinova G.Zh., Bigaliev A.B. (1997) Cytogenetic effect in human somatic cells under radiation during nuclear tests at Semipalatinsk polygon [Citogeneticheskij effect' v somaticheskih kletkah cheloveka, podvergavshihsja vozdejstviju radiacii v period jadernyh ispytanij na Semipalatinskom poligone], News of MS AS RK, Series biol. and med., no. 4, pp. 6-12.

L. Lebedeva[1] , Z. Aytasheva[1] , T.Berges[2] , B. Zhumabaeva[1] , Zh. Agadil[1] , A. Nuketay[1]

[1]Al-Farabi Kazakh National University, Almaty, Kazakhstan
[2]Laboratory STIM, *University* of Poitiers, Poitiers, France
*e-mail: lebedeva_lina1@live.kaznu.kz

Studying the impact of anthocyanin extract from black rice on regenerative abilities in the zebrafish D*anio rerio*

Abstract. Zebrafish (*Danio rerio*) is becoming more widespread in all types of biomedical researches. Owing to its high regenerative potency, zebrafish can be used in human therapy as a model organism. Anthocyanins, extracted from plants, are presented as a prospective food supplementary, demonstrating anti-bacterial, anti-fungal, anti-inflammatory, antioxidant and tumor-suppressing effects. In this study, we tested the impact of anthocyanins, extracted from black rice (*Oryza sativa*), utilized as a dietary supplement to commercial and live feed, on regeneration of amputated caudal fin in the zebrafish population. 4 months old (120 days postfertilization) newly amputated zebrafish were given anthocyanins daily during 21 days. The main ichthyological parameters, such as total length (TL) and length of caudal fin (LCF) were measured every 7 days. The obtained data was processed via T-test. Despite all predictions, the control group demonstrated better growth and regeneration than the experimental fishes. It might correlate to high concentration of anthocyanins, which in turn activates the process of apoptosis.

Key words: zebrafish, *Danio rerio*, anthocyanins, regeneration, diet.

Introduction

The zebrafish (*Danio rerio*) is a small tropical fish, which became more frequently used as as a model in biomedical researches. Owing to its high potency to regenerate amputated tissues and organs, such as heart muscle, eyes and fins, it can be useful to study the process of renovation in humans. For zebrafish, food and food supplements is an important factor, regulating many inner processes, including its growth and regeneration [1].

Anthocyanins are considered the most important group of pigmented flavonoids with more than 600 compounds identified in nature [2]. They are water-soluble compounds that provide color from red to dark-blue and black to such plant tissues as leaves, stems, roots, flowers and fruits, in dependence on pH of the medium and their structural composition [3]. In fact, there are about 25 various aglycones, detected in nature now. However, only six anthocyanidins (cyanidin, delphinidin, malvidin, pelargonidin, peonidin and petunidin) are widespread in plants, accounting for more than 90% identified anthocyanins [4-6].

The relative abundance of anthocyanins may vary according to the species depending on external and internal factors. Genetic factors and agronomic practices, intensity, processing and storage conditions influence the level of anthocyanins. Among the most common anthocyanidins in the higher plants, the glycosides of the three non-methylated anthocyanidins (cyanidin, delphinidin and pelargonidin) are the most abundant in nature, 80% of leaf pigments, 69% of fruits and 50% of flowers. The distribution of the six most common anthocyanidins in the edible parts of plants is cyanidin (50%), pelargonidin (12%), peonidin (12%), delphinidin (12%), petunidin (7%) and malvidin (7%). The most widespread anthocyanin in fruits is cyanidin-3-glucoside. Recently, anthocyanin composition and its antioxidant capacity were determined for highly pigmented edible vegetables [7-9]. Consistently, fruits contain anthocyanins which indicate the best natural source of these compounds. Red and blue highly pigmented fruits, mainly berries such as blueberry, blackberry, blackcurrant, cherry, cranberry, raspberry and strawberry fruits, have been comprehensively analyzed suggesting that anthocyanins contribute significantly to the antioxidant activity.

Interest in studying a diet rich in polyphenols, which includes anthocyanins was intensified after identifying their potential health benefits [10]. It has been detected, that high consumption of anthocyanin-rich foods might provide potential benefits on the health of people, suffering from cancer, aging, obesity, neurological diseases, inflammation, diabetes, and bacterial infections [11-13].

Anthocyanins as food supplements also have a huge impact on health and help to fight with obesity, diabetes, cardiovascular, respiratory and extractor diseases, improve mood, digestion, regeneration and so on. A large list of experiments revealed the anti-diabetic properties of anthocyanins, and simultaneous effects of these biologically active compounds, including decrease in blood glucose, preventing the production of free radicals, increased pancreatic insulin production and improvement of insulin resistance.

Materials and methods

Danio rerio husbandry. The main principles and protocols of breeding and housing of zebrafish were borrowed from "The Zebrafish Book", monograph by Westerfield. The whole population of adult *Danio rerio* was kept at 23 °C, with pH 7 ± 0, and saturation level >90%. The photoperiod was 12L: 12D. An artificial source of light was used during the experiment. The volume of both tanks was equal to 200 liters, what helped us to minimize the negative effect of overpopulation (maximum 135 fishes/ tank). To maintain water quality, 10% of water was exchanged every week. For the experiment zebrafish both males and females about 120 days-old were collected from the Laboratory of Aquaristic at al-Farabi Kazakh National University (KazNU) for amputation (dfa). For amputation only healthy fishes without any visible marks of diseases were selected.

Procedure of caudal fin elimination. Before amputation all fishes were anesthetized in 2 mL 1% lidocaine per 100 mL of water during 2 min. Caudal fin was amputated totally by a sharp razor. After the procedure zebrafish were divided into control and experimental groups and returned to the tanks, containing fresh, warm and oxygenated water. All stages of the experiment were performed fully according to the rules and standards accepted in modern practice.

Anthocyanins extraction. Black rice *(Oryza sativa)* was selected as a source of anthocyanins. To check various solvents and their ability to extract anthocyanins, distilled water, isopropyl, ethyl and methyl in the presence of HCl in different concentrations were used as a source. 2.5 g of raw material were put in a blender and crushed into homogeneous powder. Obtained substance was dunked in 25 mL of extractant and incubated for 1, 2, 3, 4, 8, 24 h under the general room temperature as well as in water baths: LOIP (Japan), IKA-WERKE basic pro 20 (Germany).

Then, 1 mL of solution was centrifuged at 10 000 rpm within 3 min, supernatant was removed, and the pellet was diluted 100 times. The optical density was measured by V-3000PC Spectrophotometer (Austria) at 538 nm. The blank corresponded to the extractant. For the further utilization of extracts of anthocyanins *in vivo* it was essential to remove the extractant. The solution was evaporated in a vacuum rotary evaporator BUCHI Rotavapor R-124 (Switzerland) at 55°C during several hours to delete any liquids. Then the pellet was suspended with 100 mL of distilled water, mixed and kept in the refrigerator.

Anthocyanins assessment. In the international scientific practice, it has been generally accepted the method of measurement of anthocyanins concentration at different pH. Moreover, the exposure time must be in the range of 15-60 min to exclude overestimated results. Buffer solutions were prepared according to the following protocol:

Solution A: 0.025 M KCl, pH 1.0

A powder of KCl weighing 0.465 g was dissolved in 240 mL of distilled water in a beaker. The pH was adjusted to 1.0 with a solution of concentrated hydrochloric acid, adding drop by drop. The resulting solution was transferred to a volumetric flask with a capacity of 250 mL and brought to the mark with distilled water, followed by pH control.

Solution B: 0.4 M CH_3COONa, pH 4.5

A weighed portion of $CH_3COONa \cdot 3H_2O$ weighing 13.6 g was dissolved in 240 mL of distilled water in a beaker. The pH was adjusted to 4.5 with a solution of concentrated hydrochloric acid, adding it dropwise. The resulting solution was transferred to a 250 mL volumetric flask and adjusted to the mark with distilled water, re-monitoring the pH.

Aliquots of the analyzed anthocyanins Va extract (with preliminary dilution selection) were transferred to Vk volumetric flasks and adjusted to the mark with solutions A and B, respectively.

The calculation of the concentration of anthocyanins was performed according to the formula:

$$(A \times MW \times DF \times 1000) / (\varepsilon \times 1),$$

where $A = (A_{520} - A_{700})$ pH 1.0 – $(A_{520} - A_{700})$ pH 4.5;

MW – molecular weight 449.2 g/mol (cyanidin-3-glucoside);

DF – number of dilutions;

ε – molar absorption coefficient 26,900 L/mol.

Behavioral extinct assessment. To assess fish behavior before and after caudal fin amputation, physical and psychological conditions, classical methods such as swimming test, light reflex, Pavlovian conditioning and anxiety test were used.

Forage preparation. To check the activity of extracts of plant anthocyanins, 150 g of frozen Aqua menu artemia (*Artemia salina*) and 100 g of tubifex (*Tubifex tubifex*) (JBL NovoFex, UK) were soaked in 100 mL of water extract of black rice for 24 h and given with Betta Menu (Tetra, Germany) to the experimental group once per day during 21 days. The control group was fed by a mix of natural and commercial food in equal proportions.

Statistical analysis and modelling. All analyzes were performed via Statistica Software (StatSoft, Russia), all graphs were generated by Excel Software. Every week the major ichthyological parameters as TL – full body length and LCF – caudal fin length were performed. To process obtained data the method of T-test was selected. To calculate it, the following formula was used:

$$t = \frac{M_1 - M_2}{\sqrt{m_1^2 + m_2^2}},$$

where M_1 and M_2 – the arithmetic mean of the first and the second groups;

m_1 and m_2 – the mean error of the first and the second groups.

All calculations were performed by Statistica software.

Live imaging. To take pictures in high resolution, the fishes were fixated in glycerol. All images and videos were obtained by Motic DM143 series and Motic Images Plus 3.0 software (Motic, China).

Results and discussion

As in alcohol homologous series the effect of extraction grows from isopropanol to ethanol and methanol, it has been decided to extract anthocyanins from black rice (*Oryza sativa*) in various spirits (Figure 1). Distilled water, isopropyl, ethyl and methyl in different concentrations were used as solvents.

a   b

Figure 1 – *Oryza sativa* as a source of anthocyanin extracts.
Note: A – raw material (x10) and B–rice powder (x10)

Isopropyl appeared not appropriate to use for anthocyanin extraction because of its low reactivity (Table 1). Maximal optical density (OD) 0.0034 at λ_{max} =538 nm was approached only after 24 h from the start of extrac-tion, whereas in the tube with ethanol higher OD was observed in 1 h, and in methanol this indicator was 2.5 times higher. Even extraction in distilled water demonstrated more significant ability to extract anthocyanins.

**Table 1** – Usage of different alcochol doses in order to extract anthocyanins, OD at λ_{max}=538 nm

Extractant	1 h	2 h	3 h	4 h	6 h	8 h	24 h
Distilled water	0.012	0.029	0.017	0.055	0.013	0.009	0.003
1% isopropanol	0.009	0.011	0.012	0.014	0.024	0.026	0.034
2% isopropanol	0.002	0.006	0.015	0.018	0.011	0.010	0.007
5% isopropanol	0.004	0.005	0.011	0.013	0.010	0.007	0.003
1% ethanol	0.042	0.061	0.067	0.092	0.103	0.106	0.099
2% ethanol	0.058	0.078	0.092	0.076	0.065	0.081	0.098
5% ethanol	0.070	0.081	0.096	0.071	0.063	0.075	0.091
1% methanol	0.113	0.148	0.168	0.201	0.172	0.141	0.123
2% methanol	0.110	0.139	0.155	0.185	0.129	0.145	0.119
5% methanol	0.108	0.144	0.146	0.143	0.140	0.142	0.131

Consequently, we can exclude isopropanol from the list of organic extractants useful for anthocyanins extraction (Figure 2).

While extraction with methyl alcohol in the presence of 1% hydrochloric acid, the peak of anthocyanin concentration was observed after 4 h of maceration. Further on anthocyanins became discolored. In 1% ethanol, the concentration of anthocyanins continued to increase slightly during the entire incubation time, however, the maximum optical density was two times lower than in samples with methyl alcohol as a solvent. An increase in the percentage ratio of hydrochloric acid did not show any significant differences; therefore, 1% ethyl and methyl alcohols can be considered as effective organic solvents for the extraction of anthocyanins from black rice powder.

According to the literature sources, the extraction of anthocyanins might be increased by maceration in a water bath or in an US-machine. In order to find out how such methods are more effective than maceration at room temperature, 2.5 g of the sample were poured into 25 mL of an organic extractant and placed under various conditions. After each hour, an aliquot of 10 microliters was diluted 100 times and the optical density of the solution was measured. The measurement results are presented below (Table 2).
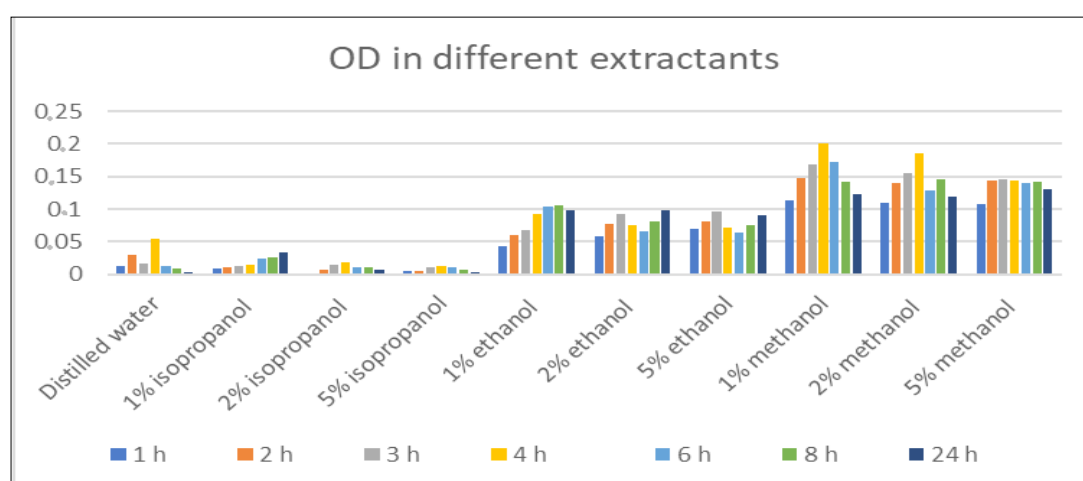
Figure 2 – Dependence of anthocyanins concentration on an extractant and time of incubation

Table 2 – The dependence of OD on different types of maceration at λ_{max}=538 nm

Conditions	1 h	2 h	3 h	4 h
Maceration at room temperature				
Ethanol	0.038	0.056	0.075	0.097
Methanol	0.139	0.147	0.165	0.185
Maceration at 75 °C in water bath				
Ethanol	0.089	0.131	0.142	0.159
Methanol	0.222	0.202	0.164	0.183
Maceration in US-machine				
Ethanol	0.195	0.156	0.122	0.117
Methanol	0.201	0.193	0.180	0.195
Maceration in both water bath and US-machine				
Ethanol	0.173	0.188	0.178	0.195
Methanol	0.192	0.178	0.189	0.183

Therefore, the optimal conditions for maceration were revealed. Figure 3 shows that the best results were obtained after 1 h maceration in the water-bath in the presence of methanol, and after 1 h maceration in the US-machine in the presence of ethanol. The usage of methyl alcohol instead of ethanol and placing the solution in a water bath for one hour allowed to increase the yield of anthocyanins by more than two times in comparison with ethanol.

A pH-spectrophotometry method was then used to calculate the concentration of anthocyanins in three samples. The total weight of anthocyanins per 100 g of raw mass is equal to 167 mg (Table 3).
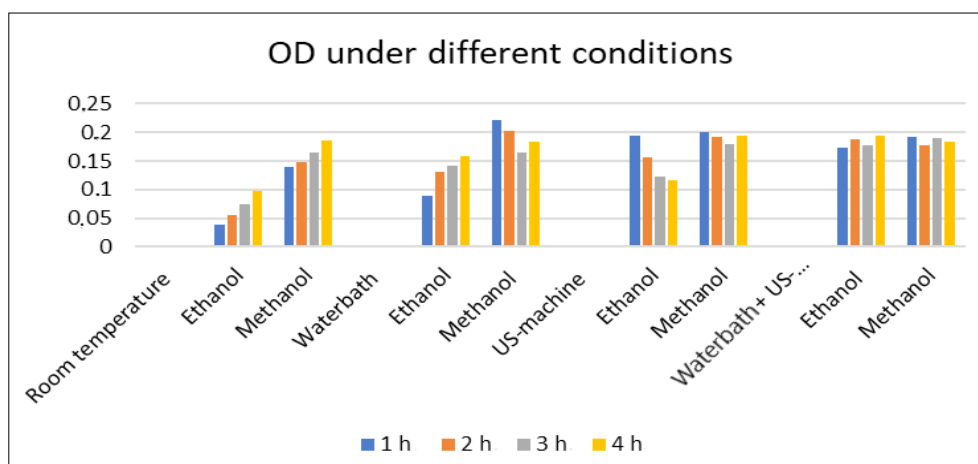
Figure 3 – The dependence of anthocyanins concentration on types of maceration

Table 3 – The total weight of anthocyanins per 100 g of raw weight

Source	pH=1.0	pH=4.5
Rice	510nm=0.030	510nm=0.015
	700nm=0.003	700nm=0.010
Note: C=167 mg/100g.		

The data obtained is confirmed with previous investigations.

Caudal fin regeneration. 264 fishes were selected randomly from the pool without any sign of diseases, physical nor anatomical abnormalities. Their length varied from 1.3 to 3.7 cm (Figure 5). The fishes were divided into two cohorts – control and experimental in equal proportions.

To avoid any mistakes and inaccuracies in the further calculations, before the experiment we measured TL and LCF (TL – total length; from the rostrum to the end of the longest fin ray, and LCF – length of caudal fin; the length of caudal rays) and processed the obtained data via T-test. It has been showed, that t_{emp} =0.8589 for TL< t_{crit} =1.972 (p=0.05, df=262), so, it can be stated, that there are not any differences in total body length for both groups. The same results were obtained for length of caudal fin. According to the calculations, t_{emp} =0.7817 for LCF< t_{crit} =1.972 (p=0.05, df=262, which proves that the cohorts of the zebrafish are homogeneous.

Table 4 – The results of TL and LCF measurements in control and experimental cohort right after the procedure of caudal fin elimination

|	$TL_{control}$	$TL_{experimental}$	$LCF_{control}$	$LCF_{experimental}$
$\overline{x}$	2.76	2.75	0.56	0.59
$m\ (\sigma/\sqrt{(n)})$	0.004	0.006	0.0217	0.0247
t_{emp}	0.8589		0.7817	
df (T)	262		262	
$t_{crit,}$ p = 0.05	1.972		1.972	

a   b

Figure 4 – *Danio rerio* species. Note: A– before elimination (x10) and B– right after (x20)

Via microscope Motic and Motic Images Plus 3.0 software the pictures of fishes right after amputation were taken (Figure 5). As we can see on the picture, no veins nor arteries, neither vertebras were harmed. All fishes survived the procedure of caudal fin elimination.

Right after amputation fishes were transferred to a temporary tank, where visual assessment of their behavior was performed. Amputees demonstrated weak reaction on light (both natural and artificial), ignored food and preferred staying at the bottom, whereas non-amputees swam actively, reacted on tapping and consumed food. Such type of behavior which was detected in the amputees signals about stress, normal for animals deprived of limbs or other structures. 1 h later all fishes successfully passed the tests and had no differences in comparison with fishes with caudal fin. These observations were repeated several times to insure that stress had short-time effect and did not result in any severe consequences for fishes´ health as chronic stress could do.

a   b
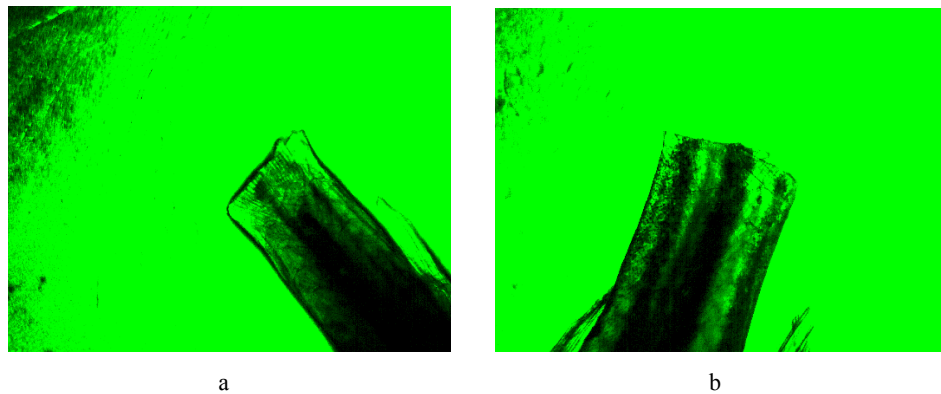
Figure 5– Caudal fins of fishes right after amputation.

Note: A– control (x100); B– experiment (x100)

Within 3 weeks since the experiment was started:
– the control group was fed by a mix of commercial and natural food;
– an experimental group consumed the same mix soaked in anthocyanins.

Two days after the start, in both tankers dead representatives were detected. Probably, traumas, obtained during catching and measuring, temperature fluctuations, bad aeration, bacterial or fungal invasion etc. could provoke death of fishes. However, there were not any outbreaks of mortality, whereas in the experimental group fishes continued dying without any visible causes.

In 7 days the secondary measurements were done. The results are presented in table (Table 5).

As we can see one week later, there is no significant difference not only in length (TL and LCF both), but also in weight. In the control group fishes were gaining mass and growing, in the experimental the processes of grow and development were slowed down (Figures 6-7).

Table 5 – The results of TL and LCF measurements in control and experimental cohorts 7 days after the procedure of caudal fin elimination

	$TL_{control}$	$TL_{experimental}$	$LCF_{control}$	$LCF_{experimental}$
$\bar{x}$	2.463	2.345	0.21	0.19
m ($\sigma/\sqrt{n}$)	0.028	0.033	0.0083	0.0077
t_{emp}	2.694		2.382	
df (T)	241		241	
$t_{crit,}$ p = 0.05	1.972		1.972	

a   b
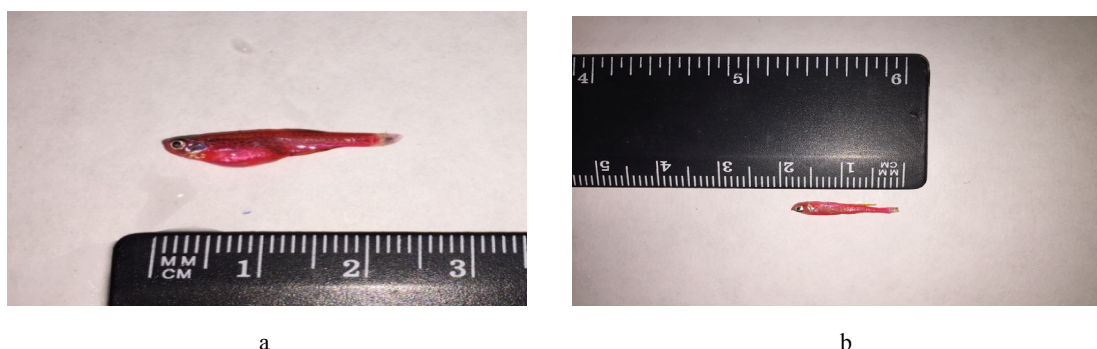
Figure 6 – The process of caudal fin regeneration with eye vision. Note: A–control (x10); B–experiment (x10)

a   b
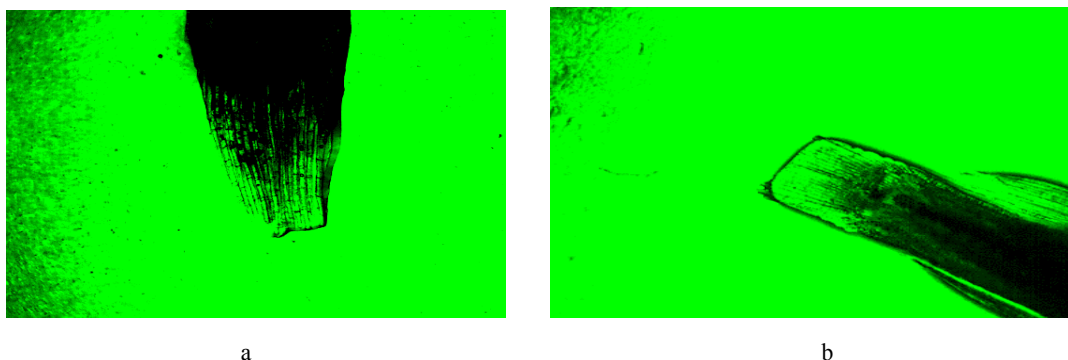
Figure 7 – The process of caudal fin regeneration. Note: A - control (x100); B - experiment (x100)

In parallel with weekly measurements, we also performed visual evaluation of physical conditions and behavioral patterns of fishes. One of the most representative parameters is speed of food consumption. In the control subpopulation it was equal to 5 min (100% of food, no wastes), in the experimental was 11 min (80%). Physical activity also decreased, all fishes were passive, did not demonstrate research behavior, schooled and did not react on any stressors, like light and sound. The control ones actively swam in the tank in all directions, searched and reacted on knocking on the glass in a normal way. These behavioral differences proved again, that anthocyanins impacted not only grow processes, but also on general health and living conditions.

Two weeks later another series of measurements was done (Table 6).

Table 6 – The results of TL and LCF measurements in control and experimental cohorts 14 days after the procedure of caudal fin elimination

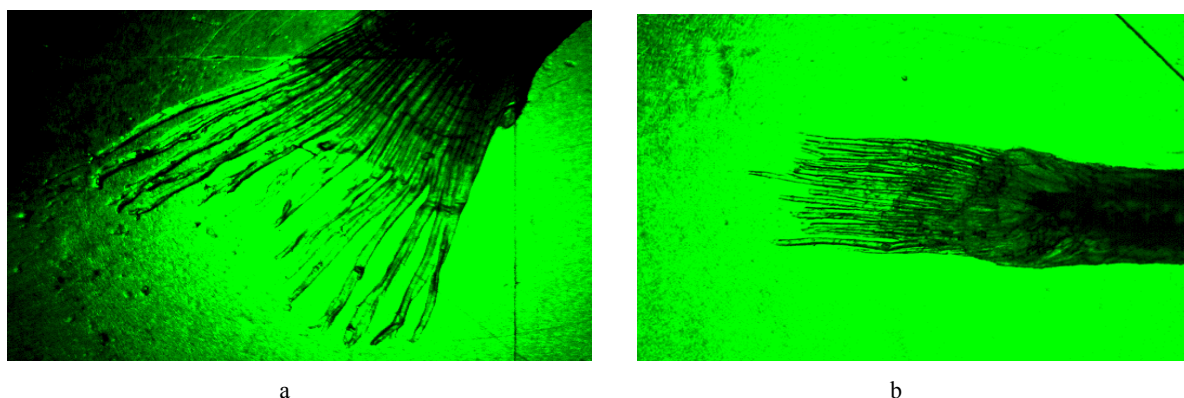|	$TL_{control}$	$TL_{experimental}$	$LCF_{control}$	$LCF_{experimental}$
$\bar{x}$	2.545	2.414	0.3	0.27
m ($\sigma/\sqrt{n}$)	0.0309	0.0428	0.0092	0.0090
t_{emp}	2.476		2.36	
df (T)	189		189	
$t_{crit,}$ p = 0.05	1.973		1.973	

As t_{epm}=2.476 for TL>t_{crit} =1.973 (p=0.05, df=189), ~~we accepted~~ $H_{(A)}$. It means, that two set of fishes are different in length. The same distinction can be observed in the length of caudal fin. t_{epm}=2.36 for LCF>t_{crit} =1.973 (p=0.05, df=189), so, in the control group the process of regeneration went better and faster in contrast to the experimental group.

Microscopic pictures allowed us to see the process of caudal fin restoration more detailed. On the left normally regenerating fin can be observed, fin rays have different length to form heterocercal lobes. On the right all fins are identical, skin fold is invis-ible, lobes cannot be detected (Figure 9). These morphological changes show that the process of regeneration has been interrupted.

Three weeks later new 18 dead experimental fishes were detected. Those fishes, that were still alive, did not show interest to food, interactions, stopped swimming and spent time lying on the bottom of the tank.

The third measurements revealed that the length of body in the control group significantly increased in comparison with the experimental group. Also, we can see the positive correlation between body length and caudal fin length.

a   b

Figure 8 – The process of caudal fin regeneration. Note: A- control (x100); B- experiment (x100)

Table 7 – The results of TL and LCF measurements in control and experimental cohorts 21 days after the procedure of caudal fin elimination

|	$TL_{control}$	$TL_{experiment}$	$LCF_{control}$	$LCF_{experiment}$
$\overline{x}$	2.647	2.311	0.42	0.34
m ($\sigma/\sqrt{(n)}$)	0.013	0.021	0.027	0.031
t_{emp}	5.65		2.0	
df (T)	157		157	
$t_{crit,}$ p = 0.05	1.977		1.977	

Obviously, that anthocyanins acted as an agent, inhibiting the processes of growth and regeneration. According to literature sources, anthocyanins are considered as a substance with antitumor effect, suppressing some type of cancer, as colorectal adenoma. Anthocyanins regulate cell proliferation and mechanism of apoptosis. However, high concentrations of anthocyanins can stop not only cancer cells, but healthy and normal ones, abolishing mitosis and essential renewal of tissues and organs.

The main organ which is responsible for effective digestion is intestine. From the inside it is covered by non-keratinized epithelium, constantly damaged as a result of mechanical impact, and thus regularly replaced by new cells. The stop of cell division and self-renewal causes perforation of intestine, inner bleeding, deterioration of normal digestion, losing weight, weakening of immune response, and, at the end, death.

Based on the obtained results, we can say, that high concentration of anthocyanins in food, consumed day by day (15% and more from total mass of food) led to failure both in amitotic and mitotic cycles and provoked weakness, growth and regeneration suppression.

In the picture it has been shown that the caudal fin in the experimental group was not only shorter than in the control, but differed from it morphologically. We can see homocercalus fin with visually distinguishable lobes. In the control fin rays are homogeneous, no signs of tumor or atypical structures have been detected. Regeneration operates correctly. In the experimental group the length of fin rays different, no lobes can be seen, skin fold is rigid, what did not allow to straighten caudal fin fully. Food containing highy concentrated anthocyanins negatively influenced the processes of cell division. So, mechanisms of proliferation and regeneration were stopped prematurely, what resulted in pathological changes in the structure of caudal fin.

As some authors reported, high concentration of anthocyanins might induce apoptosis in different somatic cells in humans and mice [14]. Anthocyanins can block cell division at different stages of mitosis, because cyanidin glycosides accumulate ROS and have cytotoxic effect on tumor cells [15]. Also, it has been found, that anthocyanins increase the concentration of caspase-3, -8 and -9, and initiate degradation of poly(ADP-ribose) polymerase [16].

a   b
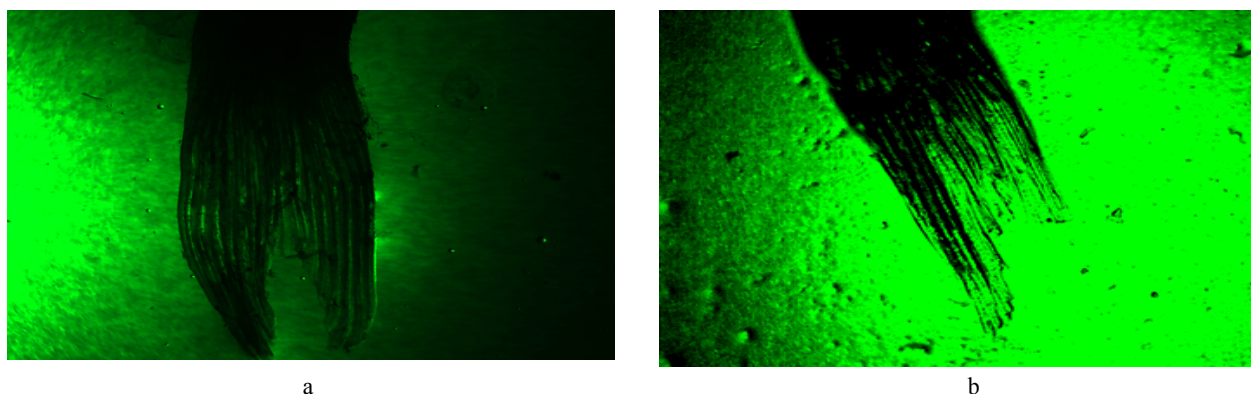
Figure 9 – Caudal fin of Danio rerio in a group. Note: A–control (x100); B–experimental (x100)

Conclusion

Anthocyanins are natural polyphenol compounds, which stimulate vivid colors to numerous vegetables, fruits and cereals. These pigments range in color from orange-red to (dark) blue-violet and could serve as natural colorants to replace artificial additives. There is a tremendous demand from consumers to have fewer artificial compounds in their foods. Despite food supplements based on anthocyanins are widely spread in the world, in fact, there are not strict evidences that they have any positive effects on human health. According to the obtained results it was defined that in high concentrations anthocyanins decrease the process of regeneration, cell proliferation and tissue formation in *Danio rerio*. In obedience to literature sources, high concentrations are associated with increase of caspase level in cells and induced caspase-dependent degradation. Major caspase cascades leading to apoptosis since they are able to slay not only tumor cell, also healthy ones. Effector caspases are responsible for initiating the hallmarks of the degradation phase of apoptosis, including DNA fragmentation, cell shrinkage and membrane blebbing. These investigations will be prolonged to unveil the inner mechanisms, provoked such critical changes in caudal fin regeneration or outer physical appearance alterations.

References

1   Detrich H.W., et al. (2016). The Zebrafish. AP, Academic Press, vol. 13, pp. 124-137. ISBN: 9780128052068.

2   Andersen Ø.M., Jordheim M. (2006). The anthocyanins. In: Flavonoids: Chemistry, Biochemistry and Applications, CRC Press, vol. 51, pp. 471-552. ISBN 9780849320217.

3   Fossen T., Andersen Ø.M., ØVstedal D.O., Pedersen A.T., Raknes Å. (2006). Characteristic anthocyanin pattern from onions and other Allium spp. Journal of Food Science, JFS, vol. 61, pp. 703-706. ISBN 9780849320217.

4   Hudson E.A., Dinh P.A., Kokubun T., Simmonds M.S., Gescher A. (2000). Characterization of potentially chemopreventive phenols in extracts of brown rice that inhibit the growth of human breast and colon cancer cells. Cancer Epidemiology, Biomarkers & Prevention, vol. 9, pp. 1163-1170. https://doi.org/10.1016/j.maturitas.2006.10.002.

5   Hassan H.A., Abdel-Aziz A.F. (2010). Evaluation of free radical-scavenging and anti-oxidant properties of black berry against fluoride toxicity in rats. Food and Chemical Toxicology journal, vol. 48, pp. 271-335. https://doi.org/10.1016/j.fct.2010.05.018.

6   Olsson M.E., Gustavsson K.E., Andersson S., Nilsson Å., Duan R.D. (2004). Inhibition of cancer cell proliferation in vitro by fruit and berry extracts and correlations with antioxidant levels. J Agr. FoodChem., vol. 52, pp. 7264-7271. https://doi.org/10.1021/jf030479p.

7   Li H., Deng Z., Zhu H., Hu C., Liu R., Young J.C., Tsao R. (2012). Highly pigmented vegetables: Anthocyanin compositions and their role in antioxidant activities. Food Research International, vol. 46, pp. 250-259, https://doi.org/10.1016/j.foodres.2011.12.014.

8   Yang Z., Zheng Y., Cao S. (2008). Effect of high oxygen atmosphere storage on quality, antioxidant enzymes, and DPPH-radical scavenging activity of Chinese bayberry fruit. J Agr Food Chem., vol. 57, pp. 176-181. https://doi.org/10.1021/jf803007j.

9   Juroszek P., Lumpkin H.M., Yang R.Y., Ledesma D.R., Ma C.H. (2009). Fruit quality and bioactive compounds with antioxidant activity of tomatoes grown on-farm: comparison of organic and conventional management systems. J Agr Food Chem., vol. 57, pp. 1188-1194. https://doi.org/10.1021/jf801992s.

10   Seeram N.P., Adams L.S., Hardy M.L., Heber D. (2004). Total cranberry extract versus its phytochemical constituents: antiproliferative and synergistic effects against human tumor cell lines. J Agr Food Chem., vol. 52, pp. 2512-2517. https://doi.org/10.1021/jf0352778.

11   Egbuna, Chukwuebuka, et al. (2018) Phytochemical Test Methods: Qualitative, Quantitative and Proximate Analysis. Phytochemistry, pp. 381-426. https://doi.org/10.1201/9780429426223-15.

12   Andersen Ø.M., Jordheim M. (2006) The anthocyanins. In: Flavonoids: Chemistry, Biochemistry and Applications. CRC Press, vol. 51, pp. 471-552. ISBN 9780849320217.

13   Andersen Ø.M., Jordheim M. (2008) Anthocyanins – food applications. Proc. 5th Int. Congr. Pigments Foods: For Quality and Health, Finland, vol. 56, pp.165-221. https://doi.org/10.1007/978-0-387-77335-3_3.

14   Lazze M.C. (2004). Anthocyanins induce cell cycle perturbations and apoptosis in different human cell lines, Carcinogenesis, vol. 25, no. 8, pp. 1427-1433, https://doi.org/10.1093/carcin/bgh138.

15   Rugină D., Sconţa Z., Leopold L., Pintea A., Bunea A., Socaciu C. (2012). Antioxidant activities of chokeberry extracts and the cytotoxic action of their anthocyanin fraction on HeLa human cervical tumor cells. J. Med. Food., vol. 6, pp. 700-706. https://doi.org/10.1089/jmf.2011.0246.

16   Lee S.H., Park S.M., Park S.M., Park J.H., Shin D.Y., Kim G.Y., Ryu C.H., Shin S.C., Jung J.M., Kang H.S., Lee W.S., Choi Y.H. (2009). Induction of apoptosis in human leukemia U937 cells by anthocyanins through down-regulation of Bcl-2 and activation of caspases. Int. J Oncol. vol. 6, pp. 1077-1083, https://doi.org/10.3892/ijo_00000234.

S.D. Atabayeva[1*] (ID), R. Minocha[2] (ID), S.C. Minocha[3] (ID), A. Rakhymgozhina[1],
A.M. Nabieva[1], A.C. Nurmahanova[1] (ID), S.S. Kenzhebayeva[1] (ID),
R.A. Alybayeva[1] (ID), S.S. Asrandina[1] (ID)

[1]Al-Farabi Kazakh National University, Research Institute of Ecology Problems, Almaty, Kazakhstan
[2]USDA Forest Service, Durham, USA
[3]Department of Biological Sciences, University of New Hampshire, Durham, USA
*e-mail: sauleat@yandex.ru

Response of plants to cadmium stress

Abstract. In this article we discuss cadmium pollution in the environment and the various ways plants take up cadmium and respond to its accumulation. The increased development of metallurgical and mining industries is primarily responsible for the increases in cadmium pollution in the environment. Another significant source of cadmium contamination of agricultural plants is the widespread use of phosphorus fertilizers, which contain cadmium. Cadmium reduces the growth and development of plants. Cadmium in the soil also competes with the basic essential mineral elements thereby reducing their uptake by plants. This article reviews the published data on the cellular and molecular mechanisms of cadmium uptake by plants, its metabolic transformations, effects on nutrient status of plants, modulation of cadmium response by polyamines and amino acids, and the growth of plants. Strategies to reduce cadmium uptake and accumulation are also discussed.

Key words: Cadmium, plants, crops, growth, toxic effect.

Introduction

The expansion of industry and agriculture to cope with increasing world population leads to an increase in the number of heavy metals in the environment. Often this increase is several orders of magnitude greater than background concentrations. The primary sources of anthropogenic contributions of heavy metals are industrial emissions associated with mining, and metallurgical and chemical industries. There is a constantly growing volume of industrial waste from new technological landscapes which have become a source of contaminated dust that extends long distances from the source, polluting the environment and posing a threat to public health and biodiversity of the region.

Contamination of soil, plants and water with heavy metals in the vicinity of large industrial centers has become one of the most pressing environmental problems. Cadmium (Cd) in unpolluted soils is present in trace amounts (0.05- 0.15 mg/kg) [1]. Nevertheless, human industrial activities and agricultural practices increase the level of Cd in the soil. The operations of metallurgical enterprises and the use of Cd containing phosphorus fertilizers and pesticides, contributes to high Cd accumulation in soil [2]. The degree of contamination of soil Cd fertilized with phosphorus fertilizers can reach 300 mg/kg dry weight [3].

Cadmium enters human body through the food chain, and it remains in the body for many years. Cadmium-contaminated food can induce chronic toxicity. Cadmium is a calcium (Ca) antagonist. Increased accumulation of Cd in the human body is responsible for diseases like Itai-Itai, which translates into reducing the content of Ca in the bones, which causes their softening [4]. The World Health Organization (WHO) has set a maximum limit of Cd in human diet to about 60-70 mg per day, and the Codex Alimentarius Commission of the US (usda.gov/codex) and the Food and Agriculture Organization (FAO) (http://www.fao.org/fao-who-codexalimen tarius /en/) has set a limit of 0.1 mg Kg^{-1} for cereals and oilseeds [5]. Because of its high solubility in the soil (~35%), Cd is more readily available than other heavy metals such as Zn, Cu, Pb, which have a higher absorption coefficients [6].

Toxic effect of cadmium on plants

The mechanism of interaction of heavy metals, including Cd, in plants is exceedingly complicated, and can be schematically represented in the following way: heavy metals → cell membranes → cell → organ → system of organs → organism → return to the ecosystem after decomposition of plants residues. Heavy metals cause inhibition of growth and a decrease in crop yields due to disruption of physiological and biochemical processes in plant cells and in the plant body as a whole. The fibrous root system of many crops like rice, which increases the absorbing surface of plants for Cd uptake [7], chelating agents, such as organic acids of rhizosphere microorganisms, and phytosiderophores, all contribute to the absorption of Cd by cereal plants [8]. It has been suggested that because of the low diffusion coefficients and generally lower concentrations of Cd in soil solution, its uptake by plant roots is mainly controlled by transpiration. Both Lux et al. [9] and Yamaguchi et al. [10] reported that abscisic acid promotes the closure of stomata leading to a decrease in transpiration, ultimately lowering the rate of transport of Cd to the aerial organs.

Cadmium-induced chromosomal aberrations including C-mitosis, chromosomal fragmentation, anaphase bridges, and chromosome adherence was observed in *Allium cepa,* which indicate a genotoxic effect [11]. Cadmium reduced the mitotic index in root cells, which correlated with the degree of decrease in root growth. C-mitosis, was the main type of chromosomal aberration, with a high degree of compaction that occurred at the root tips of barley from exposure to low concentrations (1 and 10 μM) of Cd [12].

Reduced biomass was observed in various rice varieties grown in a medium containing varying amounts of Cd [13]. In our studies, under the action of cadmium, the content of photosynthetic pigments in the studied wheat varieties was significantly reduced [14]. The content of chlorophyll *a* at a relatively low cadmium concentration (0.15 mM) decreased to the greatest extent in the variety Kazakhstanskaya rannaya (by 34%) (Figure 1).

In the varieties Kazakhstanskaya -3 and Shagala, this indicator decreased by 19 and 18%, respectively. With a doubling of the cadmium concentration, the content of chlorophyll a decreased to the greatest degree in the varieties Shagala and Kazakhstanskaya rannaya – by 34 and 43%, accordingly. To the least extent, this indicator decreased in the variety

Kazakhstanskaya-3 – by 21% relative to the control. According to the content of chlorophyll a, the varieties can be arranged as follows: Kazakhstanskaya -3 (79%) > Shagala (66%) > Kazakhstanskaya rannaya (57%).The content of chlorophyll *b* in the presence of cadmium decreased almost to the same extent as the content of chlorophyll a in all the studied wheat varieties. At 0.15 mM $CdSO_4$, the chlorophyll *b* content decreased by 35, 18, and 17% in the Kazakhstanskaya rannaya, Kazakhstanskaya-3, and Shagala varieties (Figure 2). With an increase in the concentration of cadmium (0.3 mM $CdSO_4$), the content of chlorophyll *b* in the Kazakhstanskaya rannaya variety decreased the most (by 44%). In the least degree, this indicator decreased in the Kazakhstanskaya-3 variety – by 23%, in Shagala variety – by 32%.
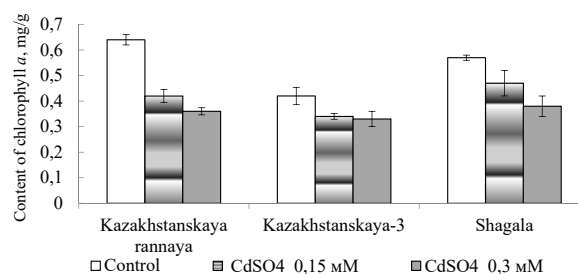
Figure 1 – Effect of cadmium on chlorophyll
a content in leaves of wheat varieties

The amount of chlorophylls (*a+b*) in the presence of cadmium in soils also decreased (Figure 3). For this indicator, with a high concentration of cadmium, the varieties were arranged as follows: Kazakhstanskaya -3 (79%) > Shagala (68%) > Kazakhstanskaya rannaya (52%).
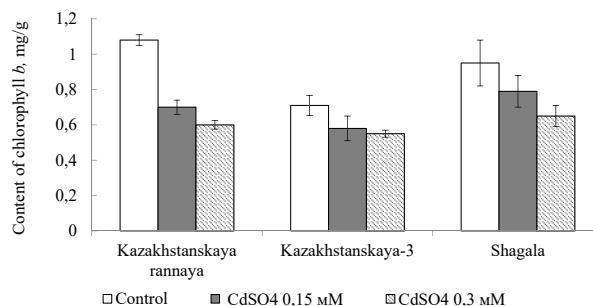
Figure 2 – Effect of cadmium on chlorophyll
b content in leaves of wheat varieties

The content of carotenoids at a relatively low concentration of cadmium (0.15 mM) decreased the most in the Shagala variety – by 61%, and the least in the Kazakhstanskaya-3 variety (by 30%) (Figure 4). In the Kazakhstanskaya rannaya variety, the content of carotenoids at a low concentration of cadmium decreased by 50%. According to the content of carotenoids at a high concentration of cadmium (0.3 mM), wheat varieties can be arranged as follows: Kazakhstanskaya -3 (63%) > Kazakhstanskaya rannaya (47%) > Shagala (19%).
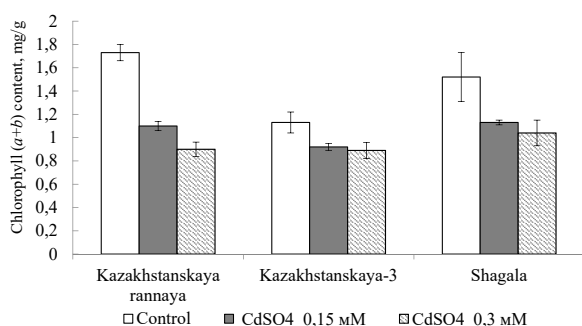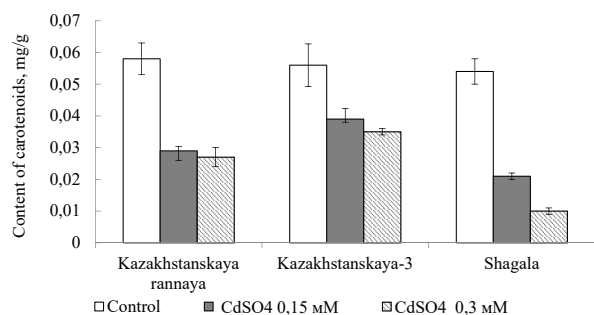

Figure 3 – Effect of cadmium on chlorophylls (a+b) content in leaves of wheat varieties

Figure 4 – Effect of cadmium on carotenoids content in leaves of wheat varieties

According to other researchers, cadmium causes disorganization of the leaf structure, reduces the intercellular space, and leads to structural changes in thylakoids in chloroplasts [15].

Under the effect of cadmium, changes in the ultrastructure of chloroplasts were observed as a result of oxidative stress [16]. Cadmium causes disorganization of the thylacoid and stroma systems and a decrease in starch grains [17]. Structural changes in chloroplasts lead to a decrease in photosynthetic activity [18].

Plants respond to environmental stresses by controlling the level and activity of various hormones. Cadmium ions have been found to reduce the content of free forms of auxin in poplar plants and increase the activity of peroxidase, which increases lignification of cell walls under stress [19].

In addition to affecting vital processes of cell division and signaling pathways, Cd ions known to cause oxidative stress in plants [20]. Cell membranes are the primary target of the action of heavy metals. Under the influence of heavy metals, including Cd, membrane permeability changes, leading to increased rates of membrane lipid peroxidation and K^+ leakage, and a decrease in chlorophyll content. The physiological and biochemical processes that control photosynthesis, water consumption efficiency, mineral nutrition, and sugar metabolism are disrupted by Cd, thus the yield of plant biomass decreases [20]. Free radicals can directly destroy proteins, amino acids and nucleic acids, and induce lipid peroxidation [21].

Cadmium, along with other heavy metals, increases the products of reactions with thiobarbituric acid (TBA), which are an index of lipid peroxidation and oxidative stress. Lipid peroxidation of membranes has a negative effect on their function and integrity and can produce irreversible damage in the function of cells. In our studies, the level of lipid peroxidation in wheat varieties increased with Cd in the growth medium [14]. In resistant varieties of wheat, lipid peroxidation increased to a lesser degree than that of non-tolerant wheat varieties.

Cadmium is not a redox metal and does not participate in Fenton-type reactions, but it can also produce oxidative stress indirectly, causing damage in chloroplasts, the formatin of reactive oxidized substances such as superoxide radicals (O^{2-}), singlet oxygen ($^1O_2$), hydrogen peroxide (H_2O_2), and hydroxyl radicals ($\cdot OH$) [21].

According to the degree of increase in the lipid peroxidation under the action of 0.3 mM $CdSO_4$, the varieties can be arranged as follows: Shagala (159) > Kazakhstanskaya-3 (139) > Kazakhstanskaya rannaya (107) (Figure 5).

In relatively resistant varieties to these stressors, the content of malonic dialdehyde increased to a lesser extent than in Shagala variety.
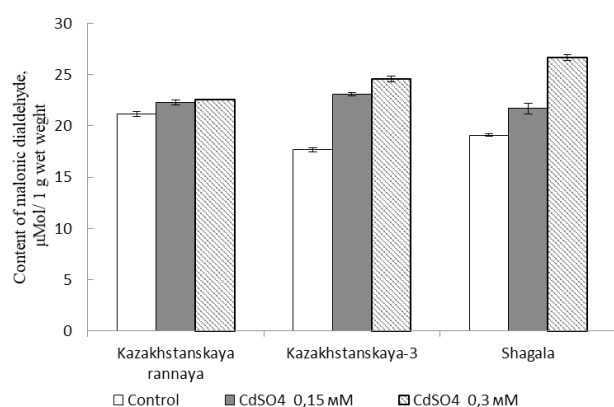
Figure 5 – Effect of cadmium on lipid peroxidation level
in several wheat varieties (*Triticum aestivum* L.)

With the increase in the overall ionic strength of the soil solution, the adsorption of Cd by soil particles decreases. Zinc (Zn) in phosphate fertilizers competes with Cd for adsorption to soil particles, which increases the concentration of Cd in the soil solution [22]. Consequently, the amount of accumulated Cd depends on various factors, such as its content in the soil, its bioavailability, genetic characteristics of the plant, the nature of the soil and its total ionic strength, and finally, the rhizosphere microbiome [23].

Cadmium especially competes with zinc, copper and iron. Silicon (Si) has been reported to decrease Cd accumulation within shoots. This effect is attributed to shoot Si-mediated down-regulation of transporter genes involved in Cd uptake and translocation [24].

The mechanisms of Cd absorption by plant roots are the key to its accumulation. One can ask the question "if Cd is not an essential metal, why would cells have Cd transporters?" Indeed, plants do not have any specific Cd-specific transporters. However, transporters of Zn^{2+} like OsZIP1, and Fe^{2+} like OsIRT1 and OsIRT2 have been shown to transport Cd ions in the roots [25].

In countries where rice is the staple food, there is generally a deficiency of micronutrients in the soil [26]. The presence of Cd ions in the soil aggravates micronutrient deficiencies in rice grains.

In our previous study, the effects of Cd on the content of minerals were determined in three varieties of rice namely: Madina, Bakanaskyi and Chapsari [27]. Plants were grown in pots containing 2 mM kg^{-1} of $CdSO_4$. Although Cd was not found in grains of these rice varieties under investigation it caused a decrease in the content of mineral nutrients like Mg, Cu, Mn, Zn in variety-specific manner (Table 1).

It has been reported that the sensitivity to Cd increases in transgenic Arabidopsis expressing the genes for AtNramp1, AtNramp3 and AtNramp4 transporters from the Nramp (natural resistance-associated macrophage protein) family, which transport Zn, Mn, Fe, Co and Ni [28]. The OsLCT1 (Low-affinity Cation Transporter1) transporter of rice participates in the transport of Cd to the phloem, and it is a homolog of the wheat gene LCT1, which presumably regulates Cd release in the plasma membrane. Expression of the OsLCT1 gene was higher in leaf blades and nodes during the reproductive period, especially at node 1; i.e., the highest node. The expression of OsLCT1 was seen in diffuse vascular bundles in the panicles [29].

Table 1 – Content of mineral elements in rice grain [27].

Rice varieties	$CdSO_4$, mMol/kg	Mg, mg/kg	Mn, mg/kg	Fe, mg/kg	Cu, mg/kg	Zn, mg/kg	Cd mg/kg
Madina	0	1363.0 ±32.3	174.2±6.2	19.3±0.63	5.8±0.19	24.9±1.1	0.0
	2	1267.0±44.6	125.7±5.5	17.1±0.58	5.3±0.21	23.2±0.9	0.0
Bakanas	0	1480.3±51.7	161.0±8.7	17.2±0.7	7.2±0.3	26.4±1.3	0.0
	2	1456.1±72.3	120.3±6.1	12.4±0.49	6.3±0.26	22.9±1.4	0.0
Barakat	0	1311.0±39.8	133.1±4.7	15.7±0.58	5.0±0.22	19.4±0.81	0.0
	2	1105.4±51.3	84.6±3.4	7.46±0.7	4.4±0.15	16.4±0.52	0.0
Chapsari	0	1403.7±80.5	170.0±7.3	12.4±0.62	6.0±0.19	21.3±0.8	0.0
	2	1212.0±44.9	121.6±5.1	7.1±0.26	5.4±0.23	18.6±1.0	0.0
	P	ns	P < 0.01	P < 0.05	P < 0.01	P < 0.01	

Clemens [30] has also suggested that there are other genes whose products participate in the subcelllular transport of Cd from the cytoplasm to the apoplast, and in its compartmentalization in the vacuole as a mechanism of tolerance by the plant.

Thus the antagonistic effects of these ions are an important factor to consider when estimating net accumulation of Cd ions in a living organism [31]. Thus, biofortification, either through plant breeding and/or transgenic approaches to the development of new varieties that accumulate high concentrations of certain nutrients [26], is one possible solution to the problem of harmful Cd effects in humans. Efforts to biofortify seeds with Fe and Zn in rice were focused on increasing the content of the ferritin protein [32], the overexpression of Zn-transporter *ZIP1* gene [33], the expression of the phytosiderophore synthesis genes (*NAS*) [34], and the increase of Fe-reductase in the roots [35]. Thus, increased accumulation of Fe^{+2} and Ca^{+2} may be one of the effective ways to decrease Cd uptake by crop plants.

Mechanisms of plant resistance to cadmium

Plants have several mechanisms in place for providing resistance to heavy metals, including Cd. These mechanisms can be divided into two groups: 1) restriction of the entry of metals into most of the plant through its accumulation mainly in the root system and isolation in the vacuole; 2) changes in the metabolism of cells, aimed at reducing the toxic effect of metals. Biochemically bonded metal ions can be deposited in organs such as cell wall and vacuoles, which limits their transport as well as their deleterious effects on the plant [36]. Dai et al. [37] suggested that root cell walls were the first and the main barrier against Cd, with intracellular Cd being mainly stored in the vacuoles.

Seregin and Ivanov [36] have proposed that the ratio of the concentration of a toxic ion present in the plant in a tightly bound vs. mobile state determines not only the degree of influence of this ion on metabolism, but also determines the cellular structures and the processes associated with its functions. The reason for greater resistance or sensitivity of certain plants to Cd (and Pb) may be related to their ability to safely compartmentalize these metals in cellular organelles. The content of metals in plant cells does not necessarily reflect their content in their cytoplasm because of their ability to effectively exclude metals from the cytoplasm by binding with chelating agents and insulating them in vacuoles and cell walls.

Another effective mechanism for detoxification of most toxic metal ions in plants is their binding by organic acids and thiols in the cytoplasm, followed by the sequestration of these complexes in vacuoles. Glutathione (GT) plays an important role in the antioxidant defense of plants. Glutathione is also a precursor to phytohelatins (PCs) that are capable of binding heavy metals [38]. The determination of SH-groups in plant cells serves as one of the integral indicators of plant responses to the action of heavy metals [39, 40].

It is known that a common response of living organisms to the accumulation of Cd (and other heavy metals) is the induction/promotion of the biosynthesis of low molecular weight, cysteine-rich proteins called metallothioneins (MTs) or peptides called phytochelatins (PCs). Chemical bonding of Cd^{+2} with organic ligands is much stronger than that of other metal ions. At high concentrations, Cd-PC complexes are transported and localized in vacuoles; at low concentrations, 86-100% of Cd was found in the cytoplasm in *Datura inoxia* [41]. At high concentrations, Cd also binds with organic acids, and at low concentrations, with GT in the cytosol.

Phytochelatins, cadastins, glutamyl-peptides, found in some algae, higher plants and fungi containing γ-glutamylcysteinyl residues, differ from the mts by the fact that they are synthesized enzymatically and not by ribosomes. Phytochelatins are compounds with the general formula $[(\gamma\text{-Glu-Cis})_n\text{-Gly}$, where n is at most 11, but more often varies from 2 to 5. The ratio of pcs and their derivatives depends on the plant species, as well as on the ratios of metals in the soil or nutrient solution [42]. For example, in *rice,* resistance to Cd is provided by hydroxymethyl-PC $[(\gamma\text{-Glu-Cis})_n\text{-Ser}]$ and cadastines, but with increasing metal concentration the ratio shifts towards the latter [43].

Modulation of cadmium response by polyamines and amino acids

Several studies have reported the role of common polyamines [PAs – putrescine (Put), spermidine (Spd) and spermine (Spm)] in the modulation of plant responses to Cd and/or other heavy metals. Nahar *et al.* [44] hypothesized that exogenous additions of 0.2 mM Put and/or nitric oxide could improve physiological processes to enhance tolerance to Cd-toxicity for up to 2.0 mM in mung bean plants via coordinated effects on antioxidant and glyoxalase systems. Pretreatment with Put caused an increase in endogenous PA content and a de-

crease in protection from Cd stress, which was accompanied by a decrease in PCs and GS levels and PCS enzyme in rice plants [45]. These authors suggested that Put pre-treatment may inhibit the expression of the PCS gene or may decrease PCS activity, probably due to the depletion of GS by increased PA metabolism. It is conceivable that the added Cd may have bound to PAs used for pre-treatment, thus reducing the amount of free Cd to below the level required for the induction of PCS activity. Thangavel et al. (2007) reported a trend in the increase of Put in response to an increased concentration of Cd (12.5 µM-200 µM) in red spruce suspension cultures but this change was not statistically significant. Exogenous PAs were not supplied to these cultures and concentrations of Cd may not have been high enough to trigger a response in the PA pathway. Another study reported a decrease in Put and Spd in discs of sunflower leaves when treated with 0.5 mM Cd [46]. However, these authors reported that in 0.5 mM Cd-treated wheat leaves there was an increase in Put that was accompanied by increases in the activities of orthinithine decarboxylase and arginine decarboxylase, the two enzymes responsible for Put biosynthesis in plants. These authors concluded that differences in the effects of Cd on PAs in these two studies may be attributed to environmental conditions and the species-specificity of responses.

Although not yet tested with Cd, the exogenous application of 1 mM Spd was shown to improve the growth of Cr-stressed seedlings of *Raphanus sativus* L., perhaps through effects on the endogenous levels of PAs, amino acids, antioxidants such as GT, ascorbic acid, proline, glycine betaine, and total phenols, along with the activities of antioxidant enzymes [47]. These observations were accompanied by increases in PCs, photosynthetic pigments, H_2O_2, and total soluble sugars in seedlings treated with Spd and Cr – all indicating better adaptation to Cr-stress. Groppa *et al.* [46] showed that the exogenous addition of Spm resulted in a partial reversal of the effects of Cd on certain antioxidant enzymes, and an increase in the levels of endogenous PAs. Differences observed in the effects of treatment with Put or higher PAs (SPD and SPM) could be explained by the possibility that the exogenous application of higher PAs may not induce the synthesis of dcSAM from SAM, while after Put

treatment, its conversion to higher PAs (Spd and Spm) would involve SAM utilization [48]. Since amino acids, PAs and PCs share common metabolites in the nitrogen pathway, cellular amino acids concentrations also change under Cd toxicity [39, 48]. Zhu *et al.* [49] also hypothesized that higher adaption of *Noccaea praecox* than *N. caerulescens* to Cd-induced stress was partially due to differences in the cellular accumulation of glycine, sarcosine and ornithine; both glycine and ornithine are precursor metabolites for the synthesis of PCs.

Higher Cd tolerance and Cd accumulation was associated with greater accumulation of free amino acids Gln and Asn, in *Crassocephalum crepidioides* (Cd hyperaccumulator) as compared to *Ageratum conyzoides* L.. Thangavel *et al.* [39] reported an increase in glutamine and arginine along with a concurrent decrease in cystine + cysteine in Cd-treated red spruce cell cultures.

The effect of cadmium on plants can be presented as in the following figure (Figure 6):

Conclusion

The degree of negative impact of Cd on plant health is the result of the interaction of many factors such as the degree of Cd pollution from the environment, changes in physiological and biochemical processes in response to Cd exposure, antagonistic relationships among other anions, the functioning of transport systems and metal transporters, and the activation of protective reactions of the plant. Because of the ubiquitous presence of Cd ions in the soil as a result of active human industrial activity, there is a danger of contamination by this metal in agricultural crops. It is worth emphasizing that even though low concentrations of Cd in the soil do not lead to the accumulation of Cd in the fruits or grain of most crops, they do negatively impact the growth and development of most plants. The strengthening of oxidative stress, decrease of antioxydative enzyme activities, changing in membrane permeability and other negative alterations lead to inhibition of growth and biomass accumulation and mechanisms of homeostasis provide the plants tolerance to cadmium. Studies are needed to identify Cd-resistant crops, taking into account endogenous and exogenous factors that determine the degree of Cd toxicity for each plant species.
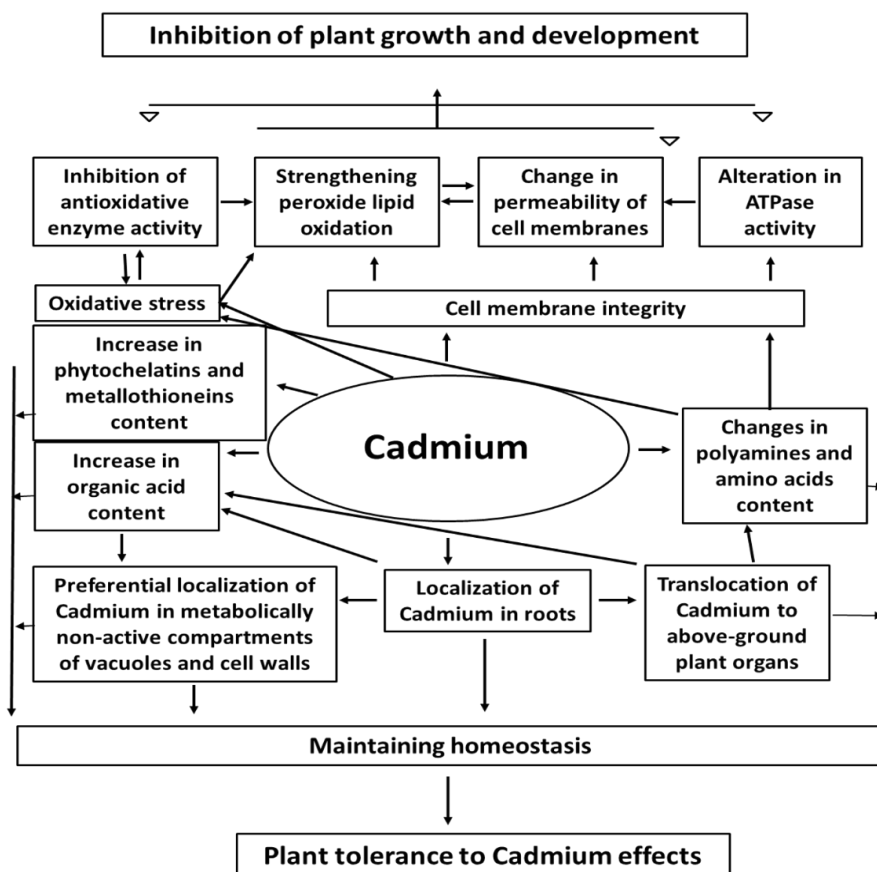
Figure 6 – Toxic effect of cadmium on plant and mechanisms of cadmium detoxification

References

1   Mynbayeva B.N., Imanbekova T.G. Estimation of regulations of soil contamination by heavy metals (analytical review) [Osenka normativov zgryaznenia pochv nyazhelymi metallami (analiticheskii obzor)]. http://nblib.library.kz/elib/library.kz/journal/Mynbaeva%20Imanbekova.pdf.

2   Kpomblekou A.K., Tabatabai M.A. (1994) Metal contents of phosphate rocks. Commun. Soil Sci. Plant Anal., no. 25, pp. 2871-2882. http://dx.doi.org/10.1080/00103629409369231.

3   Jones K.C., Johnston A.E. (1989) Cadmium in cereal grain and herbage from longterm experimental plots at Rothamsted, UK. Env. Poll., vol. 57, pp. 199-216. https://doi.org/10.1016/0269-7491(89)90012-2.

4   Bhattacharyya M.H. (2009) Cadmium osteotoxicity in experimental animals: mechanisms and relationship to human exposures. Toxic., Appl. Pharmacol., vol. 238, no 3, pp. 258-265. https://doi.org/10.1016/j.taap.2009.05.015.

5   FAO/WHO. Joint Committee on Food Additives and Contaminants. Position paper on Cd (prepared by France). 27th Session. 20-24 March, 1995. The Hague, Netherlands, 32 p.

6   Chaney R., Reeves P.G. and Angle J.S. (2001). Rice Plant Nutritional and Human Nutritional characteristics roles in human Cd toxicity. In: Plant nutrition: Food security and sustainability of agroecosystems through basic and applied research, W.J.Horst, (Ed.). Kluwer Academic Publishing, Dordrech, Netherlands, pp. 288-289. https://doi.org/10.1007/0-306-47624-X_138.

7   Coudert Y., Perin C., Courtois B., Khong N.G., Gantet P. (2010). Genetic control of root development in rice, the model cereal. Trends Plant Sci, vol. 15, no. 4, pp. 219-226. https://doi.org/10.1016/j.tplants.2010.01.008.

8   Liu H., Zhang J., Christie P. and Zhang F. (2008) Influence of iron plaque on uptake and accumulation of Cd by rice (Oryza sativa L.) seedlings grown in soil. Science of The Total Environment, vol. 394, no 2, pp. 361-368. https://doi.org/10.1016/j.scitotenv.2008.02.004.

9   Lux A., M. Martinka, M. Vaculik and White P.J. (2011). Root responses to cadmium in the rhizo-

sphere: a review. J Exp Bot., vol. 62, no. 1, pp. 21-37. https://doi.org/10.1093/jxb/erq281.

10 Yamaguchi N., Shikawa S. I, Abe T. et al. (2012). Role of the node in controlling traffic of cadmium, zinc, and manganese in rice. Journal of experimental botany, vol. 63, no 7, pp. 2729-2737. https://doi.org/10.1093/jxb/err455.

11 Zou J., Yue J., and Liu D. (2012). Effects of cadmium stress on root tip cells and some physiological indexes in Allium cepa var. Agrogarum L. Acta Biologica Cravoviensia, no 54/1, pp. 129-141. https://doi.org/10.2478/v10182-012-0015-x

12 Shi Q., Wang J., Zou J. et al. (2016). Cadmium localization and its toxic effects on root tips of barley. Zemdirbyste-Agriculture, vol. 103, no. 2, pp. 151-158. https://doi.org/10.13080/z-a.2016.103.020.

13 Ibrahim M.H., Chee Kong Y. and Mohd Zain N.A. (2017) Effect of Cadmium and Copper Exposure on Growth, Secondary Metabolites and Antioxidant Activity in the Medicinal Plant Sambung Nyawa (Gynura procumbens (Lour.) Merr). Molecules, vol. 22, no. 10, pp. 16-23. https://doi.org/10.3390/molecules22101623.

14 Atabayeva S.D., Zhardamalieva A., Nurmahanova A. et al. (2014) Vlianie deistvia ionov kadmia na uroven' POL I soderzhanie chlorophyllov u sortov pshenici (Triticum aestivum L.[Effect of cadmium on lipid peroxidation level and chlorophyll content in wheat (Triticum aestivum L.)]. Vestnik KazNU, vol. 60, no 1-2, pp. 167-171.

15 Aravind P., Prasad M.N.V. (2005) Cadmium-Zinc interactions in a hydroponic system using Cerathopyllum demersum L.: ada ptive ecophysiology, biochemistry and molecular toxicology. Brazil. J. Plant Physiol., vol.17, pp. 3-5. doi.org/10.1590/S1677-04202005000100002.

16 Choundury S., Panda S.K. (2005) Toxic effects, oxidative stress and ultrastructural changes in moss Tuxithelium nepalense (Schwaegr.) Broth. Under chromium and lead phytotoxicity. Water, Air, Soil Pollut., vol. 167, pp. 73-90.

17 Gratao P.L., Monteiro C.C., Rossi M.L. et al. (2009) Differential ultrastructural changes in tomato hormonal mutants exposed to cadmium. Environ. Exp. Bot., vol. 67, pp. 387-394.

18 Semane B., Dupae J., Cuypers A. et al. (2010). Leaf proteome responses of Arabidopsis thaliana exposed to mild cadmium stress. Journal of Plant Physiology, vol. 167, no 4, pp. 247-254. https://doi.org/10.1016/j.jplph.2009.09.015.

19 Elobeid M., Polle A., Göbel C. and Feussner I. (2012). Cadmium interferes with auxin physiology and lignification in poplar. Journal of Experimental Botany, vol. 63, no 3, pp. 1413-1421. https://doi.org/10.1093/jxb/err384.

20 Vassilev A. and Lidon F. (2011). Cd-induced membrane damages and changes in soluble protein and free amino acid contents in young barley plants. Emirates Journal of Food and Agriculture, no. 23, pp. 130-136. http://ejfa.info/.

21 Verma R., Shekhawar G.S., Sharma F. et al. (2008). Cadmium induced oxidative stress and changes in soluble and ionically bound cell wall peroxidase activities in roots of seedling and 3-4 leaf stage plants of Brassica juncea (L.) cern. Plant Cell Reports, vol. 27, pp. 1261-1269.

22 Grant C., Monreal M. A., Irvine R. B. et al. (2010) Preceding crop and phosphorus fertilization affect cadmium and zinc concentration of flaxseed under conventional and reduced tillage. Plant and Soil, vol. 333, pp. 337-350. https://doi.org/10.1007/s11104-010-0349-7.

23 Muehe E.M., Weigold P., Adaktylou I.J. et al. (2015) Rhizosphere microbial community composition affects cadmium and zinc uptake by the metal-hyperaccumulating plant Arabidopsis halleri. Applied and environmental microbiology, vol. 81, no 6, pp. 2173-2181. https://doi.org/10.1128/AEM.03359-14.

24 Feng Shao J., Che J., Yamaji N. et al. (2017) Silicon reduces cadmium accumulation by suppressing expression of transporter genes involved in cadmium uptake and translocation in rice. Journal of Experimental Botany, vol. 68, no 20, pp. 5641-5651. https://doi.org/10.1093/jxb/erx364.

25 Nakanishi H., Ogawa I., Ishimaru Y. et al. (2006) Iron deficiency enhances cadmium uptake and translocation mediated by the Fe2+ transporters OsIRT1 and OsIRT2 in rice. Soil Science and Plant Nutrition, vol. 52, no.4, pp. 464-469. https://doi.org/10.1111/j.1747-0765.2006.00055.x.

26 White P.J. and Broadley M.R. (2005) Biofortifying crops with essential mineral elements. Trends in Plant Science, vol. 10, no.12, pp. 586-593. https://doi.org/10.1016/j.tplants.2005.10.001.

27 Atabayeva S.D., Nurmakhanova A., Yernazarova G.E. et al. (2018) Effect of cadmium on mineral composition of rice grain. Research on Crops, no. 19, pp. 569-575.

28 Thomine S., Wang R.C., Ward J. et al. (2000) Cadmium and iron transport by members of a plant metal transporter family in Arabidopsis with homology to Nramp genes. PNAS, no. 97, pp. 4991-4996. https://doi.org/10.1073/ pnas.97.9.4991.

29 Uraguchi S., Fujiwara T. (2012) Cadmium transport and tolerance in rice: perspectives for reducing grain cadmium accumulation. Rice (New York, N.Y.), vol. 5, no. 1, 5 p. https://doi.org/10.1186/1939-8433-5-5.

30 Clemens S. (2001) Molecular mechanisms of plant metal tolerance and homeostasis. Planta,

vol. 212, no. 4, pp. 475-486. https://doi.org/10.1007/s004250000458.

31 Kobayashi N.I., Tanoi K., Hirose A. and Nakanishi T.M. (2012) Characterization of rapid intervascular transport of cadmium in rice stem by radioisotope imaging. Journal of Experimental Botany, vol. 64, no 2, pp. 507-517. https://doi.org/10.1093/jxb/ers344.

32 Goto F., Yoshihara T., Shigemoto N., et al. (1999) Iron fortification of rice seed by the soybean ferritin gene. Nature Biotechnology, vol.17, no 3, pp. 282-286. https://doi.org/10.1038/7029.

33 Ramesh S.A., Choimes S. and Schachtman D.P. (2004) Over-Expression of an Arabidopsis Zinc Transporter in Hordeum Vulgare Increases Short-Term Zinc Uptake after Zinc Deprivation and Seed Zinc Content. Plant Molecular Biology, vol. 54, no 3, pp. 373-385. https://doi.org/10.1023/B:PLAN.0000036370.70912.34.

34 Masuda H., Usuda K., Kobayashi T., et al. (2009). Overexpression of the Barley Nicotianamine Synthase Gene HvNAS1 Increases Iron and Zinc Concentrations in Rice Grains. Rice, vol. 2, no. 4, pp. 155-166. https://doi.org/10.1007/s12284-009-9031-1.

35 Vasconcelos M., Clemente T. and Grusak M. (2014). Evaluation of constitutive iron reductase (AtFRO2) expression on mineral accumulation and distribution in soybean (Glycine max L). Frontiers in Plant Science, no 5, 112. https://doi.org/10.3389/fpls.2014.00112.

36 Seregin I.V., Ivanov V.B. (2001). Physiological Aspects of Cadmium and Lead Toxic Effects on Higher Plants. Russian Journal of Plant Physiology, no. 48, pp. 523-544. https://doi.org/10.1023/A%3A1016719901147.

37 Dai H.P., Shan C., Wei Y. Et Al. (2012). Subcellular localization of cadmium in Hyperaccumulator Populus × Canescens. African journal of biotechnology, No. 11(16), pp. 3779-3787. https://doi.org/10.5897/Ajb11.3491.

38 Gupta S.C., Goldsbrough P.B. (1991). Phytochelatin accumulation and cadmium tolerance in selected tomato cell lines. Plant Physiology, vol. 97, no. 1, pp. 306-312. https://doi.org/10.1104/pp.97.1.306.

39 Thangavel P., Long S., Minocha R. (2007) Changes in phytochelatins and their biosynthetic intermediates in red spruce (Picea rubens Sarg.) cell suspension cultures under cadmium and zinc stress. Plant Cell, Tissue and Organ Culture, vol. 88, no 2, pp. 201-216. https://doi.org/10.1007/s11240-006-9192-1

40 Minocha R., Thangavel P., Dhankher O.P., et al. (2008) Separation and quantification of monothiols and phytochelatins from a wide variety of cell cultures and tissues of trees and other plants using high performance liquid chromatography. Journal of Chromatography A, vol. 1207, no. 1-2, pp. 72-83. https://doi.org/10.1016/j.chroma.2008.08.023

41 Rauser W.E. (1995) Phytochelatins and Related Peptides (Structure, Biosynthesis, and Function). Plant Physiology, vol. 109, no. 4, pp. 1141-1149. https://doi.org/10.1104/pp.109.4.114

42 Ahner B.A., Kong S., Morel F.M.M. (1995) Phytochelatin production in marine algae. 1. An interspecies comparison. Limnology and Oceanography, vol. 40. no. 4, pp. 649-657. https://doi.org/10.4319/lo.1995.40.4.0649.

43 Klapheck S., Fliegner W. and Zimmer I. (1994) Hydroxymethyl-phytochelatins [(gamma-glutamylcysteine)n-serine] are metal-induced peptides of the Poaceae. Plant Physiol, vol.104, no. 4, pp. 1325-1332. https://doi.org/10.1104/pp.104.4.1325.

44 Nahar K., Hasanuzzaman M., Alam M.M. et al. (2016) Polyamine and nitric oxide crosstalk: Antagonistic effects on cadmium toxicity in mung bean plants through upregulating the metal detoxification, antioxidant defense and methylglyoxal detoxification systems. Ecotoxicology and Environmental Safety, vol. 126, pp. 245-255. https://doi.org/10.1016/j.ecoenv.2015.12.026.

45 Pál M., Csavas G., Szalai G., et al. (2017) Polyamines may influence phytochelatin synthesis during Cd stress in rice. J Hazard Mater, vol. 340, pp. 272-280. https://doi.org/10.1016/j.jhazmat.2017.07.016.

46 Groppa M.D., Tomaro M.L. and Benavides M.P. (2007) Polyamines and heavy metal stress: the antioxidant behavior of spermine in cadmium- and copper-treated wheat leaves. BioMetals, vol. 20, no. 2, pp. 185-195. https://doi.org/10.1007/s10534-006-9026-y.

47 Choudhary S.P., Kanwar M., Bhardwaj R. (2012). Chromium stress mitigation by polyamine-brassinosteroid application involves phytohormonal and physiological strategies in Raphanus sativus L. PLOS ONE, vol. 7, no. 3, e33210. https://doi.org/10.1371/journal.pone.0033210.

48 Minocha R., Majumdar R. and Minocha S.C. (2014) Polyamines and abiotic stress in plants: A complex relationship. Frontiers in plant science, no. 5. https://doi.org/10.3389/fpls.2014.00175.

49 Zhu G., Xiao H., Guo Q. et al. (2018). Effects of cadmium stress on growth and amino acid metabolism in two Compositae plants. Ecotoxicology and Environmental Safety, vol. 158, pp. 300-308. https://doi.org/10.1016/j.ecoenv.2018.04.045.

G.T. Zhumaliyeva[1*], E.K. Makashev[2] ID, A.I. Zhussupova[1] ID,
S.N. Abdreshov[1,2] ID, G.A. Demchenko[2] ID

[1]Al-Farabi Kazakh National University, Almaty, Kazakhstan
[2]Institute of Human and Animal Physiology, Almaty, Kazakhstan
*e-mail: gaziza_jumalieva@mail.ru

Selected Kazakhstani plants with possible lymphatic properties

Abstract. Search for drugs that affect the functions of the lymphatic system in normal state and under various pathologies is extremely relevant and important. Intensive research is being conducted worldwide based on the idea of influencing any pathological process through the lymphatic system. One promising strategy is the use of herbal medicines as integrative, complementary and preventive therapy. The active components in medical plants have always been an important source of clinical therapeutics and their molecular pharmacology offers a great chemical diversity with often multi-pharmacological activity. In this review, we mainly analyzed the immunomodulating/anti-inflammatory and antioxidant activity of important Kazakhstani plants (*Ribes nigrum*, *Crataegus almaatensis*, *Ziziphora bungeana*, *Alhagi kirgisorum*, *Rosa majalis*, *Hypericum perforatum*, and *Bergenia crassifolia*). These plants have industrial reserves on the territory of Kazakhstan, and they have been used in traditional medicine since ancient times and are approved for use in official medicine. They are characterized by a high content of polyphenols, polysaccharides which have a stimulating effect on the lymphatic flow and promote the activation of the synthesizing apparatus and mitochondria in lymphoid cells and macrophages in the regional lymph nodes. In addition, they have a stimulating effect on the cellular composition of the lymph node and other synergistically acting biologically active compounds necessary for treatment and prevention of lymphatic system diseases.

Key words: *Ribes nigrum, Crataegus almaatensis, Ziziphora bungeana, Alhagi kirgisorum, Rosa majalis, Hypericum perforatum, Bergenia crassifolia*.
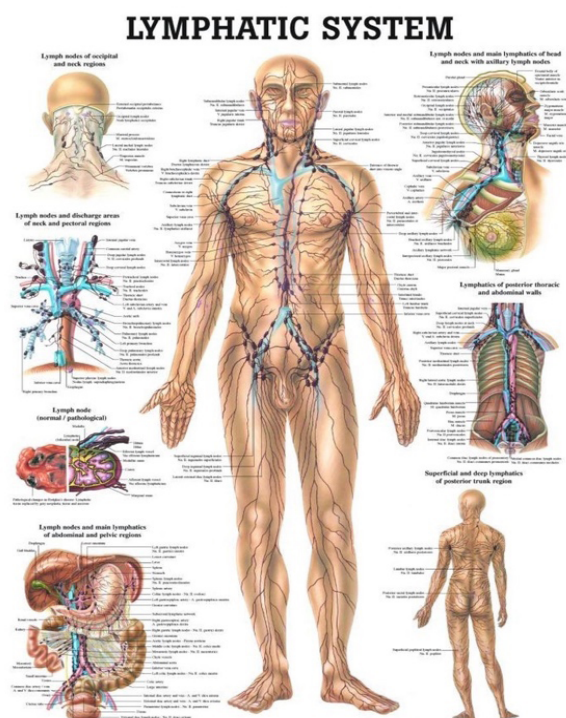
Introduction

The immune system is the body's defense system. Without a properly functioning immune system, the body quickly succumbs to infection [1].

The lymphatic system and immune system are closely linked. The lymphatic system comprises a network of vessels and nodes that circulate immune cells and provide a site for antigen presentation and immune activation. Lymphatic vessels transport lymph, a fluid containing infection-fighting white blood cells, from body tissues into lymph ducts that drain into lymph nodes. Lymph nodes are small, oval-shaped nodes that are found in clusters on either side of the neck, collar bone, armpits and groin. Lymphatic vessels run alongside arteries and veins connecting lymph nodes throughout the body. Having several times more vessels (Figure 1), the lymphatic system in the human body plays no less important role than the circulatory system [2; 3].

Since the lymph is derived from the interstitial fluid, its composition continually changes as the blood and the surrounding cells continually exchange substances with the interstitial fluid. It is generally similar to blood plasma, which is the fluid component of blood. Lymph returns proteins and excess interstitial fluid to the bloodstream. Lymph also transports fats from the digestive system (beginning in the lacteals) to the blood via chylomicrons [4].

Bacteria may enter the lymph channels and be transported to lymph nodes, where they are destroyed. Metastatic cancer cells can also be transported via lymph. In various pathological conditions, it delivers products of metabolism, necrobiosis, and other toxic substances from tissues into the blood. [5-7].

Figure 1 – The human lymphatic system

Being the first to take the products of tissue destruction, toxins and biologically active compounds under pathological processes in organs, lymph is involved in the generalization of inflammatory processes [8]. For instance, as is the case with apical periodontitis, the products of lipid peroxidation and antioxidant defense enzymes mainly enter the jugular lymph, to a lesser extent the jugular and femoral blood [9].

Under normal physiological conditions, entry into the lymphatic system is via the initial lymphatic capillaries in the interstitium. From lymphatic capillaries, lymph flows through progressively larger pre-collecting and collecting (afferent) lymphatic vessels, through the lymph nodes via lymphatic sinuses and then to post-nodal (efferent) lymphatic vessels. The collecting and post-nodal lymphatic vessels are segmented frequently by semilunar valves and are surrounded by smooth muscle cells that facilitate unidirectional lymph flow. In disease, there are substantial changes to the lymphatic system compared with normal physiological conditions (Figure 2, a).
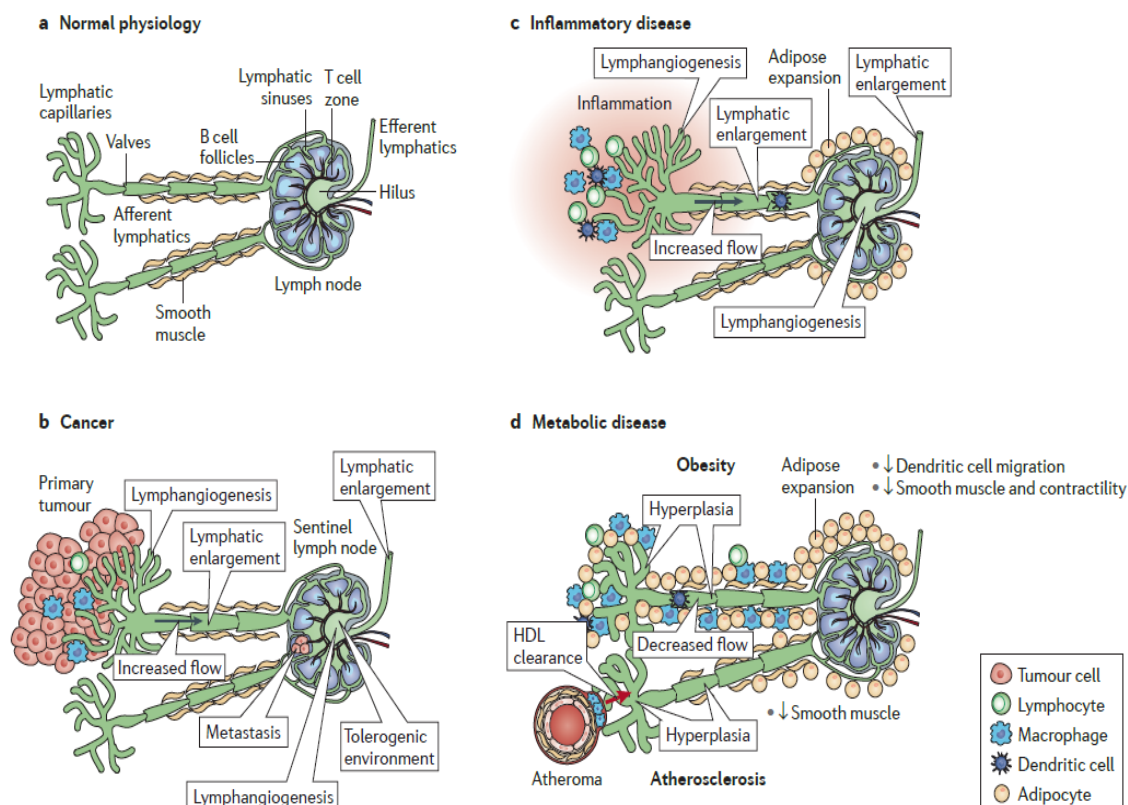
Figure 2 – Lymphatic function in health and disease [10]

In cancer, metastatic dissemination from the primary tumors often occurs via lymph vessels to the sentinel (first draining) lymph node. Tumor cells and associated macrophages induce lymph angiogenesis at the tumor site and in the draining lymph nodes via the release of pro-inflammatory and lymphangiogenic factors. Lymph angiogenesis, lymph vessel dilation and increased interstitial pressure modulate lymph flow from tumors and therefore alter immunity. Tumors may also release factors that promote immune tolerance (Figure 2, b).

In inflammatory disease, immune cells (for example, macrophages and lymphocytes) release pro-inflammatory and lymphangiogenic factors that promote lymphatic hyperplasia. These changes stimulate alterations in the flow of fluid, inflammatory mediators and dendritic cells from inflamed tissue to lymph nodes and therefore modulate immunity and inflammation. In chronic inflammation, there is also expansion of the adipose tissue surrounding the lymph node (Figure 2, c).

In metabolic disease, lymphatic function is markedly altered by high-fat diets and hypercholesterolemia. High-fat diets and/or obesity alter lymph node structure, promote lymphatic vessel hyperplasia and dilatation, reduce lymphatic smooth muscle coverage and contractility, and reduce lymph transport of fluid and dendritic cells. The lymphatics are surrounded by adipose, and impairments in lymphatic function typically increase lipid deposition in adipose, promoting obesity. Mice with hypercholesterolemia exhibit lymphatic vessel hyperplasia in the skin and loss of smooth muscle coverage. Recent data also suggest that lymphatic vessels facilitate high-density lipoprotein (HDL)-mediated cholesterol clearance from atheroma's. In this way, the lymph and lymphatics are broadly implicated in the development and progression of metabolic disease (Figure 2, d) [11].

In general, without restoration of the drainage function of the lymphatic apparatus, for which complete decongestive physiotherapy (which is a combination of four methods: manual lymphatic drainage, lymphedema rehabilitation exercises, compression therapy, skin care), a complete rehabilitation of the morphological and functional parameters of each organ is impossible [12].

The possibility of a drug effect on the lymphatic channel in order to correct violations of the homeostasis of the whole organism has been considered for a long time [13], but only with the development of clinical lymphology has this method been put into the practice. Drugs that stimulate lymph circulation and, thereby, activate the drainage function of the lymphatic system (drugs with an osmotic effect – mannitol, polyglucin, hemodes, glucose, isotonic sodium chloride solution and others) are widely used in treatment of various pathological processes [14]. In chemical terms, the structure of drugs of natural origin is close to the structure of metabolites produced by the human body, and, accordingly, is accessible to the action of its enzymatic systems, which makes drugs based on plant materials not only more effective, but also safer.

Due to its unique anatomy and physiology, potential exists to exploit the lymphatic system as a means of drug delivery. Targeting drugs into the lymph has certain advantages arising mainly from the unique anatomy and physiology of the lymphatic system (Figure 3). These advantages include avoidance of first pass metabolism, direct delivery of drugs to particular regions of the lymphatic circulation, e.g., in the treatment of disease states, and the possibility of regulating the rate of drug delivery into the systemic circulation.

The lymphatic system consists of a network of lymphatic vessels, tissues and nodes. Fluid, immune cells, macromolecules and molecules packaged into carriers such as lipoproteins, vesicles or exosomes enter the initial lymphatic capillaries to form lymph fluid. From here, lymph flows through a network of progressively larger collecting (afferent) lymphatic vessels, lymph nodes and post-nodal (efferent) lymphatic vessels to converge at either the left (or right) thoracic lymph duct. Lymph empties from the major lymph ducts directly into the venous system. Therapeutics can be targeted to the lymphatic system via mucosal, intestinal or parenteral routes. Mucosal delivery of particulate materials leads to their absorption across the epithelium into mucosa-associated lymphoid tissue (Figure 3, a). Intestinal or oral delivery of lipophilic drugs (typically logP values >5) leads to their incorporation into the process of intestinal lipoprotein assembly and transport into the intestinal lymphatics (Figure 3, b). Parenteral or interstitial delivery of macromolecular materials leads to their entry into lymphatic capillaries as these materials are too large to access the blood capillaries draining the injection site (Figure 3, c) [11].

Complications associated with the lymphatic system span a wide spectrum, including congenital disorders, cancer and side-effects of cancer treatments, cardiovascular disease, diabetes, and parasitic infections [15]. According to some estimates, 140-250 million people across the globe are affected by lymphedema [16]. While some lymphatic disorders are genetically related, lymphatic complications most

often arise as a secondary complication following cancer, cardiovascular disease, and immunological disorders [17]. For example, patients undergoing radiation therapy or surgery for breast cancer treatment are at a high risk of developing lymphedema [18]. Breast cancer is the most commonly observed cancer among women and is the second-most common type of cancer. According to the World Cancer Research Fund, an estimated 2 million cases of breast cancer were reported in 2018 across the world [19]. Another interesting aspect is that tumors may engage the lymphatic system in order to invade and metastasize [20].
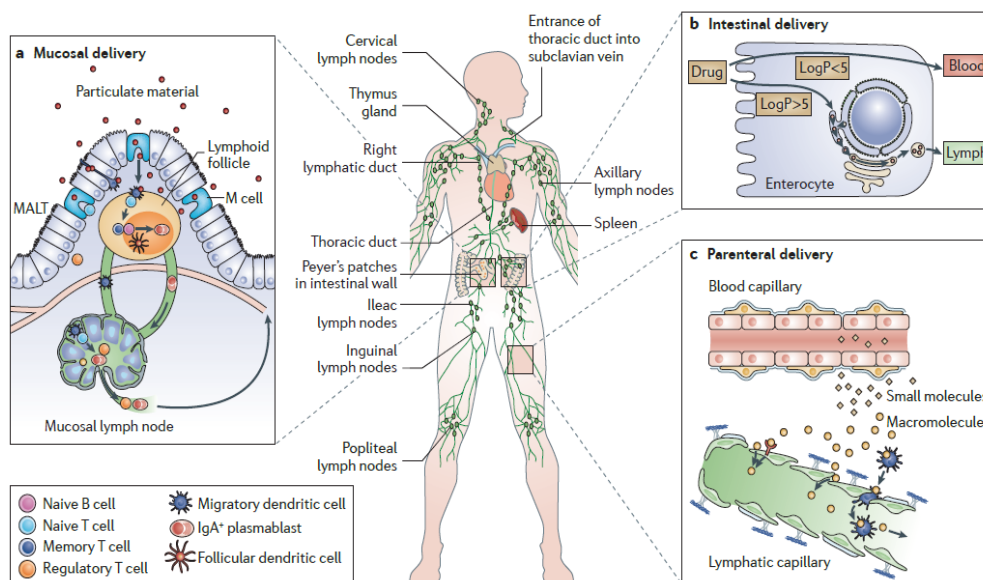
Figure 3 – Access routes to the lymphatics after oral and parenteral delivery [11]

Ongoing research for the development of novel therapies for the treatment of lymphedema is another driver of the global lymphedema treatment market. The emergence of a new direction in prophylactic lymphology, so-called lymphophytonutriciology, served as basis for the proposal to use phytocomposites with the realization of the effect of their action through the lymphatic system. The active ingredients of phlebotonic drugs with known lymphotropic effect, such as Antistax (Switzerland) and Ginkor Fort (France) are extracts of red grapes (*Vitis vinifera*) and Ginkgo bilobate (*Ginkgo bilobae*), obtained from plant materials of their own region [21; 22].

Alternative systemic approaches to development of a lymphedema-reversing pharmacology, including targeted anti-inflammatory therapy, are beginning to show promise. According to a new study conducted at the Stanford University School of Medicine, a new molecular mechanism primarily responsible for causing lymphedema, along with a drug (bestatin) that has the potential for hindering the process, was uncovered in May 2017. Bestatin is currently undergoing clinical trials for the treatment of secondary lymphedema. Positive outcome from the trials is expected to be a step forward toward developing new treatment options for the management of lymphedema [23]. Two early-stage clinical trials led by Stanford researchers have shown that ketoprofen, a nonsteroidal anti-inflammatory drug, or NSAID, can improve skin damage in patients with lymphedema. The researchers found that the buildup of lymph fluid is actually an inflammatory response within skin tissue. Thus, it is not merely a "plumbing" problem within the lymphatic system, as previously thought. They discovered that the naturally occurring inflammatory molecule LTB4 is elevated in both animal models of lymphedema and in humans with the disease, and that at elevated levels it causes tissue inflammation and impaired lymphatic function. Further research in mice showed that using ketoprofen to target LTB4 induced lymphatic repair and reversed the disease processes. This indicated that perhaps other therapies could reverse the negative impact of inflammation on lymphatic repair by targeting LTB4 [24].

The Institute of Human and Animal Physiology of the National Academy of Sciences of the Ministry of Education and Science of the Republic of Kazakhstan is the leading Institution of the

Kazakh Physiological Society, key organization in the Republic of Kazakhstan engaged in detailed studies of the activity of the lymphatic system, its morphofunctional state and direct relationship with various pathologies of metabolism, cardiovascular system, digestive tract, as well as the effects of weightlessness on the structure and function of lymphoid organs. A number of studies are conducted with leading organizations of near and far abroad, in particular with the Scientific Research Institute of Clinical and Experimental Lymphology SB RAMS [25; 26].

The consumption of certain complex natural substances derived from plants is widely accepted for their protective role in microvascular and lymphatic physiological functionality. Among the natural substances demonstrated to maintain microvascular and lymphatic homeostasis, our attention was focused on polyphenolic compounds, such as flavonoids, saponins and polysaccharides.

As is known, polyphenols have a stimulating effect on the lymphatic flow and promote the activation of the synthesizing apparatus and mitochondria in lymphoid cells and macrophages in the regional lymph nodes, and have a stimulating effect on the cellular composition of the lymph node [27].

Flavonoids are plant secondary metabolites to which such pharmacological functions as antioxidant, anti-mutagenic, antibacterial, anti-angiogenic, anti-inflammatory, anti-allergic, enzyme modulation, and anti-cancer are attributed. They are known as phytochemicals that exist either as free aglycones or glyosidic conjugates. Flavonoids are polyphenolic with a wide range of structures. they are categorized mainly into flavones, flavanols, isoflavones, flavanols, flavanones, flavanonols, and chalcones. The diverse structures of flavonoids have resulted in many properties including anti-cancer and anti-inflammatory effects. Recently, it has been shown that flavonoids can affect immune system response and might have immune-modulator effects [28].

Flavonoids like daflon, a combination of two flavonoids – hesperidin and diosmin, increase the intensity and frequency of lymphatic contraction and the total number of lymphatic capillaries. This results in the decrease of adhesion, migration, and activation of leukocytes, leading to lowering of prostaglandin's PGE2 and PGF2a and the reduction of radical oxygen species [29].

Rutin inhibits platelet aggregation and decreases capillary permeability, improving circulation. Among the other protective activities, rutin has anti-inflammatory and anti adipogenic activity [30].

Flavonoids possess different mechanisms of antioedemic action. It was determined that diosmin exerts a direct influence upon the functional state of the lymphatic system, activating proliferation of the lymphatic endothelium by means of gemmation, which leads to the formation of new capillary lymphatic networks with the resulting increase in both the total absorption area of the lymphatic capillary networks and the volume of lymph reabsorption. Troxerutin acts predominantly on the endothelium of blood capillaries, decreasing permeability in the arterial segment of the capillary, thus lowering the total volume of fluid in the interstitial space and accordingly the load on the lymphatic system [31].

Benzopyrones also have a variety of beneficial effects on the body. For example, they increase lymph drainage, reduce the fragility of capillaries. Of these, the first is coumarin (5,6-benzo-α-pyron). In Australia, coumarin is available on the market under the name "Lodema as 200 mg tablets, as well as 10% ointment. There are other oral forms of coumarin on the pharmaceutical market. For example, Venium (Limex containing 100 mg of coumarin) is produced in Switzerland and Liz Edem (15 mg of coumarin) is produced in France. There is also a drug known as Venalot-Depot (Germany), which contains 15 mg of coumarin and 90 mg of troxerutin. In addition, saponins (escin and horsechestnut extract), plant extracts (anthocyanosides – blueberries, proanthotonidols – preparations from grape seeds, Ginkgo extract), and synthetic drugs (calcium dobsilate, tribenoside, etc.) are used [32]. Polysaccharides also have positive effect on the circulatory and lymphatic systems [33].

In order to develop our own knowledge base, we started looking at the valuable properties of Kazakhstani plants with possible lymphatic properties. In this regard, valuable parts of seven medicinal plants (i.e. leaves of Ribes nigrum, fruits of *Crataegus almaatensis*, *Ziziphora bungeana* and *Alhagi* kirgisorum grass, fruits of Rosa majalis, *Hypericum perforatum* grass, and leaves and roots of *Bergenia crassifolia)* caught our special attention. These plants occur in abundance on the territory of Kazakhstan, and they have been used in traditional medicine since ancient times and are approved for use in official medicine (monographs on them are available in world pharmacopoeias). They are characterized by a high content of polyphenols, polysaccharides and other synergistically acting biologically active compounds necessary for treatment and prevention of lymphatic system diseases.

Blackcurrant (*Ribes nigrum*) is a berry that belongs to the family *Grossulariaceae*. It includes 150

cultivars and is one of the most common woody shrubs in the world. *Ribes nigrum* has a well-deserved demand because its fruits have dietary and medicinal properties. Blackcurrant contains a complex of significant biologically active compounds. Its leaves are rich in ascorbic acid (up to 470 mg%), carotene, polyphenols, phytoncides and essential oils. Due to its rich chemical composition, blackcurrant leaves are of much interest as a source of plant material, which, among other properties, display high antioxidant activity [34]. Experimental data show that consumption of blackcurrant juice prevents the development of oxidative stress, improves the state of vascular endothelium, and protects the erythrocyte membranes from destruction when exposed to free oxygen and ultraviolet radiation [35; 36]. Therefore, the extract obtained from the leaves of blackcurrant is a valuable component of the synthetic drug. Its sugar composition includes more fructose (4.2%), less glucose (1.5%) and sucrose (1.0%). Non-digestible carbohydrates are represented by fiber (up to 3%) and pectins (up to 1.5%). An important property of pectins is their ability to adsorb bacterial toxins, heavy metal ions, including radionuclides. In addition, pectins bind and remove cholesterol from the body, preventing the development of atherosclerosis and the oxidation of ascorbic acid and catechins in fresh fruits. Organic acids in blackcurrant fruits are mainly citric acid (2.0%); they also contain malic (0.25%) and oxalic (0.06%) acids. They have a positive effect on digestion by increasing the secretion of gastric glands and intestinal peristalsis [37].

Blackcurrant berries are rich in polyphenols, which range from 488 to 1116 mg and significantly determine their taste, nutritional and medicinal value. Ripe fruits are also a rich source of anthocyanins. The anthocyanin complex of black currant includes four main components: 3-glucosides and 3-rutinosides of delphinidine and cyanidine. These components ocur in all varieties of *R. nigrum* with black color, regardless of the variety and growing region. Anthocyanins have capillary-strengthening activity, antioxidant, antibacterial, anticarcinogenic properties and are effectively used in medicine for the treatment and prevention of a host of diseases. The beneficial properties of anthocyanins, cyanidins and their glycosides are due to their ability to scavenge free radicals, including the reactive oxygen species [38].

Almaty hawthorn (*Crataegus almaatensis* Pojark) is an endemic plant that grows only in the foothills of Zailiysky Alatau, Almaty region, Kazakhstan. Hawthorn fruits contain the flavonoids hyperoside, quercetin, vitexin, triterpene saponins, acids, proanthocyanides of various degrees of polymerization related to condensed tannins. They also contain a large number of such beneficial organic acids as ascorbic, tartaric, citric, malic, caffeic, chlorogenic, and vitamins (K, C, F, B) and trace elements (K, Ca, Mg, Fe, Mn, Zn) [39; 40]. Its extracts are used for treatment of cardiovascular disorders, such as arrhythmia, myocardial infarction, heart failure, as well as a hypotensive and diuretic drug [4].

Broad range of biological activities of Almaty hawthorn, such as anti-inflammatory, antioxidant, vasodilator, positive inotropic and cholesterol synthesis inhibiting properties has been described as being important for medical practices. These activities are significantly affected by the presence of antioxidant molecules in the extracts of hawthorn, which have the ability to absorb free radicals formed as a result of biochemical and physiological reactions in the human body. Furthemore, oligomeric procyanidins, triterpenes, flavonoids, polysaccharides and catecholamines have been identified in hawthorn extracts, and they are thought to have pharmacological potential [41; 42]. Fresh or dried fruits, flowers and leaves are used as a source of extracts for the production of various dosage forms of over-the-counter medicines or dietary supplements [43].

Ziziphora bungeana Juz. is found in meadows and highlands of Kazakhstan. Capsules obtained on its basis are used for treatment of various viral infections of the upper respiratory tract; a preparation from its flavonoid fraction is recommended for treatment of cardiovascular diseases. Its chemical composition includes monoterpene essential oil, polyphenols and triterpenes [44]. Industrial reserves and cultivation capability, experience in traditional medicine and the rich chemical composition of *Ziziphora* suggest that its extract be added to the formulae.

The antibacterial and antiseptic activities of *Ziziphora* species are determined by their content of essential oils such as thymol and carvacrol. Some components of the essential oils of *Ziziphora* (terpinolene, thymol, borneol, karyofillen, carvacrol) show antioxidant activity. Moreover, flavonoids from *Ziziphora* grass show antioxidant, anti-inflammatory and antitumor activity. Flavonoids such as chrysin, apigenin, linarin, luteolin have anti-inflammatory effects [45].

Ziziphora extracts that had a high concentration of polyphenolic substances showed vasodilator activity. The presence of a 4-hydroxy group without methyl substitution in flavonoids and the absence of constant substitution at positions 5, 6 and 7 of the

flavonoid structure are apparently responsible for the vasodilator effect [46].

The world flora includes 7 species of the genus *Alhagi,* of which 5 species grow in Central Asia: *Alhagi pseudalhagi* (M.Bieb.) Desv. ex Shap., *Alhagi sparsifolia* Shop., *Alhagi canescens* (Regel) B. Keller & Shap., *Alhagi kirghisorum* Schrenk. and *Alhagi persarum* Boiss. & Buhse. The phytochemical profile of two species (*Alhagi pseudalhagi* and *Alhagi sparsifolia)* have been most studied to date. These species of camel thorn have been shown to produce biologically active alkaloids, phenolic compounds and terpenoids. Kyrgyz camel thorn (*Alhagi* kirgisorum Schrenk.) grows in southern part of Kazakhstan. Polyphenols in the form of flavonols, their glycosides, phenolic acids, condensed tannins, and heteropolysaccharides were isolated from its aerial parts. On the basis of the substance "Alkhidin", the following dosage forms were developed: alchidin ointment, 5%, "Zhantak" syrup, introduced into the medicine [47].

For the purpose of treatment the roots of the Kyrgyz camel thorn is recommended. Infusions and decoctions of yantak are widely used in traditional medicine as a diuretic, diaphoretic, and laxative. Its extract is widely used in medicine as an anti-inflammatory and wound healing agent. The following phenolic compounds were isolated and identified from the aboveground part of *Alhagi kirghisorum*: gallic acid, (+)- catechin, narcissin and rutin. Gallic acid has strong antioxidant properties and also exhibits hepatoprotective properties when it is part of more complex substances. Catechin enhances the hepatotoxic effect of carbon tetrachloride, and it was found to increases the killer activity of T-lymphocytes. Narcissine can have an spasmolytic effects on the heart vessels, and is used in cardiological practice. Rutin is a strong antioxidant that prevents the formation of carcinogens, strengthens the walls of blood vessels, improves blood circulation, including blood circulation in the capillaries of the joints and spine, provides the flow of necessary nutrients to the joints, improving their function [45; 47].

Rose hip (*Rosa* L.) is a genus of wild plants in the family *Rosaceae*. It is an erect, large-leaved shrub, reaching a height of 1-2 m. There are more than 120 species of wild rose that are widely distributed in Europe, Asia, the Middle East and North America. Plants are resistant to harsh environmental conditions (rocky and sloping terrain, poor soil, and lack of water). It is of great scientific interest as a source of biologically active compounds and is widely used as medicinal, vitamin and food raw materials. Its posi-

tive effect has been demonstrated in reducing the risk of cardiovascular diseases, various forms of cancer, diarrhea, bladder infection, and diabetes. Rosehip preparations have a wide pharmacological spectrum of action. They have a strong antioxidant, restorative effect, stimulate nonspecific resistance of the body, reduce vascular permeability, enhance hormone synthesis and tissue regeneration, and have anti-inflammatory, immunostimulating, and choleretic properties. In traditional medicine, fruits, flowers, leaves and roots of a plant are used [48; 49].

The value of rose hips is determined by a complex of such biologically active compounds as ascorbic acid, carotenoids, flavonoids (quercetin, kempferol, isocvercetin), catechins (epigallocatechin, gallocatechin, epigallocatechin gallate), carbohydrates, organic acids, vitamins of group B, K1, Pac, E, Pol, E, Pol, E, Pol, E, Pol , pectic substances, salts of potassium, sodium, calcium, magnesium, phosphorus, iron, etc. It is considered the richest natural source of vitamin C. In this case, the biological role of vitamin C is manifested in the presence of organic acids and P-active compounds, which include anthocyanins, catechins, leucoanthocyanins and flavonols, which differ in chemical composition, but have a similar effect on the human body. Flavonoids act as antioxidants and inactivate free radicals in the presence of metals. In the fruits of the plant genus *Rosa* L., they are represented in particular by hyperoside, quercetin, rutin, astragalin, kaempferol-3-arabinoside, kaempferol-3-rhamnoglucoside, and others. Fruits *Rosa majalis* Herrm. are used as vitamin supplement [48; 49]. Fruits of May rose hips (*Rosa majalis* Herrn.) contain vitamins C, B2, K, E, provitamin A, polyphenols, a complex of higher organic acids with a predominant content of polyenes, and it is part of vitamin and multivitamin collection and Traskov's anti-asthma potion, Hepar immunostimulant. The strongest anti-scurring agent, rosehip oil and Karotolin, used as wound healing agents, Holosas syrup, used for hepatitis, cholecystitis, biliary dyskinesia, are obtained from the fruits of *Rosa majalis*. Drugs from rose hips are prescribed for disorders of carbohydrate metabolism and impaired functions of the bone marrow, liver and pancreas [49]. The immunostimulating properties of the extract from *Rosa majalis* will contribute to such in new formulation.

St. John's wort (*Hypericum perforatum* L.) is a promising source of such biologically active compounds as naphthodianthrones pigments and flavonoids, widely used in traditional and scientific medicine, and it is included in the pharmacopeias of many countries. *St John's wort (Hypericum perforatum* L.)

is widespread in Kazakhstan in the foothills of Zailiysky and Dzhungarsky Alatau, and it has been used in the treatment of genitourinary and gastrointestinal inflammations since ancient times. Both in folk and scientific medicine, preparations from St. John's wort are used as astringents, anti-inflammatory and antiseptic agents for treatment of various wounds and burns. The chemical composition of plants of the genus *Hypericum* L. is complex and diverse in the type of structures of biologically active compounds. Lead role in the therapeutic properties of the species of this genus is played by naphthodianthrones (anthraquinones), flavonoids and derivatives of hyperforin. Vitamins C, PP, carotenoids tone up, improve brain activity; flavonoids normalize the nervous system and positively affect reproductive function, which indicates the importance of including this component in the developed phytocomposite. St. John's wort has a strong anti-inflammatory effect, including improving microcirculation and dissolves infiltrates that helps to cure serious diseases and the penetration of antibiotics to the source of infection. In homeopathic practice, the entire St. John's wort plant is used, as well as its individual parts as an analgesic, hemostatic and regenerating agent, as well as for lesions of the central and peripheral nervous systems [50; 51].

Badan thick-leaved (*Bergenia crassifolia* (L.) Fritsch) perennial herb of the family Saxifragaceae. Badan thick-leaved has industrial reserves in Eastern Kazakhstan. It contains up to 35% of mixture of pyrocatechol and pyrogall hydrolyzable tannins, gallic acid, vitamin C, carotenes, oxidized and reduced flavonoids, coumarins, mineral salts, essential oils and resins, trace elements Mn, Fe, Cu, and carbohydrates. By the content of glycoside arbutin (22%), badan is the richest plant source in the world. Infusions and decoctions from it are used to treat pulmonary tuberculosis, throat diseases, rheumatism, diseases of the gastrointestinal tract, high blood pressure, as well as in gynecological practice as a hemostatic agent and for the treatment of cervical dysplasia [52]. A complex of biologically active compounds from this plant is appropriate for inclusion in the formulated drug. Badan refers to plants that accumulate tannins. Quite large amounts of tannins accumulate in the rhizomes of badan from 6 to 30%. Simple phenols, flavonoids, and catechins found in various parts are precursors of tannins and serve as building materials for polymeric phenols [53]. Modern pharmacological studies have revealed a number of medicinal properties of preparations from the leaves of badan. Badan leaves are used for diseases of the digestive system (colitis, enterocolitis, hyposecretory gastritis), allergies, and to normalize metabolism. The decoction of leaves has

an anti-hypoxic and choleretic effect, and it has antibacterial activity against gram-positive bacteria in gynecological practice to treat various bleedings. Dry leaves of badan are used for Mongolian tea, which has tonic properties, improves metabolism in the body and normalizes blood pressure [54]. Research to be continued.

Conclusion

The active components in medical plants have always represented an important source of clinical therapeutics since they offer tremendous chemical diversity that is often associated with a large number of pharmacological activities and the absence of cumulative and side effects. Their use in traditional medicine for their properties and health benefits is well recognized since ancient times. In this paper our focus was on some biologically active compounds from selected Kazakhstani plants, which might be potentially valuable for creation of drug enhancing lymphotropic activity and immune status of the human organism. Authors are thankful to Prof. Asim Esen Virginia Polytechnic Institute and State University (Blacksburg, USA) for his kind assistance in preparing the manuscript.

References

1 McMahon S.B., La Russa F., Bennett D.L. (2015) Crosstalk between the nociceptive and immune systems in host defence and disease. Nat Rev Neurosci. vol. 16, no. 7, pp. 389□402. https://doi.org/10.1038/nrn3946.

2 Andrade M.F.C.d, Jacomo A.L. (2007). Anatomy of the human lymphatic system. Cancer treatment and research. vol. 135, pp. 55-77.

3 Myers K., Hannah P. (2017). Manual of venous and lymphatic diseases. CRC Press, 335 p.

4 The Editors of Encyclopaedia Britannica. Lymphatic system // Encyclopædia Britannica, inc. March 20, 2020. Available at: https://www.britannica.com/science/lymphatic-system.

5 Rudiger Anatomie. The human lymphatic system laminated anatomy chart, A-104187. Anatomy Warehouse, 2020. Available at: https://anatomywarehouse.com/the-human-lymphatic-system-anatomy-chart-a-104187.

6 Chen J., Alexander J.S., Orr A.W. (2012) Integrins and their extracellular matrix ligands in lymphangiogenesis and lymph node metastasis. International Journal of Cell Biology, 853703.

7 Semyachkina-Glushkovskaya O., Postnov D., Kurths J. (2018). Blood-brain barrier, lymphatic

clearance, and recovery: Ariadne's thread in labyrinths of hypotheses. International Journal of Molecular Sciences. vol. 19, no. 12, 3818.

8 Sweeney M.D., Zlokovic B.V. (2018). A lymphatic waste-disposal system implicated in Alzheimer's disease. Nature, vol. 560, no. 7717, pp.172-174.

9 Schwager S., Detmar M. (2019) Inflammation and lymphatic function. Frontiers in Immunology. vol. 10, p. 308.

10 Bora C.R., Prabhu R.H., Patravale V.B. (2017). Lymphatic Delivery: concept, challenges and applications. Indian Drugs. vol. 54, pp. 5-22.

11 Trevaskis N.L., Kaminskas L.M., Porter C.J. (2015) From sewer to saviour – targeting the lymphatic system to promote drug exposure and activity. Nat. Rev. Drug Discov. vol. 14, no. 11, pp. 781□803. https://doi.org/10.1038/nrd4608.

12 I2. Tzani I., Tsichlaki M., Zerva E., Papathanasiou G., Dimakakos E. (2018). Physiotherapeutic rehabilitation of lymphedema: state-of-the-art. Lymphology. vol. 51, pp. 1-12.

13 Oliveira M.M.F.d, Gurgel M.S.C., Amorim B.J., Ramos C.D., Derchain S., Furlan-Santos N., Santos C.C.d, Sarian L.O. (2018). Long term effects of manual lymphatic drainage and active exercises on physical morbidities, lymphoscintigraphy parameters and lymphedema formation in patients operated due to breast cancer: a clinical trial. PLOS ONE, vol. 13, no. 1, e0189176.

14 Solari E., Marcozzi C., Negrini D., Moriondo A. (2018). Fluid osmolarity acutely and differentially modulates lymphatic vessels intrinsic contractions and lymph flow. Front. Physiol., vol. 9, no. 871. https://doi.org/10.3389/fphys.2018.00871.

15 Nazeh M. Al-Abd, Zurainee Mohamed Nor, Abdulelah H. Al-Adhroey, Anwar Suhaimi, S. Sivanandam. (2013). Recent advances on the use of biochemical extracts as filaricidal agents. Evid Based Complement Alternat Med., 986573. https://doi.org/10.1155/2013/986573.

16 Lymphedema treatment market analysis by size, share, top key manufacturers, demand overview, regional outlook and growth forecast to 2026. Available at: https://coleofduty.com/military-news/2020/04/22/lymphedema-treatment-market-analysis-by-size-share-top-key-manufacturers-demand-overview-regional-outlook-and-growth-forecast-to-2026/, 22 April 2020.

17 Alderfer L., Wei A., Hanjaya-Putra D. (2018). Lymphatic tissue engineering and regeneration. J Biol Eng. vol. 12, no. 32. https://doi.org/10.1186/s13036-018-0122-7.

18 Fu M.R. (2014) Breast cancer-related lymphedema: Symptoms, diagnosis, risk reduction, and management. World. J Clin. Oncol. vol. 5, no. 3, pp. 241□247. https://doi.org/10.5306/wjco.v5.i3.241.

19 Bray F., Ferlay J., Soerjomataram I., Siegel R.L., Torre L.A., Jemal A. (2018). Global cancer statistics 2018: GLOBOCAN estimates of incidence and mortality worldwide for 36 cancers in 185 countries CA Cancer J Clin., http://dx.doi.org/10.3322/caac.21492.

20 Jones D. (2020). Parallels of resistance between angiogenesis and lymphangiogenesis inhibition in cancer therapy. Cells, vol. 9, no. 3, p. 762, https://doi.org/10.3390/cells9030762.

21 Stücker M., Rabe E., Meyer K., Ottillinger B., Schütt T. (2019). Therapeutic approach to chronic venous insufficiency – clinical benefits of red-vine-leaf-extract AS 195 (Antistax®). Pharmazie, vol. 74, no. 4, pp. 193□200. https://doi.org/10.1691/ph.2019.9326.

22 Pokrovskii A.V., Sapelkin S.V., Galaktionova L.A., Fedorov E.E. (2005). The assessment of medical therapy effectiveness of patients with lower limb chronic venous insufficiency: the results of prospective study with Ginkor Fort. [rus.]. Angiology and Vascular Surgery. vol. 11, no. 3, pp. 47□52.

23 Tian W., Rockson S.G., Jiang X., et al. (2017) Leukotriene B4 antagonism ameliorates experimental lymphedema. Science Translational Medicine, vol. 9, no. 389, eaal3920. https://doi.org/10.1126/scitranslmed.aal3920.

24 Rockson SG., et al. (2018). Pilot studies demonstrate the potential benefits of antiinflammatory therapy in human lymphedema. JCI Insight. vol. 3, no. 20, e123775.

25 Bulekbaeva L.E., Ilyin E.A., Erofeeva L.M., Demchenko G.A., Gorchakova O.V. (2015). State microstructure lymphoid nodules of the small intestine of mice on the background of the 30-day space flight / HABERLERI, proceedings of the National Academy of Sciences of the Republic of Kazakhstan, vol. 4, no. 310, pp. 9-12.

26 Demchenko G.A., Abdreshov S.N. & Nurmakhanova B.A. (2019) Contractile activity of lymph nodes in young, middle-aged, and old rats. Bull. Exp. Biol. Med., vol. 167, pp. 194-197. https://doi.org/10.1007/s10517-019-04489-x.

27 Yahfoufi N., Alsadi N., Jambi M., Matar C. (2018). The immunomodulatory and anti-inflammatory role of polyphenols. Nutrients, vol. 10, no. 11, p. 1618.

28 Hosseinzade A., Sadeghi O., Naghdipour Biregani A., et. al. (2019). Immunomodulatory Effects of Flavonoids: Possible Induction of T CD4+ Regulatory Cells Through Suppression

of mTOR Pathway Signaling Activity. Front. Immunol., vol. 10, p. 51. https://doi.org/10.3389/fimmu.2019.00051.

29 Lemole G.M. (2016). The importance of the lymphatic system in vascular disease. J Integr. Cardiol., 2. https://doi.org/0.15761/JIC.1000188.

30 Ciccone V., Monti M., Antonini G., Mattoli L., et al. (2016). Efficacy of AdipoDren in reducing interleukin-1-induced lymphatic endothelial hyperpermeability. J Vasc. Res., vol. 53, pp. 255-268. https://doi.org/10.1159/000452798.

31 Shishlo V., Malinin A., Diurzhanov A. (2013). Mechanisms of antioedemic effect of bioflavonoids in experiment [Mechanismi antiedemicheskogo effecta bioflavonoidov v experimente]. Angiology and vascular surgery. vol. 19, pp. 25-33.

32 Wanchai A., Armer J.M., Stewart B.R. (2013). Complementary and alternative medicine and lymphedema. Seminars in Oncology Nursing, vol. 29, no. 1, pp. 41-49. https://doi.org/10.1016/j.soncn.2012.11.006.

33 Minquan H., Tiyu C., Yinglun L. (1996). Effects of polysaccharides from Dendrobium candidum on white blood cells and lymph cell moving inhibition factor of mice. Natural Product Research and Development, vol. 8, no. 3, pp. 39-41.

34 Karomatov I.D., Rustamova G.U. (2018) . The healing properties of currants [Lechebnye svojstva smorodiny]. Biology and Integrative Medicine. no. 5, pp. 32-47.

35 Huebbe P., Giller K., de Pascual-Teresa S., Arkenau A., Adolphi B., Portius S., Arkenau C.N., Rimbach G. (2012). Effects of blackcurrant-based juice on atherosclerosis-related biomarkers in cultured macrophages and in human subjects after consumption of a high-energy meal. Br. J. Nutr., vol. 108, no. 2, pp. 234-244.

36 Bonarska-Kujawa D., Cyboran S., Żyłka R., Oszmiański J., Kleszczyńska H. (2014). Biological activity of blackcurrant extracts (Ribes nigrum L.) in relation to erythrocyte membranes. Biomed. Res. Int., 783059.

37 Ashigai H., Komano Y., Wang G., Kawachi Y., Sunaga K., Yamamoto R., Takata R., Miyake M., Yanai T. (2017). Polysaccharide from black currant (Ribes nigrum L.) stimulates dendritic cells through TLR4 signaling. Bioscience of Microbiota. Food and Health, vol. 36, no. 4, pp. 141-145.

38 Kim B., Bae M., Park Y.K., Ma H., Yuan T., Seeram N.P., Lee J.Y. (2018). Blackcurrant anthocyanins stimulated cholesterol transport via post-transcriptional induction of LDL receptor in Caco-2 cells. European Journal of Nutrition. vol. 57, no. 1, pp. 405-415.

39 Tadic V.M., Dobric S., Markovic G.M., Sofija M., Tanja S. (2008). Antiinflammatory, gastroprotective, free–radical scavenging and antimicrobial activities of hawthorn berries ethanol extract. J. Agr. Food Chem, vol. 56, pp. 7700-7709.

40 Wu J., Peng W., Qin R., Zhou H. (2014). Crataegus pinnatifida: chemical constituents, pharmacology, and potential applications. Molecules, vol. 19, no. 2, pp. 1685-1712.

41 Degenring F.H., Suter A., Weber M., Saller R. (2003). A randomised double blind placebo controlled clinical trial of a standardised extract of fresh Crataegus berries (Crataegisan®) in the treatment of patients with congestive heart failure NYHA II, Phytomedicine, vol. 10, pp. 363-369.

42 Dinesh K., Vikrant A., Zulfiqar B., Nisar K., Deo P. (2012) The genus Crataegus (Rosaceae): chemical and pharmacological perspectives. Rev. Bras. Farmacogn., vol. 22, pp. 1187-1200.

43 Claudia A.M, Dana C., Madosa E., Ghiocel M., Lucian C. (2016). The chemical composition and pharmaceutical usage of Hawthorn (Crataegus monogyna L.) extracts, J Biotechnol. vol. 231, S59.

44 Smejkal K., Malaník M., Zhaparkulova K., Sakipova Z., Ibragimova L., Ibadullaeva G., ZemliCka M. (2016). Kazakh Ziziphora species as sources of bioactive substances. Molecules, vol. 12, no. 7, p. 826.

45 Radulovic N.S., Blagojevic P.D., Stojanovic-Radic Z.Z., Stojanovic N.M. (2013). Antimicrobial plant metabolites: structural diversity and mechanism of action. Curr Med Chem., vol. 20, no. 7, pp. 932-952.

46 Tian S., Shi Y., Zhou X., et. al. (2011). Total polyphenolic (flavonoids) content and antioxidant capacity of different Ziziphora clinopodioides Lam. extracts. Pharmacogn Mag., vol. 7, no. 25, pp. 65-68. https://doi.org/10.4103/0973-1296.75904.

47 Eskalieva B., Burasheva G. (2002). Flavonoids of Alhagi persarum. Chem. Nat. Comp., vol. 38, pp. 102-103.

48 Bhave A., Schulzova V., Chmelarova H., Mrnka L., Hajslova J. (2017). Assessment of rosehips based on the content of their biologically active compounds. Journal of food and drug analysis, vol. 25, no. 3, pp. 681-690.

49 Winther K., Vinther Hansen A.S., Campbell-Tofte J. (2016). Bioactive ingredients of rose hips (Rosa canina L.) with special reference to antioxidative and anti-inflammatory properties: in vitro studies. Botanics: targets and therapy. vol. 2016, no. 6, pp. 11-23.

50 Süntar I.P., Akkol E.K., Yılmazer D., Baykal T., Kırmızıbekmez H., Alper M., Yeşilada E. (2010).

Investigations on the in vivo wound healing potential of Hypericum perforatum L. J Ethnopharm., vol. 127, no. 2, pp. 468-477.

51 Russo E., Scicchitano F., Whalley B.J., Mazzitello C., Ciriaco M., Esposito S., Patanè M., Upton R., Pugliese M., Chimirri S., Mammì M., Palleria C., De Sarro G. (2014). Hypericum perforatum: pharmacokinetic, mechanism of action, tolerability, and clinical drug-drug interactions. Phytotherapy Research, vol. 28, no. 5, pp. 643–655.

52 Arok R., Végh K., Alberti A., Kéry Á. Phytochemical comparison and analysis of Bergenia crassifolia L. (Fritsch.) and Bergenia cordifolia Sternb. (2012). Eur. Chem. Bull., vol. 1, no. 1-2, pp. 31-34.

53 Zafar R., Ullah H., Zahoor M. et al. (2019). Isolation of bioactive compounds from Bergenia ciliata (haw.) Sternb rhizome and their antioxidant and anticholinesterase activities. BMC Complement Altern Med., 2019, vol. 19, no. 296, 13 p.

54 Yakovlev G.P. (2010). Pharmacognosy. Medicinal raw materials of plant and animal origin [Farmakognozija: Lekarstvennoe syr'e rastitel'nogo i zhivotnogo proishozhdenija. 2 izd. SPb., SpecLit, 863.]

D.A. Gritsenko[1*] , K.P. Aubakirova[1] ,
I. Voitsekhovskiy[1] , I. Soldatova[3] , N.N. Galiakparov[1]

[1] Institute of Plant Biology and Biotechnology, Almaty, Kazakhstan
[2] Charles University, Prague, Czech Republic
*e-mail: d.kopytina@gmail.com

Simultaneous detection of five apple viruses by RT-PCR

Abstract. Apple market takes third place in the world after bananas and grapes. Apple trees are affected by viruses and virus-like diseases, which cause significant economic losses. The most common viruses in the apple tree are Apple chlorotic leafspot virus (ACLSV), Apple stem pitting virus (ASPV), and Apple stem grooving virus (ASGV). Tomato ringspot virus (ToRSV) and apple mosaic virus (ApMV) also cause significant economic losses. Timely detection of viruses and using virus-free planting materials will reduce crop losses. In this work, we performed genetic analysis of ACLSV, ASGV, ASPV, ApMV, ToRSV, and developed RT-PCR test-system for simultaneous detection of these viruses in apple tree materials. The sequences of the developed primers for the test-system are patented. The planting materials imported from Turkey and Italy were investigated for the presence of apple viruses. The most common virus in the samples is ACLSV (60%) followed by ASPV (34%), ASGV (30%) and ApMV (2%). ToRSV virus was not detected at all. Analysis of samples showed that 60% of planting materials were infected with at least one virus, some samples were infected with 3 viruses simultaneously. Mandatory certification of imported planting materials will reduce crop losses of apple orchards.
Key words: apple viruses, ACLSV, ApMV, ToRSV, ASGV, ASPV, RT-PCR, primers.

Introduction

Apple market takes third place in the world after bananas and grapes. There are over 7,500 apple tree varieties worldwide. The most common apple varieties in the world are the Red Delicious, Gala, Granny Smith, Golden delicious, Lady, Baldwin, McIntosh, Honey crisp, Fuji, and Cortland. World apple production has increased by 37.5% since 2000 and reached 59.1 million tons in 2017. The growth of the production was achieved by increasing yield, while the total planting area decreased by 10% during this time [1]. Apple export from Europe was 36.9% ($2.8 billion) of the global export. The largest exporters of apples in the world are China (US$1.3 billion or 17% of total apple export), United States ($1 billion or 13.3%), Italy ($814.1 million or 10.7%), Chile ($703.5 million or 9.2%), France ($573.4 million, or 7.5%) [2]. In 2019, apple imports to Kazakhstan reached 101 thousand tons, which amounted to 31.5% of the total consumption [3].

Apple trees are affected by at least 12 viruses and virus-like diseases, which cause significant eco-nomic losses [4-6]. Most apple viruses are transmitted through grafting. ToRSV is an exception, and it causes apple union necrosis and decline. Some apple varieties are susceptible to certain viruses. For example, it is known that all varieties of apples are susceptible to ApMV, but Golden Delicious, Jonathan, and Granny Smith are very susceptible [7]. According to various estimates, an infection can lead to loss of up to 40% of the yield, depending on the apple cultivar. ToRSV is distributed by nematodes, *Xiphinema americanum*. In the case of latent infection, viruses spread in apple trees without causing symptoms. Latent infection can lead to delaying bud blooming and decreasing in leaves size. The growth of shoots is also reduced. Further development of the disease can cause severe tree damage or death [8].

The most common viruses in the apple tree are ACLSV, ASPV, and ASGV. These viruses can be present individually or together and can cause disease in other fruit crops. Apple tree infected by these viruses shows decreasing in bud survival ability from 20% to 67%. The degree of tree damage depends on the pathogen and its strain in combination with apple

cultivar, the supply of nutrients, and the age of the tree, rhizome [9-12].

Viral control is mainly based on the prevention of possible infection by planting healthy materials and eradication of infected plants. Therefore, reliable and effective methods for early detection of viruses are important for the successful propagation of healthy plants. Within the framework of the existing programs for the agro-industrial complex development of the Republic of Kazakhstan, it was decided to create an effective system for controlling viral infections.

Apple production traditionally remains one of the main sectors of agribusiness in the South Kazakhstan region. The investigation of local strains of apple tree viruses is important since the South Kazakhstan region is located in the foothills of the Western Tien Shan, which is the natural habitat for wild apple trees *Malus sieversii* and *Malus niedzwetzkyana*. Identification of orchards affected by the virus will also provide objective data on the spreading of viruses in the country. Timely detection of viruses and using virus-free planting materials will reduce crop losses. In this work, we performed genetic analysis of ACLSV, ASGV, ASPV, ApMV, ToRSV, and developed RT-PCR test-system for simultaneous detection of these viruses in apple tree materials.

Materials and methods

Genetic analysis of five apple viruses. Analysis of genomic and gene sequences of apple viruses was performed by using Ugene V.34 programm (Russia). Genomic and gene sequences were downloaded from NCBI, S1. Multiple alignments were performed using the Muscle algorithm [13].

Development of primers for detection of apple viruses. Forward and reverse specific primers for every virus were developed by using NCBI (Primer-BLAST module) and Ugene program. The specific primers did not overlap with other nucleic acid sequences available in the NCBI database, nt-Blast. All primers were analyzed by OligoAnalyzer Tool (Merck KGaA, Germany) for their properties (GC content, Melting temperature (T_m), Secondary structure, Self-dimer & heterodimer tendencies), and compatibility in term of simultaneous detection of five viruses in a single tube.

RNA isolation. 50 samples of apple were analyzed in this work: 10 samples – Jerome (Italy), 10 samples – Pinova (Italy), 10 samples – Jerome (Turkey), 10 samples – Golden Delicious (Turkey), 10 samples – Gala (Turkey). Leaves from symptomatic

trees were collected during the period of mid-April to mid-May 2019. RNA isolation from leaves was performed according to a methodology with modifications. [14]. In details, 100 mg of leaves were homogenized by grinding in a porcelain mortar with the addition of 1 ml of extraction buffer (0.1M Tris-HCl; 25mM EDTA; 2M NaCl; 2% CTAB; 2% PVP). 400 µl of homogenate were incubated at 65 °C for 10 min. After incubation, an equal volume of chloroform was added to the sample with the following centrifugation at 15,500 g for 10 min. The supernatant was transferred to a clean tube. RNA was precipitated by ethanol. The dried precipitate was dissolved in 40 µl of water.

Multiplex RT-PCR analysis. RT-PCR (reverse transcription – PCR) method was used for the simultaneous detection of five viruses. Reverse transcription was performed with a specific reverse primer for each virus (Table 1). Reverse transcription was carried out in 2 steps. Step 1 – incubation with primers: 13 µl of the reaction mixture (1 µl (150 ng) of total RNA, 1 µl (10 mM) of the specific reverse primer for each gene, 11 µl of water) was incubated for 10 min at 65 °C. Further, the reaction mixture was cooled on ice for 5 minutes. Step 2 – reverse transcription: 4 µl of 5 × RT buffer (250 mM Tris-HCl (pH 8.3 at 25 °C), 250 mM KCl, 20 mM $MgCl_2$, 50 mM DTT), 2 µl dNTP (10 mM dNTP mixture) and 1 µL (200U) reverse transcriptase (RevertAid H Minus Reverse Transcriptase) were added to the 13 µl of reaction mixture obtained in Step 1. The final reaction mixture was incubated at 42 °C for 1.5 h. Subsequently, cDNA was used for PCR with specific forward and reverse primers.

To amplify specific genomic regions of five viruses, the reaction mixture contained: 4 µL DNA from reverse transcription (cDNA), five pairs of primers at a concentration of 0.25 mM, PCR buffer, dNTP at a concentration of 0.2 mM, deionized sterile water, 1.25 U of Taq-DNA polymerase. The amplification mixture was 25 µL. PCR program for amplification: Stage 1: 1 cycle – 2 min at 94 °C; Stage 2 (35 cycles): step 1 – 20 sec at 94 °C; step 2 – 20 sec at 60 °C; step 2 min at 72 °C. Stage 3: 1 cycle – 10 min at 72 °C. All reagents used for RT and PCR were purchased from Thermo Fisher Scientific.

Results and discussion

Genetic analysis of ACLSV, ASGV, ASPV, ApMV, and ToRSV was performed to develop a highly sensitive system for detecting these viruses simultaneously in one tube. We investigated genomic regions

of viruses and selected perspective ones for primer design. These regions are highly conservative in every virus genome and do not overlap with other nucleic acid sequences available in the NCBI database.

All isolates containing complete genome of ACLSV were obtained from NCBI database.

The number of isolates was 39. The max hamming dissimilarity in 29-30 % was showed for Ta Tao 5 regarding other isolates. The min hamming dissimilarity in 8%, 5%, 0% was indicated for SY01 and SY02, BR-Gala3 and 38/85-A, QD-13 and Shanxi_14, respectively. The results of the genetic analysis of 39 genomes were used to select conservative regions for the design of forward and reverse primers. Selected regions were located in 3'- region of ORF1 encoding RNA-depended RNA-polymerase, Figure 1.

Specific primers for the capsid protein gene were used to detect ApMV [15]. Complete ApMV capsid protein genes of 29 isolates were obtained from NCBI to design specific primers, Figure 2.

Genetic analysis showed that AM490197.2 isolate of ApMV had an insertion mutation of 58 bp fragment at 3'- terminus before stop codon of capsid protein. This isolate was originated from China, isolation source – Yunnan Dounan.

All complete RNA 2 genomic sequences encoding capsid protein of ToRSV were obtained from NCBI. The number of isolates was 8. Conservative regions of RNA 2 were used to design forward and reverse primers for virus detection, figure 3. 5'- and 3'- termini are highly variable in the ToRSV genomic RNA 2.
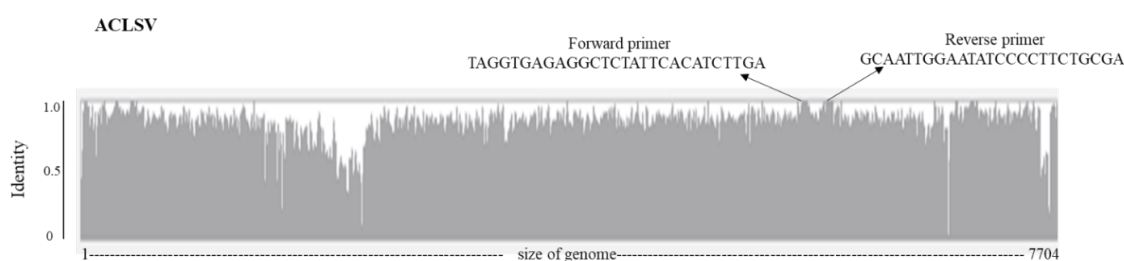
Figure 1 – Identity diagram of 39 ACLSV genomes from
NCBI and primer sequences for virus detection
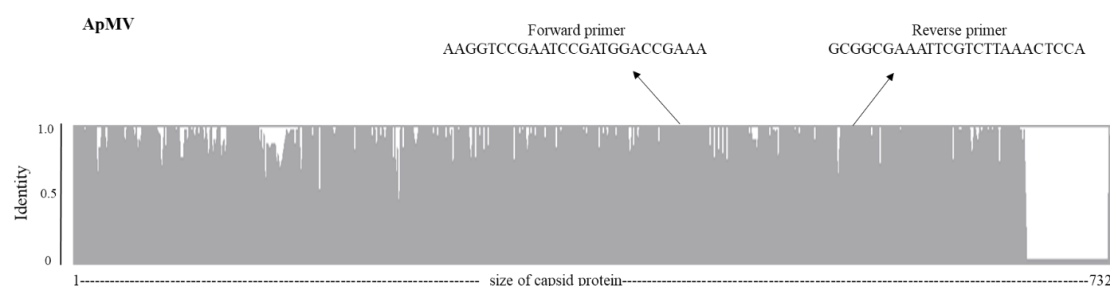
Figure 2 – Identity diagram of 29 ApMV capsid protein genes
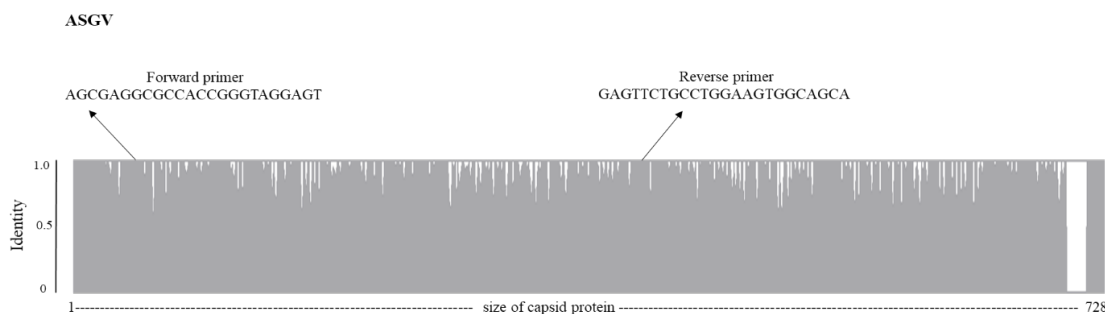from NCBI and primer sequences for virus detection
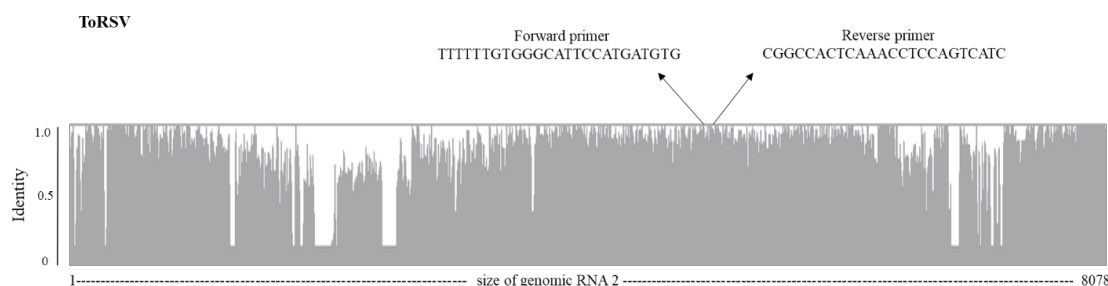
Figure 3 – Identity diagram of 8 ToRSV genomic RNA 2 sequences
from NCBI and primer sequences for virus detection

ToRSV virus had multiple insertions and deletions in genomic RNA2. The largest insertion of 150 bp fragment was observed in GYV-2014 isolate.

Also, the capsid protein genes were used to design specific primers for ASGV. 130 complete capsid protein genes from NCBI were used for genetic analysis followed by primer design,

Figure 4. Conservative and variable regions are shown on Figure 4.

Specific primers for ASPV were designed by genetic analysis of complete genomes of 25 isolates from NCBI. Conservative regions of RNA-depended RNA-polymerase were used for primer design, Figure 5.

Figure 4 – Identity diagram of 130 ASGV capsid protein genes
from NCBI and primer sequences for virus detection
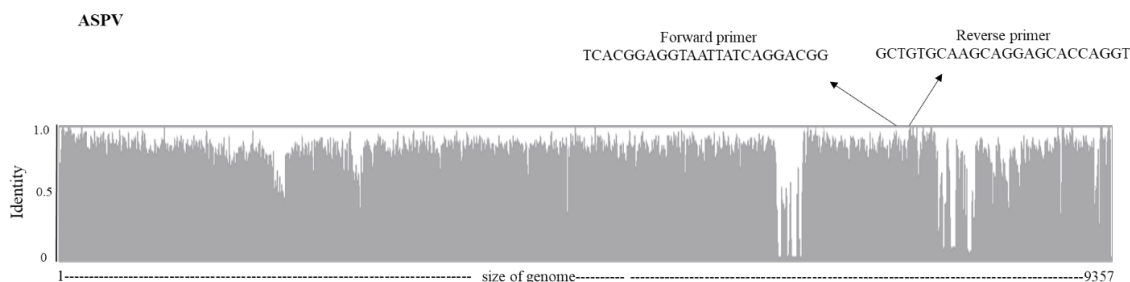
Figure 5 – Identity diagram of 25 ASPV complete genome sequences
from NCBI and primer sequences for virus detection

The results of the genetic analysis revealed that the 3'-terminus of the genome encoding the triple gene protein and the capsid protein has higher variability than the 5'-terminus encoding the RNA-dependent RNA-polymerase.

The developed multiplex detection system, including specific primers for each virus, was tested on positive and negative controls. The sizes of PCR products for each virus were ACLSV – 203 bp, ApMV – 142 bp, ToRSV – 914 bp, ASGV – 378 bp, ASPV – 166 bp.

In the work, the planting materials imported from Turkey and Italy were investigated. These planting materials did not have certificates to confirm the absence of viral infection. 36 of the 50 investigated samples were infected with viruses, Figure 6.
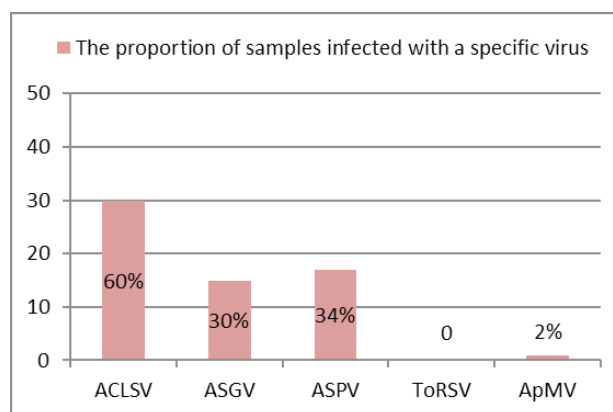
Figure 6 – Presence of five apple viruses
in the planting materials from Turkey and Italy

6 samples were infected simultaneously with 3 viruses (ASGV, ACLSV, ASPV), 6 samples with 2 viruses (ASGV, ACLSV), 1 sample with ASGV and ASPV, 1 sample with ASGV and ApMV. The remaining samples were infected with only one virus. The figure shows that the most common virus in the samples is ACLSV (60%) followed by ASPV (34%), ASGV (30%), and ApMV (2%). ToRSV virus was not detected at all. All 10 Golden Delicious, 5 Jeromin, and 5 Gala planting materials from Turkey were infected with ACLSV.

Conclusion

Virus evolution is based on successful strategies that allow these intracellular parasites to multiply by utilizing the molecular mechanisms of host cells. A lot of methods have been developed to detect plant viruses, such as microscopical observation, serological techniques, molecular methods [16].

Molecular methods are used to detect viruses with high efficiency. These methods are more often used in the laboratory due to their high accuracy and sensitivity compared to serological methods. Molecular methods include PCR, PCR combined with reverse transcription (RT-PCR), multiplex PCR, isothermal amplification, microarray (oligonucleotide array).

Numerous PCR variants (multiplex PCR, nested PCR, real-time PCR) are used for virus detection. RT-PCR is very popular as a relatively cheap and reliable method for detecting plant viruses.

We performed a genetic analysis of five apple viruses and developed highly specific primers for multiplex RT-PCR test-system. Conservative and variable regions of the viral genomes were also identified by genetic analysis. Conservative regions of the viral genomes were selected for the design of species-specific primers. The primers for ACLSV and ASPV detection are specific to RNA-dependent RNA polymerase genes. Primers for ToRSV, ASGV, ASPV detection are specific to conserved regions located in the capsid protein genes. The developed primers had high specificity without formation of non-specific binding. The sequences of the developed primers are patented and can be used to detect viruses in planting materials. Controlling the possible contamination of planting materials with viral infections should be a priority in the framework of import and export programs. In this work, apple planting materials imported from Turkey and Italy were investigated by using the developed test-system. Analysis of samples showed that 60% of planting materials were infected with, at least, one virus, some samples had 3 viruses,

simultaneously. Viral pathogens from infected imported planting materials can be potentially aggressive to local apple varieties. Mandatory certification of imported planting materials will reduce this threat and prevent a decrease in the yield of apple orchards.

Acknowledgments

References

1   Shahbandeh M. (from Aug 29, 2019, accessed at March 15, 2020) Major apple producing countries worldwide 2018/2019. https://www.statista.com/statistics/279555/global-top-apple-producing-countries/.

2   Workman D. (from April 1, 2020, accessed at March 15, 2020) Apples Exports by Country. http://www.worldstopexports.com/apples-exports-by-country/.

3   Forbes.kz (from December 27, 2019, accessed at March 17, 2020) The Minister of Agriculture of the Republic of Kazakhstan reported about new approaches to supporting the agricultural sector [O novyh podhodah po podderzhke APK rasskazal ministr sel'skogo hozyajstva RK]. forbes.kz/news/2019/12/27/newsid_215734.

4   Kim, N. Y., Oh, J., Lee, S. H., Kim, H., et al. (2018). Rapid and Specific Detection of Apple stem grooving virus by Reverse Transcription-recombinase Polymerase Amplification. Plant Pathol J., vol. 34, no. 6, pp. 575–579. https://doi.org/10.5423/PPJ.NT.06.2018.0108

5   Maliogka V.I., Minafra A., Saldarelli P., Ruiz-García A.B., et al. (2018) Recent Advances on Detection and Characterization of Fruit Tree Viruses Using High-Throughput Sequencing Technologies. Viruses, 1 vol. 10, no. 8, pp. 1-23. https://doi.org/10.3390/v10080436.

6   Umer M., Liu J., You H., Xu C., et al. (2019) Genomic, Morphological and Biological Traits of the Viruses Infecting Major Fruit Trees. Viruses, vol. 11, no. 6, pp. 1-12. https://doi.org/10.3390/v11060515.

7   Hadidi A., Barba M., Candresse T., Jelkmann, W. (2011) Virus and Virus-like Diseases of Pome and Stone Fruits. USA: The American Phytopathological Societ, pp.17-48. ISBN:978-0-89054-501-0.

8   Bitterlin M.W., Gonsales D. (1987) Spartial distribution of Xiphinema riversi and persis-

tence of tomato ringspot virus and its vector in soil. Plant Disease, vol. 71, pp. 408-411. https://doi.org/10.1094/PD-71-0408.

9   Beaver-Kanuya E., Szostek S.A., Harper S.J. (2019) Development of real-time RT-PCR assays for two viruses infecting pome fruit. J Virol Methods., vol. 266, pp. 25-29. https://doi.org/10.1016/j.jviromet.2018.12.008.

10   Hao L., Xie J., Chen S., Wang S., et al. (2016) A multiple RT-PCR assay for simultaneous detection and differentiation of latent viruses and apscarviroids in apple trees. J Virol Methods., vol. 234, pp. 16-21. https://doi.org/10.1016/j.jviromet.2016.04.003.

11   Ji Z., Zhao X., Duan H., Hu T., et al. (2013) Multiplex RT-PCR detection and distribution of four apple viruses in China. Acta Virol., vol. 57, no. 4, pp. 435-41. https://doi.org/10.4149/av_2013_04_435.

12   Peng D., Xie J., Qiang W., Ling K.S. (2017) One-step reverse transcription loop-mediated isothermal amplification assay for detection of Apple chlorotic leaf spot virus. J Virol Methods, vol. 248, pp.154-158. https://doi.org/10.1016/j.jviromet.2017.07.002.

13   Edgar R.C. (2004) MUSCLE: multiple sequence alignment with high accuracy and high throughput. Nucleic Acids Res., vol. 32, no. 5, pp. 1792-1797. https://doi.org/10.1093/nar/gkh340.

14   Gambino G., Perrone I., Gribaudo I. (2008) A Rapid and effective method for RNA extraction from different tissues of grapevine and other woody plants. Phytochem Anal., vol. 19, no. 6, pp. 520-525. https://doi.org/10.1002/pca.1078.

15   Koonin E. V., Dolja V. V. (1993) Evolution and taxonomy of positive-strand RNA viruses: Implications of comparative analysis of amino acid sequences. Crit. Rev. Biochem. Mol. Biol., vol. 28, pp. 375-430. https://doi.org/10.3109/10409239309078440.

16   Pallás V., Sánchez-Navarro J., James D. (2018) Recent Advances on the Multiplex Molecular Detection of Plant Viruses and Viroids. Front Microbiol., vol. 9, p. 1-11. https://doi.org/10.3389/fmicb.2018.02087.

M. Derakhshan[1] iD , A.H. Elhamirad[1] iD , M. Javanmard[2*] iD ,
P. Sharayei[3] iD , M.Armin[1] iD

[1]Department of Food Science & Technology, Sabzevar Branch, Islamic Azad University, Sabzevar, Iran
[2] Food technologies group, Chemical Engineering Institute,
Iranian Research Organization for Science & Technology (IROST), Tehran, Iran
[3]Agricultural Engineering Research Department, Khorasan Razavi Agricultural and
Natural Resources Research and Education Center, AREEO, Mashhad, Iran
*e-mail: javanmard@irost.ir

Optimization of conditions of ultrasound-assisted extraction of effective compounds from apple pomace (*malus domestica*)

Abstract. Every year millions of tons of fruit peels, such as that from apples, oranges and pomegranates are disposed of as juice factory wastes in our country as well as globally. Unfortunately, Iran with a 15.2-30% green waste production, currently holds the first place in the world fruit waste production. The current study was carried out with the goal of optimizing the ultrasound-assisted extraction of antioxidant compounds from apple pomace. In this study the optimal conditions of ultrasound-assisted extraction (US) of effective compounds from the ethanolic extract of apple pomace by use of the response surface method (Box-Behnken design) with three variables consisting of ultrasound amplitude (20, 60 and 100 %), ultrasound exposure time (15, 35 and 55 min) and ultrasound temperature (35, 50 and 65 °C). According to Derringer's desired function approach, the optimal conditions based on both individual and combinations of all process variables were ultrasound amplitude 82.36%, ultrasound exposure time 35.24 min and ultrasound temperature 51.48 °C. At this optimum condition, the predicted maximum values of the total phenolic compound (TPC) 1,1-diphenyl-picrylhydrazyl free radical scavenging (DPPH) and extraction yield (EY) were 74.53% of gallic/ 100 g, 83.85% and 17.74%, respectively. The experimental values were in a good agreement with the predicted values. Also, the TPC, DPPH and EY maceration method were 11.10 mg of gallic acid/100 g, the free-radical scavenging as 2.79% and the extraction efficiency as 4.46%. The results demonstrated that US could be a very effective method for continuous extraction of natural compounds.
Key words: apple pomace extract, Box-Behnken design, total phenolic compounds, ultrasound.

Introduction

Every year millions of tons of fruit peels such as that from apples, oranges, and pomegranates are disposed of as juice factory wastes in our country all the while in the world as we know it today special attention is given to optimum use of plant wastes and extraction of bioactive compounds, namely, antioxidants and antimicrobials. Unfortunately, Iran with a 15.2-30% green waste production, currently holds the first place in the world fruit waste production. On the one hand, wastes lead to loss of national resources, on the other hand, the disposal of which causes some difficulties. For example, wastes rich in phenolic compounds which are usually buried in the ground, in addition to being expensive, cause environmental problems [1].

One of the valuable sources for the production of natural additives is apple pomace. Apple pomace is the main product of the juice and apple center industries which consists of 25% of the original fruit volume with a humidity content (wb) of 85% [2].

Pomace is rich in raw fiber, protein, vitamin, and minerals. Its main compounds are simple sugars such as glucose, fructose, and arabinose while its insignificant compounds include sucrose, galactose, and xylose. Hence, several microorganisms are able to make use of apple residue as a substrate for growth [3].

Phenolic and flavonoid compounds are often gathered in apple fruit peel, and the major of which

are phenolic acids, flavonols, quercetin, glycoside, di-hydrochalcones and anthocyanin [4].

The extraction method of the plant extract is one of the main factors which can affect the properties of effective constituents of extracts [5]. Thermal extraction causes antioxidant degradation and reduces the antioxidative activity of the produced extract. There are different extraction methods from plants and fruits [6-8]. Although, use of novel and practical methods such as the ultrasound process for extraction of higher quality, more stable, soluble in water and remaining safe solvents extracts along with reduced related expenses (high efficiency and low energy and water consumption), seems essential [9, 10].

Ultrasound-assisted extraction (UAE) is an emerging potential technology that can accelerate heat and mass transfer and has been successively used in extraction field. UAE is a clean method that avoids the use of large quantity of solvent along with cutting down in the working time. Ultrasounds are successively employed in plant extraction field [11, 12].

Hammi et al. (2015) has found that the optimum operating conditions for extraction of antioxidant from *Zyzyphus lotus* fruit by ultrasound was ethanol concentration of 50 %, extraction time of 25 min, extraction temperature of 63°C. The obtained extract exhibited a high content of phenolic compounds (40.782 mg gallic acid equivalents/g dry matter) with significant antioxidant properties (the total antioxidant activity was 75.981 mg gallic acid equivalents/g dry matter and the 2,2-diphenyl-1-picrylhydrazyl (DPPH) radical scavenging activity was 0.289 mg/mL) [13]. Similarly, Luengo et al. (2014) reported that the use of ultrasound has been proved as a promising technology to extract carotenoids from tomato by-product (skin, seeds, and part of the pulp). Ultrasound significantly increased the extraction yield (143 %) without any degradation of carotenoids in comparison with conventional extraction [14].

The study by Sharayei et al. (2017) was performed with the purpose of optimum use of pomegranate peel as the residue of agriculture and pomegranate juice factories, and extraction of bioactive compounds (antioxidative and antimicrobial), employing the ultrasound-assisted method. Results showed that all aqueous extracts of pomegranate and peel, possessed the antioxidative activity and antioxidative strength of aqueous extract of pomegranate peel with a 6% concentration and was roughly the same as that of synthetic butylated hydroxytoluene antioxidants [15]. Kalamara et al. (2014) extracted pomegranate seed oil utilizing ultrasound and then dried it via spray drying. The results of this study demonstrated that the ultra-sound method increases production efficiency and reduces extraction time by 12 times [16]. Rosangela et al. (2007) examined the chemical composition of yerba mate tea (*Ilex paraguariensis* leaves) using the ultrasound-assisted method. The use of ultrasound waves led to improved caffeine and palmitic acid amounts efficiencies in methanol solvent [17].

Again, in this study, optimization ultrasound-assisted extraction of TPC from apple pomace, and later comparison between the two methods, i.e., maceration and ultrasound are dealt with. The following study was performed due to the importance of optimum use of residue of agricultural products and food industry factories (apple juice factories) and the extraction of bioactive compounds from them.

Materials and methods

Plant materials

Apple wastes were purchased from Iran Citrus Co., located in Tonekabon, Mazandaran Province in August 2016. The apple wastes, after collection at room temperature and away from sunlight, were then completely dried and then ground by using an electric grinder and passed through a mesh strainer No. 20 and kept at a dark, cold and dry place.

Chemical and reagents

All chemicals and reagents used in this study, were analytical grade consisting of Folin-Ciocalteu (FC), gallic acid, DPPH were provided from Sigma-Aldrich (St. Louis, MO), and chemical and organic solvents were purchased from Merck (Darmstadt, Germany).

Extraction procedures

In order to produce extracts from apple wastes, the maceration and ultrasound-assisted methods were used. The solvent used in both methods was 70% ethanol.

Maceration extraction method

For this purpose, 100 g of powdered apple pomace was carefully weighed and poured into a 1000 ml in a beaker containing 70% ethanol solvent and performed on a shaker (Unimax 1010, Heidolph, Germany) for 24 hours at room temperature. The solution was then filtered under vacuum and concentrated up to the point of full dewatering using a rotary dryer (Laborota 4000 efficient model, made in Germany) at 45 ^{0}C in an oven until reaching constant weight under vacuum [18].

Ultrasound-assisted extraction method

For the purpose of extraction of bioactive compounds from apple pomace, a 100 g of powdered

apple pomace was carefully weighed and poured into a 1000 ml beaker containing 70% ethanol solvent and moved to the special ultrasound chamber. For ultrasound, the ultrasonic device model UP400S, made by Heilscher in Germany with 400 W of power and H7 type probe made from titanium and a diameter of 7 mm and a length of 100 mm, was used. For extraction, the effects of ultrasound exposure time (15, 35 and 55 min), ultrasound amplitude (20, 60 and 100%) and ultrasound temperature (35, 50 and 65 ^{0}C) with the sound frequency of 24 kHz based on the variables surfaces predicted in the Box-Behnken design, according to Table 2.

In order to investigate the effect of the Time period of the process, temperature and amplitude on the optimization of extraction conditions of phenolic, tests were performed based on an RSM design in 3 factors and 3 design surfaces and a Box-Behnken design. The software in use was Design Expert and graphs were drawn by Microsoft Excel. The coded and actual levels of each of the variables are given in Table 1.

Table 1 – Valuable codes, independence variables and actual value used in ultrasound method

Independence variables	Valuable codes	Actual value
Time (min)	-1, 0, +1	15, 35, 55
Temperature (^{0}C)	-1, 0, +1	35, 50, 65
Amplitude (%)	-1, 0, +1	20, 60, 100

Table 2 – Random treatments of the Box-Behnken design experiment

Treatment	Time (min) (A)	Temperature (^{0}C) (B)	Amplitude (%) (C)
1	35	50	60
2	35	50	60
3	35	50	60
4	35	65	20
5	55	50	100
6	15	50	20
7	15	35	60
8	55	65	60
9	15	50	100
10	55	50	20
11	35	65	100
12	35	35	100
13	35	35	20
14	15	65	60
15	35	50	60

Measurement of TPC

The TPC amount in the extract produced from the two extraction methods, maceration and ultrasound, was determined using Folin-Ciocalteu methods [19].

For 500 μl test sample (100 mg extract in 10 mL of Methanol), 6 ml of distilled water twice and 500 μl of the reagent Folin– Ciocalteau were added, after waiting for 8.8 minutes at room temperature, 1.5 ml of sodium carbonate (20% w/v) was added to the solution. The solution was mixed and allowed to remain for 30 min, and the spectrophotometric analysis was performed at 765 nm. The standard curve was obtained by plotting gallic acid adsorption data at 765 nm at a concentration of 0.04-0.4 mg/ml. The results were reported in terms of mg of gallic acid per 100 g.

Determination of antioxidant capacity

Determination of the free radical-scavenging activity was performed through the use of the DPPH test and 2, 2-diphenyl picrylhydrazyl reagent [20].

The radical-scavenging activity was calculated as a percentage of DPPH discoloration using the Eq. (1):

$$DPPH\% = [(A_{DPPH} - A_S)/A_{DPPH}] \times 100 \qquad (1)$$

where A_S is the absorbance of the solution when the sample is added at a particular level and A_{DPPH} is the absorbance of the DPPH solution.

Extraction Yield

The extraction yield is given by the following formula (Eq. 2).

$$EY = \frac{dried\ extraction\ weight}{inital\ sample\ weight} * 100 \qquad (2)$$

Results and discussion

Model fitting

After data analysis with the goal of determining the best-suggested model from the 5 existing Mean, cubic, 2FI, Linear, variance analysis, the model, for which the sum of squares had significant differences, and the Lack of fit was insignificant, was selected as the best model. Given this subject and after examining the results obtained and a comparison between the existing regression models, the results indicated that the Quadratic model for total phenolic compound, DPPH Free radical-scavenging capacity and measured extraction efficiency tests in this study, had a significant difference compared to the other models.

There models for which the Lack of fit was undefined (Table 3). Consequently, the Quadratic model was selected for examining the trend of variations of the parameters measured in this study. After selecting the best model in the desired statistical surface (1% or 5%), in order to examine the effective parameters in the study, with regard to the variance table, the parameter for which the F test insignificant ($P>0.05$), is eliminated and the rest of parameters which had significant differences were kept.

It is worth mentioning that in the case that the linear parameter of a variable in a model, does not have a significant effect, yet its mutual effect with one of the other variables, which has a significant effect in the model, does have a significant effect, then that parameter is kept in the model and afterward the general equation is derived for any parameter, by the given coefficients. Ultimately, from amongst the different parameters, the parameter which has the highest sum of squares is selected as the most effective parameter.

Table 3 – Regression coefficients of predicted polynomial models for the investigated responses from apple pomace extract

Source	df	EY (%)		TPC (mg GA/100 g)		DPPH (%)	
		Coefficient	Sum of Squares	Coefficient	Sum of Squares	Coefficient	Sum of Squares
Model	9	3.56	48.97	-183.29	9911.71	36.93	1732.43
Linear							
Time (A)	1	0.09	7.26	0.025	3257.05	-0.097	0.0015
Temperature (B)	1	0.01	0.80	7.87	904.83	0.366	208.28
Amplitude (C)	1	0.19	12.70	3.28	1371.83	0.774	633.86
Quadratic							
A*A	1	-0.0029	5.14	-0.0084	41.87	-0.019	228.91
B*B	1	-0.0004	0.044	-0.064	780.33	-0.0087	14.42
C*C	1	-0.0013	18.12	-0.016	2639.61	-0.0021	44.04
Interaction							
A*B	1	0.002	2.82	-0.018	121.88	0.029	320.77
A*C	1	0.00036	0.34	0.0079	160.53	-0.0002	0.198
B*C	1	-0.0014	3.06	-0.024	876.75	-0.014	305.20
Residuals	5		4.84		195.15		82.71
Lack of Fit	3		0.95		128.66		14.76
Pure Error	2		3.88		66.49		67.95
Total	14		53.80		12077.7		1815.14
Std. Dev		0.98		15.04		4.07	
Mean		8.93		63.37		45.36	
CV (%)		11.02		23.73		8.97	
R^2		0.91		0.89		0.95	
Adj R^2		0.74		0.71		0.87	

Std. Dev: Standard Deviation

Table 4 – Box-Behnken design of three variables with their observed responses of ultrasound-assisted extract

Time (min)	Temperature (⁰C)	Amplitude (%)	EY (%)		TPC (ml GA/100 g)		DPPH (%)	
			Real Values	Predicted Values	Real Values	Predicted Values	Real Values	Predicted Values
35	50	60	19.80	20.40	15.31	22.52	84.61	77.52
35	50	60	9.00	7.50	50.66	52.73	72.51	69.94
35	50	60	13.80	13.20	23.63	16.42	43.25	49.86
35	65	20	18.80	17.13	73.13	72.86	78.72	81.82
55	50	100	20.60	18.50	51.34	46.21	66.49	62.11
15	50	20	8.00	8.00	8.90	8.90	77.41	69.94
35	50	60	10.20	12.30	49.46	54.59	21.47	26.82
15	35	60	18.41	17.13	68.24	72.86	77.93	81.82
55	65	60	16.26	17.13	80.34	72.86	85.52	81.82
15	50	100	11.00	10.40	85.24	78.03	72.12	76.80
55	50	20	20.00	17.90	10.43	5.30	58.12	49.86
35	65	100	7.60	9.70	34.17	39.31	70.73	77.52
35	35	100	17.00	17.60	22.34	29.55	60.47	56.76
35	35	20	15.03	17.13	69.75	72.86	83.17	81.82
15	65	60	20.40	21.90	12.42	10.34	69.47	77.57

Investigating the effect of independent variables on qualitative and quantitative properties of Apple pomace

Effects of process variables on TPC extraction

The results from the variance analysis (Table 3) illustrates that the linear models of time (A) and ultrasound amplitude (C) and the square of temperature (B^2) have a significant effect on the TPC amount.

With regard to Equation 3 and Table 3, the parameter B^2 (the mutual effect of temperature), was selected as the most effective factor in the extraction of TPC.

$$TPC = -361/31926 -0/88101A +17/37277B + \\ +1/06101C -0/031319A2 -0/19439B2 - \\ -5/15113E\text{-}003C2 +0/049792AB - \\ -2/11781E\text{-}003AC -2/36167E\text{-}003BC \quad (3)$$

In the RSM methodology, there is a step called verification. In this step, the value for TPC extraction in the extermination step should be statistically compared to the value predicted by the model. In this examination, after having carried out this step, the observed values were compared to the predicted values and the calculations may be seen in Table 4. The results are demonstrative of the good correlation between results obtained from the experimental method and the values predicted with the statistical method.

Regarding the mutual effect of temperature and ultrasound amplitude, the response surface plot (Figure 1, A), with temperature rising up to 48 ⁰C, the TPC percentage increased, both in low and high ultrasound intensities and a trend of decrease was observed in the TPC, which was stronger at high ultrasound intensities. Additionally, at both low and high temperatures, with an increase in ultrasound amplitude up to 60%, the TPC level expanded and up to 80% this growing trend was observed gradually, and its amount had dropped thereafter. Such findings are in line with by the Pinelo *et al.* (2005) they declared that at high temperatures, drops in the phenolic compounds extraction amount has been witnessed [21]. This scholar has stated the reason behind this to be the polymerization reactions of phenolic compounds. Furthermore, in the study performed, the explanation for the TPC extraction amount decrease, according to the response surface diagram, may be solvent satura-

tion at lower temperatures and dissolution of TPC at high temperatures. In the research carried out on the extraction of polyphenolic compounds from some kind of raspberry, the highest polyphenolic compounds extraction efficiency was reported at 60 ^{0}C.

Investigation of the phenol variations against temperature and time showed that at both the start and finish of the experiment, with a rise in temperature up to 47.21^{0}C, the TPC increased and then a trend of decrease was observed in the TPC extraction amount. Considering Figure 1, B, it can be said that temperature and time are significantly effective on the amount of TPC extraction such that with an increase in temperature and time, a trend of increase has been witnessed in the TPC extraction amount. Rises in temperature lead to a growth in the solvent penetration rate and also increases the mass transfer period. Taking into account, the fact that the sample/solvent ratio was assumed to be constant in this study, the explanation for the TPC extraction amount decrease, according to the response surface diagram, may be solvent saturation at lower temperatures and dissolution of TPC at high temperatures.

The contents of TPC extracted from wheat bran at different times of sonication increase of the total phenolics content was observed up to 30 min, remaining constant until 50 min. A significant increase of the total phenolic content was observed over the extraction temperature range (25–75 ^{0}C), and the total phenolic content reached a maximum of around 2.80 mg GAE/g of wheat bran at 65 ^{0}C. At a higher temperature, the solubility of phenolic compounds in wheat bran could be enhanced, and the viscosity of wheat bran extracts was decreased, accelerating the whole extraction [19].

Spigno *et al.* (2007) investigated the relationship of extraction temperature and extraction time with TPC was demonstrate both of the factors displayed significant linear and quadratic effect (at least at *p*<0.05) on TPC. With regard to extraction temperature, TPC of limau purut peels extracts increased readily with increasing temperature up to 47.5^{o}C and followed by a slight decrease afterwards (22). This suggested that incubation in warm water did improve phenolics extraction, yet was gentle enough to avoid heat degradation of the target phenolic antioxidants. Mild heating might soften the plant tissue, weaken the cell wall integrity, hydrolyze the bonds of bound phenolic compounds (phenol-protein or phenol-polysaccharide) as well as enhance phenolics solubility, thus more phenolics would distribute to the solvent [23, 24]. At optimum extraction temperature (about 47.5^{o}C), higher amounts of phenolic contents were

obtained with short extraction time. In other words, long extraction time may compensate the beneficial effects of moderate temperature by inducing oxidation or degradation of phenolic compounds, yielding low TPC [23, 25].

In the research carried out by Ya-Qin *et al.* (2009) for all detected phenolic acids under study, their yields depended dramatically on extraction time and temperature. At relatively lower temperature (15 and 30 ^{0}C), the yields of phenolic acids increased with increased extraction time. For example, after UAE at 15 ^{0}C for 40 min, the yields of caffeic, p-coumaric, ferulic, p-hydroxy-benzoic acid increased from 15.4 to 103.7, 36.4 to 171.3, 452.3 to 1672.3, 18.3 to 42.0 µg/g of DW, respectively (26). In agreement with these results, Sueli and Pinto (2007) reported that extraction time significantly affected the yields of phenolic compounds from coconut shell powder. Likewise, the yield of phenolic compounds increased also with extraction temperature increased. For example, after UAE from 15 to 30 ^{0}C for 20 min, the yield of caffeic acid increased from 36.9 to 86.7 lg/g DW, 80.0 to 165.3 lg/g DW in p-coumaric acid, 951.8 to 2283.3 lg/g DW in ferulic acid, 27.0 to 43.4 lg/g DW in p-hydroxy-benzoic acid, respectively [27].

Results acquired from the Ahmadian and Niazmand study (2016) illustrate the specific effect of the mean temperature (43$^{°}$C) on the extraction of polyphenolic compounds from the saffron petal [28]. The effect of temperature on increasing extraction efficiency is most probably due to the improvement of mass transfer at a higher temperature and therefore increasing the solubility of phenolic compounds, increasing the penetration rate and decreasing the coefficient of viscosity, of the solvent. In addition, the rise in extraction temperature, bringing about the dissociation of the bonds of the phenolic compounds with the rest of the compounds and affecting the membrane structure of plant cells can be responsible for extraction procedure facilitation.

In agreement with this research, also researchers showed that the extraction yield increased with increasing temperature. When extraction temperature increased from 30 to 50 °C, the extraction yield increased from 17.6±0.4 to 30±0.8%. Similarly, the total phenolic content also increased from 21±0.6 to 23± 0.3 mg/g DW. A rise in extraction temperature can break the phenolic matrix bonds and influence the membrane structure of plant cells making them less selective by coagulation of lipoproteins [29]. The dielectric constant of water decreases and solvent property and capacity change at higher temperature, resulting in a better extraction of phenolic [5].

However, further increase in extraction temperature could degrade phenolic compounds [30, 31].

On the mutual effect of time and ultrasound amplitude in the response surface diagram (Figure 1, C), by raising the ultrasound amplitude up to 60%, the amount of TPC increases and then until 87.93% of amplitude a marginally rising trend was observed and extraction declined thereafter. Yet, by increasing time at low ultrasound intensities, the extraction amount, until 25 minutes, had a slowly increasing trend and then a sensible declining trend in the amount of TPC extraction was observed. In addition, at higher sound intensities, at times higher than 35 minutes, the declining trend occurred more steeply. The principal mechanism of ultrasound-assisted extraction is due to the cavitation phenomenon which leads to the generation of micro bubbles and subsequently an implosion within the liquid mass. The implosion of these bubbles is often accompanied by release vast amounts of energy which is exerted on the nearby environment in the form of shear stress [32]. The decline in the effective constituent extraction amount, caused by increasing the ultrasound amplitude from 80% to 100%, is probably a result of the destruction of some active natural compounds because of the high amplitude of the waves [33]. Moreover, it has been reported that application of ultrasonic waves with high intensities and time periods, having brought about the enhanced cell wall disruption, leads to the extraction of insoluble compounds within the solvent, which results in the lower solvent penetration of cells [34, 35].
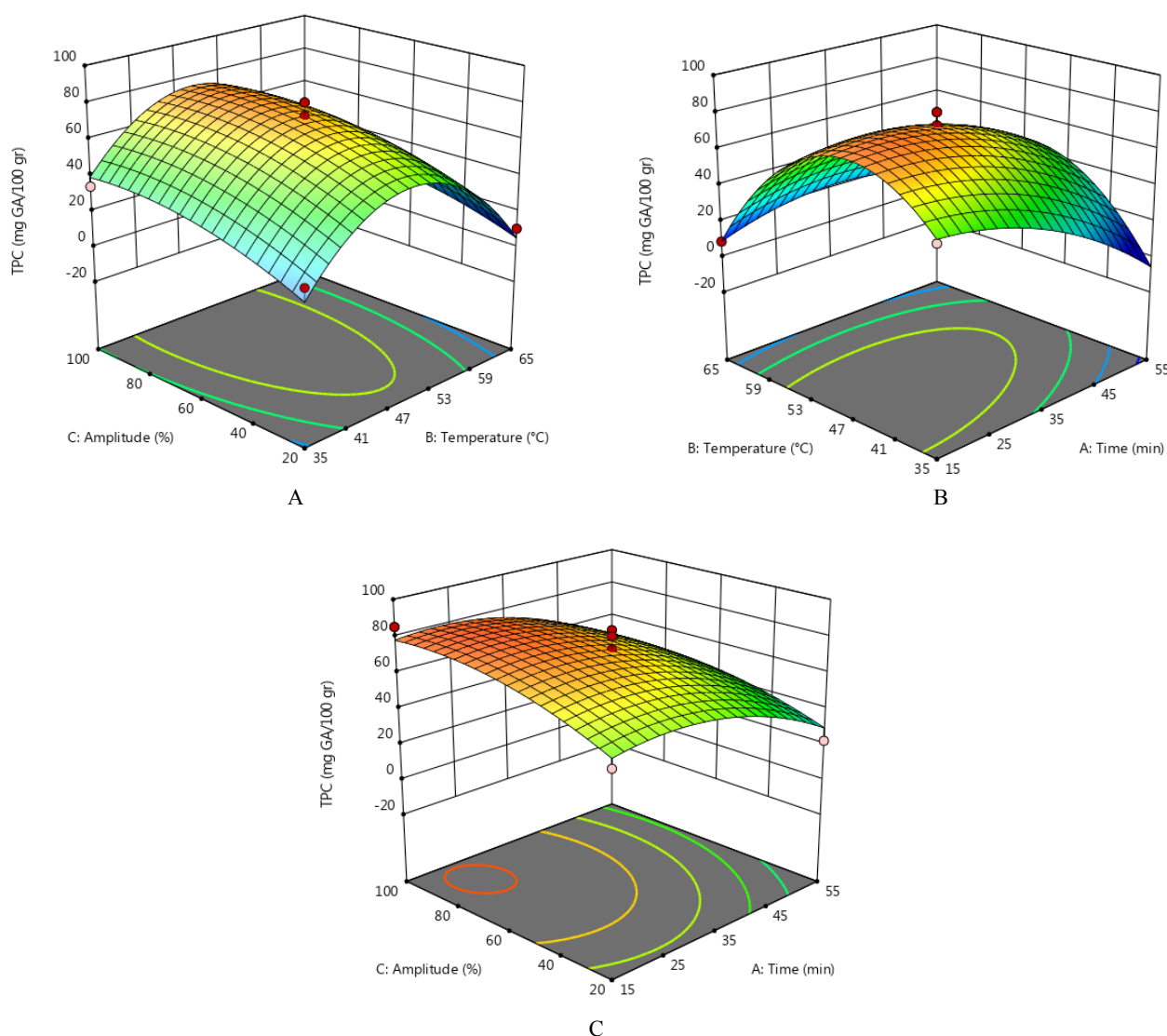
Figure 1 – Response surface plots of the total phenolic contents (TPC) of apple pomace extract as affected by A: ultrasound amplitude and ultrasound exposure time, B: temperature and time C: ultrasound amplitude and time

Effects of process variables on antioxidant activity

The results of the variance analysis (Table 3) showed that the linear amplitude model, the square of the amplitude (C^2) and the mutual effect of time and amplitude have a significant effect on the free-radical scavenging capacity.

With regard to Equation 4 and Table 3, the amplitude and the temperature parameters were reported as to possessing the most and least effective parameter upon the scavenging of free radicals, respectively.

$$DPPH= -40.38433 +2.43910A +2.19379C - -0.020167A^2 -0.011332C^2 -0.013948AC \quad (4)$$

On the mutual effects of time and amplitude in the response surface diagram (Figure 2), by increasing the amplitude to 60%, the free-radical scavenging amount is increased and thereafter until 76.94% of amplitude, a marginally increasing trend was observed and the scavenging capacity was reduced. At low sound intensities, through increasing time, at first, the scavenging amount grew until 35.91 minutes and then was diminished. More on the matter, a trend of decrease was observed at higher sound intensities.

The cause behind the aforementioned findings may either be oxidization of phenolic compounds due to prolonged extraction time or increase in impurities as a result of ultra-sonication time [36]. Heidari *et al.* (2011) investigated the antioxidantal properties of *Flomidoschema parviflora* [37]. These researchers reported that by means of increasing the time and temperature, the free-radical scavenging has risen which is because of the growth of TPC extraction with the increase in time and their inhibition effect on the free radicals. Yet, with increasing time (times greater than 46 minutes) this trend has become very gradual and the free-radical scavenging amount declines, with which study, the results from the relation by increasing time to 36 minutes, agree.

In the research on grape peels conducted by Ghafoor (2009) in order to optimize the conditions of ultrasound-assisted extraction, by means of the two extraction temperature and ultrasound amplitude parameters, it was determined that with rises in the extraction temperature and ultrasound amplitude the free-radical scavenging capacity increases [38].

Researchers demonstrated that when the results for fruits were omitted from the regression analysis, the relationship between the phenolic contents and antioxidant activities was significant ($p < 0.05$). This indicates that factors other than total phenolic can play a major role in the antioxidant activity of plant materials such as sea buckthorn [39].

In the research carried out by Ahmadian and Niazmand (2016) the results showed that with an increase in the amplitude, the free-radical scavenging amount has grown, in such a way that at 100% of amplitude, the highest inhibition percentage was observed. In fact, this is a result of the higher poly phenolic compounds extraction at this amplitude and therefore increasing cell wall destruction and expanded exit and access of such materials. Additionally, by raising the extraction time up to the maximum (15 minutes), a significant increase of inhibition percentage was witnessed. According to the results obtained, an increase in poly phenolic compounds extraction was also observed by increasing time. Therefore, one may relate the growth in inhibition percentage to the enhanced extraction of such compounds by increasing time and in the current study, by means of increasing the amplitude up to 76%, the highest free-radical scavenging capacity was observed as well [28].
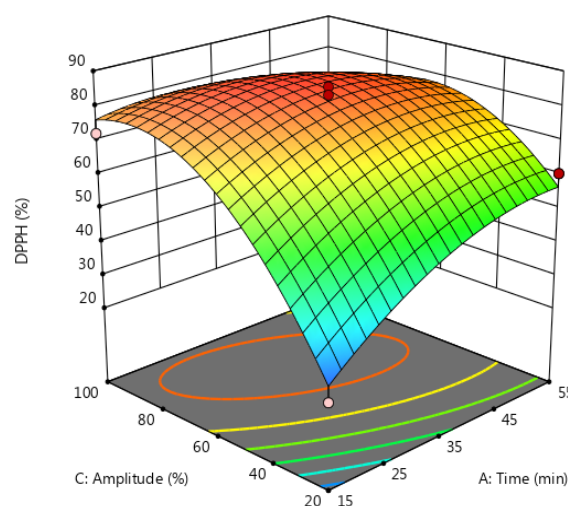
Figure 2 – Response surface plots of the DPPH of pomace extract as affected by ultrasound amplitude and ultrasound exposure time

Effects of process variables on Extraction yield

The variance analysis table (Table 3) shows that the linear models of time (A) and temperature (B)

have a significant effect on the amount of extraction efficiency.

With regard to the data from the sum of squares column, the effect of temperature was introduced as the most significant.

$$\text{yield} = -9.14488 + 0.094688A + 0.89222B - 0.22844C - 8.28125E\text{-}003A^2 - 0.012056B^2 + 5.54688E\text{-}004C^2 + 0.012000AB + 8.75000E\text{-}004AC + 2.50000E\text{-}003BC \quad (5)$$

On the mutual effect of time and temperature, taking the response surface diagram (Figure 2, A) into account, at low times, with an increase in temperature up to 60 ^{0}C, the extraction efficiency is increased and then was diminished. Yet at high times, with a rise in temperature up to 65 ^{0}C, the extraction efficiency ratio grew and also at low temperatures, with a time increase up to 51.97 minutes, the extraction efficiency ratio was enhanced and then it was lowered, and at high temperatures up to 55 minutes of time, it was added on the extraction amount, as well. Temperature is one of the key factors in the extraction efficiency amount, in a way that the rise in temperature causes an increase in the solvent penetration rate. The drop in the effective constituents' extraction amount with rises in temperature from 60 to 65 ^{0}C and time from 51 to 55 minutes is probably due to the destruction of some active natural compounds.

On the mutual effects of time and amplitude in the response surface (Figure 2, B), at low sound intensities, with an increase in time up to 44 minutes, the extraction efficiency ratio is enhanced and then declines with a steep slope. Moreover, also at high sound intensities, the extraction efficiency amount rises with a sharp incline and reduced with a very gradual incline and in which case of the extraction time is constant, with a rise in the amplitude amount, the extraction efficiency amount increases. The extraction amount growth by an increase in amplitude is probably because of the cavitation phenomenon resultant of the ultrasound; the cavitation phenomenon leads to increased plant tissue [40]. The decline in the effective constituent's extraction amount, caused by increasing the ultrasound amplitude from 80% to 100%, is probably a result of the destruction of some active natural compounds because of the high amplitude of the waves [33].

Considering the response surface diagram (Figure 2, C), at low sound intensities, with a rise in temperature up to 57.51 ^{0}C, the extraction efficiency

amount increases and was reduced thereafter with a smooth slope and also at high sound intensities up to 65 ^{0}C, it grew. In addition, with increases in temperature at low sound intensities, the extraction efficiency grew but with more rapid incline at high sound intensities.

A study on the carambola or star fruit, and lemon peels in order to find the optimal extraction conditions approves of our result [25].

***Optimization comparison ultrasound-assisted extraction with conventional extraction***

The measurement of TPC, free-radical scavenging, and extraction efficiency amount through maceration and ultrasound methods demonstrated the method of extraction has a profound effect on the total amount of TPC in terms of gallic acid. As apparent, the ultrasound method has extracted more TPC compared to the maceration method (for the ultrasound method, the TPC amount in terms of mg of gallic acid/ 100 g was obtained as 74.52 mg, the free-radical scavenging amount as 73.85% and the extraction efficiency as 17.75% and for the maceration method the TPC amount was obtained as 11.10 mg of gallic acid/ 100 g, the free-radical scavenging as 2.79% and the extraction efficiency as 4.46%). It can be said the shear stress exerted by ultrasonic waves lead to the breakdown of large polymer molecules which in turn results in the better extraction of TPC compared to the maceration method. These results are in accordance with the report by Albu *et al.* (2004) and they reported utilization of the ultrasound method has brought about the added extraction of carnosic acid from rosemary [41].

Hemwimol *et al.* (2006) investigated the use of ultrasound-assisted extraction for improvement of anthraquinones from roots *morinda citrifolia* with solvent [42]. Ultrasound-assisted extraction in a system (water-ethanol), led to a 75% decrease in time and extraction efficiency as compared to samples not treated with ultrasonic waves.

In agreement with this research, also Heidari majd *et al.* (2012) demonstrate that yield extraction of phenolic compounds in ultrasound method is more than maceration method [37].

C´ujic. N *et al.* (2016) showed that extract obtained by maceration contained higher yield of TP (27.6 mg GAE/g) than extracts obtained by ultrasonic-assisted extraction for 30 min (25.4 mg GAE/g). These preliminary results indicate that maceration could be preferable method for the extraction of polyphenols from chokeberry fruit under tested conditions [43].
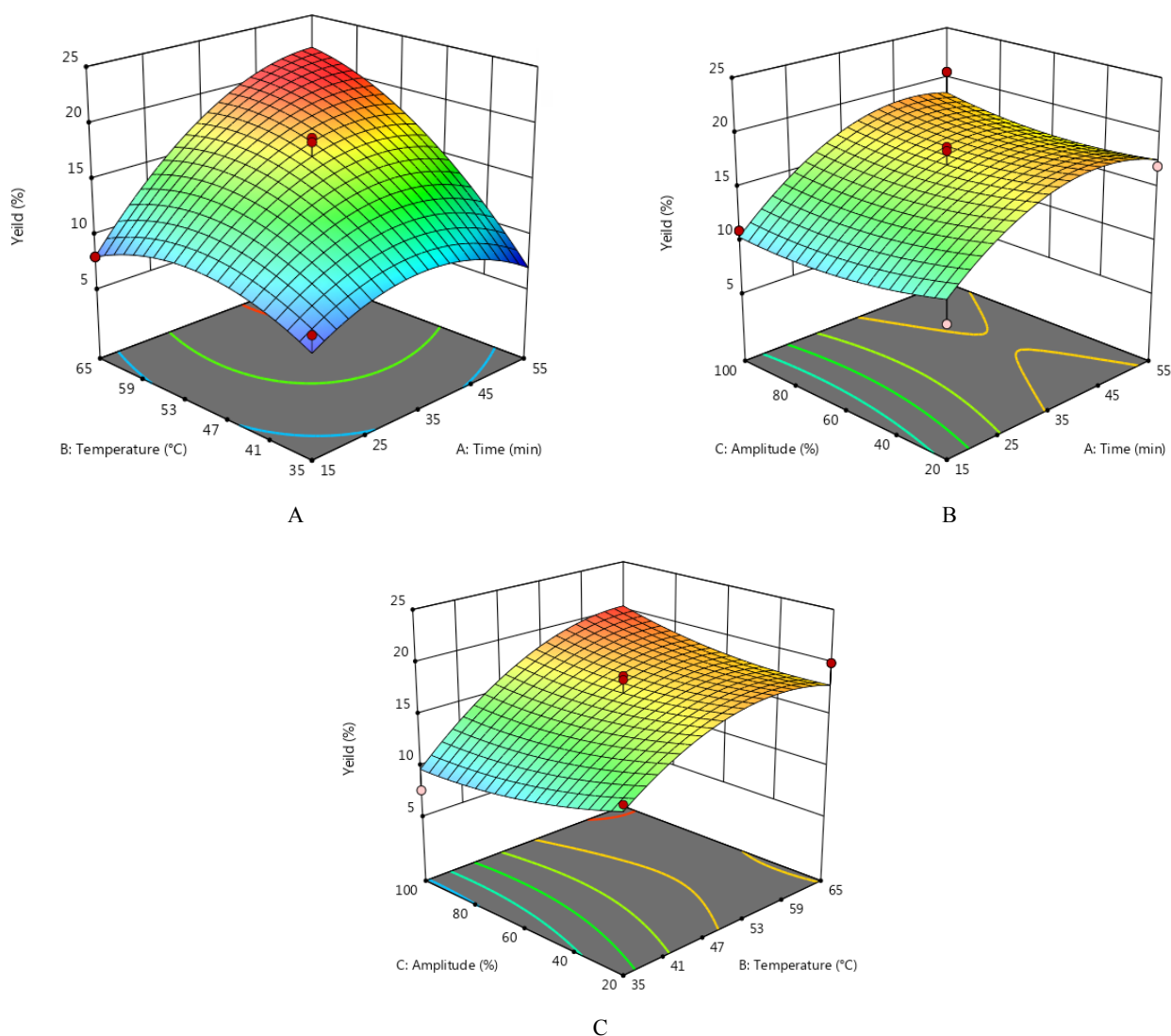
Figure 3 – Response surface plots of the extraction yield (Yield) of apple pomace extract as affected by A:
ultrasound amplitude and ultrasound exposure time, B: temperature and time C: ultrasound amplitude and time

Table 5 – Comparison of the maceration and ultrasound methods

Ultrasound	Maceration	
74.53	11.70± 0.28	TPC (mg GA/100 g)
83.85	2.79± 0.38	DPPH (%)
17.74	4.49± 0.14	YIELD (%)

Mean ± standard deviation

Conclusion

Apple pomace has agreeable antioxidantive activity due to possessing high amounts of polyphenolic compounds and flavonoids. Therefore, it is possible to have it introduced as a natural antioxidant source within the food industry. Analysis of the Box-Behnken design response surface with 3 independent variables consisting of time, temperature and device ultrasound amplitude serving as effective parameters on the extraction of antimicrobial compounds from apple pomace was carried out. All three extraction temperature, extraction time and ultrasound amplitude led to the increasing antioxidantal activity of the treatments. In this study, a model which its sum of squares amount had a significant difference and its lack of fit was insignificant was selected as the best model. On the one hand, by utilizing the models, adjustment of the extraction conditions is made possible, and on the other, considering the utilized extraction conditions, predict and rectify the desired properties.

References

1   Negro C., Tommasi L., Miceli A. (2003) Phenolic compounds and antioxidant activity from red grape marce extracts. Bioresource Technology., no. 87, pp. 41- 44. https://doi.org/10.1016/S0960-8524 (02)00202-X.

2   Sun H., Ge X., Hao Z., Peng M. (2010) Biotechnology Cellulase production by Trichoderma sp. on apple pomace under solid state fermentation. African Journal of Biotechnology. no. 9, pp. 163-166.

3   Kosseva, M.R. (2011) Management and Processing of Food Wastes, in: Moo-Young, M. (Ed.), Comprehensive Biotechnology. Environmental Biotechnology and Safety. no. 6.

4   Takos A., Jaffé F., Jacob S., Bogs J., Robinson S., Walker A. (2006) Light-Induced Expression of a MYB Gene Regulates Anthocyanin Biosynthesis in Red Apples. Plant Physiol., vol. 3, no. 142, pp. 1216–1232.

5   Corrales M., Garcia A., Butz P., Tauscher B. (2009) Extraction of anthocyanins from grape skins assisted by high hydrostatic pressure. Journal of Food Engineering. no. 90, pp. 415–421.

6   Adamez J., Samino E.G., Sanchez E.V., Gomez D.G. (2012) In vitro estimation of the antibacterial activity and antioxidant capacity of aqueous extracts from grape-seeds (Vitis vinifera L.). Food Control. no. 24, pp.136- 141.

7   Martin J., Porto E., Correa C., Alencar M., Gloria E., Cabral I., Aquino L. (2012) Antimicrobial potential and chemical composition of agro-industrial wastes. Journal of Natural Products., no. 5, pp. 27- 36.

8   Sagdic O., Ozturk I., Kisi O. (2012) Modeling antimicrobial effect of different grape pomace and extracts on S. aureus and E. coli in vegetable soup using artificial neural network and fuzzy logic system. Expert Systems with Applications., vol. 39, vo. 8, pp. 6792- 6798. https://doi.org/10.1016/j.eswa.2011.12.047

9   Porto C.D., Porretto E., Decorti D. (2013) Comparison of ultrasound-assisted extraction with conventional extraction methods of oil and polyphenols from grape (Vitis vinifera L.) seeds. Ultrasonics Sonochemistry., no. 20, pp. 1076- 1080. https://doi.org/10.1016/j.ultsonch.2012.12.002.

10   Wijngaard H., Hossain M.B., Rai D.K., Brunton N. (2012) Techniques to extract bioactive compounds from food by-products of plant origin. Food Research International., vol. 46, no. 2, pp. 505-513. https://doi.org/10.1016/j.foodres.2011.09.027.

11   Luque-Garci´a J.L., Luque De Castro M.D. (2003) Ultrasound: a powerful tool for Leaching. TrAC Trends in Analytical Chemistry., vol. 22, no. 1, pp. 41–47. https://doi.org/10.1016/S0165-9936(03)00102-X.

12   Lopez-Avila V., Young R., Teplitsky N. (1996) Microwave-assisted extraction as an Alternative to soxhlet, sonication, and supercritical fluid extraction. Journal of AOAC Int., no. 79, pp. 142–156. https://doi.org/10.1093/jaoac/79.1.142.

13   Hammi K. M., Jdey A., Abdelly C., Majdoub H., Ksouri R. (2015) Optimization of ultrasound-assisted extraction of antioxidant compounds from Tunisian Zizyphus lotus fruits using response surface methodology. Food Chemistry., vol. 184, pp. 80-89. https://doi.org/10.1016/j.foodchem.2015.03.047.

14   Luengo E., Condon-Abanto S., Condón S., Alvarez I., Raso J. (2014) Improving the extraction of carotenoids from tomato waste by application of ultrasound under pressure. Separation and Purification Technology., vol. 136, pp. 130-136. https://doi.org/10.1016/j.seppur.2014.09.008.

15   Sharayei P., Azarpazhouh A. (2017) Investigating the effect of ultrasound on antioxidant and antifungal properties of pomegranate peel. Agricultural and Natural Resources Research and Education Center, AREEO, Mashhad, Iran, 2017.

16   Kalamara E., Goula A. M., Adamopoulos K.G. (2014) An integrated process for utilization of pomegranate wastes–Seeds. Innovative Food Science and Emerging Technologies., vol. 27, pp.144-153. https://doi.org/10.1016/j.ifset.2014.12.001.

17   Rosangela J., Lisiane F., Valeria P., Claudio D., Ana Paula O., Jose O. (2007) The use of ultrasound in the extraction of Ilex paraguariensis leaves: a comparison with maceration. Ultrasonics Sonochemistry., vol. 14, no. 1, pp. 6-12. https://doi.org/10.1016/j.ultsonch.2005.11.007.

18   Harborne J.B. (1973) Phytochemical methods: a guide to modern techniques of plant analysis. London: Chapman & Hall; New York: [Distributed in the USA by Halsted Press, a Division of John Wiley & Sons].

19   Wang J., Sun B., Cao Y., Tian Y., Li X. (2008) Optimization of ultrasound-assisted extraction of phenolic compounds from wheat bran. Food

Chem., vol. 136, no. 2, pp. 804-810. https://doi.org/10.1016/j.foodchem.2007.06.062.

20 Von Gadow A., Joubert E., Hansmann C.F. (1997) Comparison of the antioxidant activity of aspalathin with that of other plant phenols of rooibos tea (Aspalathus linearis), α-tocopherol, BHT, and BHA. J. Agric. Food. Chem., vol. 3, no. 45, pp. 632-638. https://doi.org/10.1021/jf960281n.

21 Pinelo M., Rubilar M., Jerez M., Sineiro J., Núñez M.J. (2005) Effect of Solvent, Temperature, and Solvent-to-Solid Ratio on the Total Phenolic Content and Antiradical Activity of Extracts from Different Components of Grape Pomace. Journal of Agricultural and Food Chemistry., vol. 53, no. 6, pp. 2111-2117. https://doi.org/10.1021/jf0488110.

22 Spigno G., Tramelli L., Faveri D. M. D. (2007) Effects of extraction time, temperature and solvent on concentration and antioxidant activity of grape marc phenolics. Journal of Food Engineering., vol. 81, no.1, pp. 200-208. https://doi.org/10.1016/j.jfoodeng.2006.10.021.

23 Juntachote T., Berghofer E., Bauer F., Siebenhandl S. (2006) The application of response surface methodology to the production of phenolic extracts of lemon grass, galangal, holy basil and rosemary. International Journal of Food Science and Technology., vol. 41, no. 2, pp. 121-133. https://doi.org/10.1111/j.1365-2621.2005.00987.x.

24 Li B.B., Smith B., Hossain M.M. (2006) Extraction of phenolic from citrus peels II. Enzyme-assisted extraction method. Separation and Purification Technology., vol. 48, no. 2, pp. 189-196. https://doi.org/10.1016/j.seppur.2005.07.019.

25 Chan S., Lee C., Yap C., Mustapha W.A.W., Ho C. (2009) Optimization of extraction conditions for phenolic compounds from limau purut (Citrus hystrix) peels. Int. Food Res. J., vol. 2, no. 16, pp. 203-213.

26 Ya-Qin Ma., Jian-Chu Chen. (2009) Simultaneous extraction of phenolic compound of citrus peel extracts: Effect of ultrasound. Journal of Ultrasonics Sonochemistry., vol.16, no. 1, pp. 57-62. https://doi.org/10.1016/j.ultsonch.2008.04.012.

27 Sueli R., Pinto G.A.S. (2007) Ultrasound extraction of phenolic compounds from coconut (Cocos nucifera) shell powder. Journal of Food Engineering., vol. 80, no. 3, pp. 869–872. https://doi.org/10.1016/j.jfoodeng.2006.08.009.

28 Ahmadian koochaksarayee Z., Niazmand R. (2016) Optimization of Extraction of effective compounds from saffron petals by ultrasound-assay method. Novel food technology., no. 13, pp. 121-135.

29 Fernandez D. P., Goodwin A. R. H., Lemmon E. W., Levelt-sengers J. M. H., Williams R. C. (1997) A formulation for the static permitivity of water and steam at temperature from 238 K to 873 K at pressures up to 1200 MPa, including derivatives and Deby–Hückel coefficients. Journal of Physical Chemistry., vol. 26, pp. 1125−1166.

30 Durling N. E., Catchpole O. J., Grey J. B., Webby R. F., Mitchell K. A., Foo L. Y., Perry, N.B. (2007) Extraction of phenolics and essential oil from dried sage (Salvia officianlis) using ethanol-water mixtures. Food Chemistry., vol. 101, no. 4, pp. 1417−1424. https://doi.org/10.1016/j.foodchem.2006.03.050.

31 Prasad N. K., Yang B., Zhao M., Wang B., Chen F., Jiang Y. (2008) Effects of high pressure treatment on the extraction yield, phenolic content and antioxidant activity of litchi (Litchi chinensis Sonn.) fruit pericarp. International Journal of Food Science and Technology.doi:10.1111/j.1365-2621.2008.01768.x

32 Ji J.B., Lu X.H., Cai M.Q., Xu Z.C. (2006) Improvement of leaching process of Geniposide with ultrasound. Ultrasonics sonochemistry., vol. 13, no. 5, pp. 455-462. https://doi.org/10.1016/j.ultsonch.2005.08.003.

33 Lianfu Z., Zelong L. (2008) Optimization and comparison of ultrasound/microwave assisted extraction (UMAE) and ultrasonic assisted extraction (UAE) of lycopene from tomatoes. Ultrasonics sonochemistry., vol. 15, no. 5, pp. 731-737. https://doi.org/10.1016/j.ultsonch.2007.12.001.

34 Liu S., Yang F., Zhang C., Ji H., Hong P., Deng C (2009) Optimization of process parameters for supercritical carbon dioxide extraction of Passiflora seed oil by response surface methodology. The Journal of Supercritical Fluids., vol. 48, no. 1, pp. 9-14. https://doi.org/10.1016/j.supflu.2008.09.013.

35 Tian Y., Xu Z., Zheng B., Lo Y.M. (2013) Optimization of ultrasonic-assisted extraction of pomegranate (Punica granatum L.) Seed oil. Ultrasonics Sonochemistry., vol. 20, no.1, pp. 202–208. https://doi.org/10.1016/j.ultsonch.2012.07.010.

36 Zhang L. (2011) Estimating covariation: Epps effect and microstructure noise. Journal of Econometrics., vol. 160, no. 1, pp. 33–47. https://doi.org/10.1016/j.jeconom.2010.03.012.

37 Heydari Majd M., Mortazavi A., Asili J., Bolouriyan Sh. (2012) Optimization of Extraction of Phenolic compounds from Flomidoschema parviflora by ultrasound-assay method Herbal Medicine., no 1, pp. 7-13.

38 Ghafoor K,. Choi Y., Yeong Jeon, Ju., Hee Jo. (2009) Optimization of Ultrasound-Assisted Extraction of Phenolic Compounds, Antioxidants, and Anthocyanins from Grape (Vitis vinifera) Seeds. Agric. Food Chem., vol. 11, no. 57, pp. 4988–4994. https://doi.org/10.1021/jf9001439.

39 Velioglu Y.S., Oomah B.D. (1998) Antioxidant activity and total phenolic in selected fruits, vegetables and grain products. Journal of agricultural and food chemistry., vol. 46, pp. 4113-4117. https://doi.org/10.1021/jf9801973.

40 Vilkhu K., Mawson R., Simons L., Bates D. (2008) Applications and opportunities for ultrasound assisted extraction in the food industry – A review. Innovative Food Science & Emerging Technologies., vol. 9, no. 2, pp. 161-169. https://doi.org/10.1016/j.ifset.2007.04.014.

41 Albu S., Joyce E., Paniwnyk L., Lorimer J., Mason T. (2004) Potential for the use of ultrasound in the extraction of antioxidants from Rosmarinus officinalis for the food and pharmaceutical industry. Ultrasonic Sonochemistry., vol. 11, no. 3-4, pp. 261-265. https://doi.org/10.1016/j.ultsonch.2004.01.015.

42 Hemwimol S., Pavasant P., Shotipruk A. (2006) Ultrasonic-assisted extraction of anthraquinones from roots of Morinda citrifolia. Ultrasonics Sonochemistry., vol. 13, no. 6, pp. 543-548. https://doi.org/10.1016/j.ultsonch.2005.09.009.

43 Ujic N., Šavikin K., Jankovic T., Pljevljakušic D., Zdunic G., Ibric S. (2016) Optimization of polyphenols extraction from dried chokeberry using maceration as traditional technique. Food Chemistry., vol. 194, pp. 135–142. https://doi.org/10.1016/j.foodchem.2015.08.008.

E.M. Yergaliyeva[1] ⓘD , *K.B. Bazhykova[1] ⓘD ,

D.N. Mukhan[1] ⓘD , P. Langer[2] ⓘD

[1]Al-Farabi Kazakh National University, Almaty, Kazakhstan
[2]University of Rostock, Rostock, Germany
*e-mail: bazhikova@bk.ru

Synthesis of substituted tetrahydropyran-4-one and its oxime

Abstract, Tetrahydropyranone derivatives are promising starting materials for the synthesis of various heterocyclic compounds with biological activity. Oximes obtained on the basis of heterocyclic compounds, which include 3,5-substituted tetrahydropyran-4-one, possess antibacterial activity. We studied the optimal conditions for the synthesis of 3,5 substituted tetrahydropyran-4-one and its oxime, to confirm the obtained structures, and to perform quantum-chemical calculations of the conformations of the target compounds. The optimal method for the 3,5-dimethyleneoxytetrahydropyran-4-one (III) synthesis was the condensation of acetone with formaldehyde in a ratio of 1:4 in the presence of K_2CO_3; the yield was 67.4 %. The reaction of (III) with hydroxylamine hydrochloride was studied in the presence of NaOH and AcONa at different temperatures. The optimal yield (65.3%) of the product (IV) was obtained in the presence of AcONa with heating below 80 ^{0}C. To determine the composition of obtained compounds elemental analysis was used. Functional composition and structural elements were identified using IR spectroscopy. To prove the structure of the synthesized oxime, ^{1}H and ^{13}C NMR spectra were taken on a JNN-ECA Jeol 400 spectrometer (at a frequency of 399.78 MHz and 100.53 MHz) with a $CDCl_3$ solvent. Quantum-chemical calculations of stable conformations of (III) and (IV) was performed using *ab initio* DFT B3LYP method and 6-31G (d) and 6-311+G(3df,2p) basis sets. Calculated total energies and dipole moments allow to find the geometry of the most stable conformers. The most stable conformer of (IV) is the 3a5a configuration of substituents, which can be explained by the formation of intramolecular hydrogen bonds. Calculations show that the syn- and anti-isomers of 3,5-dimethyleneoxytetrahydropyran-4-one oxime are energetically equivalent.
Key words: tetrahydropyranone, acetone, formaldehyde, oxime, synthesis, condensation, conformational analysis.

Introduction

Pyran systems are an important group of six-membered oxygen-containing heterocycles that have diverse biological properties; they are found in many natural compounds [1-2]. Tetrahydropyranones can serve as precursors in the fine organic synthesis of new biologically active compounds. In medicine and modern technologies, substituted tetrahydropyran-4-ones, their derivatives [3-5] and isomers [6-7] are widely used.

Oximes of aldehydes and ketones are used to protect and selectively activate groups, to produce amides and nitriles. They act as intermediates in many reactions, such as the production of amides by Beckmann rearrangement [8]. Oximes find application in transition-metal catalysis [9-12]. Oximes and their ethers are present in some biologically active compounds that exhibit healing properties [13-14]. Tetrahydropyran-4-one linker-containing oximes show the antiproliferative activity [15].

3,5-dimethyleneoxytetrahydropyran-4-one and its oxime were synthesized in order to obtain their derivatives to study their properties and biological activity.

Earlier, we reported on synthesis and quantum chemical calculations of the conformation of 3,5-substituted tetrahydropyranone [16]. Theoretical calculations of the conformation of the obtained oxime were also performed. In order to confirm structures, NMR ^{13}C and ^{1}H spectra were studied.

Materials and methods

Earlier, we reported on the synthesis of oxime of 3,5-dimethyleneoxytetrahydropyran-4-one (IV) [16]. In the present work we studied the different conditions of 3,5-substituted tetrahydropyranone synthesis according to the scheme below.
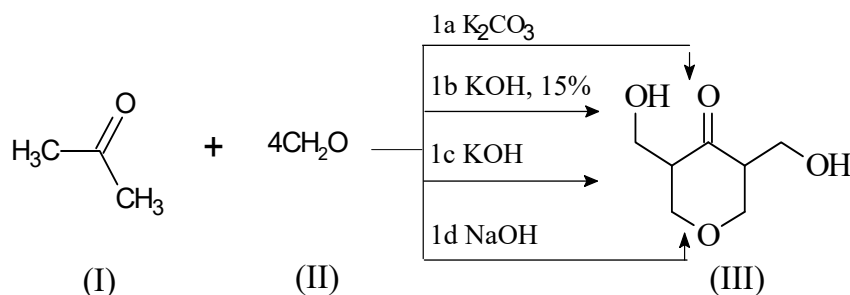
Figure 1 – Synthesis of 3,5-substituted tetrahydropyranone

1a) The method of (III) synthesis in the presence of K_2CO_3 is described in the article [16]. Yield is 67.4 %.

1b) 11.6 g (0.2 mol) of acetone, a formalin solution containing 0.8 mol of formaldehyde, 15% KOH solution (0.04 mol) were added to a round bottom flask equipped with a mechanical stirrer. It was refluxed for 7 days at a temperature of 35-40 °C. To control the reaction by TLC, the mobile phase ethanol-hexane (6: 4) was used. To develop chromatographic zones, the plate was treated with iodine vapor. Yield was 65.7 %.

1c) A formalin solution containing 0.8 mol of formaldehyde, 2.24 g of KOH (0.04 mol) were added

in a flask. After stirring and cooling of the reaction mixture, 11.6 g (0.2 mol) of acetone were added. The reaction takes place within a few minutes with the release of heat. Yield is 58.2 %.

1d) Similar to procedure 1c, but instead of KOH, 1.6 g of NaOH (0.04 mol) were added. Yield was 56.8 %.

In order to study the conditions of (IV) synthesis we carried out the reaction of equivalent amounts of (III) and hydroxylamine hydrochloride in an alkaline medium and in the presence of sodium acetate according to the scheme [17].
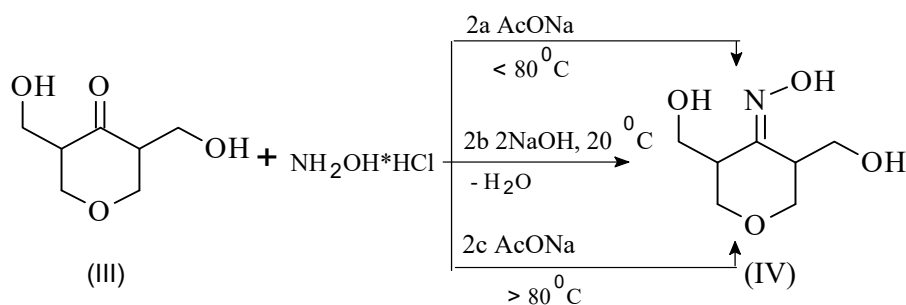
Figure 2 – Synthesis of 3,5-dimethyleneoxytetrahydropyran-4-one oxime

2a) 1.5 g (0.02 mol) of hydroxylamine hydrochloride (15% water solution), 3.2 g (0.02 mol) of (III) (ethanol solution) and 2 g of AcONa (0.02 mol) were added to a round-bottom flask. The reaction mixture was refluxed and heated (< 80 °C) for 40 minutes. After completion of the reaction, 60 g of cold water were added and the unreacted (III) was filtered off. Pieces of ice were added to the filtrate and acidified

with sulfuric acid. The resulting product was filtered and dried at 70-80 °C. Yield was 65.3 % in the powder form.

2b) 1.6 g (0.01 mol) of (III) and 0.75 g (0.01 mol) of hydroxylamine hydrochloride in sodium hydroxide were added to a round bottom flask. The reaction mixture was stirred and refluxed at 20 °C for 7 days. The progress of the reactions was monitored by TLC

in the system butanol: acetic acid: water (40:12.5:29). After completion of the reaction, 50 ml of benzene and desiccant (calcium chloride) were added. Calcium chloride was filtered off and the mixture was washed again with benzene. The product was separated by vacuum distillation in the form of a brown powdery substance. Yield was 62.5 %.

2c) Similar to method 2.1, but at temperature above 80 °C. Yield was 60.9 %.

Results and discussion

The condensation of acetone and formaldehyde in a ratio of 1: 4 was studied under mild alkaline conditions in the presence of K_2CO_3 (1a). The product (III) yield was 67.4 %, while the reaction time was 7 days. Heating above 50 °C leads to the formation of by-products and a decrease in the yield of the reaction. In the presence of a 15% KOH solution (1b), the

product yield was 65.7 %. In the presence of KOH (1c) or NaOH (1d) side reactions of polymerization occur, which reduces the yield of the product (58.2 % and 56.8 % respectively). Thus, method 1a is optimal (Table 1).

Reactions of (III) with hydroxylamine hydrochloride in the presence of CH_3COONa and NaOH were investigated at different temperatures. In the presence of sodium acetate, (IV) was synthesized with 65.3% yield at the most optimum state and high flow rate, at a temperature below 80 °C (Table 2).

The physical constants of recrystallized purified (III) and (IV) were determined. The results are shown in Table 3.

The low melting range of the obtained compounds indicates the purity of the isolated substances. The functional groups were identified by the results of IR spectra. The results of the IR spectrum analysis are shown in Table 4.

Table 1 – Optimization of (III) synthesis by condensation of acetone[1] and formaldehyde[2]

Entry	Molar ratio	Solvent	Temperature, ^{0}C	Time	Yield, %
1a	1[1]: 4[2]: 0.1 (K_2CO_3)	water	35-40	7 days	67.4
1b	1[1]: 4[2]: 0.2 (KOH)	water	35-40	7 days	65.7
1c	1[1]: 4[2]: 0.2 (KOH)	water	25	3-5 min.	58.2
1d	1[1]: 4[2]: 0.2 (NaOH)	water	25	3-5 min.	56.8

Table 2 – Optimization of (IV) synthesis by reaction of (III)[1] with hydroxylamine hydrochloride[2]

Entry	Molar ratio	Solvent	Temperature, ^{0}C	Time	Yield, %
2a	1[1]: 1[2]: 1 (AcONa)	water	< 80	40 min	65.3
2b	1[1]: 1[2]: 1 (NaOH)	water	20	7 days	62.5
2c	1[1]: 1[2]: 1 (AcONa)	water	80-90	40 min	60.9

Table 3 – Physical constants of (III) and (IV)

Product	T_m, °C	R_f (ethanol-hexane (6: 4)	Yield, %
1a	138-140	0.210	67.4
1b		0.228	65.7
1c		0.230	58.2
1d		0.215	56.8
		R_f (butanol: acetic acid: water (40:12.5:29)	
2a	128-129	0.410	65.3
2b		0.413	62.5
2c		0.411	60.9

Table 4 – The results of the IR spectrum of (III) and (IV)

Compound	Frequency, ν, cm^{-1}				
	C=O	OH	C-O-C	CH$_2$	C-C
III	1703	3432	1101	2933,29	1657,14
	C=N	N-OH	C-O-C	CH$_2$	C-C
IV	1650	3414	1180.93	2892	1657

To identify the structure of the synthesized compounds, ^{1}H and ^{13}C NMR spectra were obtained. The ^{1}H NMR spectra were recorded on a JNN-ECA Jeol 400 spectrometer (at a frequency of 399.78 MHz) with a solvent CDCl$_3$ (Table 5).

The ^{13}C NMR spectra were recorded on a JNN-ECA Jeol 400 spectrometer (at a frequency of 100.53 MHz) with a solvent CDCl$_3$. The results are given in Table 6.

As reported in a previous article, we carried out the conformational analysis of (III) using the methods of quantum chemistry. The ab-initio calculation method and results were described there [16]. Similar calculations were performed for (IV). The results are shown in Table 7.

According to the calculations, one of the stable geometry of 3,5-dimethyleneoxytetrahydropyran-4-one is the conformation (III)3a5a in which the substituents are located in the axial position.

Table 5 – ^{1}H NMR spectra of (III) and (IV)

Compound	Chemical shift, σ				
	CH$_2$(C^{2,6})	CH (C^{3,5})	CH$_2$(C^{7,8})	OH$^{(9,10)}$	OH$^{(11)}$
III	3.61 (dd)	2.19 (tp)	3.53 (tp)	5.15 (tp)	-
IV	3.82 (dd)	1.61 (tp)	3.03 (tp)	5.25 (tp)	6.8 (s)

Table 6 – ^{13}C NMR spectrum of (III) and (IV)

Compound	Chemical shift, σ			
	CH$_2$(C^{2,6})	CH (C)	CH$_2$(C^{7,8})	C^4
III	66.18	50.39	62.02	215.19
IV	51.37	30.95	44.76	157.19

Table 7 – Total energy and dipole moment of (IV) conformations calculated by the DFT method B3LYP density functional and the 6-31G basis sets

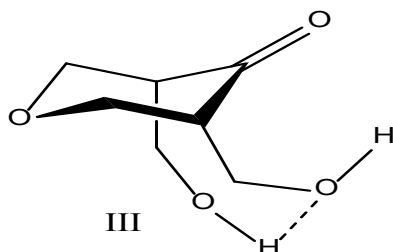| Conformation	Total energy, Hartree	Dipole moment, Debye
(IV) 3e5e	-626.16560	4.76
(IV) 3a5e	-626.16183	0.94
(IV) 3e5a	-626.16715	1.07
(IV) 3a5a	-626.17215	4.46

Figure 3 – The conformation (III)3a5a

This may be explained by the formation of intramolecular hydrogen bonds between the hydroxyl groups. The difference from the molecule of (III), where the energy (III) 3e5e is quite low and approaches the value of the (III) 3a5a conformation energy, for oxime (IV) conformation 3a5a is the most stable (Table 7). This can be explained by the interaction with the functional group of (IV).
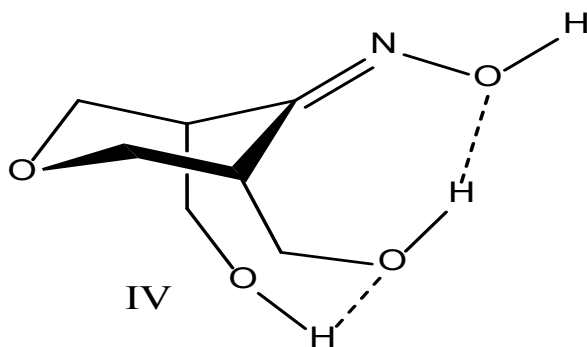

Figure 4 – The conformation (IV)3a5a

For oximes, syn- and anti-isomerism are characteristic. However, due to the symmetric arrangement of the substituents, no significant differences in energy were revealed for the syn- and anti-isomers of oxime.

Conclusion

Based on the processing of experimental data, optimal synthesis conditions of 3,5-dimethyleneoxytetrahydropyran-4-one synthesis by acetone and formaldehyde condensation are determined. It has been established that the basicity of the reaction mixture has the greatest influence on the yield of the product. An increase in temperature affects the side processes of polymerization. The presence of concentrated alkalis also leads to an increase in temperature (due to an exothermic reaction) and side reactions, which reduces the yield of the product. Therefore, methods 1c and 1d give a lower product yield compared to methods 1a and 1b. The optimal condition for the conden-

sation of acetone and formaldehyde is the presence of potassium carbonate and heating no higher than 40 ^{0}C (1a). In the presence of K_2CO_3 at 40 ^{0}C the product yield was 67.4%. The methods 1a and 1b are highly time-dependent, but more economical in reagent requirements.

For the production of oxime, the optimal conditions were the presence of AcONa and heating not higher than 80 ^{0}C (2a method). Yield of product was 65.3%. Method 2b gives a higher yield than 2c, but depends more on the reaction time. An increase in temperature above 80 ^{0}C reduces the yield of the product.

The structure of the synthesized compounds was determined and identified by IR spectroscopy, elemental analysis and NMR spectroscopy. The obtained experimental data can be used to develop a technological scheme for the production of 3,5 substituted tetrahydropyran-4-one and its oxime.

Quantum-chemical calculations of stable conformations of 3,5-dimethyleneoxytetrahydropyran-4-one oxime was performed. The total energies and dipole moments of the conformers are calculated. The most stable is the 3a5a configuration of substituents, which can be explained by the formation of intramolecular hydrogen bonds. The syn- and anti-isomers of 3,5-dimethyleneoxytetrahydropyran-4-one oxime are energetically equivalent. A more detailed conformational analysis of 3,5 substituted tetrahydropyran-4-one and its oxime can be carried out after obtaining two-dimensional ^{13}C and ^{1}H NMR spectra.

References

1   Jacques R., Pal R., Parker N.A., Sear C.E., et al. (2016) Recent applications in natural product synthesis of dihydrofuran and -pyran formation by ring-closing alkene metathesis. Organic & Biomolecular Chemistry, vol. 14, no 25, pp. 5875–5893. https://doi.org/10.1039/c6ob00593d.

2   Luhavaya H., Dias M.V., Williams S.R., Hong H., et al. (2015) Enzymology of Pyran ring a formation in salinomycin biosynthesis. Angew Chem Int Ed Engl, vol. 54, no 46, pp. 13622-13625. https://doi.org/10.1002/anie.201507090.

3   Lemos L.M.S., Martins T.B., Tanajura G.H., Gazoni V.F., et al. (2012) Evaluation of antiulcer activity of chromanone fraction from Calophyllum brasiliesnse Camb. Journal of Ethnopharmacology, vol. 141, no 1, pp. 432–439. https://doi.org/10.1016/j.jep.2012.03.006.

4   Kandhare A.D., Raygude K.S., Ghosh P. et al. (2012) Neuroprotective effect of naringin by modulation of endogenous biomarkers in streptozotocin induced painful diabetic neuropathy. Fitoterapia, vol. 83, no 4, pp.650-659. http://dx.doi.org/10.1016/j.fitote.2012.01.010.

5   Uesugi S., Watanabe T., Imaizumi T., Ota Y., et al. (2015) Total Synthesis and Biological Evaluation of Irciniastatin A (a.k.a. Psymberin) and Irciniastatin B. The Journal of Organic Chemistry, vol. 80, no 24, pp. 12333–12350. https://doi.org/10.1021/ol1000389.

6   Nottelet B., Patterer M., François B. et al. (2012) Nanoaggregates of biodegradable amphiphilic random polycations for delivering water-insoluble drugs. Biomacromolecules, vol. 13, no 5, pp.1544–1553. http://dx.doi.org/10.1021/bm300251j.

7   Brückner M., Westphal S., Domschke W., Kucharzik T., Lügering A. (2012) Green tea polyphenol epigallocatechin-3-gallate shows therapeutic antioxidative effects in a murine model of colitis. Journal of Crohn's and Colitis, vol. 6, no 2, pp. 226–235. https://doi.org/10.1016/j.crohns.2011.08.012.

8   Gopalakrishnan M., Thanusu J., Kanagarajan V. (2009) A facile solid-state synthesis and in vitro antimicrobial activities of some 2,6-diarylpiperidin/tetrahydrothiopyran and tetrahydropyran-4-one oximes. Journal of Enzyme Inhibition and Medicinal Chemistry, vol. 24, no 3, pp. 669-675. https://doi.org/10.1080/14756360802323902.

9   Tan Y., Hartwig J.F. (2010) Palladium-Catalyzed Amination of Aromatic C−H Bonds with Oxime Esters. Journal of the American Chemical Society, vol. 132, no 11, pp. 3676–3677. https://doi.org/10.1021/ja100676r.

10   Too P.C., Chua S.H., Wong S.H., Chiba S. (2011) Synthesis of Azaheterocycles from Aryl Ketone O-Acetyl Oximes and Internal Alkynes by Cu–Rh Bimetallic Relay Catalysts. The Journal of Organic Chemistry, vol. 76, no 15, pp. 6159–6168. https://doi.org/10.1021/jo200897q.

11   Neely J.M., Rovis T. (2012) Rh(III)-Catalyzed Regioselective Synthesis of Pyridines from Alkenes and α,β-Unsaturated Oxime Esters. Journal of the American Chemical Society, vol. 135, no 1, pp. 66–69. https://doi.org/10.1021/ja3104389.

12   Xia J., Huang X., You S., Cai M. (2019) Heterogeneous copper☐catalyzed oxidative coupling of oxime acetates with sodium sulfinates: An efficient and practical synthesis of β☐keto sulfones. Applied Organometallic Chemistry, e5001. https://doi.org/10.1002/aoc.5001.

13   Setamdideh D., Karimi Z., Alipouramjad A. (2013) NaBH4/DOWEX(R)50WX4: A Convenient Reducing System for Fast and Efficient Reduction of Carbonyl Compounds to Their Corresponding Alcohols. Journal of the Chinese Chemical Society, vol. 60, no 6, pp. 590–596. https://doi.org/10.1002/jccs.201300014.

14   Mirjafary Z., Abdoli M., Saeidian H., Boroon S., Kakanejadifard A. (2015) Oxime ethers as versatile precursors in organic synthesis: a review. RSC Advances, vol. 5, no 97, pp. 79361–79384. https://doi.org/10.1039/c5ra15299b.

15   Qin H.-L., Leng J., Youssif B.G.M. Amjad M.W., et al. (2017) Synthesis and mechanistic studies of curcumin analog-based oximes as potential anticancer agents. Chemical Biology & Drug Design, vol. 9, no 3, pp. 443–449. https://doi.org/10.1111/cbdd.12964.

16   Bazhykova K.B., Langer P., Yergaliyeva E.M., Seylkhanov T.M., Abilov Z. (2018) Synthesis and identification of 3,5-bis(hydroxymethyl)tetrahydro-4H-pyran-4-one. Chemical Bulletin of Kazakh National University, vol. 4, pp. 4-9. https://doi.org/10.15328/cb1039.

17   Bazhykova K.B., Yergaliyeva E.M., Abduali G.A., Mukhan D.N., et al. (2019) Synthesis of few hetrocyclic compounds from a number of substituted tetrahydropyranones. New Materials, Compounds and Appliccations, vol. 1, no 3, pp. 47-51.

A.K. Kenessova[1*] (iD) , G.A. Seilkhanova[1,2] (iD) ,

A.B. Rakhym[1] (iD) , Yitzhak Mastai[3] (iD)

[1]Al-Farabi Kazakh National University, Almaty, Kazakhstan
[2]Center of Physicochemical Methods of Research and Analysis, Almaty, Kazakhstan
[3] Bar-Ilan University, Department of Chemistry and the Institute of Nanotechnology, Israel
*e-mail: kenessova.aruzhan@gmail.com

Composite materials based on orange and pomegranate peels for Cu (II) and Zn (II) ions extraction

Abstract. The method of obtaining composite materials based on orange (OP) and pomegranate (PP) peels is described. The fruit peels were modified by polyethylene glycol (PEG). Sorption ability of obtained composite materials towards heavy metal ions (Zn and Cu) was studied. The effect of the mass of composite materials and PEG concentration were studied. The optimal concentration of PEG was determined as 0.1%. The maximum removal degree of heavy metals was at 2 and 2.5 g per 100 ml of solution for orange and pomegranate peels respectively. Three different adsorption models were used to describe the sorption process (Langmuir, Freundlich, and BET). The most applicable for the sorption of Zn (II) and Cu (II) ions by both OP and PP is Freundlich theory. Hence, the sorption of Zn (II) and Cu (II) ions by modified peels of orange and pomegranate occurs at a heterogeneous system where the active centers are unevenly filled.
Key words: composite material, orange peel, pomegranate peel, polyethylene glycol, sorption, heavy metal.

Introduction

Thousand tons of fruits are eaten every day around the world. In order of utilization of their peels they can be used as sorbents of heavy metals (HM) from wastewater. In accordance with the WHO (World Health Organization), drinking of low quality water can cause human ailments accounted about 80% of health problems' total amount [1]. Purification of water from various pollutants is currently a relevant task, which requires the application of new approaches as well as environmentally-friendly and resource-saving technologies. All these approaches should give the opportunity to use the purified water in production processes, thus decreasing the consumption of freshwater [2].

Many methods and technologies have been developed for the treatment of wastewater from different types of pollutants, particularly from HM ions. They are electrodialysis, coagulation, reverse osmosis, sedimentation, ion exchange, filtration, flocculation and precipitation [3–6]. However these conventional methods are quite expensive [7]. Among all of the developed methods for the treatment of

wastewater, containing HM ions, an important place is taken by sorption methods. They allow to provide the most complete removal of toxicions, especially from solutions with low concentrations [8, 9]. Hence, adsorption is one of the promising methods for purification of wastewater and industrial effluents [10].

Such composite materials based on fruit peels and other plant raw materials are low-cost and effective. Low-cost bioadsorbents are based on using household wastes, such as peels of banana, orange, kiwi, pomegranate, tangerine, tomato, potato and pumpkin, also tea wastes and pineapple [11]. Agricultural wastes are also used in bio-sorption [12]. The wastes of crops are one of the sources that are rich of low-cost sorbents. Agricultural wastes show ability to adsorb toxic heavy metal ions, such as mercury, lead, cadmium, nickel, zinc and chromium. According to investigated works [13], sorbents based on agricultural wastes are effective for removal of cadmium ions.

Such household waste as eggshell is also used as bioadsorbent. In the work devoted to removal of copper and lead ions from water eggshell [14], banana

peels and pumpkin were used as bioadsorbents. Yellow passion-fruit shell was used as adsorbent for removal of ions of Cr (III) and Pb (II) from water. The highest removal efficiency was observed at pH = 5 both for chromium and lead. The removal efficiency of Cr (III) ions was about 63% and about 20% for Pb (II) [15].

Banana peel was used as adsorbent to remove Cr (VI) ions from industrial wastewater [16]. The sorption process was carried out at the pH range of 1-9. Maximum Cr (VI) removal was observed at pH = 2, the removal degree reaches more than 95 %. Another work has been provided using banana peel as adsorbent for treatment of wastewater collected from Gelox paints, Kaduna state, Nigeria [17].

A lot of research works were performed using orange peel as an adsorbent for heavy metal ions removal [18-20]. Orange peel along with date palm fibers were used to remove copper (II), lead (II) and arsenic (V) ions from aqueous solutions [21].

A lot of researches have been done using peel of pomegranate [22, 23]. Pomegranate peel was used to adsorb copper, cadmium, nickel and zinc ions [24]. Biosorbent shows the highest adsorption capacity of heavy metals at pH 4.5. Adsorption of copper and cadmium ions represents the highest results, followed by ions of zinc and nickel. Adsorption of Cr (VI) is the lowest at pH 4.5. The maximum removal of copper ions was 0.0677 mmol/g at initial 0.787 mmol/l of the solution.

Thus, an analysis of the literature has shown that composite materials based on orange peel and pomegranate peel are of practical interest for use in the process of sorption of heavy metal ions, but they should be modified to increase the sorption activity. For our knowledge, there is no data on the use of polyethylene glycol (PEG) as a modifier for the preparation of composite materials based on orange peel and pomegranate peel in the literature. The previous studies [25] have shown that PEG can be used as an effective modifier of sorbents based on natural materials. The adsorption activity of PEG-modified OP and PP towards copper (II) and zinc (II) ions was studied in the current work.

Materials and methods

Composite materials preparation

Orange (OP) and pomegranate (PP) peels were collected from local markets and juice-producing shops. At first, peels were washed with distilled water, finely cleaned and left to dry at room temperature. Then the dry peels were mechanically ground till fine powder was obtained.

Obtainment of the composite materials based on the peels was carried out according to two-step procedure: first with a solution of sodium hydroxide (NaOH), then with a solution of polyethylene glycol (PEG).

Obtaining the composite material based on orange peel was carried out according to the following procedure. Orange peel powder weighing 5 g is placed in a glass; 100 ml of an aqueous solution containing 0.1 M NaOH is poured into this glass. Next, the resulting solution with the OP is stirred with a glass rod to prevent lumps, and then continued mixing using magnetic stirrer at 100 rpm for 60 min. The resulting gelatinous solution is left over night. On the next day the process of polymer modification begins. First, solution is rinsed with distilled water until a neutral medium is reached (pH of 6-7). Then the solution is filtered. After that the sorbent remaining on the filter paper is dried and subjected to polymer modification. For this purpose, 100 cm^3 of 0.1 % polyethylene glycol is poured into a glass with a sorbent obtained in the previous step. After 60 minutes of stirring on a mixer, composite material is dried in an oven at 100 °C for 2 hours, then left to dry until completely drying at room temperature. The obtained composite material was ground in order to further study of its characteristics.

The composite material based on pomegranate peel was obtained by the same method as in the case of orange peel.

Adsorption experiments

The following solutions containing heavy metal ions of various concentrations are prepared for the experiment:

– solution of the $CuCl_2 \cdot 2H_2O$ salt with a metal concentration of 10-50 μg/ml;

– solution of $ZnCl_2$ salt with a metal concentration of 10-50 μg/ml.

The sorption process was carried out under static conditions with outstirring, at the room temperature equal to T = 298 K.

Sorbent with a mass of 1 g is placed and 100 ml of solution is poured into a measuring cup (flask) with a capacity of 100 cm^3. Furthermore, an aliquot of the solution is taken after a certain period of time and kept at room temperature until equilibrium was established.

Results and discussions

Sorption characteristics of initial and modified composite materials based on orange and pomegranate peels

A comparative analysis sorption activity of the initial materials (orange and pomegranate peels) towards TM ions is represented in Figure 1. It can be seen from the graphs that the peels show different adsorption properties for each metal ion. As can be seen from Figure 1 (a) the removal degree of Zn^{2+}

and Cu^{2+} ions reaches about 70 % (67 % and 71 %). The results in Figure 2 (b) show that PP adsorbs copper (II) ions much better than zinc (II) ions (41 % and 28 %). It can be concluded that initial OP has better adsorption properties towards Zn^{2+} and Cu^{2+} ions than initial PP.
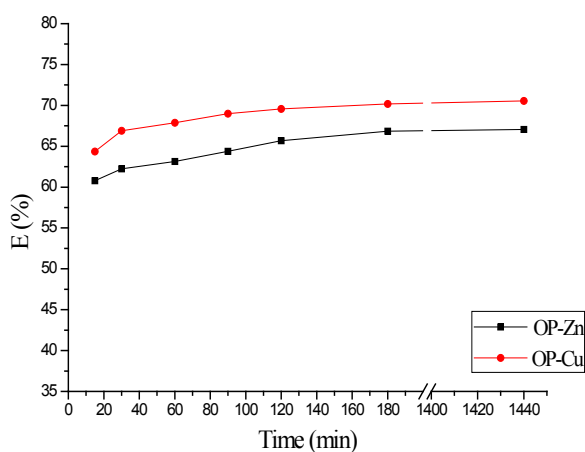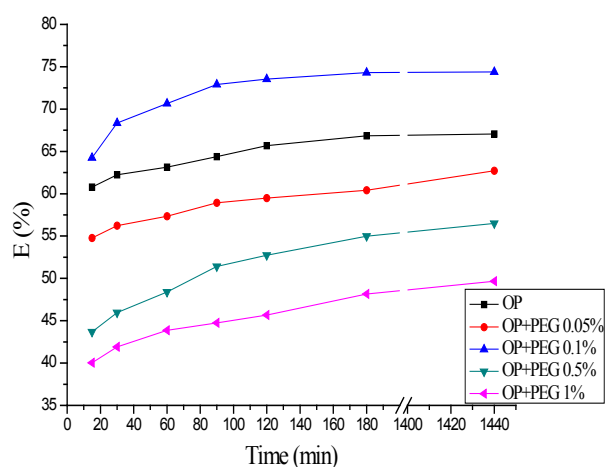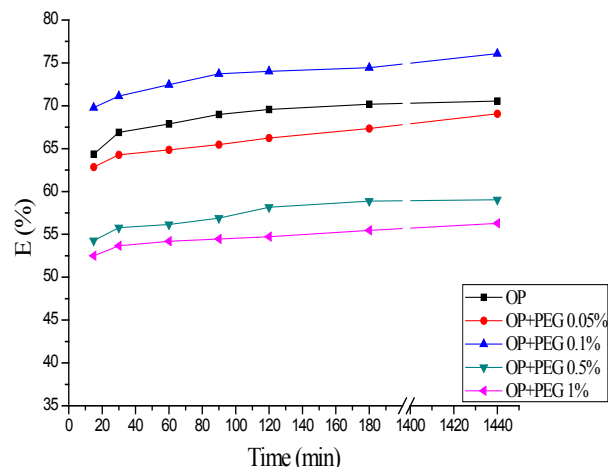

a) initial OP
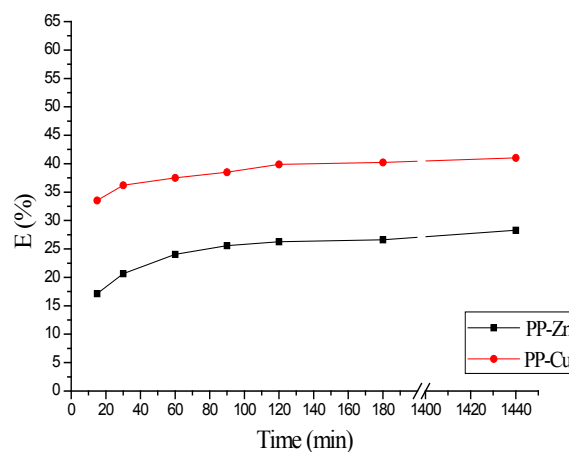
b) initial PP

Figure 1 – Dependence of removal degree (%) of Zn^{2+} and Cu^{2+} ions by initial (a) OP and (b) PP on time (T = 298 K, C_{in} = 10 mg/l)

a) Zn^{2+}

b) Cu^{2+}

Figure 2 – Dependence of removal degree (%) of (a) Zn^{2+} and (b) Cu^{2+} ions by modified OP at different concentrations of PEG on time (T = 298 K, C_{in} = 10 mg/l)

A comparative analysis of Zn^{2+} and Cu^{2+} ions sorption by modified OP at different concentrations of PEG is represented in Figure 2.

It can be seen from the graphs that the modification of OP by PEG 0.1 % enhanced the sorption

ability of the initial peel. The removal degree of Zn^{2+} and Cu^{2+} reaches 74 % and 76 % respectively. However, in both cases, the other concentrations of PEG are not effective compared to the initial OP. It can be concluded that the 0.05 % concentra-

tion of PEG is not enough to improve the sorption activity of OP. Meanwhile increasing the concentration of modifier reduces the removal degree of the metal ions due to closing the active centers of peel surface.
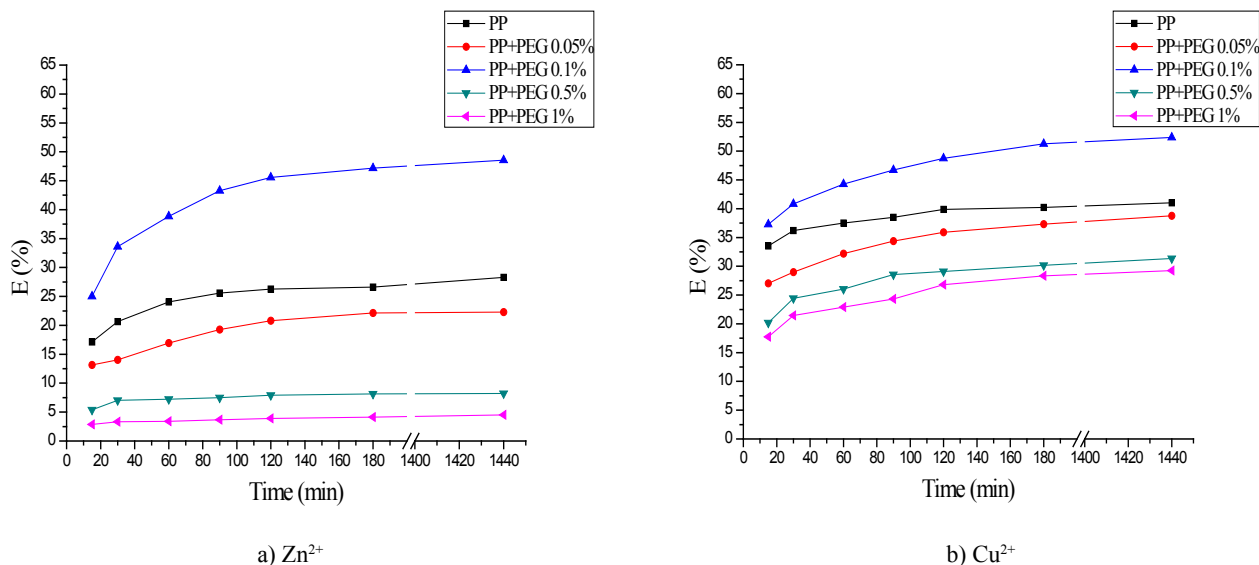
Figure 3 represents a comparative analysis of Zn^{2+} and Cu^{2+} ions sorption by modified PP at different concentrations of PEG.

The consequence of sorption activity of modified pomegranate peels are the same as in the case of modified orange peels: 0.1 % > 0.05 % > 0.5 % > 1 %. The removal degree of zinc (II) ions by PP-PEG 0.1 % highly increases in comparison to the initial pomegranate peel (49 %). The lowest removal degree of zinc (II) ions by modified PP (about 5 %) has been observed at the concentration of PEG = 1 %.

a) Zn^{2+} b) Cu^{2+}

Figure 3 – Dependence of removal degree (%) of (a) Zn^{2+} and (b) Cu^{2+} ions on time by modified PP at different concentrations of PEG

The adsorption ability of modified PP towards Cu^{2+} ions are shown in Figure 3 (b). The extraction degree of copper (II) ions by modified polyethylene glycol reaches 52%.

According to the results from the graphs of removal degree dependence of HM ions from time, it can be concluded that the optimal time of equilibrium establishment is 180 minutes. The concentration of the modifier (PEG) equal to 0.1% is optimal to reach the highest removal degree of the metal ions from aqueous solutions, while the lowest results are observed at 1 %. The removal of Zn^{2+} and Cu^{2+} ions by modified OP is about 75 % and the removal degree by modified PP reaches up to 50 %.

Figure 4 shows a comparative analysis of Zn^{2+} and Cu^{2+} ions sorption by modified OP at different masses of sorbents. It can be seen from the graphs that with increasing the mass of the modified orange peel the removal degree of zinc (II) and copper (II) ions also increase. However, there is no considerable difference between the removal degree at 2 g and 2.5 g. Hence, 2 g of modified orange peel was chosen

as the optimal mass of sorbent for removal of both Zn^{2+} and Cu^{2+} ions. The removal degree of Zn^{2+} and Cu^{2+} ions by the optimal mass of modified OP reaches about 80 %.

Figure 5 represents a comparative analysis of Zn^{2+} and Cu^{2+} ions sorption by modified PP at different masses of sorbents. In the case of modified pomegranate peel, 2.5 g was the most effective for sorption of zinc (II) and copper (II) ions. The removal degree of Zn^{2+} ions was 80 % and of Cu^{2+} ions was 70 %.

Analysis of isotherms of the sorption process of Zn^{2+} and Cu^{2+} ions from aqueous solutions

Sorption isotherms are of great importance for describing the sorption process. There is no unified model that accurately and fully describe all types of adsorption on different interfaces. Three of the most frequently used models (Langmuir, Freundlich and BET) were used to describe the process of HM ions sorption by the obtained composite materials. Table 1 summarizes the isotherm constants of sorption by composite materials, where K is adsorption equilib-

rium constant, A_∞ is maximum adsorption, K_{BET} is BET equilibrium constant, K_F and $1/n$ are Freundlich isotherm constants. According to the data in Table 1, the BET isotherm model does not describe the sorption process. Langmuir theory does not fully describe the process, while the correlation coefficient values of the Freundlich model show better results. Consequently, sorption of Zn^{2+} and Cu^{2+} ions by modified OP and PP occurs at a heterogeneous system with an uneven filling of active centers.
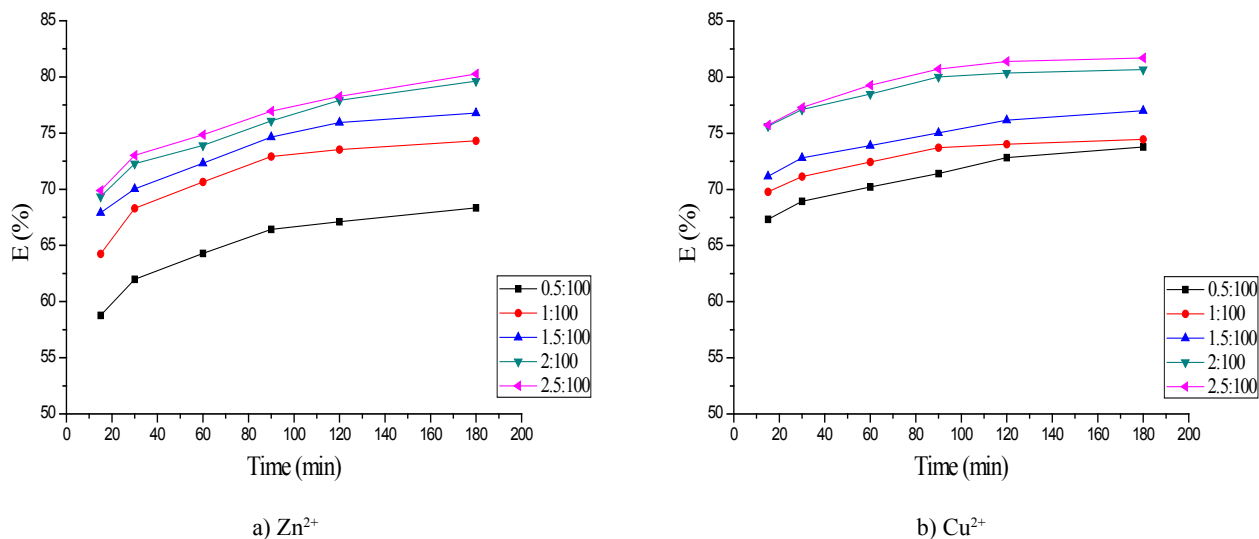
a) Zn^{2+}

b) Cu^{2+}

Figure 4 – Dependence of removal degree (%) of (a) Zn^{2+}
and (b) Cu^{2+} ions by modified OP at different masses of composite material on time
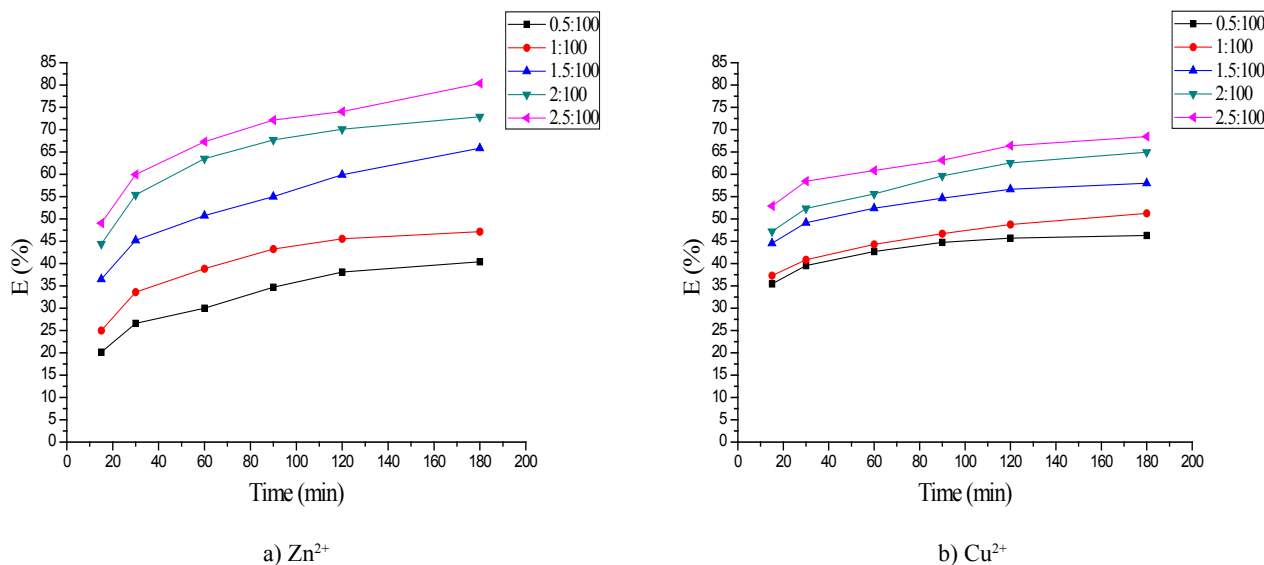
a) Zn^{2+}

b) Cu^{2+}

Figure 5 – Dependence of removal degree (%) of (a) Zn^{2+}
and (b) Cu^{2+} ions by modified PP at different masses of composite material on time

Table 1 – Isotherm constants of sorption process by modified peels

Model parameters		OP-PEG		PP-PEG	
		Zn^{2+}	Cu^{2+}	Zn^{2+}	Cu^{2+}
Langmuir theory	K	0.0011	0.0038	0.0156	0.0175
	A_∞, mg/l	26.1780	10.9529	2.0903	1.6150
	R^2	0.0066	0.9436	0.9717	0.9591
Freundlich theory	K_F	0.0501	0.0488	0.0552	0.0499
	1/n	0.8789	0.9157	0.7241	0.7036
	R^2	0.9936	0.9995	0.9976	0.9904
BET theory	K_{BET}	-0.4981	-1.7127	0.8663	0.5803
	A_∞, mg/l	-1.8126	-0.4610	0.8481	0.6141
	R^2	0.2037	0.8642	0.0447	0.1295

Conclusion

The method of obtaining composite materials based on orange and pomegranate peels was developed. Sorbents based on orange and pomegranate peels modified by PEG were used to remove Zn (II) and Cu (II) ions from water and the following conclusions were made:

1. It has been established that the modification of fruit peels by polyethylene glycol (PEG) increases their sorption activity in comparison to the initial peels. The degree of removal of Zn^{2+} and Cu^{2+} ions by the modified orange peel reaches (80 ± 4) %. In case of modified PP the removal degree of Zn^{2+} ions is (80 ± 3) % and of Cu^{2+} ions is (70 ± 5) %.

2. Based on study results the optimal concentration of PEG (0.1 %) and optimal mass of sorbents (2 g for OP+PEG and 2.5 g for PP+PEG) were determined.

3. For the description of process mechanism Langmuir, Freundlich and BET model isotherms were used. The most applicable was Freundlich theory, at which the correlation coefficients were equal to $R^2 = 0.9936$ (OP-PEG-Zn), $R^2 = 0.9995$ (OP-PEG-Cu), $R^2 = 0.9976$ (PP-PEG-Zn) and $R^2 = 0.9904$ (PP-PEG-Cu). It means that the adsorption process goes on a heterogeneous surface with uneven filling and multilayers of adsorbates are formed.

References

1 Malkin P. (2018) Wastewater treatment from heavy metal ions using nanoactivated complexes of natural zeolite and diatomite. Nanotechnologies in Construction, vol. 10, no. 2, pp. 21–41. https://doi.org/10.15828/2075-8545-2018-10-2-21-41.

2 Osokin V.M., Somin V.A. (2013) Research on the production of new sorbents from plant materials for water purification [Issledovanija po polucheniju novyh sorbentov iz rastitel'nogo syr'ja dlja ochistki vody]. Polzunovsky Bulletin [Polzunovskij Vestnik], no. 1, pp. 280–282.

3 Czikkely M., Neubauer E., Fekete I., Ymeri P., Fogarassy C. (2018) Review of heavy metal adsorption processes by several organic matters from wastewaters. Water-Sui., vol. 10, no. 10. https://doi.org/10.3390/w10101377.

4 Ince M., Ince O.K. (2017) An overview of adsorption technique for heavy metal removal from water / wastewater: A critical review. International Journal in Physical and Applied Sciences, vol. 3, no. 2, pp. 10–19. https://doi.org/10.29132/ijpas.372335.

5 Prabhu P.P., Prabhu B. (2018) A Review on Removal of Heavy Metal Ions from Waste Water Using Natural/Modified Bentonite. Matec Web Conf., vol. 144, pp. 1–13. https://doi.org/10.1051/matecconf/201714402021.

6 Ravindra K. Gautam, Sanjay K. Sharma, Suresh Mahiya, Mahesh C. Chattopadhyaya (2015) Chapter 1. Contamination of Heavy Metals in Aquatic Media: Transport, Toxicity and Technologies for Remediation. Heavy Metals In Water, pp. 1–24. https://doi.org/10.1039/9781782620174-00001.

7 Lim A.P., Aris A.Z. (2014) A Review on Economically Adsorbents on Heavy Metals Removal in Water and Wastewater. Rev Environ Sci Bio., vol. 13, no. 2, pp. 163–181. https://doi.org/10.1007/s11157-013-9330-2.

8 Pathak P.D., Mandavgane S.A. (2015) Fruit Peel Waste as a Novel Low-Cost Bio Adsorbent. Rev Chem EngG., vol. 31, no. 4, pp. 361–381. https://doi.org/10.1515/revce-2014-0041.

9 Redinova A.V., Grabelnykh V.A., Levanova E.P., Korchevin N.A. (2013) Extraction of heavy metal ions from aqueous solutions by sulfur-containing polymer sorbents [Izvlechenie ionov tjazhelyh metallov iz vodnyh rastvorov serosoderzhashhimi polimernymi sorbentami]. Bulletin of Irkutsk State Technical University [Vestnik Irkutskogo gosudarstvennogo tehnicheskogo universiteta], vol. 72, no. 1, pp. 113–116.

10 Bonilla-Petriciolet A., Mendoza-Castillo D.I., Reynel-Ávila H.E. (2017) Adsorption Processes for Water Treatment and Purification. Springer. ISBN 978-331-95-8136-1.

11 Bharat S., Manchanda D. (2017) Efficient Bio Adsorbents for Removal of Heavy Metals from Water: A Review. Internatonal Journal of Chemical Studies, vol. 5, no. 4, pp. 1691–1694.

12 Bobade V., Eshtiagi N. (2015) Heavy Metals Removal from Wastewater by Adsorption Process: A Review. Proceedings of APCChE 2015 Congress Incorporating Chemeca 2015. Melbourne, Victoria, pp. 312–317.

13 Hlihor R. M., Gavrilescu M. (2009) Removal of Some Environmentally Relevant Heavy Metals Using Low-Cost Natural Sorbents. Environ Eng Manag J., vol. 8, no. 2, pp. 353–372. https://doi.org/10.30638/eemj.2009.051.

14 Kanyal M., Bhatt A.A. (2015) Removal of Heavy Metals from Water (Cu and Pb) Using Household Waste as an Adsorbent Bior Emediation & Biodegradation. Journal of Bioremediation & Biodegradation, vol. 6, no. 1, pp. 1–6. https://doi.org/10.4172/2155-6199.1000269.

15 Jacques R.A., Lima E.C., Dias S.L.P., Mazzocato A.C., Pavan F.A. (2007) Yellow Passion-Fruit Shell as Biosorbent to Remove Cr (III) and Pb (II) from Aqueous Solution. Sep Purif Technol., vol. 57, no. 1, pp. 193–198. https://10.1016/j.seppur.2007.01.018.

16 Memon J.R., Memon S.Q., Bhanger M.I., El-turki A., Hallam K.R., Allen G.C. (2009) Colloids and Surfaces B: Biointerfaces Banana Peel: A Green and Economical Sorbent for the Selective Removal of Cr (VI) from Industrial Wastewater. Colloid Surface B., vol. 70, no. 2, pp. 232–37. https://doi.org/10.1016/j.colsurfb.2008.12.032.

17 Jimoh A., Saka A.A., Afolabi A.S. (2013) Development of Adsorbent from Banana Peel for Wastewater Treatment. Appl Mech Mater., vol. 248, pp. 310–315. https://doi.org/10.4028/www.scientific.net/AMM.248.310.

18 Annadurai G., Juang R.S., Lee D.J. (2003) Adsorption of Heavy Metals from Water Using Banana and Orange Peels. Water Sci Technol., vol. 47, no. 1, pp. 185–190. https://doi.org/10.2166/wst.2003.0049.

19 Schiewer S., Balaria A. (2009) Biosorption of Pb^{2+} by Original and Protonated Citrus Peels: Equilibrium, Kinetics, and Mechanism. Chem Eng J., vol. 146, no. 2, pp. 211–219. https://doi.org/10.1016/j.cej.2008.05.034.

20 De Souza J.V.T.M., Diniz K.M., Massocatto C.L., Tarley C.R.T., Caetano J., Dragunski D.C. (2012) Removal Of Pb (II) From Aqueous Solution With Orange Sub-Products Chemically Modified As Biosorbent. Bioresources, vol. 7, no. 2, pp. 2300–2318. https://doi.org/10.15376/biores.7.2.2300-2318.

21 Amin M.T., Alazba A.A., Amin M.N. (2017) Absorption Behaviours of Copper, Lead, and Arsenic in Aqueous Solution Using Date Palm Fibres and Orange Peel: Kinetics and Thermodynamics. Pol J Environ Stud., vol. 26, no. 2, pp. 543–557. https://doi.org/10.15244/pjoes/66963.

22 Shartooh S.M., Al-Azzawi M.N.A., Al-Hiyaly S.A.K. (2013) Pomegranate Peels as Biosorbent Material to Remove Heavy Metal Ions from Industerial Wastewater. Iraqi Journal of Science., vol. 54, no. 4, pp. 823–831.

23 Zainab Abdulrazak N. (2016) Pomegranate Peel As A Sorbent In The Removal Of Pb (II) From Wastewater. Journal of Engineering and Sustainable Development, vol. 20, no. 03, pp. 25–35.

24 Rifaqat Ali Khan Rao. (2015) Adsorption of Heavy Metal Ions on Pomegranate (Punica Granatum) Peel: Removal and Recovery of Cr (VI) Ions from a Multi-Metal Ion System. Adsorpt Sci Technol., vol. 28, no. 3, pp. 195–211. https://doi.org/10.1260/0263-6174.28.3.195.

25 Seilkhanova G.A., Imangaliyeva A.N., Mastai Y., Rakhym A.B. (2019) Bentonite polymer composite for water purification. B Mater Sci., 42:60. https://doi.org/10.1007/s12034-019-1752-1.

I.Yu. Silachyov iD

Institute of Nuclear Physics, Almaty, Kazakhstan
e-mail: silachyov@inp.kz

Instrumental neutron activation analysis of rhenium in uranium raw material

Abstract. The application of comparator instrumental neutron activation analysis combined with the internal standard method was considered to study rhenium content of the uranium raw material core samples collected in Chu-Sarysu uranium province in the Southern Kazakhstan. Iron content of the samples as the internal comparator was determined by X-ray fluorescence analysis with the help of a laboratory energy dispersive X-ray spectrometer. Rhenium was analyzed by its long-lived radionuclide [186]Re using a planar type HPGe detector. Six certified reference materials of complex ores and non-ferrous metal concentrates were analyzed to verify the accuracy of the method. Rhenium and its main interfering elements were determined in the samples from three different sites of the uranium province. Due to reverse correlation dependence, selenium was found as a simple predictor of industrially significant rhenium contents. The method can be used to analyse rhenium mass fractions more than ≈0.02 mg/kg in the ores with uranium content of the samples not exceeding several hundreds mg/kg.
Key words: Neutron activation analysis, internal standard, rhenium, uranium ore.

Introduction

Rhenium, a valuable element for modern industry, belongs to the scattered element group and does not form its own deposits. Main raw material sources of rhenium by-product extraction in the world are molybdenum, copper-molybdenum porphyry ores and cupreous sandstones [1, 2]. Alternative rhenium industrial sources include copper pyrite and copper nickel fields, carbonaceous rocks, coals, liquid carbohydrates and some other objects [3]. In recent times the "blanket oxidation zone deposits" or "sandstone type deposits" were related to an important non-traditional rhenium source [2]. Such zones are well known in the world due to localization of the bedded infiltration uranium deposits which are worked out everywhere by underground leaching [4]. In Kazakhstan the numerous sandstone uranium deposits are localized within the Near Tien Shan uranium mega-province including Chu-Sarysu and Syr Darya uranium basins [5, 6]. Uranium ores of the province are distinguished by their complex character and contain a range of rare elements, but mainly in low contents.

Rhenium content in the Southern Kazakhstan uranium basins corresponds to sundry degree of knowledge. The study for associated elements during uranium deposit exploration was carried out in different time (including several decades ago), by the methods differing in their sensitivity, using individual or combined core samples. In some deposits rare elements were not determined at all [7]. However, in view of the continuing search and exploration of new uranium fields by JSC "NAC Kazatomprom" to promote uranium branch in Kazakhstan, development of simple up-to-date methods of rhenium analysis became vital now to predict the scopes of its by-product production.

A lot of methods of rocks and mineral raw material analysis for rhenium content are known at present [8]. Most of them suffer from insufficient sensitivity and poor selectivity. To overcome these disadvantages sample decomposition with subsequent rhenium preconcentration and separation from the matrix is used in spectrophotometric methods and X-ray fluorescence (XRF) analysis [8, 9]. Widely used inductively coupled plasma atomic emission spectrometry offers better sensitivity, but rhenium analytical lines are partly overlapped with the lines of concomitant elements [10, 11]. Mass spectrometry with inductively coupled plasma (ICP-MS) is one of the most sensitive methods of rhenium determination, but this advantage can be reached only after rhenium quantitative separation of the matrix using some way or another [12-14].

Moreover, ICP-MS is usually affected by matrix effects, isobaric interferences and signal drift.

Sample decomposition with subsequent rhenium preconcentration additionally complicated by high volatility of rhenium compounds is the most serious drawback of all the methods above. In this respect non-destructive neutron activation analysis as one of the most sensitive methods of trace element determination is an attractive option. However, the application of its instrumental variant (INAA) is restricted by low rhenium contents of geological samples and high matrix activity. Preliminary rhenium concentration can be used in this case [15, 16], but the necessity in supra pure reagents makes the method not in current use. Radiochemical neutron activation analysis (RNAA) based on ion-exchange chromatographic separation is far more prevalent, when rhenium is determined together with platinum group elements [17-19].

In this work comparator INAA using the XRF-based internal standard method and iron content of the samples as the internal comparator [20, 21] was tried to analyze rhenium content of the uranium ore core samples collected from several sites of the Shu-Sarysu uranium province in the Southern Kazakhstan.

Materials and methods

A great number of grinded ore samples studied by gamma-ray spectrometric method were preliminary inspected. The samples with the uranium content of no more than ≈300 mg/kg were selected based on the previous experience [22] to prevent counting and other problems. The chosen samples were then analyzed by XRF technique using an energy dispersive spectrometer RLP-21T by JSC "AspapGeo" (Almaty, Kazakhstan) for iron mass fraction as an internal standard to realize comparator INAA [20]. The spectrometer was designed to analyze rocks, ores, concentrates and so on. The accuracy of its software was repeatedly confirmed with the help of different corresponding certified reference materials (CRMs). The ascribed uncertainty of iron content measuring in rock samples is 2–8%. RLP-21T is enrolled in the State Register of Measuring Devices, and the corresponding analytical technique is registered by the National Body for Certification of Kazakhstan.

INAA of the same samples for rhenium and some other element contents by the long-lived radionuclides was then carried out. About 100 mg of the assays divided into several parties were sealed in small thin double polyethylene bags and packed in aluminium foil. There wasn't any need in sample precise weighing using an analytical balance since an independent method to determine the internal comparator content was applied. Every package included ten samples and a zirconium monitor to evaluate epithermal to thermal neutron flux ratio (10 mg of ZrO_2). Package length was about 10 mm.

All the packages were irradiated in different days for 2.5 hours in the position № 4 inside the water channel № 10-6 of the research reactor WWR-K by thermal neutron (< 0.625 eV) flux density 8.9×10^{13} cm^{-2} s^{-1}; the fast neutron (0.1–1.15 MeV) flux density amounted to 6.0×10^{12} cm^{-2} s^{-1} [23]. To reduce the influence of neutron flux gradient, the packages were oriented along the channel axis.

Direct rhenium determination by the long-lived radionuclide ^{186}Re in rocks is highly impeded by substantial spectral interferences from hafnium, selenium and sometimes from other elements (ytterbium). Since ^{186}Re spectrum is characterized by the single analytical gamma-line, its count rate can be hardly measured correctly using a coaxial type semiconductor detector due to its insufficient resolution. That is why a planar type detector was preferred notwithstanding its far lower total efficiency.

The irradiated samples were counted by a planar HPGe detector GLP36360 with the crystal dimensions 36×13 mm and an energy resolution of 585 eV at the 122 keV peak of ^{57}Co connected to an ORTEC multi-channel analyzer DSPEC LF. Spectra collection was carried by the MAESTRO software. Detector calibration for relative detection efficiency was made with the help of a multi-gamma ray standard (^{152}Eu, ^{154}Eu, ^{155}Eu) and an isotopic source ^{133}Ba, both by Canberra. Before measuring rhenium content of the samples, 9–12 days of the decay time elapsed to make radionuclide ^{24}Na almost completely decayed and Compton background from uranium fission products essentially reduced. This made possible to use very close counting geometry – 10 mm to the detector cap. The approximate time of spectra collection was 30–60 minutes. The first counting was also used to evaluate ytterbium and uranium contents. The samples were counted once again a fortnight later to determine selenium and hafnium mass fractions.

Spectra treatment was carried out by the "AnalGamma" software developed in the Institute of Nuclear Physics to provide gamma-ray spectrometric analysis. The software approximates a part of gamma-ray spectrum in the treatment

window by Gaussian curves and a flat background and calculates peak count rates J in cps. Partly overlapping peaks can be reliably resolved. Quality of the approximation is checked by the χ^2 test. Then the other software converts J values of the analytical peaks into the element contents C_a of the samples.

C_a values (%) were calculated according to the next model based on the single comparator method (SCM) of standardization [24] using the internal standard method [20] (lower case indices a and c mean an analyzed element and the comparator, respectively):

$$C_a = C_c \frac{k_c N_{p,a} \varepsilon(E_c)(f + Q_0^c)(SDC)_c G_c F_c}{k_a N_{p,c} \varepsilon(E_a)(f + Q_0^a)(SDC)_a G_a F_a} K_{a,c} , \qquad (1)$$

where C_c is the element comparator content of the sample (%), N_p is net peak area of the measured gamma-line (cps), $\varepsilon(E)$ is the relative detection efficiency of the measured gamma-line (%), Q_0 is the resonance integral I_0 (cm^2) to thermal neutron cross-section σ_0 (cm^2) ratio, f is the thermal to epithermal neutron flux ratio, $S = 1 - \exp(-\lambda t_{irr})$ is saturation factor, $D = \exp(-\lambda t_d)$ is decay factor, $C = (1 - \exp(-\lambda t_m))/\lambda t_m$ is the counting factor (t_{irr}, t_d, and t_m are irradiation, decay and measuring time), G is the correction factor for neutron self-shielding by the sample, F is the correction factor for analytical gamma-ray self-absorption by the sample, and the k-factor is composed of nuclear constant product:

$$k = \sigma_0 \theta P_\gamma M^{-1} , \qquad (2)$$

where θ is isotopic abundance (%), P_γ is the yield of the measured gamma-line (%), M is the atomic mass (Da).

The empirical correction factor $K_{a,c}$ accessed by the CRMs is used to compensate for a bias caused by the errors of the detector calibration and other reasons and to adjust the model for the specific counting geometry. That is why there is no need both in α-parameter to correct I_0 for nonideal epithermal neutron flux distribution, and in J correction for true coincidences.

Correction factors G is ignorable for the 100 mg uranium ore samples not distinguished by high contents of rare earths or other elements with anomalous σ_0 values. Coefficient F is very close to unity in case of rock analysis since there is no appreciable self-absorption of ^{186}Re analytical gamma-line (137.16 keV) in a thin ($<$ 1 mm) light source such as an aluminum-siliceous matrix.

The model ratio of $1/f$ was evaluated by the "bare bi-isotopic method" [25] with the help of a monitor of the neutron flux spectral composition – a ZrO$_2$ sample [20]:

$$\frac{1}{f} = \frac{\sigma_{0.2} - B\sigma_{0.1}}{BI_{0.1} - I_{0.2}} ,$$

$$B = \frac{N_{p,2} \varepsilon(E_1) \theta_1 P_{\gamma,1} (SD)_1}{N_{p,1} \varepsilon(E_2) \theta_2 P_{\gamma,2} (SD)_2} , \qquad (3)$$

where lower indices 1 and 2 correspond to two Zr isotopes ($Q_{0.1} \ll Q_{0.2}$). C factor in Eq. 3 is ignorable due to a very short counting time. The ratio can be simply reevaluated for every irradiation. During the investigation the resonance to thermal neutron flux ratio in the irradiation position varied within 0.028–0.034.

Table 1 – Main nuclear data used to calculate rhenium, its interfering elements and uranium by comparator INAA

Activated isotope	Isotopic abundance, %	σ_0, cm^2	I_0, cm^2	Target radionuclide	Half-life, days	Energy, keV	Quantum yield, %
^{185}Re	37.4	110	1694	^{186}Re	3.72	137.16	9.47
^{74}Se	0.89	51.8	545.4	^{75}Se	119.8	136.00	58.3
^{180}Hf	35.2	13.5	34	^{181}Hf	42.39	133.02 136.26 136.86	43.3 5.85 0.86
^{174}Yb	31.8	63.4	29.2	^{175}Yb	4.19	396.33 137.66	13.2 0.235
^{238}U	99.28	2.68	277	^{239}Np(^{239}U)	2.36	277.60	0.144
^{58}Fe	0.28	1.28	1.25	^{59}Fe	44.50	192.34	3.08

The main nuclear data used to calculate rhenium content (including iron as the internal standard) and to evaluate interfering element contents are presented in Table 1 [26]. [181]Hf and [175]Yb spectral interferences to [186]Re are tabulated as well. Uranium was enrolled too since its mass fraction is one of the basic restrictions of the approach.

Results and discussion

To assess accuracy of rhenium determination by comparator INAA, several CRMs of complex ores and non-ferrous metal concentrates certified for rhenium content were used (Table 2). OSO 528 was produced by the All-Russian Scientific-research Institution of Mineral Resources (FSBI VIMS), Moscow, and the other five – by JSC "Tsentrgeolanalit", Republic of Kazakhstan. The CRM samples were prepared, irradiated and analyzed as described above. To avoid overirradiation and diminish gamma-ray self-absorption, the sample mass of concentrate and uranium ore CRMs was diminished to 30–50 mg. A single measurement of each CRM was carried out.

The first three CRMs are characterized by rather low content of the main elements impeding rhenium determination. [186]Re analytical gamma-line is distinctly resolved from a ^{75}Se gamma-line (136.00 keV) and from a rather intensive [181]Hf gamma-line (136.26 keV, $P_\gamma = 5.85\%$). Contribution of a 136.26 keV low-intensive [181]Hf gamma-line ($P_\gamma = 0.86\%$) is simply taken into account with another one (133.02 keV, $P_\gamma = 43.3\%$). Corrections to [186]Re count rate

(137.16 keV) appeared rather small, within 1.5–3.5%. The same is true for OSO 528 too, but a partly resolved low-intensive gamma-line of [175]Yb (137.66 keV, $P_\gamma = 0.235\%$, $C_{Yb} = 40.2$ mg/kg) in the spectrum of this CRM with the enhanced rare-earth contents makes the result less reliable.

The samples of concentrates are practically deprived of hafnium and selenium according to their gamma-spectra but contain high contents of heavy metals: 61% of lead in GSO 2890 and 40.4% of copper in GSO 2891, both apart from some minor contents of another heavy elements. For these CRMs the self-absorption correction (Eq. 1) was estimated in the approximation of a thin irradiating layer:

$$\frac{F_c}{F_a} = \frac{\mu(E_a)(1-\exp(-\rho\mu(E_c)d))}{\mu(E_c)(1-\exp(-\rho\mu(E_a)d))}, \quad (4)$$

where $\mu(E)$ is photon mass attenuation coefficient (cm^2 g^{-1}); ρ is sample density (g sm^{-3}) and d is sample thickness (cm). $\mu(E)$ values of [186]Re and ^{59}Fe analytical gamma-lines in different matter were picked up from a NIST database [27]. Sample bulk density having been independently evaluated, the self-absorption correction appeared about 10% in case of lead concentrate analysis and no more than 1% for copper one. Such moderate corrections resulted from both application of the internal standard method and not too far difference between E_a (137.16 keV) and E_c (192.34 keV).

Relative expanded uncertainty of the INAA results was estimated as follows ($P = 0.95$):

$$\frac{U(C_a)}{C_a} \approx 2\sqrt{\frac{u(J_a)^2}{J_a^2} + \frac{u(J_c)^2}{J_c^2} + \frac{u(C_c)^2}{C_c^2} + s_a^2}, \quad (5)$$

where $u(J_a)$, $u(J_c)$, and $u(C_c)$ are standard uncertainties of the corresponding values as in Eq. 1, s_a is the standard deviation of element analysis (methodical uncertainty) by SCM (all the ratios and s_a are in %). The last value assessed earlier with the help of the CRMs equals ≈4%. Standard uncertainty of iron internal comparator content of a sample by XRF corresponded to the ascribed values according to the certified analytical technique.

The results of CRM analyses for rhenium content by comparator INAA using Eq. 1 and Eq. 2 ($P = 0.95$) are presented in Table 2. Iron content of

the samples was determined by XRF. The measured values are well comparable with the certified ones with < 4% of discrepancy.

On the other hand, E_n-number usually used as a recommended by IUPAC criterion to verify laboratory performance [28] also showed good agreement between all certified and measured values within acceptable value ±1 (Table 2).

So the demonstrated accuracy of rhenium determination in a range of CRMs by comparator INAA enabled to try this approach for real geological samples.

Table 2 – Rhenium content of CRMs by comparator INAA using iron as the internal standard ($P = 0.95$)

CRM number	CRM type	Fe, %	Re, mg/kg		E_n-number
			Certified value	Measured value	
GSO 3029	Copper porphyritic ore	2.99 ± 0.17	0.43 ± 0.02	0.430 ± 0.044	0
GSO 3030	Copper molybdemum scarn ore	13.61 ± 0.45	0.30 ± 0.02	0.291 ± 0.030	-0.25
GSO 3031	Copper molybdemum scarn ore	15.31 ± 0.45	0.40 ± 0.03	0.394 ± 0.040	-0.12
OSO 528	Phosphorus rare earth uranium ore	15.53 ± 0.45	0.79 ± 0.04	0.82 ± 0.11	0.26
GSO 2890	Lead concentrate	1.393 ± 0.081	21.4 ± 1.0	21.2 ± 2.8	0.13
GSO 2891	Copper concentrate	5.84 ± 0.30	28.2 ± 1.2	27.8 ± 3.3	-0.11

Tables 3–5 presents the results of rhenium and two its main interfering element contents by comparator INAA ($P = 0.95$) of the uranium ore core samples collected from three different sites of the Shu-Sarysu uranium province. Ytterbium contents as a possible interfering element were evaluated as well. Iron mass fractions by XRF are presented with the ascribed uncertainties corresponding to the certain intervals of iron contents. Uranium mass fraction was determined by its daughter long-lived radionuclide [239]Np using iron content of the samples, as the other elements.

Eight of ten samples from site I (Table 3) revealed rhenium contents up to 0.3 mg/kg. Low mass fraction of the interfering elements not far differing from their Clarke (crust average) contents didn't hinder from rhenium determination. In two samples, with selenium contents exceeding its Clarke value (0.05 mg/kg) by three orders of magnitude, rhenium wasn't found. The upper assessment of rhenium content of these two samples approximately corresponds to its limit of identification (lowest content that can be safely detected, LOI) as double limit of detection (LOD) [29]. The latter was estimated in the way commonly used in spectroscopic methods: LOD ≈ three counting statistics of total background counts at the peak area.

Table 3 – Rhenium, uranium, internal standard, and interfering element content of the uranium ore samples from site I ($P = 0.95$)

Sample number	Re, mg/kg	Se, mg/kg	Hf, mg/kg	Yb, mg/kg	U, mg/kg	Fe, %
556	0.059 ± 0.009	1.88 ± 0.28	3.35 ± 0.33	1.74 ± 0.19	170 ± 17	0.988 ± 0.080
561	0.095 ± 0.014	< 0.2	2.72 ± 0.29	1.50 ± 0.18	188 ± 19	0.556 ± 0.080
571	0.308 ± 0.034	< 0.2	6.00 ± 0.53	2.30 ± 0.25	187 ± 19	1.818 ± 0.081
576	< 0.02	46.5 ± 4.2	3.00 ± 0.30	1.31 ± 0.13	304 ± 30	0.758 ± 0.080
597	0.043 ± 0.009	< 0.2	1.37 ± 0.15	0.84 ± 0.11	199 ± 20	0.472 ± 0.048
600	0.020 ± 0.007	0.21 ± 0.07	3.02 ± 0.30	1.84 ± 0.23	245 ± 25	0.619 ± 0.080
608	0.174 ± 0.023	1.33 ± 0.21	2.93 ± 0.29	2.73 ± 0.32	234 ± 24	0.698 ± 0.080
628	0.182 ± 0.022	< 0.2	6.27 ± 0.61	3.43 ± 0.35	106 ± 11	2.89 ± 0.17
630	0.016 ± 0.006	1.90 ± 0.30	6.43 ± 0.64	3.58 ± 0.35	133 ± 13	3.07 ± 0.17
649	< 0.02	198 ± 19	3.29 ± 0.30	1.36 ± 0.13	208 ± 21	0.654 ± 0.080

Almost in all samples from site II (Table 4) rhenium contents appeared lower their LOI and accompanied by very high selenium contents, with the exception of № 316. As for site I, increased rhenium mass fraction of the sample agrees with selenium content lower LOI of the latter.

A part of gamma-ray spectrum of sample № 316 counted for 30 minutes after 10 days of decay is presented in Fig. 1 in a log-linear scale. It displays clearly that [186]Re background/peak ratio is quite enough to obtain reliable results in case of even far lower rhenium contents. This ratio substantially depends on the intensities of some gamma-lines of [239]Np and the uranium fission products (including not shown in Figure 1). The dependence increases sharply with the uranium mass fraction growth. [186]Re half-life is comparable with that of [239]Np, [99]Mo, [140]La and less than the half-lives of [141]Ce, [147]Nd, ^{131}I, and [140]Ba. That's why, to gain the best sensitivity, there should be a minimum decay time to make possible

counting in a close geometry. Decay time is assessed empirically and in case of uranium content no more than 250 mg/kg begins from 8-9 days, actually right after [24]Na has practically decayed.

[59]Fe gamma-peak of sample № 316 ($C_{Fe} = 2.31\%$) is not too expressed against background (Figure 1) but its count rate is enough to use it as the internal standard.

Table 4 – Rhenium, uranium, internal standard, and interfering element content of the uranium ore samples from site II ($P = 0.95$)

Sample number	Re, mg/kg	Se, mg/kg	Hf, mg/kg	Yb, mg/kg	U, mg/kg	Fe, %
232	< 0.03	401 ± 40	3.40 ± 0.34	1.94 ± 0.25	202 ± 20	0.587 ± 0.080
241	< 0.03	955 ± 83	5.21 ± 0.52	2.31 ± 0.27	115 ± 12	1.500 ± 0.081
254	< 0.05	2460 ± 220	3.82 ± 0.38	1.48 ± 0.19	192 ± 19	1.161 ± 0.081
265	< 0.04	968 ± 97	4.41 ± 0.44	1.73 ± 0.21	180 ± 18	1.180 ± 0.081
268	< 0.03	265 ± 23	2.39 ± 0.24	1.81 ± 0.19	134 ± 14	6.39 ± 0.30
291	< 0.03	420 ± 42	3.16 ± 0.32	1.36 ± 0.18	212 ± 22	0.855 ± 0.080
304	< 0.02	173 ± 16	3.61 ± 0.36	1.77 ± 0.19	160 ± 16	2.60 ± 0.17
308	< 0.05	2730 ± 230	1.67 ± 0.25	2.78 ± 0.37	162 ± 17	18.79 ± 0.45
316	0.738 ± 0.075	< 0.2	5.81 ± 0.51	4.02 ± 0.43	142 ± 14	2.31 ± 0.17
324	< 0.03	936 ± 94	2.29 ± 0.26	1.09 ± 0.14	1.77 ± 0.19	0.891 ± 0.080
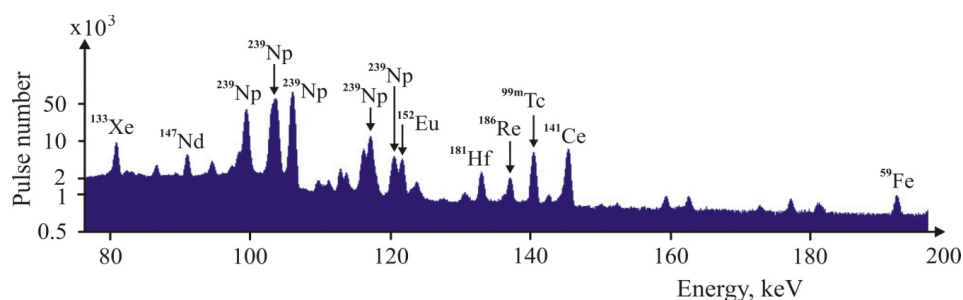
Figure 1 – A part of gamma-ray spectrum of uranium ore sample № 316
counted by GLP36360 (in log-linear scale)
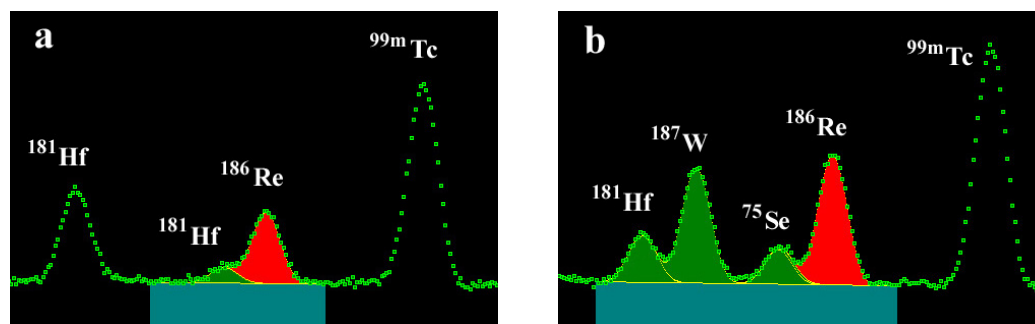
Figure 2 – net peak area of [186]Re and adjacent radionuclides
in "AnalGamma" treatment window: sample № 316 (a) and № 10 (b)

The zoomed fragment of the spectrum № 316 in the vicinity of [186]Re 137.16 keV gamma-line is shown in more details in Figure 2(a) in the treatment window of the "AnalGamma" software. Only rhenium and hafnium (136.26 keV) gamma-lines were approximated by Gaussian curves. The

treatment interval is marked by a different colour.

Site III (Table 5) appeared the most promising among the studied three with respect to the rhenium content. All the ten samples revealed surely quantitative rhenium mass fractions and two of them – more than 1 mg/kg. Selenium content is lower its

LOI or not too high comparing with the samples from site II.

Figure 2(b) presents the treatment area including rhenium gamma-line for the sample № 10. The spectrum counted for 20 minutes after 8 days of decay is distinguished by a distinct gamma-line of ^{187}W (134.25 keV). This is an atypical situation since only several samples contained tungsten among the dozens of the investigated ones. The presence of ^{187}W gamma-line changed practically nothing, but in the cases of its much higher intensities the decay time should be apparently increased to get a reliable net peak area of ^{181}Hf (to take into account its contribution to ^{186}Re count rate). Rather moderate ^{75}Se gamma-line is surely resolved with the ^{186}Re one and doesn't hinder rhenium determination.

Table 5 – Rhenium, uranium, internal standard, and interfering element content of the uranium ore samples from site III ($P = 0.95$)

Sample number	Re, mg/kg	Se, mg/kg	Hf, mg/kg	Yb, mg/kg	U, mg/kg	Fe, %
1	0.232 ± 0.032	< 0.2	3.43 ± 0.35	1.01 ± 0.13	159 ± 16	0.247 ± 0.048
10	1.27 ± 0.14	11.8 ± 1.2	2.52 ± 0.25	0.74 ± 0.09	131 ± 13	2.43 ± 0.17
24	0.399 ± 0.052	< 0.2	6.73 ± 0.67	2.29 ± 0.30	215 ± 22	0.576 ± 0.080
25	0.478 ± 0.062	< 0.2	9.40 ± 0.94	1.62 ± 0.22	191 ± 19	0.610 ± 0.080
48	0.707 ± 0.092	< 0.2	3.43 ± 0.37	1.57 ± 0.22	251 ± 25	0.420 ± 0.048
51	0.046 ± 0.06	40.8 ± 4.9	6.08 ± 0.66	1.38 ± 0.14	180 ± 18	0.309 ± 0.048
73	2.90 ± 0.30	< 0.2	6.62 ± 0.66	4.10 ± 0.45	133 ± 13	2.23 ± 0.17
81	0.95 ± 0.12	2.49 ± 0.39	14.5 ± 1.4	1.69 ± 0.23	162 ± 16	0.722 ± 0.080
88	0.116 ± 0.018	< 0.2	4.50 ± 0.45	0.88 ± 0.12	219 ± 22	0.670 ± 0.080
529	0.663 ± 0.073	8.51 ± 0.77	1.85 ± 0.18	1.02 ± 0.13	137 ± 14	0.459 ± 0.048

To verify the noticed reverse dependence between rhenium and selenium contents a range of uranium ore samples from another two sites located in Chu-Sarysu and Syr Darya provinces were additionally investigated using the same approach. With rhenium mass fraction of the samples amounting to 0.65 mg/kg, this relationship was confirmed. The whole pattern including all the studied samples is depicted graphically in Fig. 3 in regular and semi-logarithmic coordinates. LOI assessments were replaced by numerical values. To avoid negative magnitudes of common logarithms, selenium contents (in mg/kg) were multiplied by ten.
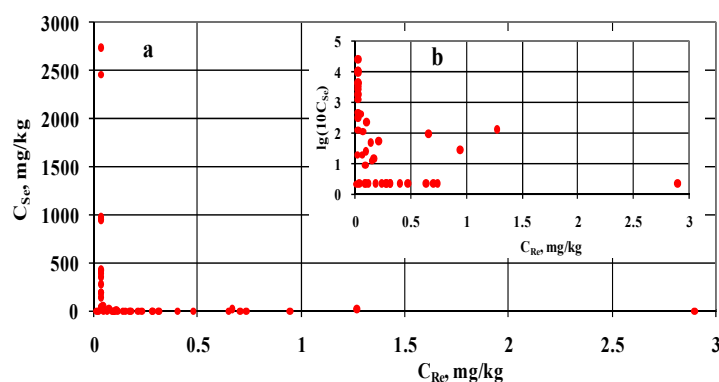
Figure 3 – Interrelation between rhenium and selenium contents in the uranium samples in regular (a) and semi-logarithmic (b) scales

As Figure 3 demonstrates the following prognostic feature may be apparently applied. Rhenium can not be obviously found in the samples characterized by very high selenium content, more than a hundred mg/kg. (It corresponds to 3 in Figure 3(b)). All the samples with selenium mass fraction lower than approximately 50 mg/kg are considered as relevant ones. Only these samples should be

investigated by INAA. Preliminary screening can be carried out by a prompt method, i.e. XRF.

As this investigation revealed, high uranium content of the samples evidently presents main drawback for INAA. Neither of the elements (hafnium, selenium or any other) making unacceptable a coaxial type detector doesn't impede seriously rhenium determination in case a planar detector is applied. Several hundreds mg/kg are apparently the uranium maximum content making possible conducting analysis under the conditions above (neutron flux density, sample mass, and irradiation time). The gained limit of rhenium identification in the investigated samples doesn't exceed 0.05 mg/kg. This value corresponds to the accessed industrially significant rhenium content of complex ores as a by-product [30].

If uranium content is higher than $\approx$ 300 mg/kg, as of the vast majority of the previewed samples, to implement INAA sample mass or irradiation time must be inevitably reduced. But this sharply diminishes sensitivity and accuracy of the methods. Beginning from some uranium content, preliminary rhenium concentration or radiochemical NAA can be the only option.

Conclusion

Comparator INAA using a planar type HPGe detector and iron as the internal standard proved its applicability to determine industrially significant contents of rhenium as a by-product in a part of uranium ore samples collected from Southern Kazakhstan uranium provinces. Distinct reverse correlation between rhenium and selenium mass fractions makes possible to apply XRF both for iron analysis and relevant sample selection to conduct INAA afterwards. Rhenium contents more than (0.02-0.05) mg/kg are available for direct determinations if uranium mass fraction of the samples doesn't exceed several hundreds mg/kg. Otherwise, one or another way of uranium separation must be applied to realize NAA.

Acknowledgments

References

1   Engalychev S.Yu. (2019) New data on the mineral composition of unique rhenium U–Mo–Re ores of the Briketno-Zheltukhinskoe deposit in the Moscow basin. *RAS* [Doklady Akademii nauk], *ser. geol.*, vol. 485(4), pp. 464-467. https://doi.org/ 10.31857/S0869-56524854464-467 (in Russian).

2   Trach G.N., Beskin S.M. (2011) Rhenium resources potential of the Russian territory. *Prospect and Protection of Mineral Resources* [Razvedka i ohrana nedr], vol. 6, pp. 26-33 (in Russian).

3   Troshkina I.D., Shilyaev A.B., Abdrakhmanov T.G., Maiboroda A.B. (2011) Rhenium in non-traditional raw materials: distribution and the possibility of recovery. *Prospect and Protection of Mineral Resources* [Razvedka i ohrana nedr], vol. 6, pp. 87-90 (in Russian).

4   Kremenetskiy A.A., Luneva N.V., Kulikova I.M. (2011) Belskoe Re-Mo-U deposit: mineralogical and geochemical characteristics, conditions of formation, technology of rhenium extraction. *Prospect and Protection of Mineral Resources* [Razvedka i ohrana nedr], vol. 6, pp. 33-41 (in Russian).

5   IAEA-TECDOC-1629   (2009)   World Distribution of Uranium Deposits (UDEPO) with Uranium Deposit Classification. IAEA, Vienna. ISBN: 978-92-0-110509-7.

6   Sushko S.M., Shishkov I.A., Vershkov A.F. (2013) Uranium mining industry in Kazakhstan and the prospects for its development. *News of the Academy of Sciences of RK*, *ser. geol. & tech. sci.*, vol. 401(5), pp. 61-69 (in Russian).

7   Ministry of Industry and Infrastructural Development of the Republic of Kazakhstan. Committee of Geology and Subsoil Use. (accessed May 19, 2020) https://www.info.geology.gov.kz/ ru/informatsiya/spravochnik-mestorozhdenij-kazakhstana/tverdye-poleznye-iskopaemye.

8   Evdokimova O.V., Pechishcheva N.V., Shunyaev K.Yu. (2012) Up-to-date methods for the determination of rhenium. *J Anal Chem*, vol. 67(9), pp.   741-753   https://doi.org/10.1134/ S1061934812090043.

9   Kolpakova N.A., Buinovskii A.S., Mel'nikova I.A. (2009) Determination of rhenium in gold-containing ores by X-ray fluorescence spectrometry. *J Anal Chem*, vol. 64(2), pp. 144-148. https://doi.org/10.1134/S1061934809020099.

10 Karadjov M., Velitchkova N., Veleva O., et al. (2016) Spectral interferences in the determination of rhenium in molybdenum and copper concentrates by inductively coupled plasma optical emission spectrometry (ICP-OES). *Spectrochim Acta*, Part B. vol.   119,   pp.   76-82.   https://doi.org/10.1016/ j.sab.2016.03.011.

11 Evdokimova O., Zaitceva P., Pechishcheva N.V., et al. (2014) The rhenium determination in

copper and molybdenum ores and concentrates by ICP atomic emission spectrometry. *Curr Anal Chem*, vol. 10(4), pp. 449-456. https://doi.org/10.2174/157341101004140701102351.

12 Liu Y., Qi L., Gao J., Huang Z. (2016) Determination of rhenium and osmium by ICP-MS for galena and sphalerite. *Acta Geochim*, vol. 35(1), pp. 43-49. https://doi.org/10.1007/s11631-015-0076-0.

13 Li J., Zhong L.-F., Xu J.-F., et al. (2014) Determination of PGE concentration(s) and Re-Os isotope(s) using ID-ICP-MS and N-TIMS from a single digestion after two-stage column separation. *Geostand Geoanal Res*, vol. 38(1), pp. 37-50. https://doi.org/10.1111/j.1751-908X.2013.00242.x.

14 Pearce C., Cohen A., Parkinson I. (2009) Quantitative separation of molybdenum and rhenium from geological materials for isotopic determination by MC-ICP-MS. *Geostand Geoanal Res*, vol. 33(2), pp. 219-229. https://doi.org/10.1111/j.1751-908X.2009.00012.x.

15 Swain K., Kayasth S. (2007) Preconcentration of traces of rhenium in geological matrix by NAA. *J Radioanal Nucl Chem*, vol. 271(1), pp. 129-131. https://doi.org/1007/s10967-007-0118-0.

16 Wang H., Li J., Chen Y. (1992) Neutron activation analysis of rhenium in rocks after preliminary extraction with acetone. *J Radioanal Nucl Chem*, vol. 161, pp. 227-231. https://doi.org/10.1007/BF02034895.

17 Zinovyev V.G., Ablesimov N.E., Egorov A.I., et al. (2017) Instrumental and radiochemical neutron activation analysis of the quartz adularia veins from the deposit Milogradovka, the Far East, Primorye. *J Radioanal Nucl Chem*, vol. 311(1), pp. 141-153. https://doi.org/10.1007/s10967-016-4948-5.

18 Zinovyev V.G., Egorov A.I., Shulyak G.I., et al. (2016) Neutron activation analysis of the tagamite and suevite from the Kara astrobleme. *J Radioanal Nucl Chem*, vol. 307(2), pp. 1315-1324. https://doi.org/10.1007/s10967-015-4480-z.

19 Dai X., Koeberl C., Fröschl H. (2001) Determination of platinum group elements in impact breccias using neutron activation analysis and ultrasonic nebulization inductively coupled plasma mass spectrometry after anion exchange preconcentration. *Anal Chim Acta*, vol. 436(1), pp. 79-85. https://doi.org/10.1016/S0003-2670(01)00902-3.

20 Silachyov I. (2016) Rare earths analysis of rock samples by instrumental neutron activation analysis, internal standard method. *J Radioanal Nucl Chem*, vol. 310(2), pp. 573-582. https://doi.org/10.1007/s10967-016-4903-5.

21 Silachyov I. (2020) Elemental analysis of vegetation samples by INAA internal standard method. *J Radioanal Nucl Chem*, vol. 324(1), pp. 97-108. https://doi.org/10.1007/s10967-020-07051-6.

22 Silachyov I. Yu. (2018) Determination of rare earths in uranium raw material by neutron activation analysis and X-ray fluorescence. *News of the Academy of Sciences of RK, ser. chem. & technol.*, vol. 429(3), pp. 28-38.

23 Koltochnik S.N., Sairanbayev D.S., Chekushina L.V., et al. (2018) Comparison of neutron spectrum in the WWR-K reactor with LEU fuel against HEU one. *NNC RK Bulletin* [Vestnik NYATS RK], vol. 76(4), pp. 14-17 (in Russian).

24 Kafala S.I., MacMahon T.D. (2007) Comparison of neutron activation analysis methods. *J Radioanal Nucl Chem*, vol. 271(2), p. 507-516. https://doi.org/10.1007/s10967-007-0238-6.

25 Simonits A., De Corte F., Hoste J. (1976) Zirconium as a multi-isotopic flux ratio monitor and a single comparator in reactor-neutron activation. *J Radioanal Nucl Chem*, vol. 31, pp. 467-586.

26 Nuclear data sub-committee. (accessed May 19, 2020) k_0-neutron activation analysis link page. http://www.kayzero.com/k0naa/k0naaorg/Links.html.

27 Hubbell J.H., Seltzer S.M. (accessed May 19, 2020) X-ray mass attenuation coefficients. NIST standard reference database 126. https://www.nist.gov/pml/x-ray-mass-attenuation-coefficients (31.03.2020).

28 Kuzelman I., Fajgelj A. (2010) IUPAC/CITAC guide: Selection and use of proficiency testing schemes for a limited number of participants – chemical analytical laboratories. *Pure Appl Chem*, vol. 82(5), pp. 1099-1135. https://doi:10.1351/PAC-REP-09-08-15.

29 Vogelgesang J., Hädrich J. (1998) Limits of detection, identification and determination: a statistical approach for practitioners. *Accred Qual Assur*, vol. 3, pp. 242-255. https://doi.org/10.1007/s007690050234.

30 Samoilov A.G., Engalychev S.Yu., Zozyrev N.Yu., et al. (2018) Rhenium potential of the Upper Jurassic oil shale in the central part of the Volga Shale Basin. *Regional Geology and Metallogeny* [Regionalnaya geologiya i metallogeniya], vol. 75, pp. 67-78 (in Russian).

Zh. Kassenova

Innovative Eurasian University, Pavlodar, Kazakhstan
e-mail: zhanar.kassenova@gmail.com

Study of the partitioning behaviour
of a quaternary ammonium salt between oil and water phases

Abstract. Partitioning of corrosion inhibitors between oil/ water phases is one of main factors governing the inhibitor performance. It is important for the inhibitor to be dissolved in water phase at a particular concentration in order to provide protection from corrosion. Partitioning behaviour of a quaternary ammonium salt that is widely used as a corrosion inhibitor was studied by carrying out partitioning tests and determining the concentration of the inhibitors by conventional colorimentry method. The tests were performed using various water cuts, hydrocarbon phases, and concentrations in order to find out the effects of these factors. Comparison of partitioning behaviour of the inhibitors in low and high water cut mixtures resulted in some loss of the inhibitor from bulk water phase as water cut decreased. Partitioning of quaternary ammonium compound seems to be dependent on the nature of the hydrocarbon phase. Also, general suggestions about silanisation procedure of glassware were made.

Key words: corrosion inhibitors, partitioning, oil, water cut.

Introduction

Metallic corrosion in its broad meaning can be described as a destructive process of metal caused by its interaction with the environment. The majority of corrosive processes in the Oil and Gas industry incorporate electrochemical reactions. Inhibitors are compounds that are added in a small amount to the system to slow down a chemical reaction. Corrosion inhibitors are used in the Oil and Gas industry as a part of corrosion mitigation program. These chemicals affect the destructive process by retarding the rate of either electrochemical reaction. In practice, the chemicals are used as formulations and complex mixtures rather than a single component. It is done because synergism and cooperation, that enhance protective properties, exist between different inhibitors. Although numerous chemicals that act as inhibitors are known, few of them are utilized in practice. This happens because of environmental legislations, cost, and availability [1].

Oil field inhibitors are usually utilised in a small concentration (<0.1%). Corrosion inhibitor formulations may include up to six individual surface active ingredients, and may contain up to 30% w/w of them. The inhibitors are usually dissolved in a carrier solvent which may be water, hydrocarbon, or alcohol. The solvent makes the inhibitors easier to inject into the system since it reduces their viscosity. Corrosion inhibitors used for petroleum production can be soluble, dispersible, or insoluble in either the oil or water phases. However, the classification is not strict due to the fact that the inhibitors in most cases partition between hydrocarbon and aqueous phases. The examples of preferentially water soluble inhibitors are quaternary amines, amine salts, and salted imidazolines. These chemicals are susceptible to desorption and may lose solubility in high temperatures and in highly mineralised brines respectively [2]. The protective film formed by water soluble inhibitors is not as tenacious as formed by oil soluble inhibitors; therefore, they must be continuously supplied to maintain system protection. Inhibitors that are preferentially oil soluble are primary amines, phosphate esters, fatty acids, and imidazolines [3].

Partitioning behaviour of the corrosion inhibitor is one of the key factors along with efficiency, solubility, optimum concentration, and film stability. Partitioning test is an irreplaceable and highly recognised standard procedure for inhibitor selection, which aims to find out the adequate inhibitor dosage required for injection in total fluids. Ideally, real field

fluids from production sites should be used for the tests [4]. However, clean untreated fluids are not always available. Therefore, sometimes synthetic fluids are prepared in the testing laboratories. Corrosion takes place mainly at the surface, which has a contact with water. Thus, corrosion inhibitors should present in the aqueous phase in order to provide protection. Logically, the practical purpose of any partitioning test is to reach adequate amount of an inhibitor in aqueous phase. Partitioning coefficient is not a fixed value. For instance, the inhibitor distribution depends on water cut, i.e. the ratio of the aqueous phase to the total fluid volume. That is why partitioning test also should include fluids with different water cuts. It is important because in the oil production water cut is not constant and tends to change as time passes. If results from partitioning studies are available, the injection rate of the corrosion inhibitors can be adjusted to the current water cut [5].

The literature review shows that there is a need for an extensive study of partitioning of oil field corrosion inhibitors between oil and water phases under various conditions, for example, different concentrations of the chemicals and water cuts. The aim of the project is to study the partitioning behaviour of an individual corrosion inhibitor like quaternary ammonium salt.

Materials and methods

Standard solutions. Stock standard solutions of benzyldimethylcocoalkylammonium chloride (10,000 ppm-parts per million) were prepared by weighing and dissolution in 1% NaCl solution or in Forties brine. An analytical balance with accuracy up to ±0.0001 g was used for weighing. Working solutions were prepared by dilution of the stock standard solutions in blank aqueous phase for colorimetry.

Silanisation of glassware. Quaternary ammonium compounds are surfactants that have tendency to be adsorbed on glassware surface. To prevent this all glassware was silanised before each partitioning experiments. Before silanisation the glassware was rinsed with acetone and placed in a drying oven for 30 minutes. Clean dry glassware was submerged in the silanisation solution and kept there for 2-3 minutes. The procedure was repeated with acetone. Silanised glassware was placed in the oven for 30 minutes to dry.

Partitioning test. Both 1% NaCl dissolved in deionised (DI) water and Forties brine were used as a water phase for partitioning experiments. Composition of Forties brine was taken from published lit-

erature sources [6]. Required amounts of salts were weighed using an analytical balance accurate to ±0.0001 g and dissolved in DI water. Undissolved solid particles were removed by simple filtration. 1% NaCl solution and synthetic Forties brine were saturated with carbon dioxide gas until they reached pH 4 and 5.5 respectively. LAWS (low aromatic white spirit), Tiffany crude oil, kerosene, and toluene were used as the hydrocarbon phase for the experiments with the corrosion inhibitors. The total volume of water and hydrocarbon phases was 100 mL and kept constant for all partitioning tests. Required amount of the stock solution of the inhibitor (10,000 ppm) was pipetted into the mixture and shaken with the Flask shaker SF1 (Stuart Scientific, Essex, UK) for 30 minutes in a maximum mode of 800 oscillations per minute. After shaking, the mixture was kept for equilibration for 3 hours. Water and hydrocarbon phases were separated using separation funnels. The concentration of the inhibitor in the water phase was measured by colorimetry. Blank sample, i.e. mixture of hydrocarbon and water phases without any addition of corrosion inhibitors, was shaken simultaneously for each partitioning experiment. Three different water/hydrocarbon ratios were applied for the experiments: 1:3 (25 mL:75 mL), 1:1 (50 mL:50mL), and 3:1 (75 mL: 25 mL).

Colorimetry (Molecular absorbance). Concentration of quaternary ammonium chloride was measured using molecular absorbance spectroscopy. Hach Lange DR 2800 was supplied by HACH LANGE Company, Berlin, Germany.

Fluorescence spectroscopy. For Tiffany crude oil excitation (200-500 nm) and emission (300-500 nm) ranges were used. For LAWS, kerosene, and toluene full excitation (200-800 nm) and emission (200-900 nm) ranges were used in order to find out the region of maximum absorption and emission spectra. Fluorescence analysis was performed with LS55 Luminescence spectrometer supplied by Perkin Elmer (Massachusetts, USA).

Results and discussion

Partitioning behaviour of quaternary ammonium compound was studied using different hydrocarbon phases and different water cuts. After each partitioning test the residual concentration of quat (quaternary ammonium compound) in aqueous phase was measured and percentage of the amount that partitioned into aqueous phase was calculated. Table 1 represents results from partitioning tests using 1% NaCl solution (pH=4) as the water phase and LAWS as the hydro-

carbon phase. Total concentration of quaternary ammonium compound in the mixture was kept constant for all three water cuts. Total volume of the mixture was also the same (100 mL) for all three experiments. The measurements were done with three replicates. Precision of obtained sets of the results was estimated with different chemometrics factors. The calculated RSD (relative standard deviation) values showed satisfactory results in terms of repeatability (>5%).

Table 1 – Partitioning of quaternary ammonium salt between aqueous (1% NaCl, pH=4) and LAWS phase

Water: LAWS	Quat (total), ppm	Quat (aqueous phase), ppm	% in aqueous phase
1:3	5.00	19.00	95
1:1	5.00	9.90	99
3:1	5.00	6.66	100

The results in Table 1 show that concentration of quat in aqueous phase after partitioning decreased as water content in the mixture was significantly reduced. Also, the data show that in the mixture of high water content (3:1) 100% of added quat partitioned into the aqueous phase. However, at low water content (1:3) the residual concentration of quat in aqueous phase was 95% of the total added amount of the inhibitor. The 5% decrease is greater than the experimental error. This was concluded by processing obtained data with Analysis of variance (ANOVA).

The next partitioning experiment with quat was performed using synthetic Forties brine (pH=5.5) with dissolved carbon dioxide and untreated Tiffany crude oil. Total concentration in the mixture was maintained as in the previous experiment (5 ppm). However, the measured concentration of quat in the water phase after the partitioning test was lower than limit of quantification (LOQ=6.2 ppm) but higher than limit of detection (LOD=1.8 ppm). The measured value is not justified to be quoted but with certain degree of confidence it can be reported that some amount of the inhibitor was present in the brine. The amount of added inhibitor was gradually raised to 100 ppm to obtain a concentration in the brine higher than LOQ. The results are shown in Table 2. All partitioning experiments were done with three replicates in order to avoid random errors. Precision and repeatability was assessed with basic statistical analysis and concluded to be adequate (RSD<5%).

Water cut (1:1) was kept constant for all partitioning tests. For the first three concentrations (5, 15, and 40 ppm) percentage of the inhibitor that partitioned into the brine cannot be given as a single value due to the fact that measured concentrations were lower than LOQ.

Table 2 – Partitioning of quaternary ammonium salt between Forties brine (pH=5.5) and Tiffany crude oil phases

Brine: Oil	Quat (total), ppm	Quat (aqueous phase), ppm	% in aqueous phase
1:1	5.0	<6.2	<62
	15.0	<6.2	<20
	40.0	<6.2	<8
	60.0	9.6	8
	100.0	12.0	6

The results in Table 2 show that significant proportion of quat was lost from the aqueous solution whereas in the previous experiment with LAWS and 1% NaCl solution the same inhibitor distributed itself almost fully (95-100%) in aqueous phase. This implies that quat significantly changed its partitioning behaviour when different aqueous and hydrocarbon phases were applied. The reason for quat to partition less into the brine in the latter experiment could be because of high salinity level of Forties brine (58,000 ppm Cl⁻) or due to chemical differences between LAWS and Tiffany crude oil. Therefore, the initial experiment (Table 1) was repeated but with Forties brine as the aqueous phase. Table 3 represents results of the experiment. All tests were carried out with three replicates that showed good precision, reproducibility, and absence of random error (RSD<5%).

Table 3 – Partitioning of quaternary ammonium salt between Forties brine (pH=5.5) and LAWS phases

Brine: LAWS	Quat (total), ppm	Quat (aqueous phase), ppm	% in aqueous phase
1:3	5.00	19.20	96
1:1	5.00	9.90	99
3:1	5.00	6.66	100

Statistical analysis with ANOVA showed that decrease in percentage of the inhibitor that partitioned into the brine (4%) is higher than variation within

replicates. Hence, decrease in water content caused quat to lose some part of the inhibitor from aqueous phase. The results from Table 3 shows that majority of the inhibitor partitioned into Forties brine. Also, quat lost 4% of the total added amount from the aqueous phase in the low water cut mixture (1:3). A similar partitioning pattern was observed in the previous experiment with the mixture of LAWS and 1% NaCl solution (Table 1).

This result imply that partitioning behaviour of the inhibitor was not affected by the high salinity of Forties brine. Probably, the significant loss of quat in the mixture of crude oil and Forties brine (Table 2) occurred because of the effect of crude oil. Therefore, it was decided to perform a series of partitioning tests with the following hydrocarbon phases: LAWS, kerosene, toluene, and Tiffany crude oil to determine effect of various hydrocarbon phases. For the best comparison, total concentration of quat (100 ppm) and water: hydrocarbon ratio (1:1) was kept constant for all tests. The total concentration was chosen as 100 ppm to ensure that the residual concentration would not be lower than LOQ. The results are summarised in Table 4. All partitioning tests were done with three replicates. The measurements showed good precision and repeatability.

Table 4 – Partitioning of Quat between Forties brine (pH=5.5) and selected hydrocarbon phases

| Hydrocarbon phase	Quat (total), ppm	Quat (residual), ppm	% in aqueous phase
LAWS		200	100
Kerosene		190	95
Toluene	100	22	11
Tiffany crude		12	6

The results show that in the case of LAWS and kerosene, the quat partitioned mostly into aqueous phase (100% and 95%, respectively). Only 11% and 6% partitioned into the brine in the experiments where toluene and crude oil were used as hydrocarbon phases. Toluene is aromatic solvent whereas low aromatic white spirit, as the name implies, has low content (usually less than 5%) of aromatic hydrocarbons [7]. Kerosene is a distillate product of crude oil that usually does not contain aromatics and unsaturated hydrocarbons to give satisfactory properties as burning oil [8]. There is no available information about the exact composition of Tiffany oil but usu-

ally crude oil contains up to 30% of aromatic hydrocarbons. Therefore, one of the possible reasons for quaternary ammonium compound to lose a significant part of it from aqueous phase could be due to high content of aromatics in the hydrocarbon phase. The affinity of the dissolved inhibitor toward arenes could result in migration of quat from aqueous bulk solution to the liquid-liquid interface or even to bulk hydrocarbon phase. The fact that highest percentage of the quaternary compound was lost not in the pure aromatic hydrocarbon phase, i.e. toluene, but in crude oil phase could be attributed to the fact that oils usually contain various polycyclic arenes. This could affect the distribution of quat in the favour of hydrocarbon phase.
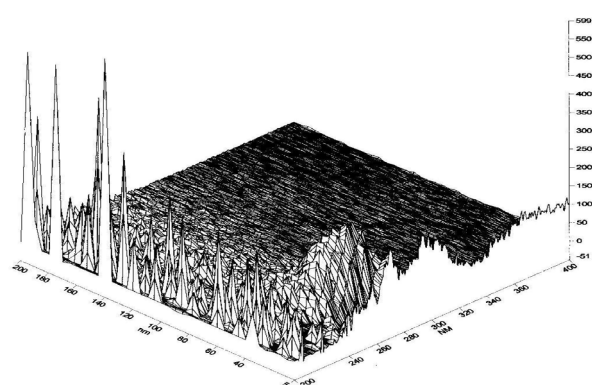
Fluorescence analysis of toluene, kerosene, LAWS, and Tiffany crude oil was carried out in order to compare their fluorescence patterns. Figures 1-4 illustrate 3D view of emission and excitation wavelengths of each hydrocarbon sample.
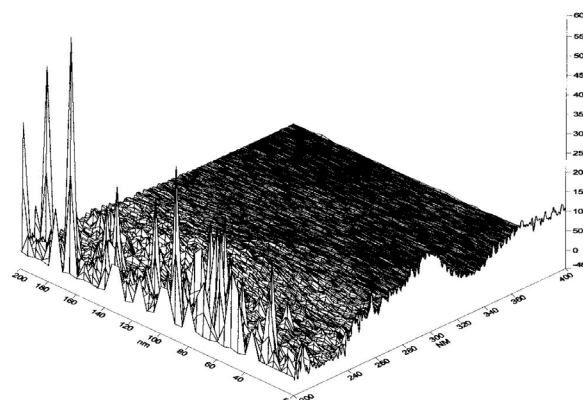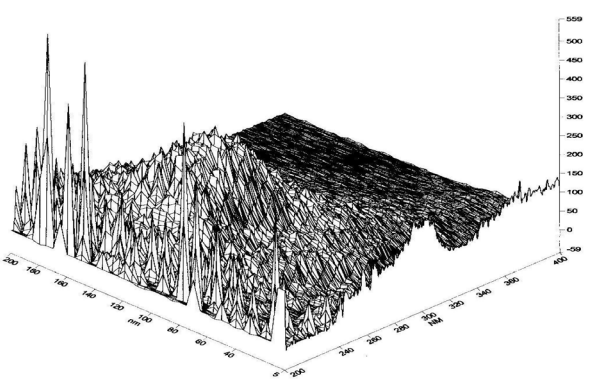

Figure 1 – 3D view of emission and excitation wavelength (LAWS)
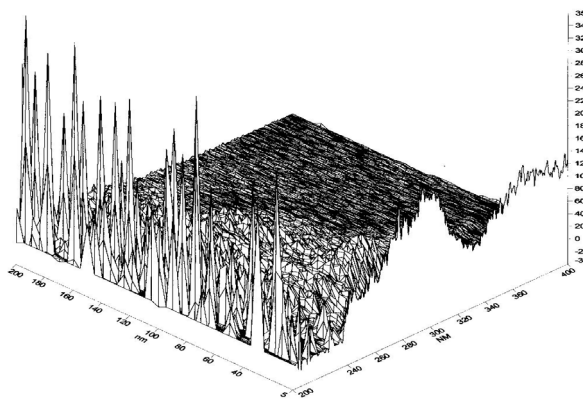
Figure 2 – 3D view of emission and excitation wavelength (Kerosene)

Figure 3 – 3D view of emission and excitation wavelength (Toluene)

Figure 4 – 3D view of emission and excitation wavelength (Tiffany crude oil)

Fluorescence of crude oils and their fractions is attributed to presence of aromatic hydrocarbons: both mono-ring and poly-aromatic compounds. 3D excitation-emission view is a result of multiple wavelength scan, which involves measuring fluorescence intensities at individual emission wavelengths. The obtained spectra are frequently used to characterise crude oils and petroleum products that contain aromatic species [9]. Fluorescence intensities are directly proportional to the concentration and number of benzene rings; polyaromatic hydrocarbons give more intense spectra than single-ring compounds. Visual comparison of the 3D spectra of 4 different samples (Figures 1-4) reinforced theoretical information about low aromatic content of LAWS and kerosene: the 3D surfaces are quiet flat. However, surface projection of kerosene spectra has slightly more intense regions than in the case of LAWS. Probably, kerosene contains more aromatics than LAWS and as a result 5% of quat partitioned into kerosene phase. Fluorescence pattern of Tiffany crude oil and toluene differ with more intense and complicated 3D view pictures.

However, it is not possible to state that loss of quaternary ammonium salt was due to its partitioning into hydrocarbon phase. Quats having asymmetric structure of surfactants could stabilise emulsions and adsorb on the water-hydrocarbon interface.

Quaternary ammonium salts are considered to be preferentially water soluble corrosion inhibitors. As it was observed from the results of the quat partitioning between aqueous phases and LAWS (Tables 1 and 3), the inhibitor was distributed mostly (95-100%) into aqueous phase. Quats have both polar and non-polar parts, i.e. ionic "head" and hydrocarbon "tail", in the strong ionic character seems to be predominant factor that governed partitioning in described systems. If the inhibitor tends to distribute itself largely into aqueous phase, hydrophilicity of the polar group exceeds hydrophobicity of the non-polar group [10]. When the inhibitor solution was added to the mixture of 75 mL LAWS and 25 mL water (1% NaCl and Forties brine), 4-5% of quat could not reach the aqueous phase and stayed in LAWS. The reason of the tendency of quats to partition more into water phase as the water content is increased in the mixture could be poor dispersibility of quat in hydrocarbon phase.

Another possible reason for the 5% loss of quat from the aqueous phase is the fact that the inhibitors as surface active agents tend to adsorb on the water-hydrocarbon interface and lower the interfacial tension. Surfactant molecules adsorb onto the interface orientating themselves with polar "head" into water phase and with non-polar "tail" into hydrocarbon phase. When concentration of a surfactant is increased in a media and reaches the point that is called critical micelle concentration (CMC), aggregations of surfactant molecules start to form in the system [11]. This happens when oil-hydrocarbon interface becomes saturated with surfactant molecules. In 1:3 (water: LAWS) mixture concentration of quat in the water phase was increased even though total applied amount of the inhibitor was not changed. Thus, increase in concentration could lead to saturated solution of the quat in water phase with adsorption of some of the molecules on the liquid-liquid interface. This could be checked by measuring and comparing interfacial tension in the applied water cuts.

The significant loss of quat from aqueous phase during the partitioning tests between Tiffany crude oil and Forties brine (Table 2) was observed. One of the possible reasons for this phenomenon could be the fact that quaternary ammonium salt is a strong surfactant, which has a tendency to stabilise oil and water microemulsions. When most part of the surfactant is concentrated in the non-polar hydrocarbon

phase, water-in-oil microemulsions are formed (Winsor II systems) [12].

Microemulsions are thermodynamically stable systems that are optically clear due to the very small sizes of suspended microdroplets (5-100 nm) which do not scatter visible light. Figure 4-6 illustrates the structure of water-in-oil microemulsion.
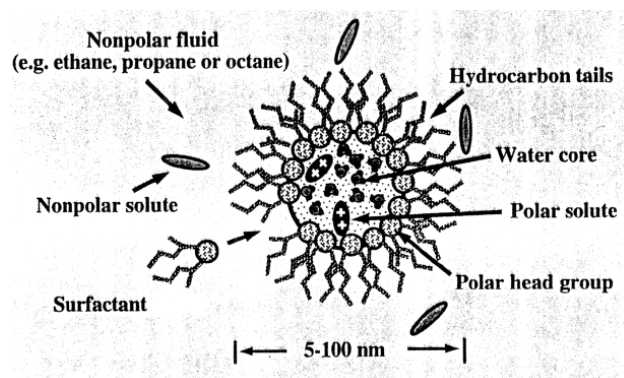

Figure 5 – Structure of water-in-oil microemulsions [13]

The surfactant molecules are adsorbed on the liquid-liquid interfaces and form a micelle-type structure by attaching to the water microdroplets with polar head group and projecting tail groups into the non-polar medium. As a result, some part of the dissolved surfactant can be lost from the bulk solution. Microemulsions are formed when the concentration of a surfactant exceeds Critical Microemulsion Concentration. When it occurs, the surfactant starts to form aggregates around microemulsion droplets to reduce the interfacial tension. Formation of emulsions can be critical for corrosion inhibition due to excessive "parasitic" consumption of the inhibitors to liquid-liquid interface and subsequent increase of corrosion risk [14].

More microdroplets form as the surfactant concentration increases in the system. Thus, more inhibitor molecules form aggregates at the interface and less monomeric forms reside in the bullk solution. Concentration of an added inhibitor directly affect the consumption of the inhibitor from the aqueous bulk solution [15]. To conclude, higher concentration of quat gave a larger interfacial area between oil and brine.

Conclusion

Partitioning behaviour of a quaternary ammonium salt was investigated with application of different water cuts. General tendency for the quat inhibitors is that they tend to lose some part during the partitioning in low water cut regions. This could happen as result of obtaining saturated surfactant solutions and formation of micelles that adsorb on the oil-water interface.

Investigation of partitioning pattern of quaternary ammonium compound revealed that the inhibitor partitioned almost fully into aqueous phase when LAWS and kerosene was used as the hydrocarbon phases. However, in the cases of Tiffany crude oil and toluene, significant part was lost from aqueous phase. The loss could be explained by the effect of high content of aromatics in the hydrocarbon phase or tendency to form of microemulsions with particular phases. Therefore, partitioning tests should take into consideration application of specially prepared model oil that has similar content as crude oil.

To conclude, partitioning of film-forming corrosion inhibitors cannot be expressed with a single value due to the fact that distribution of these compounds between oil and brine depends on factors like water cut, concentration, chemical composition of hydrocarbon phase, and presence of other chemicals.

The results obtained from the experimental part showed that there is a need for the extensive study of partitioning behaviour of corrosion inhibitors. As it is observed from results of the experiments with quaternary ammonium compound, the partitioning of the inhibitor depends not only on factors like water cut but also on the composition of the hydrocarbon phase. In order to check the assumption that cocobenzyl quaternary ammonium salt partitions more into the hydrocarbon phase if it has a high content of aromatics, different oils with known hydrocarbon composition must be applied for the tests. The effect of a type of aromatics, such as mono-ring and polycyclic arenes, on the partitioning is needed to be studied. Also, the new method for quantification of corrosion inhibitors with low LOD and LOQ should be developed to study the effect of concentrations on the partitioning.

Another way of studying partitioning behaviour of the inhibitors could be done by measuring surface tension at liquid-liquid interfaces. It would be possible to study micelle and microemulsion formation and its effect to partitioning behaviour of the inhibitors. These studies could help to identify factors that influence "parasitic" consumptions of the inhibitors due to adsorption on the liquid-liquid interfaces.

References

1   Energy Institute (2018) Guidance for corrosion management in oil and gas production and pro-

cessing. London: Energy Institute. pp.10-15. ISBN 9781787250642.

2   Javaherdashti R., Nwaoha C., Tan H. (2013) Corrosion and materials in the Oil and Gas industries. Boca Raton, Florida, USA: CRC Press. 21 p. ISBN: 9781466556249.

3   Palmer J.W., Hedges W., Dawson J.L. (2004) A working party report on the use of corrosion inhibitors in oil and gas production. London: Institute of Materials, Minerals and Mining, pp. 35-40. ISBN 9781907747885.

4   Achour M., Johlman C.L., Blumer D.J. (2008) Understanding the corrosion inhibitor partitioning in oil and gas pipelines. Proceedings of the Abu Dhabi International Petroleum Exhibition and Conference. Abu Dhabi, UAE. 95 p.

5   Kiran S.K., Nace V.M, Silvestri M.A. (2014) The HLD study of surfactant partitioning for oilfiled corrosion inhibitors. J. Surfac. Deterg., vol. 17, no. 1, pp. 1193-1201. https://doi.org/10.1007/s11743-014-1631-0.

6   Turnbull A. (2009) A multi-electrode approach to evaluating inhibition of underdeposit corrosion in CO_2 environments. Proceedings of International Corrosion Conference. Atlanta, USA. p. 50.

7   World health organization (1996) Environmental health criteria 187. White Spirit. Geneva, Switzerland.

8   Speight J.G. (2007) Chemistry and technology of petroleum. Boca Raton: CRC Press/Taylor & Francis, pp. 114-116. ISBN 0849390672.

9   Ryder A.G. (2005) Analysis of crude petrolerum oils using fluorescence spectroscopy. Boston, MA: Springer. 32 p. ISBN 978-0-387-23628-5.

10   Horsup D.I. (2007) "I Put It In, But Where Does It Go?"- The Fate Of Corrosion Inhibitors In Multiphase Systems. Proceedings of International Corrosion Conference. Nashville, Tennessee, USA. pp. 149-150.

11   Li C. (2009) Effect of corrosion inhibitor on water wetting and carbon dioxide corrosion in oil-water two-phase flow. Dr of Philosophy thesis, Ohio University. p. 55.

12   Wang Z. (2008) A downstream process with microemulsion extraction for microbial transformation in cloud point system. Biochemical Eng. J., vol. 41, no. 1, pp. 24-29. https://doi.org/10.1016/j.bej.2008.03.002.

13   McHardy, J. Sawan S.P. (1998) Supercritical Fluid Cleaning – Fundamentals, Technology, and Applications. Westwood, N.J.: Noyes Publications, 68 p. ISBN 9780815514169.

14   Gulbrandsen E., Kvarekval J. (2004) Effect of Oil-in-Water Emulsions on the Performance of CO_2 Corrosion Inhibitors. Proceedings of International Corrosion Conference. New Orleans, La, USA. pp. 236-238.

15   Knag M., Sjoblom J., Gulbrandsen E. (2006) Partitioning of a model corrosion inhibitor in emulsions. J. Disper. Sci. Technol., vol. 27, no. 1, pp. 65-75.

*F.Zh. Akhmetova[1] iD , Y.A. Aubakirov[1] iD , L.R. Sassykova[1] iD , H. Arbag[2] iD

[1]al-Farabi Kazakh National University, Almaty, Kazakhstan
[2]Gazi University, Ankara, Turkey
*e-mail: firuza.92@mail.ru

Research of composite catalysts for the process of thermocatalytic hydrogenation processing of plastic waste

Abstract. Processing plastic waste in landfills is becoming unprofitable due to the increasing costs and poor biodegradability of commonly used polymers, as well as due to large public objections. Thus, the recycling of mechanical or chemical waste seems to be the only way to handle plastic waste in the direction of sustainable development. Polyolefins, mainly polyethylene (LDPE or HDPE) and polypropylene (PP) are the main type of thermoplastics used worldwide in a wide variety of applications. In the process of thermocatalytic hydrogenation during processing of polymer waste, hydrocarbon fractions similar to motor fuels will be obtained. In general, this will allow us to process secondary raw materials, add additional fuel materials to the market and have a positive impact on the environment. Studies of new catalysts based on natural zeolite from the Taizhuzgen deposit modified with tungsten and molybdenum salt were carried out in order to jointly study the processes of thermocatalytic hydrogenation of plastic waste and optimize the process. The purpose of the study is to study the characteristics and composition of catalysts based on natural zeolite, which contain active metals for the process of thermocatalytic hydrogenation using physical and chemical methods.

Key words: fuels, plastic, recycling, polymer, Taizhuzgen zeolite, composite catalyst.

Introduction

In recent years, due to the growing need for environmental problems, especially in developing countries, and a decrease in demand for heavy oils, there are high concentrations of macromolecules and the substances contained in them, which must comply with strict environmental norms and standards. Thus, the processes that turn high molecular weight oil solutions into clean and light products have attracted the attention of researchers [1–3]. Polymers have become common materials in our daily existence and many of their properties such as service life, universalism and light weight can be an essential factor in achieving significant elaboration. However, the use of polymeric materials also increases the amount of solid waste generated, as polymeric products are often only used once before being recycled. The problem of recycling is not only technical, but also has social, economic and even political dimensions. It is for this reason that several different methods have been investigated and applied to solve problems related to the management and disposal of polymer waste [4].

The key parameter is the use of plastic waste as a source of hydrocarbon fuel. The habit of discarding plastic waste has created many environmental problems and threats to water bodies. To solve this problem, various thermochemical recycling processes have been adopted, namely thermocatalytic, pyrolysis, incineration, gasification, pyrolysis-reforming strategies for converting plastic waste into fuel-class transport hydrocarbons.

Type of thermochemical process chosen for converting plastic waste into useful energy depends on the existence of feedstock and the conversion efficiency. All processes are multi-stage and require a special type of reactor to overcome the problems of toxic gas emissions into the atmosphere [5–9]. In this study, a method for using plastic waste for the synthesis of carbon-containing materials for energy production and the use of capacitors is proposed. Environmental problems caused by plastic waste are addressed properly [10].

Processing takes place thanks to hydrothermal liquefaction – waste melts at ultra-high temperatures and dissolves in supercritical water. After that, it turns

into naphtha, which can be easily processed into fuel. The amount of fuel that can be obtained by recycling plastic will cover the need for gasoline by about 5%. Currently, it is considered as a method that develops the most the spectrum of environmental protection. Plastic waste can be processed into valuable gaseous and liquid fuels using chemical processing methods such as hydrogenation, chemical depolymerization, gasification, thermal cracking and catalytic transformations [10–12].

In addition, in order to ensure high conversion and selectivity for the target product, the catalysis is a great opportunity for converting polymer waste, since the catalysis provides low temperature and pressure, as well as high conversion and selectivity for the target product. Catalysts for energy recovery processes such as chemical processing and cracking, hydrocracking, and gasification have been studied. It is shown the effectiveness of zeolite for processing polymer waste by cracking and hydrocracking. In addition, zeolites are materials whose properties meet the requirements of the reaction, since in the liquid phase, the most important aspects are the restrictions taken into account by weight and thermal conductivity in the macromolecule of polymers of high viscosity and large size during the process of catalytic processing of the polymer in the liquid phase. Recently, the method of hydrogenation of polymer waste is used for processing various polymers, such as polyethylene (PE), polypropylene (PP), polystyrene (PS), polyethylene terphthalate (PET) and its compounds. The reaction is carried out mainly under hydrogen at a pressure of 150 atmospheric, in some cases in an describet autoclave at a temperature of 400-450 °C in the presence of solvents. Scientists have described the process of diluting PE, PP, PET and their waste in the presence of hydrogen at a temperature of 420-450 °C (54 atmospheres of cold hydrogen) with the addition of oil and tetralin used as a solvent. The results of heat treatment are compared with the results of the latter process in the presence of ZSM-5 zeolite and a highly dispersed Fe catalyst (ferrihydrite, treated citric acid). One of the directions of using production wastes and polymers as secondary raw materials is thermal and thermocatalytic modification of hydrocarbon fractions used as high-quality motor fuels. In the process of thermocatalytic hydrogenation of polymer waste, hydrocarbon fractions similar to motor fuels will be obtained. In general, this will allow us to process secondary raw materials, add additional fuel materials to the market, and have a positive impact on the environment. New catalysts based on natural zeolite from the Taizhuzgen deposit modi-

fied with Mo (VI) salt were studied in order to jointly study the processes of thermocatalytic hydrogenation of plastic waste and optimize the process [13].

The purpose of the work was to develop resource-saving technologies for the preparation and joint processing of industrial and household waste based on carbon-containing raw materials and solid fuels into fuel materials; and to establish the mechanism and regularities of chemical transformations of hydrocarbons on composite catalysts made of natural zeolites modified with active metals, as well as to develop and pilot test the technology of joint thermocatalytic hydrogenation processing of coal, shale, rubber and plastic waste in motor fuels on the developed catalysts. Improving the technology of the process and the use of appropriate catalysts can minimize losses and produce high-quality fuel distillates from spent carbon and hydrogen-containing raw materials.

Materials and methods

The experimental work in this paper differs from previous studies [13] in that the process was first studied in a continuous catalytic reactor operating under pressure in a cyclo-mixing mode with catalysis and hydrogenation of raw materials by direct distillation of liquid distillate and removal of gases. The process was carried out without the stage of draining the liquid product and its further distillation. Liquid products of thermocatalytic hydrogenation processing of polymer waste in the presence of a new composite catalyst were divided into fractions with boiling points: up to 180 °C, 180-250 °C and 250-320 °C. At the end of the process, the product is divided into fractions at a boiling point of 0-180 °C, 180-250 °C and 250-320 °C as described in the article [13].

The raw material used was a mixture of polymer waste-fuel oil with particle sizes of 2.0-6.0 mm and catalysts based on natural zeolites from the Taizhuzgen field (Kazakhstan). Natural zeolite of the Taizhuzgen deposit was activated with a solution of NH_4Cl without 1 M acid and with 1.0% Mo and 1.0 % W by the method of absorption with activated zeolite. The catalyst obtained during application is 2.0% of the total mass. The process was carried out in a continuous mixing mode at a pressure of 0.5-0.6 MPa at a temperature of 450 °C. The duration of the experience is 15 minutes [13]. To determine the crystal nature of the materials, a powder X-ray diffraction analysis was performed using a RigakuUltima IV diffractometer equipped with a Cu Kα radiation source (λ=0.15406 Nm). XPS analysis was made on the technical characteristics of the 300 device. The

XPS analysis data was adjusted for charge bias using the standard C1s 284.5 eV binding energy.

Results and discussion

The results of the study of the process of processing polymer waste showed that the nature of the catalysts affected the yield of liquid products and the optimal catalyst was 1Mo1W@Taizhuzgen; and the yield of liquid products in the thermocatalytic processing of waste polymers with heavy oil residue was high.

According to the TGA results the thermal decomposition of catalysts does not affect the processing of polymer waste, since the process takes place at a temperature of 800ºC. The results of samples of TGA composite catalysts are shown in Figure 1.
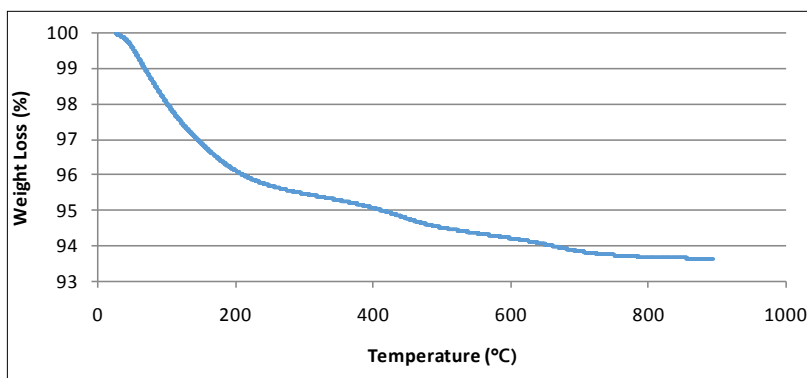

Figure 1 – TGA samples of a composite catalyst based on natural zeolite of Taizhuzgen: 1Mo1W@Taizhuzgen

The XRD pattern of the composite catalysts is shown in Figure 2. The study of the effect of the introduction of various transition metals-active components of catalysts on the heat resistance of zeolites was carried out at the next stage [14]. Figure 2 shows X-ray spectra of the Taizhuzgen zeolite and the composite catalyst 1Mo1W@Taizhuzgen, as well as catalysts based on them after heating in air at 500 °C for 1 hour. It was found that the introduction of transition metals contributes to the modification of the crystal structure of aluminosilicates, especially after high-temperature calcination [15]. The introduction of cations of group VIII elements of molybdenum and tungsten contributes to the preservation of the zeolite framework (Figure 2). It was found that the amount of MoO_3 and WO_3 oxides varies depending on the method and supporting procedure.

Thus, X-ray data indicate that significant changes in the structure of the catalyst, leading to the formation of amorphous aluminosilicate. All the regularities are valid both for natural zeolites and for 1Mo1W@Taizhuzgen.
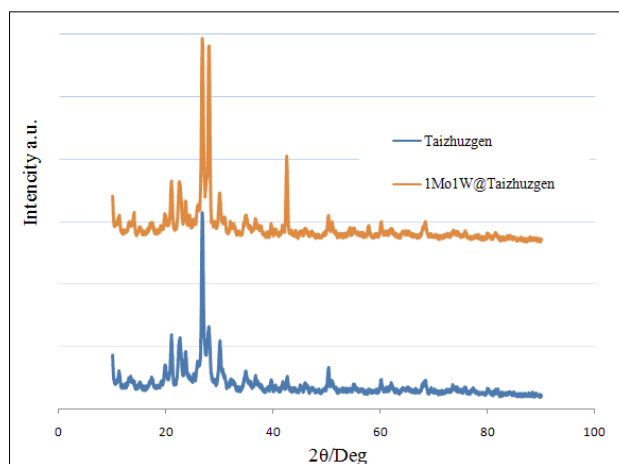
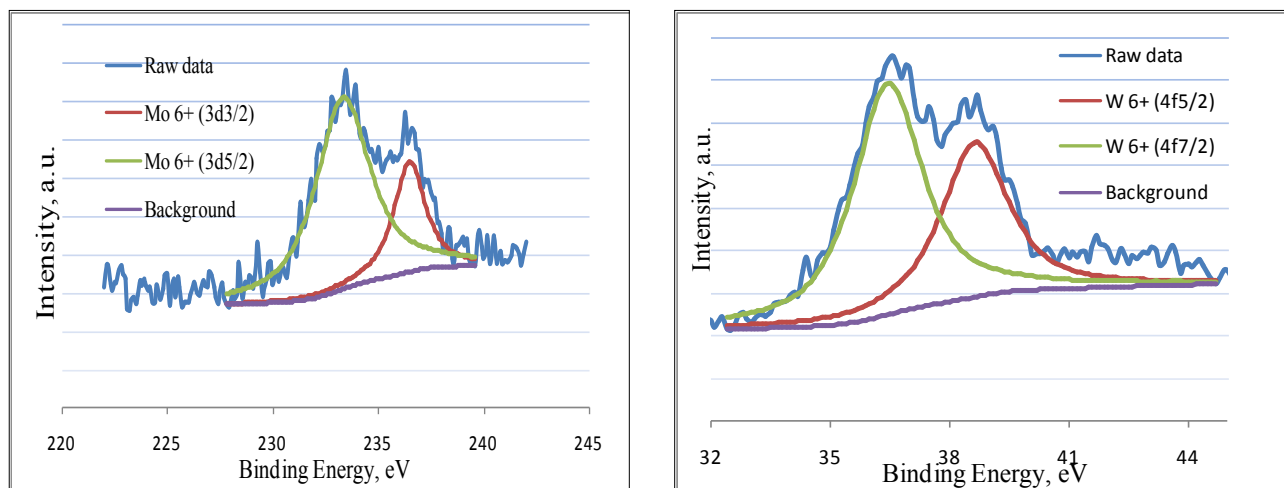**Figure 2** – XRD pattern of the catalyst 1Mo1W@Taizhuzgen

Figure 3 – XPS spectra of the catalyst 1Mo1W@Taizhuzgen

To determine the nature of the compounds, X-ray structural analysis of the catalyst was performed and the full spectra of molybdenum and tungsten were collected (Figure 3). The results of the XPS analysis determined the oxide forms of Mo and W metals in the structure of the catalysts. In the XPS 1Mo1W@Taizhuzgen spectra, two peaks refer to the Mo^{6+} oxidation of molybdenum and two peaks to the W^{6+} oxidation of tungsten. These peaks are for MoO_3 (3d3/2 and 3d5/2) and WO_3 (4f5/2 and 4f7/2).

Conclusion

To date, the most effective processes for processing rubber and polymer waste is the process of thermocatalytic hydrogenation. This is, for the purpose of searching for alternative sources of hydrocarbons for oil and natural gases, secondly, allows these processes to be carried out with the participation of cheap and effective catalysts and in soft conditions. For the resource-saving technology of thermocatalized hydrogenation of polymer waste on liquid motor fuel, a catalyst was developed with the method of impregnation of 1.0% molybdenum ion and 1.0% tungsten ion on non-acid activated Taizhuzgen zeolite, and demonstrated the activity of a new composite catalyst. In addition, it was shown that modification in combination with zeolite salts of molybdenum and tungsten salts has different effects on the catalyst morphology and on the yield of the hydrogenation process of thermocatalytic treatment of hydrocarbons and the chemical composition of liquid fractions. On the basis of physical and chemical studies of the products of the process of hydrogenation of plastic waste in the presence of a new composite catalyst, the possibility of implementing a resource-saving technology for the process of recycling waste into synthetic motor fuels is shown.

Conflict of interest

All authors have read and are familiar with the content of the article and have no conflict of interest.

References

1   Park H.B., Kim K.D., Lee Y.K. (2018) Promoting asphaltene conversion by tetralin for hydrocracking of petroleum pitch, Fuel, 222, pp. 105–113. https://doi.org/10.1016/j.fuel.2018.02.154.

2   Duan A., Wan G., Zhang Y., Zhao Z., Jiang G., Liu J. (2011) Optimal synthesis of micro/mesoporous beta zeolite from kaolin clay and catalytic performance for hydrodesulfurization of diesel. Catal. Today, 175, pp. 485–493. https://doi.org/10.1016/j.cattod.2011.03.044.

3   Ebrahiminejad M., Karimzadeh R. (2019) Hydrocracking and hydrodesulfurization of diesel over zeolite beta-containing NiMo supported on activated red mud. Adv. Powder Technol, 30, pp. 1450–1461. https://doi.org/10.1016/j.apt.2019.04.021.

4   Dargo Beyene H. (2014) Recycling of Plastic Waste into Fuels, a Review, Int. J. Sci. Technol. Soc., 2, p. 190. https://doi.org/10.11648/j.ijsts.20140206.15.

5   Upare D.P., Park S., Kim M.S., Jeon Y.P., Kim J., Lee D., Lee J., Chang H., Choi S., Choi W., Park Y.K., Lee C.W. (2017) Selective hydrocracking of pyrolysis fuel oil into benzene, toluene and xylene over CoMo/beta zeolite catalyst, J. Ind. Eng.

Chem., 46, pp. 356–363. https://doi.org/10.1016/j.jiec.2016.11.004.

6 Zhang Y., Nahil M.A., Wu C., Williams P.T. (2017) Pyrolysis–catalysis of waste plastic using a nickel–stainless-steel mesh catalyst for high-value carbon products, Environ. Technol. (United Kingdom), 38, pp. 2889–2897. https://doi.org/10.1080/09593330.2017.1281351.

7 Ragaert K., Delva L., Geem K. Van. (2017) Mechanical and chemical recycling of solid plastic waste, Waste Manag., 69, pp. 24–58. https://doi.org/10.1016/j.wasman.2017.07.044.

8 Munir D., Irfan M.F., Usman M.R. (2018) Hydrocracking of virgin and waste plastics: A detailed review, Renew. Sustain. Energy Rev., 90, pp. 490–515. https://doi.org/10.1016/j.rser.2018.03.034.

9 Weitkamp J. (2012) Catalytic Hydrocracking-Mechanisms and Versatility of the Process, ChemCatChem., 4, pp. 292–306. https://doi.org/10.1002/cctc.201100315.

10 Mir R.A., Pandey O.P. (2019) Waste plastic derived carbon supported Mo_2C composite catalysts for hydrogen production and energy storage applications. J. Clean. Prod., 218, pp. 644–655. https://doi.org/10.1016/j.jclepro.2019.02.004.

11 Munir D., Abdullah, Piepenbreier F., Usman M.R. (2017) Hydrocracking of a plastic mixture over various micro-mesoporous composite zeolites, Powder Technol., 316, pp. 542–550. https://doi.org/10.1016/j.powtec.2017.01.037.

12 Wong S.L., Ngadi N., Abdullah T.A.T., Inuwa I.M. (2015) Current state and future prospects of plastic waste as source of fuel: A review. Renew. Sustain. Energy Rev, 50, pp. 1167–1180. https://doi.org/10.1016/j.rser.2015.04.063.

13 Aubakirov Y.A., Sassykova L.R., Tashmukhambetova Z.K., Akhmetova F.Z., Sendilvelan S., Sharipov K.O., Kubekova S.N., Batyrbayeva A.A., Azhigulova R.N., Ryskaliyeva R.G., Zhussupova A.K., Abildin T.S. (2019) Thermo-catalytic processing of polymer waste over catalysts on the basis of natural zeolite from the tayzhuzgen field (Kazakhstan) modified by molybdenum, Rasayan J. Chem., 12, pp. 1701–1709. https://doi.org/10.31788/RJC.2019.1245435.

14 Li J., Liu X., Han Q., Yao X., Wang X. (2013) Formation of WO_3 nanotube-based bundles directed by $NaHSO_4$ and its application in water treatment. J. Mater. Chem. A., 1, pp. 1246–1253. https://doi.org/10.1039/c2ta00382a.

15 Wdowin M., Franus M., Panek R., Badura L., Franus W. (2014) The conversion technology of fly ash into zeolites. Clean Technol. Environ. Policy., 16, pp. 1217–1223. https://doi.org/10.1007/s10098-014-0719-6.

*O.V. Dryuk (iD) , Zh.T.Mynbaeva (iD)

Kostanay State University named after A. Baitursynova, Kostanay, Kazakhstan
*e-mail: tiptop0105@mail.ru

Amino acid composition of some plants growing in the conditions of Northern Kazakhstan

Abstract. Using gas chromatography, the amino acid composition of plants of the species *Amaranthus retroflexus L., Atriplex fera L. Bunge, Elytrigia repens L. Nevski, Bassia hyssopifolia (Pall.) Kuntze, Xanthium strumarium L.,* growing in the conditions of Northern Kazakhstan was established. The studied plants contain a number of essential and partially replaceable amino acids, such as lysine, leucine and isoleucine, methionine, valine, threonine, arginine, histidine, tryptophan and phenylalanine. Glutamine amino acid, aspartic acid, alanine, arginine, leucine, and isoleucine are found in the largest quantities. *Xanthium strumarium L.* also contains a large amount of proline. 20 amino acids were detected, including traces of ornithine and hydroxyproline for *Amaranthus retroflexus L., Atriplex fera L., Elytrigia repens L., Xanthium strumarium L.* For plants of the species *Bassia hyssopifolia (Pall.) Kuntze*, the presence of 18 amino acids was recorded and it was noted that the accumulation of amino acids is lower compared to other species that we have previously studied. The amino acid composition of plants growing in the conditions of Northern Kazakhstan has its own characteristics. Differences in the qualitative and quantitative amino acid composition of the studied species were established with known data on plants growing in the climatic conditions of Northern Siberia and Southern Kazakhstan for *Amaranthus retroflexus L., Elytrigia repens L., Xanthium strumarium L.*

Key words: amino acids, *Amaranthus retroflexus L., Atriplex fera L. Bunge, Elytrigia repens L. Nevski, Bassia hyssopifolia (Pall.) Kuntze, Xanthium strumarium L.*

Introduction

In the condition of the agricultural orientation of the Northern region of Kazakhstan, the search of plants with the rich amount of protein and free amino acids, suitable as feed additives for farm animals and raw materials for obtaining of biologically active substances necessary in the medical and food industry, becomes urgent.

The aim of our research was studying of the amino acid composition of some wild plants from the flora of Northern Kazakhstan.

In addition to studying the qualitative and quantitative amino acid composition, the objective of the research was determining differences in the content and component composition of amino acids compared with the available data on plants growing in other geographical conditions.

Amaranthus retroflexus L., Atriplex fera L. Bunge, Elytrigia repens L. Nevski, Bassia hyssopifolia (Pall.) Kuntze, Xanthium strumarium L. growing in the conditions of Northern Kazakhstan were taken as objects of study. All plants are widespread and they form the large raw materials arrays, with *Amaranthus retroflexus L., Atriplex fera L., Elytrigia repens L.* compete. The amino acid composition of *Amaranthus retroflexus L., Elytrigia repens L.* contains numerous data on plants of some climatic zones. For *Atriplex fera L., Xanthium strumarium L.*, there are data on the qualitative amino acid composition, while the quantitative composition in the literature is not adequately covered. *Bassia hyssopifolia (Pall.)* is almost not studied.

It is known that the proteins of various types of *Amaranthus* can differ in the quantitative composition of amino acids [1]. The amino acid composition of *Amaranthus Caudatus L., Amaranthus hypohondriacus L., Amaranthus cruentus L., Amaranthus edulis L., Amaranthus hybridus L.* was studied. It has been established that in various species of amaranth, seeds are richest in arginine, serine, leucine and isoleucine [2]. For plants of *Amaranthus* species, a high

lysine content is observed, which determines the usefulness of the protein. The amino acid composition of *Amaranthus caudatus L.* seeds was studied by Korejskoj I.M., Parfenovym A.A and coauthors. 19 amino acids, of which 8 are essential and 11 are nonessential was found. Traces of cystine and ornithine are noted [3, 4].

The amino acid composition of *Amaranthus retroflexus L.* seeds studied for plants growing in Central Yakutia. The content of 14 amino acids was revealed and the dominance of arginine, serine, leucine and isoleucine was established [5, 6].

According to some reports, growing *Amaranthus* at low ambient temperatures leads to a redistribution of amino acids in the overall complex: the content of serine, glutamate, proline, alanine, isoleucine and lysine increases [7].

According to *Elytrigia repens L.*, there are data on the content of a large number of lectins [8].

Elevsjuzova A.T. and Aralbaeva A.N. investigated the amino acid composition of the stems, rhizomes and seeds of *Elytrigia repens L.* growing in the conditions of Southern Kazakhstan. The authors note a high content of essential acid threonine. The limiting amino acids are phenylalanine and methionine [9].

Voronov I.V. carried out a comparative studying of the amino acid composition of seeds and middle leaves of *Atriplex patula L.* and *Amaranthus retroflexus L.* of flora of Central Yakutia. The presence of 14 amino acids was revealed, including 9 essential amino acids (lysine, leucine and isoleucine, methionine, valine, threonine, arginine, histidine and phenylalanine). Essential amino acids are tyrosine, proline, serine, alanine, and glycine. The author notes the absence of the histidine amino acid and the low content of phenylalanine in the seeds and leaves of *Atriplex patula L.* as compared to *Amaranthus retroflexus L.* [6].

The plants of the genus *Xanthium* are characterized the presence of a large number of fatty amino acids. So, the amino acid composition of the seeds of *Xanthium californicum L.* was determined by Gubanovoj L.B. and the presence of essential amino acids was revealed [10].

Based on the known data, we hypothesized that the amino acid composition of plants growing in the conditions of Northern Kazakhstan will have its own characteristics.

Materials and methods

The objects of study were air-dried raw materials of *Amaranthus retroflexus L., Atriplex fera L.*

Bunge, Elytrigia repens L. Nevski, Bassia hyssopifolia (Pall.) Kuntze, Xanthium strumarium L. Plants were harvested in the Kostanay region in August-September 2019.

The determination of amino acids was carried out by gas chromatography. Chromatography was performed on a CARLO-ERBA- 4200 gas chromatograph.

The dried, crushed feed was hydrolyzed with hydrochloric acid for 24 hours. The obtained hydrolyzate was evaporated three times to dryness in a rotary vacuum evaporator at 40° C and the final precipitate was dissolved in sulfosalicylic acid, after centrifugation at a speed of 2.5 thousand rpm. The amino acids were eluted by NH_4OH through an ion exchange column. The eluates were evaporated to dryness on a rotary evaporator, then a freshly prepared solution of tin chloride II, 2,2-dimethoxypropane and propanol saturated with hydrochloric acid were added to the flask, the mixture were heated at 110 ° C for 20 minutes, and the contents of the flask were again evaporated on a rotary evaporator. Freshly prepared acylating reagent (1 volume of acetic anhydride, 2 volumes of triethylamine, 5 volumes of acetone) was introduced into the flask, the samples were evaporated to dryness, ethyl acetate and saturated sodium chloride solution were added. The contents of the flask were thoroughly mixed and, as two layers formed, they took the top layer (ethyl acetate) for gas chromatographic analysis.

Results and discussion
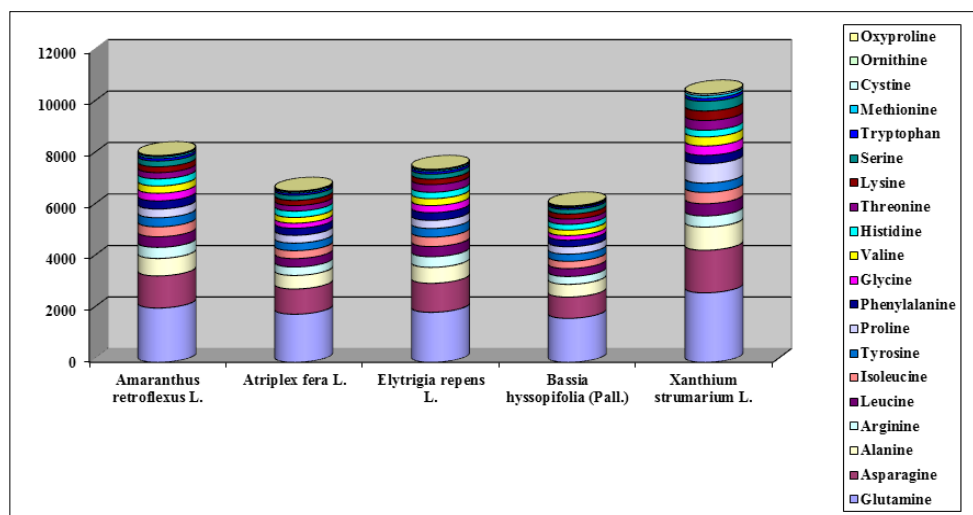
The analysis of the amino acid composition of the studied plants are shown in Table 1 and Figure 1.

The composition of *Amaranthus retroflexus L., Atriplex fera L., Elytrigia repens L., Xanthium strumarium L.*, growing in the sharply continental climate of Northern Kazakhstan, revealed the presence of 20 amino acids. Glutamate, aspartate, alanine, arginine, leucine, and isoleucine were found in the largest quantities. Traces of ornithine and hydroxyproline were found.

In the aboveground mass of *Xanthium strumarium L.*, the qualitative composition of amino acids is about 20 amino acids, of which asparagine, alanine and proline are found in the greatest amounts. After analysis of literature sources it follows that when studying the amino acid composition of the seeds of *Xanthium californicum* and *Xanthium strumarium L.*, amino acids in mainly total quantities were previously detected [10, 11]. The total amino acid content is 10.4%, of which 31% are irreplaceable and partially replaceable amino acids.

Table 1 – Amino acid composition of the studied plants

№	Amino Acid	Content, mg / 100 g				
		Amaranthus ret-roflexus L.	*Atriplex fera L.*	*Elytrigia repens L.*	*Bassia hyssopi-folia (Pall.)*	*Xanthium stru-marium L.*
1	Glutamine	2110	1870	1945	1710	2700
2	Asparagine	1248	980	1126	825	1654
3	Alanine	678	526	620	496	902
4	Arginine	430	328	415	304	431
5	Leucine	412	328	392	305	476
6	Isoleucine	388	306	368	286	439
7	Tyrosine	352	294	335	278	360
8	Proline	338	303	315	288	750
9	Phenylalanine	315	275	298	254	328
10	Glycine	296	195	276	178	365
11	Valine	285	225	270	215	352
12	Histidine	278	246	246	222	259
13	Threonine	240	214	299	204	378
14	Lysine	227	202	212	196	370
15	Serine	225	196	196	180	381
16	Tryptophan	96	75	90	62	110
17	Methionine	67	52	58	45	105
18	Cystine	44	34	35	27	64
19	Ornithine	2	1	1	-	2
20	Oxyproline	2	1	1	-	2

Figure 1 – Amino acids

Amaranthus retroflexus L. contains higher levels of tyrosine, phenylalanine, leucine, isoleucine, and alanine, the amount of arginine, proline, and threonine are lower than the amino acid composition of plants growing in Siberia [5]. It should also be noted a very high content of glutamate and aspartate compared with other types of *Amaranthus* [2-4, 12]. The total amino acid content is 8.0%, of

which 34% are irreplaceable and partially replaceable amino acids.

The amino acid composition of *Atriplex fera L.* in Northern Kazakhstan differs from *Atriplex patula L.* in Southern Siberia. The presence of small amounts of tryptophan, ornithine, oxyproline, cystine is noted. In general, the content of interchangeable and irreplaceable amino acids is higher [6]. The total amino acid content is 6.7 %, of which 34 % are irreplaceable and partially replaceable amino acids.

Differences in the content of essential amino acids *Elytrigia repens L.* are noted in comparison with plants growing in Southern Kazakhstan: the mass fraction of leucine, isoleucine and histidine is higher, and the mass fraction of threonine, valine, arginine is lower [9]. The total amino acid content is 7.5%, of which 35% are irreplaceable and partially replaceable amino acids.

In the studying samples of *Bassia hyssopifolia (Pall.)*, growing near Lake Kushmurun, in Kostanay region, the presence of 18 amino acids was established. Glutamic and aspartic acids were found in the greatest quantities. The amino acid composition of *Bassia hyssopifolia (Pall.)* also includes small amounts of tryptophan, cysteine, methionine. The total amino acid content is 6.1%, of which 34% are irreplaceable and partially replaceable amino acids.

Conclusion

The wild plants containing a large number of amino acids are of interest as the medicinal raw materials, food additives and food supply. Amino acids are a plastic material in the biosynthesis of proteins, nitrogen-containing non-protein substances, such as creatine and choline. Maintaining nitrogen balance in humans and animals depends on them. Plants rich in amino acids are a valuable raw material. The high content of amino acids in plants contributes to their effective effect on the body, as well as improved absorption, prolongation of the therapeutic effect of other biologically active substances [13-16].

As recent studies have shown, in plants about 25-30% of amino acids in free or bound form are contained. The wide distribution of amino acids in plants and their high biological activity contribute to the positive effect on the body of medicinal raw materials and medicines derived from it. So, for example, methionine as a hepatoprotective agent, aspartic acid compounds are used for the treatment of diseases of the cardiovascular system, glutamic acid can be used for the treatment of diseases of the central nervous system, histidine is used for peptic ulcers, aspartic

acid are used to normalize coronary circulation, serine are used to normalize fat metabolism, maintaining immunity [1].

The plant species studied by us are characterized by a large list of amino acids. *Amaranthus retroflexus L., Atriplex fera L., Elytrigia repens L., Xanthium strumarium L.* contain 20 amino acids, including trace amounts of ornithine and oxyproline. For plants of the species *Bassia hyssopifolia (Pall.)* the presence of 18 amino acids was recorded and it was noted that the accumulation of amino acids is lower compared to other species studied by us. The studied plants contain irreplaceable and partially replaceable amino acids: lysine, leucine and isoleucine, methionine, valine, threonine, tryptophan, phenylalanine, arginine and histidine, which make up 31-35 % of the total number of amino acids. The total amino acid content varies from 6.1 to 10.4 %.

The obtained experimental data confirm that these plant species can be used as raw materials for the production of biologically active substances necessary in the medical and food industries.

Thus, according to the results of the research, the plants *Amaranthus retroflexus L., Atriplex fera L., Elytrigia repens L., Bassia hyssopifolia (Pall.), Xanthium strumarium L.*, growing in the conditions of Northern Kazakhstan, contain large amounts of amino acids, including essential leucine, isoleucine, arginine, etc., trace amounts of ornithine and oxyproline.

References

1   Minjaeva O.A. (2016) Amino acids, as biological objects, in aqueous solutions [Aminokisloty, kak biologicheskie ob"ekty, v vodnyh rastvorah]. Scientific Review. Biological sciences [Nauchnoe obozrenie. Biologicheskie nauki], no. 6, pp. 43-47.

2   Kol'tyugina O.V. (2011) The use of amaranth seeds in dairy products [Ispol'zovanie semyan amaranta v molochnyh produktah]. Polzunovsky Bulletin [Polzunovskij vestnik], no. 3/2, pp. 163-166.

3   Parfenov A.A., Dzhurko Ju.A., Korenskaja I.M., Kornievskij Yu.I., Solennikova S.N., Borodin L.I., Fursa N.S. (2012) The study of the amino acid composition of the seeds of amaranth of the sad variety Voronezh before and after extraction with hexane [Izuchenie aminokislotnogo sostava semyan amaranta pechal'nogo sorta voronezhskij do i posle ekstrakcii geksanom].

4   Korejskaja I.M. (2013) Pharmacognostic study of seeds of various varieties of *Amarant pechal'nogo (Amaranthus hypochondriacus L.)* [Farmakognosticheskoe izuchenie semyan razlichnyh

sortov amaranta pechal'nogo *(Amaranthus hypochondriacus,* L.)]. Manuscript of the dissertation for the degree of candidate of pharmacological sciences. Permian [Rukopis' dissertacii na soiskanie uchenoj stepeni kandidata farmakologicheskih nauk. Perm'].

5   Poskachina E.R. (2014) Ecological, physiological and biochemical features of the shhiricy zaprokinutoj *(Amaranthus retroflexus,* L.), growing in the conditions of central Yakutia and the prospects for its use [Jekologo-fiziologicheskie i biohimicheskie osobennosti shhiricy zaprokinutoj *(Amaranthus retroflexus,* L.), proizrastajushhej v uslovijah central'noj Jakutii i perspektivy ee ispol'zovanija]. Manuscript of the dissertation for the degree of candidate of biological sciences. Yakutia [Rukopis' dissertacii na soiskanie uchenoj stepeni kandidata biologicheskih nauk. Jakutija].

6   Voronov I.V. (2018) Amino-acid composition of *Atriplex patula,* L. and *Amaranthus retroflexus,* L. (Amaranthaceae) growing in Central Yakutia [Aminokislotnyj sostav *Atriplex patula,* L. i *Amaranthus retroflexus,* L. *(Amaranthaceae),* proizrastajushhih v Central'noj Jakutii]. Chemistry of plant materials [Khimija rastitel'nogo syr'ja], no. 3, pp. 69-74. https://doi.org/10.14258/jcprm.2018033610.

7   Gasimova G.A., Degtjareva I.A. (2016) Complete vegetable protein as a means of improving the productivity of agricultural [Polnocennyj rastitel'nyj belok kak sredstvo povyshenija produktivnosti sel'skohozjajstvennyh zhivotnyh]. Journal, Scientific notes of Kazan State Academy of Veterinary Medicine named after N.E. Bauman [Zootehnija, Uchenye zapiski Kazanskoj gosudarstvennoj akademii veterinarnoj mediciny im. N.Je. Baumana].

8   Cammue B., Stinissen H.M., Peumans W.J. (1985) A new type of cereal lectin from leaves of couch grass *(Agropyrumrépen).* Eur. J. Biochem, 148, pp. 315-322. https://doi.org/10.1111/j.1432-1033.1985.tb08841.x

9   Elevsjuzova A.T., Aralbaeva A.N. (2019) Assessment of the biological value of different parts of pyreja polzuchego [Ocenka biologicheskoj cennosti raznyh chastej pyreja polzuchego]. Eurasian Union of Scientists (ESU) [Evrazijskij Sojuz Uchenyh (ESU)], no. 2 (59), pp. 10-12.

10   Gubanova L.B., Beklemesh E.H. (2008). The study of the amino acid composition of the flowers of the durnishnika kalifornijskogo [Izuchenie aminokislotnogo sostava semjan durnishnika kalifornijsk-

ogo]. Development, research and marketing of new pharmaceutical products. Pyatigorsk [Razrabotka, issledovanie i marketing novoj farmacevticheskoj produkcii]. Pjatigorsk, vol. 63, pp. 798.

11   Klimakhin G. I., Fonin V. S., Maslyakov V. Yu., Fadeev N. B., Semikin V. V., and Pel'gunova L. A. (2015) Biochemical features of common cocklebur *(Xanthium strumarium,* L.) Pharmaceutical chemistry Journal, vol. 49, no. 8, November, 2015 (Russian Original vol. 49, no. 8, August, 2015). https://doi.org/10.1007/s11094-015-1324-7.

12   Volkova G.A., Shirshova T.I., Beshlej I.V., Matistov N.V., Ufimcev K.G. (2017) *Amaranth (Amaranthus,* L.): chemical composition and prospects of introduction in the north [*Amarant (Amaranthus,* L.): himicheskij sostav i perspektivy introdukcii na severe]. Bulletin of the Komi Scientific Center, Ural Branch of the Russian Academy of Sciences, Syktyvkar [Izvestija Komi nauchnogo centra UrO RAN, Syktyvkar], no. 3 (31), pp.5-14.

13   Vysochina G.I. (2013) *Amaranth (Amaranthus,* L.): chemical composition and prospects of using (review) [Amaranth (*Amaranthus,* L.): himicheskij sostav i perspektivy ispol'zovaniya (obzor)] Chemistry of plant materials [Khimija rastitel'nogo syr'ja], no.2. pp. 5–14. https://doi.org/10.14258/jcprm.1302005

14   Trineeva O.V., Sinkevich A.V., Slivkin A.I. (2015) Study of the amino acid composition of plant extracts objects [Issledovanie aminokislotnogo sostava izvlechenij iz rastitel'nyh ob"ektov]. Chemistry of plant materials [Khimija rastitel'nogo syr'ja], no.2, pp. 141–148. https://doi.org/10.14258/jcprm.201502292

15   Sechin E.N., Marakaev O.A., Gavrilov G.B. (2019) Amino acid composition of vegetative organs *Dactylorhiza Maculata,* L. *Soó (Orchidaceae)* [Aminokislotnyj sostav vegetativnyh organov *Dactylorhiza Maculata,* L. *Soó (Orchidaceae)*]. Chemistry of plant materials [Khimija rastitel'nogo syr'ja], no. 2, pp.135-142. https://doi.org/10.14258/jcprm.2019024364

16   Bakova E.Ju., Plugatar' Ju.V., Bakova N.N., Konovalov D.A. (2019) Mineral and amino acid composition of the leaves of *Myrtus communis,* L. [Mineral'nyj i aminokislotnyj sostav list'ev *Myrtus Communis,* L]. Chemistry of plant materials [Khimija rastitel'nogo syr'ja], no. 3, pp. 217-223. https://doi.org/10.14258/jcprm.2019034917.